

**Petrographic and geochemical investigation of Sn - W - Nb - Ta -
pegmatites and mineralized quartz veins in southeastern Rwanda**

by

Jean-Claude Ngaruye

Thesis submitted in fulfillment of the requirements for the degree of

MAGISTER SCIENTIAE

in

GEOLOGY

Faculty of Natural and Agricultural Sciences

University of the Free State

Bloemfontein, South Africa

Supervisor: Professor Christoph Gauert

Co-supervisor: Professor Willem van der Westhuizen

September 2011

Declaration

I, Jean-Claude Ngaruye, herewith declare that the content of this dissertation is my own work and that I have referenced the material and results that are not original to it. It is being submitted for the degree Magister Scientiae at the University of the Free State, Bloemfontein, South Africa and has not been submitted before for any degree or examination at any other University.

Bloemfontein,

Jean-Claude Ngaruye

ABSTRACT

The Musha-Ntungwa, Bugarura-Kuluti-Bibare and Rwinkwavu mineral districts of Eastern Rwanda are historically known to host cassiterite, wolframite and columbite-tantalite mineralization. The geology of that area is dominated by meta-sedimentary rocks of Mesoproterozoic age deformed during the Kibaran Orogeny (1.4 to 1 Ga) and intruded by two granite generations: G1-3 granites of ca. 1380 \pm 10 Ma and G4- granites of ca. 986 \pm 8 Ma. The Sn, W and coltan deposits exploited in the E-Rwanda are associated with late magmatic phases of the youngest granite generation (G4) which probably functioned as the heat source for the mineralizing fluids. The trace and major element analyses of igneous rock samples from the study area resulted in peraluminous and S-type granites depleted in Sn, W, Nb and Ta corresponding possibly to the G1 - 3 granites. Moreover, Sn, W, Nb-Ta-rich pegmatites derived from granites equivalent to the “tin” granites (or G4-granites), were also identified. Meta-sediments hosting pegmatites/hydrothermal veins contain very low amounts of Sn, W, Nb and Ta and therefore, here like or no direct importance as source for the Sn, W and Nb-Ta mineralization. In cassiterite samples from Bugarura-Kuluti, the dominant substitution was Sn⁴⁺ replaced by (Ta, Nb)⁴⁺ whereas in cassiterite from Musha-Ntungwa and Rwinkwavu prospects, the 3 Sn⁴⁺ replaced by 2(Ta, Nb)⁵⁺ + (Fe, Mn)²⁺ and/or that of Sn⁴⁺ + O²⁻ by Fe³⁺ + OH⁻ types were predominant. The cassiterite samples also showed intergrowths with W-rich mineral phases. The wolframite samples were ferberite; coltan mineralization from increasingly distal veins showed evolution trends from ferro-columbite to mangano-tantalite compositions indicating the increase of Ta and Mn with advanced differentiation of pegmatites. Fluid inclusion studies showed a wide variation in salinities of fluids (0.5-17.5 wt. % NaCl equivalent) and formation temperatures (T_f) ranging from 150°C to 560°C confirming that the coltan precipitation closer to the granites occurred from intermediate to high temperature and relatively more saline fluids. This may indicate pneumatolytic conditions. The cassiterite and ferberite mineralization precipitated from less saline, relatively low temperature fluids possibly representing a mixture between primary magmatic fluids and meteoric to connate waters. Based on this study and various works on granite-related ore deposits in the Kibaran Belt and worldwide, a conceptual six - phase metallogenetic model involving multi-stage circulation of hydrothermal fluids caused by progressive granitic magmatism is suggested.

Key words: Kibaran Belt, South-eastern Rwanda, meta-sedimentary rocks, G4 granites, mineral chemistry, cassiterite, wolframite, coltan, fluid inclusions, hydrothermal alteration, metallogenetic model.

TABLE OF CONTENTS

DECLARATION	I
ABSTRACT	II
TABLE OF CONTENTS	III
LIST OF FIGURES	VI
LIST OF TABLES	X
LIST OF ABBREVIATIONS	XII
ACKNOWLEDGEMENTS	XIV
CHAPTER 1. INTRODUCTION	1
1.1 LOCATION AND ACCESSIBILITY	2
1.2 RWANDA SUPERGROUP: PART OF THE KIBARA OROGEN AND ITS EVOLUTION	3
1.3 EXPLORATION AND MINING HISTORY OF THE STUDY AREA.....	6
1.4 PREVIOUS WORK.....	7
1.5 OBJECTIVES OF INVESTIGATION	8
CHAPTER 2. GEOLOGICAL SETTING	9
2.1 STRATIGRAPHIC UNITS	9
2.1.1 Mesoproterozoic magmatic complexes.....	9
2.1.2 Mesoproterozoic sequences of meta-sedimentary rocks.....	10
2.1.3 Quaternary laterites and alluviums	11
2.2 STRUCTURAL GEOLOGY	14
CHAPTER 3. COUNTRY-ROCK CHARACTERIZATION	19
3.1 PETROGRAPHY AND WHOLE ROCK CHEMISTRY OF IGNEOUS ROCKS	21
3.1.1 Petrography of igneous rocks.....	21
3.1.2 Whole rock geochemistry of igneous rocks.....	21
3.2 CHEMICAL CHARACTERIZATION OF META-SEDIMENTARY ROCKS.....	27
3.2.1 Chemical composition based on major elements.....	29
3.2.2 Correlation coefficients-Discrimination plots (major elements)-Alteration estimate.....	29
3.2.3 Depletion-enrichment trends based on trace element analyses.....	33
3.2.4 Classification of the meta-sedimentary rock samples from the study area (Herron, 1988) ..	34
3.2.5 Provenance of the sediments (Roser and Korsch, 1988).....	36
3.3 MINERAL CHEMISTRY OF TOURMALINE.....	37

CHAPTER 4. PROSPECTS.	37
4.1 RWINKWAVU TIN-TUNGSTEN DEPOSIT	37
4.1.1 Geological mapping (Figures 4.1 and 4.4).....	38
4.1.2 Deformation	39
4.1.3 Mineralization	41
4.1.4. Petrography	46
4.1.5. Mineral chemistry of cassiterite and wolframite.....	54
4.2 MUSHA-NTUNGA PROSPECT	68
4.2.1 Geological setting	69
4.2.2 Deformation	71
4.2.3 Mineral occurrence and mineralization.....	72
4.2.4 Petrography	75
4.2.5 Mineral chemistry of cassiterite and coltan	77
4.3 BUGARURA-KULUTI-BIBARE PROSPECT	87
4.3.1 Geological setting	87
4.3.2 Deformation	90
4.3.3 Mineralization	90
4.3.4 Petrography	91
4.3.5 Mineral chemistry of cassiterite, coltan and wolframite.....	92
CHAPTER 5. FLUID INCLUSION INVESTIGATIONS.	102
5.1 INTRODUCTION	102
5.2 MINERALIZING FLUID PROPERTIES AND EVOLUTIONARY TREND.....	102
CHAPTER 6. DISCUSSION	115
6.1 METAMORPHISM AND HYDROTHERMAL MINERAL ALTERATION	115
6.2 CONTACT METASOMATISM OF THE COUNTRY ROCKS BY ORE ELEMENTS (Sn, W, Nb-Ta, B).....	115
6.3 ORIGIN OF FERTILE PEGMATITE MELTS- POSSIBLE SOURCES FOR Sn, W AND Nb-Ta	116
6.4 DEFORMATION CONTROL ON EMPLACEMENT OF PEGMATITIC / QUARTZ VEINS	118
6.5 STRATIGRAPHIC POSITION OF THE MINERALIZATION.....	119
6.6 PARAGENETIC SCHEME AND PRECIPITATION MODEL OF MINERALIZATION.....	120
6.7 MINERAL CHEMISTRY OF Sn, W AND COLTAN POINTING TOWARDS PRECIPITATION CONDITIONS.	122
6.8 FLUID EVOLUTION.....	125

CHAPTER 7. DEVELOPMENT OF A CONCEPTUAL METALLOGENETIC MODEL.....	127
CHAPTER 8. CONCLUSIONS	134
9. REFERENCES	135
APPENDIX 1: METHODOLOGY.....	145
APPENDIX 2: JUNE-AUGUST 2010 FIELD DATA.	147
APPENDIX 3: SAMPLING SITES.....	154
APPENDIX 4: REPRESENTATIVE SCANNING ELECTRON MICROSCOPE (SEM) DATA ...	156
APPENDIX 5: MINERAL CHEMISTRY OF TOURMALINE.	163
APPENDIX 6: WHOLE-ROCK GEOCHEMISTRY DATA.....	164

LIST OF FIGURES

Figure 1.1: Location map of the study area on the mineral deposits map of Rwanda (1:250 000). (OGMR, 2009).....	2
Figure 1.2: Map of the geological regional setting of the Karagwe-Ankole belt (KAB) in its Proterozoic and Archean framework (Fernandez-Alonso, 2007)	4
Figure 2.1: Geological map of south-eastern Rwanda (modified after Theunissen et al., 1991).....	12
Figure 2.2: Simplified stratigraphic column combined with magmatic and metallogenic events in the study area adapted after Dewaele et al. (2011), Tack et al. (2010) and Baudet et al. (1989).	13
Figure 2.3: Rose diagram of the strike and dip direction of the stratification planes	15
Figure 2.4a: Density equal area projection of strike and dip direction of the stratification planes in the study area	15
Figure 2.4b: Equal area projection strike and dip direction of the stratification planes in the study area (lower hemisphere projection)	15
Figure 2.5: Photograph of Rwinkwavu anticline structure with some mining sites	16
Figure 2.6: Interpreted shear zone map of Rwanda (Paterson, Grant & Watson Ltd, 2009) on a regional Landsat 3D-image (RTI, 2009).....	17
Figure 2.7: Right lateral strike-slip fault cross-cutting Kibaya sandstones.....	17
Figure 2.8: Structural map of the SE-Rwanda showing major faults and magmatic intrusions (modified after Theunissen et al., 1991)	18
Figure 3.1: Photograph of the coarse-grained granite of Ngarama area (2010 field work)	21
Figure 3.2: Chemical classification and nomenclature of igneous rock samples from east-Rwanda using total alkalis vs. silica –TAS (Le Maitre et al., 1989).....	25
Figure 3.3: Selected trace elements for 4 granites from E-Rwanda normalized to the phosphorous poor “tin” granite GRAN26 from Les Chatelliers-French Variscan (Raimbault et al. 1995 in Cerny et al. 2005).....	27
Figure 3.4a: Harker diagram of SiO ₂ vs. Al ₂ O ₃ , TiO ₂ , Fe ₂ O ₃ and MgO of the meta-sedimentary rock samples from the study area.....	31
Figure 3.4b: Harker diagram of SiO ₂ vs. CaO and Na ₂ O of the meta-sedimentary rock samples from the study area.	32
Figure 3.5: Al ₂ O ₃ vs. Al ₂ O ₃ / (Al ₂ O ₃ +Na ₂ O+CaO+K ₂ O) plot used to evaluate the extent of alteration of the meta-sedimentary rocks from the study area (after Nesbitt and Young, 1982).....	33
Figure 3.6: Multi-element normalized plot for some of the study area meta-sediments, normalized against the French Variscan tin granite (after Raimbault et al., 1995).....	34

Figure 3.7: Chemical classification of meta-sedimentary samples from East-Rwanda based on Herron (1988).....	35
Figure 3.8: Discriminant diagram of sedimentary provenance signatures of studied samples after Roser and Korsch (1988).	36
Figure 3.9: Fe vs. Mg discrimination diagram of tourmalines from the study area.....	37
Figure 4.1: Geological detail map around Mount Rwinkwavu showing field data of 2010	40
Figure 4.2: Photograph of the quartzite of Kibaya formation.....	42
Figure 4.3: Boulders of schists from Rukira formation (hand-picked specimens)	43
Figure 4.4: Geological and location map of the sampling sites in the Rwinkwavu area	47
Figure 4.5: Microphotographs showing general characteristics of the studied tourmalinized schists; a) PPL, x10; b)XPL, x20; c)XPL, x20; d) PPL, x4; e) XPL, x2; f) PPL, x4	49
Figure 4.6: Scanned thin-sections of meta-pelites from the Rukira formation within Rwinkwavu anticline	50
Figure 4.7: Mineralized quartz vein (Kirimbari tungsten mine)	52
Figure 4.8: Microphotographs of gangue minerals of mineralized nodes.....	53
Figure 4.9: Discrimination diagrams of major element - oxides in cassiterite from Rwinkwavu mines using WO_3 vs. Ta_2O_5 and Fe_2O_3 ; Fe_2O_3 vs. Ta_2O_5 and TiO_2 correlations.	59
Figure 4.10: Correlation diagram of cassiterite samples of Rwinkwavu using $\log [(Ta+Nb)/Sn]$ vs. $\log [(Fe+Mn)/Sn]$ after Möller et al. (1988).....	63
Figure 4.11: Correlation diagram for selected cassiterite samples using $\log [W/Sn]$ vs. $\log [(Fe+Mn)/Sn]$ after Möller et al. (1988).....	64
Figure 4.12: Binary plot Fe vs. Mn (in a.p.f.u) for wolframite data from the study area.	68
Figure 4.13: Geological map of Musha-Ntungwa area with the sampling site locations.	70
Figure 4.14: Satellite image of the Musha-Ntungwa mining district	72
Figure 4.15: Mining operations at Ntungwa tin mine	73
Figure 4.16: Mining operations at Musha mine	74
Figure 4.17: NW-SE quartz-veins in Musha area and pegmatite vein bordered by tourmaline-rich halos of alteration.....	74
Figure 4.18a: Discrimination plot of Sn vs. Nb (in apfu) in cassiterite of Musha-Ntungwa	81
Figure 4.18b: Discrimination plot of Sn vs. Ta (in apfu) in cassiterite of Musha-Ntungwa.....	82
Figure 4.18c: Discrimination plot of Sn vs. Fe (in apfu) in cassiterite of Musha-Ntungwa	82
Figure 4.18d: Discrimination plot of Sn vs. Ti (in apfu) in cassiterite of Musha-Ntungwa	83
Figure 4.19a: Correlation diagram of selected cassiterite samples from Ntungwa using $\log [(Ta+Nb)/Sn]$ vs. $\log [(Fe+Mn)/Sn]$ after Möller et al., 1988).	84

Figure 4.19b: Correlation diagram of selected cassiterite samples from Ntungwa using $\log [W/Sn]$ vs. $\log [(Fe+Mn)/Sn]$ after Möller et al. (1988).	84
Figure 4.20: Chemical composition of selected columbite-tantalite samples from Musha-Ntungwa represented in the FeTa-FeNb-MnNb-MnTa quadrilateral after Beurlen et al. (2008).....	87
Figure 4.21: Geological map of Bugarura-Kuluti-Bibare prospect (adapted after Theunissen et al. 1991).	89
Figure 4.22: Bivariate diagrams of SnO_2 against WO_3 , TiO_2 , Fe_2O_3 , Nb_2O_5 , Ta_2O_5 and MnO for the cassiterite samples from Bugarura-Kuluti.....	94
Figure 4.23: Correlation diagram of analyses for cassiterite samples from Bugarura using $\log [(Ta+Nb)/Sn]$ vs. $\log [(Fe+Mn)/Sn]$ after Möller et al. (1988)	95
Figure 4.24: Correlation diagram of analyses for cassiterite samples from Bugarura using $\log [W/Sn]$ vs. $\log [(Fe+Mn)/Sn]$ after Möller et al. (1988).....	97
Figure 4.25: Chemical composition of selected analyses of columbite-tantalite samples from Bugarura-Kuluti (this study) and from Cyubi, Ruhanga and Gasasa (Melcher et al., 2009) plotted in the FeTa-FeNb-MnNb-MnTa quadrilateral after Beurlen et al. (2008).	99
Figure 5.1: Microphotographs showing fluid inclusions in the selected thick sections from quartz crystal samples from the study area	104
Figure 5.2a: Frequency distribution of investigated fluid inclusions sizes (in μm) from the study area	105
Figure 5.2b: Frequency distribution of the total melting temperature of ice- T_m ($^{\circ}C$).....	106
Figure 5.2c: Frequency distribution of homogenization temperatures of fluid inclusions of investigated samples from the study area.	106
Figure 5.2d: Histogram showing the frequency distribution of salinities (after Bodnar and Vityk, 1994)	107
Figure 5.3: Bivariate diagram of salinities in wt. % NaCl equivalent versus homogenization temperatures (T_h) for the two phase inclusions in the studied samples	108
Figure 6.1: Photograph of one of the small intrusive kaolinized pegmatites outcropping in the Ntungwa Sn-mine.	116
Figure 6.2: Paragenetic scheme of Bugarura-Kuluti-Bibare/Musha-Ntungwa and Rwinkwavu mineralization	121
Figure 6.3: Discrimination plots of selected cassiterite samples from the study area using $\log [(Nb+Ta)/Sn]$ vs. $\log [(Fe+Mn)/Sn]$ and $\log [W/Sn]$ vs. $\log [(Fe+Mn)/Sn]$ (after Möller et al., 1988) in comparison with cassiterite samples from granites of the Egyptian Pan-African Orogeny (Abdalla et al., 2008).	123

Figure 6.4: Columbite quadrilateral binary plot of Mn/(Fe+Mn) vs. Ta/(Ta+Nb) in a.p.f.u (Beurlen et al., 2008) for the coltan samples of the study area, of selected mines in Rwanda (Melcher et al., 2009) and of Podlesi in Czech Republic (Breiter et al., 2007). 125

Figure 6.5: Frequency distribution of the eutectic temperatures T_e (°C) 126

Figure 7.1: Eh-pH diagram for the W-C-Fe-Mn-H₂O system at 25°C, 100°C, 300°C and 400°C (Haung et al., 2002) 130

Figure 7.2: Conceptual metallogenic model adapted after Varlamoff (1948, 1972); MINETAİN in RMCA's Archives (1965); Cerny (1993b) and Cerny et al. (2005). 132

LIST OF TABLES

Table 3.1: Overview list of rock-samples from the country rock and gangue minerals of veins.....	19
Table 3.1: (continued).....	20
Table 3.2: Geochemical composition of the igneous rocks from various localities of the study area obtained using XRF techniques	22
Table 3.2: (Continued).....	23
Table 3.3: Sample/clarke ratios of selected trace-elements (ppm) of investigated felsite samples	26
Table 3.4: Chemical composition of meta-sedimentary rock samples from the study area.....	28
Table 3.5: Pearson correlation matrix and coefficients for major elements	30
Table 4.1.1: Overview of mineral deposits in the Rwinkwavu mining concession	44
Table 4.1.2: Description of sampled rocks within the Rwinkwavu mining concession	48
Table 4.1.3: Summary of oxide contents in the cassiterite samples from Rwinkwavu area	56
Table 4.1.4: Pearson correlation: Samples of cassiterite from Rwinkwavu.....	57
Table 4.1.5: Chemical composition of selected cassiterite samples from Rwinkwavu	60
Table 4.1.5: (continued).....	61
Table 4.1.5: (continued).....	62
Table 4.1.6: Chemical composition of selected wolframite samples from Rwinkwavu -Kirimbari (sample JC-KRM) using SEM-EDX/WDX.....	64
Table 4.1.7: Determination of the bulk chemical formulae of selected wolframite samples from Kirimbari (JC-KRM and JC-KRM-1 676):.....	67
Table 4.2.1: Summary of the characteristics of sampled rocks in Musha - Ntungwa concession	76
Table 4.2.2: Average chemical compositions of cassiterite group minerals from Musha - Ntungwa (JEOL JSM-6610 SEM-EDX in wt. %)......	77
Table 4.2.3: Chemical composition of selected cassiterite samples from Musha-Ntungwa	79
Table 4.2.3: (continued).....	80
Table 4.2.4: Chemical composition of analyses of coltan sample JC-25 from Musha-Ntungwa	85
Table 4.2.5: Structural chemical formula and nomenclature of “coltan” analyses from Musha-Ntungwa	86
Table 4.3.1: List of geographic location and rock-types of samples from Bugarura-Kuluti-Bibare.....	92
Table 4.3.2: Average chemical compositions of cassiterite group minerals from Bugarura – Kuluti-Bibare.....	93
Table 4.3.3: Chemical composition of coltan analyses of sample JC-34 from Bugarura-Kuluti (this study) compared to those of the Cyubi, Ruhanga and Gasasa mines (Melcher et al.; 2009)	98

Table 4.3.4: Structural chemical formula and nomenclature of “coltan” analyses from Bugarura-Kuluti	99
Table 4.3.5: Summary of the chemical composition of investigated tungsten-bearing ore samples from Bibare mining concession (Rwankuba mine)	100
Table 5.1: Estimated temperatures of formation at P = 2kbars (Bodnar and Vityk, 1994).....	108
Table 5.2: Microthermometric data from aqueous fluid inclusions in the studied samples	109
Table 5.2: (continued).....	110
Table 5.2: (continued).....	111
Table 5.2: (continued).....	112
Table 5.2: (continued).....	113
Table 5.2: (continued).....	114

LIST OF ABBREVIATIONS

A/CNK	$[\text{Al}_2\text{O}_3 / (\text{CaO} + \text{Na}_2\text{O} + \text{K}_2\text{O})]$
Apfu	Atoms per formula unit
BRGM	Bureau de Recherches Géologiques et Minières
BSE	Back-scattered electron image
Ca.	Around, circa
CIA	Chemical index of alteration
COPIMAR	Coopérative de Promotion de l'Industrie Minière Artisanale au Rwanda
DRC	Democratic Republic of Congo
EARS	East-African Rift System
Eh	Potential redox
Elev.	Elevation/altitude
Ga	Billion years
GEORUANDA	Compagnie Géologique et Minière du Ruanda-Urundi
GPS	Global Positioning System
IGN	Institut Géographique National (Belgium)
KAB	Karagwe-Ankolean Belt
KIB	Kibara Belt
LLD	Lower limit of detection
LOI	Loss on ignition
Ma	Million years
MINETAÏN	Société des Mines d'Étain du Ruanda-Urundi
MINICOM	Ministry of Trade and Industry (Rwanda)
MINITRAPE	Ministère des Travaux Publics et de l'Énergie (Rwanda)
NRG	New Resolution Geophysics (South Africa)
OGMR	Rwanda Geology and Mines Authority
P	Pressure
Pers. comm.	Personal communication
PGE	Platinum Group Elements
pH	Potential hydrogen (acidity)
PPL	Plane Polarized Light
REDEMI	Régie d'Exploitation et de Développement des Mines
RMCA	Royal Museum for Central Africa (Belgium)
RTI	Radar Technologies International (France)

S0	Stratification bedding plane
S1	Cleavage or foliation plane
SEM-EDX/WDX	Scanning electron microscope-Energy Dispersive Spectrometer/Wavelength Dispersive Spectrometer
SOMIRWA	Société Minière du Rwanda
SOMUKI	Société Minière de Muhinga et de Kigali
SRTM-DEM	Shuttle Radar Topography Mission-Digital Elevation Model
TAS	Total Alkali versus Silica diagram
T_e	Eutectic temperature
T_f	Formation (or trapping) temperature
T_h	Homogenization temperature
T_{hCO_2}	Homogenization temperature of CO ₂
T_m (or $T_{m_{ice}}$)	Total melting temperature of ice
$T_{m_{CL}}$	Melting temperature of clathrate
$T_{m_{CO_2}}$	Melting temperature of CO ₂
UNCTAD	United Nations Conference on Trade and Development
UNDP	United Nations Development Programme
U-Pb SHRIMP	U-Pb Sensitive High Resolution Ion Microprobe datation
WID	Western Internal Domain
WMP	Wolfram Mining and Processing Ltd
XPL	Crossed Nichols Light microscopy
XRF	X-Ray Fluorescence

Acknowledgement

The positive atmosphere and relations with the staff of the Department of Geology and other postgraduate students played a key-role in changing my attitude to science and to life. I want to thank all whom I had the pleasure of meeting, getting to know, to work with and who have contributed not only to this research work but also to my life here in Bloemfontein.

To be more specific and giving credit where credit is due, I owe a considerable debt to my supervisor Prof. Christoph Gauert who stimulated my interest in economic geology and introduced me to various modern laboratory techniques. Your advice, guidance, continuous encouragement, fruitful discussions even at late hours and support to my daily living in Bloemfontein should not be left unacknowledged.

I would like to express my heartfelt gratitude to the Department of Geology and specifically to Prof. Willem van der Westhuizen for giving me the opportunity to attend this programme, the financial support and the tireless guidance throughout its duration.

It is also a pleasure to acknowledge the Government of Rwanda especially the Ministry of Education for funding my MSc-programme and OGMR for allowing me to participate in this research-programme.

A special word of thanks to the following company and individuals who, directly or indirectly, helped in the accomplishment of this research project: the RMCA-Tervuren for multiple guidance in terms of geology and metallogeny of Rwanda, in providing me various documents from their archives and rock samples from their collections and their support during the 06-08/2010 field survey; Profs. Haggerty, S. and Tredoux, M.; Prof. Cerny, P. for his useful correspondence; Dr. Roelofse, F. for his constructive observations & criticisms; Mrs. Immelman, CEM. and Swart, PS.; Mr. Roodt, PH., Choane, J., Felix, A. and Radikgomo, D.

To conclude I want to thank my family for their patience and for supporting me, when I needed it. I dedicate this work to my wife Marie-Louise, my daughters Vaudine, Jennifer-Victoria, Vanessa-Assumpta and Natalia and my son Lionel.

1. INTRODUCTION

Despite the relatively limited knowledge of the geology, the insufficiency of qualified miners and geologists and the absence of a professional mining structure, the mines remain one of the key-sectors of the Rwandan economy in terms of yearly incomes (UNCTAD and MINICOM, 2010).

Important reforms were elaborated and are progressively implemented since 2008 by the government of Rwanda and by various stakeholders in the mining sector. These improving measures are based on five pillars which are the following:

- Initiation and implementation of the Rwanda Geology and Mines Authority (OGMR) with concise duties: geological and mining research, supervision and inspection of the mining industry for a better quality of mining activities, permanent capacity building of the miners, etc.
- The new mining law of 2008 and regulations which may assist in its implementation are new creations in favour of more investments in the mining sector;
- The privatization process of twenty (20) mining concessions owned until 2007 by REDEMI, a former state mining company and the discoveries of new ore deposits mostly along Akagera national park;
- The promotion and technical support to tin, tungsten and other mineralization processing for the value addition;
- The strengthening of international cooperation and capacity building of the mining companies and the OGMR staff members.

Looking at the first results and the current estimated mineral ore reserves, there is hope that the mining activities would lead the Rwandan economy for another twenty to thirty years.

This study is part of various improving measures initiated. The result was a set of valuable petrographic and geochemical information which may provide a tool in mineral exploration for the south-eastern Rwanda. The present research document comprises seven chapters: chapter one is an introduction. Chapter two is a compilation of the geologic background of the study area. Chapter three consists of the country rock characterization and describes the igneous rocks, which are considered likely to act as heat sources governing the mineralization aspects and the meta-sedimentary rocks hosting the ore deposits. Chapter four gives more details on the three prospects, the mineral chemistry of their economically exploitable ores and the paragenetic schemes of each prospect. The fluid inclusion investigation results are compiled in chapter five. Chapter six is the discussion of the results whereas chapter seven is the development of a metallogenic model and chapter eight the conclusion.

1.1. Location and accessibility

The study area consists of three mining districts located in the Eastern Province of Rwanda in the vicinity of Rwamagana town, 45km from Kigali and some tens of kilometers from Akagera National Park. The three mining areas are recorded among the first mines exploited for cassiterite, wolframite and columbite/tantalite mineralization and are namely: Musha-Ntunga, Bugarura-Kuluti-Bibare and Rwinkwavu concessions (Figure 1.1).

The general topography is dominated by a succession of low and flat lands with altitudes ranging from 1300 m (Lake Muhazi) to 1750 m (Mount Gahengeri) and the three mining concessions are accessible via respectively, Kigali-Rwamagana, Kigali-Kayonza-Nyagatare, and Kigali-Kayonza-Kabarondo-Rwinkwavu roads.

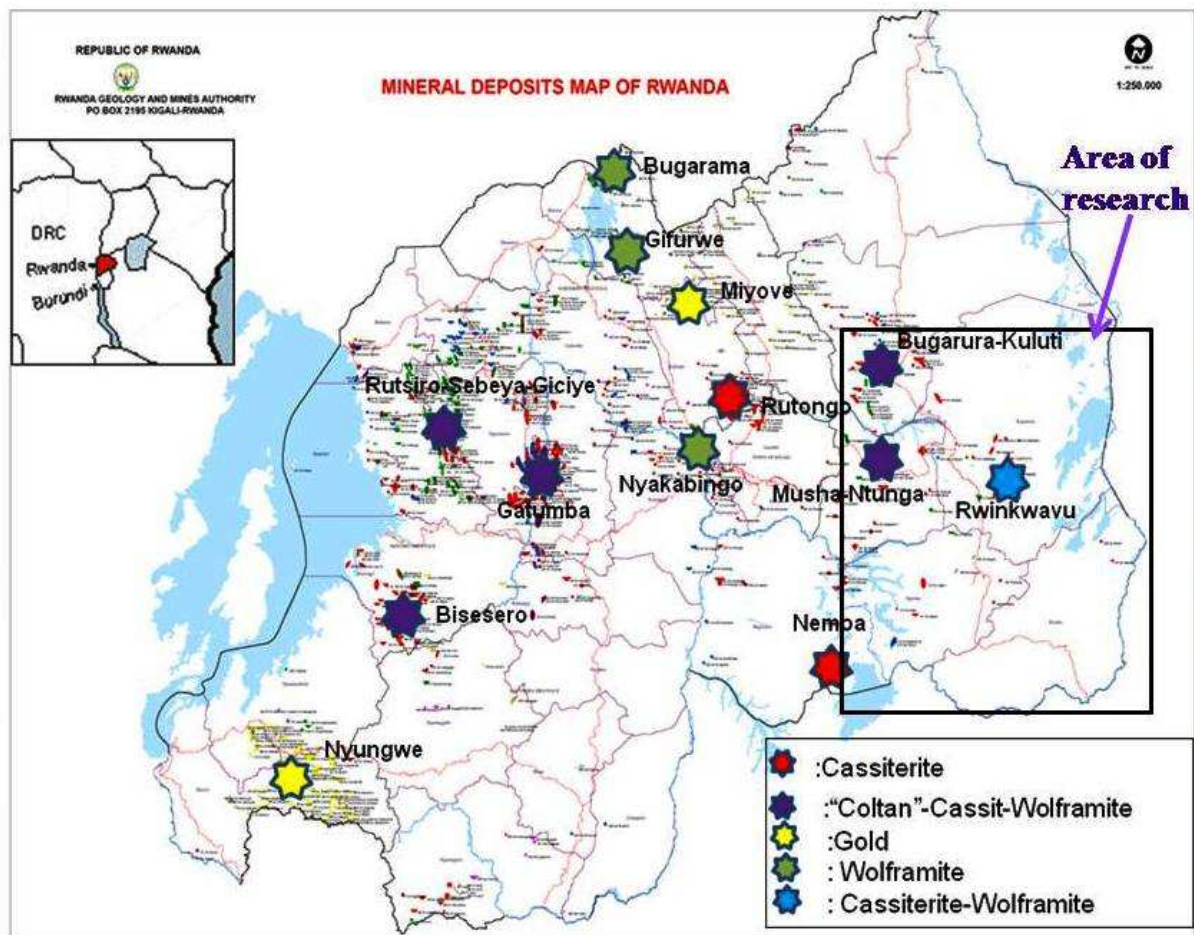


Figure 1.1: Location map of the study area on the mineral deposits map of Rwanda (1:250 000). The stars indicate the main mining concessions of the country (OGMR, 2009).

1.2 Rwanda Supergroup as a part of the Kibara orogen and its evolution

Rwanda has been located by various authors in the Kibaran metallogenic Province of the Central African Kibaran Belt (Dewaele et al., 2010; Pohl and Günther, 1991). The latter has been defined as a belt of Mesoproterozoic supracrustal units, comprising mostly meta-sedimentary rocks with locally meta-volcanic series, intruded by voluminous peraluminous S-type granitoids and subordinate mafic bodies, also of Mesoproterozoic age (Cahen et al., 1984). It has often been portrayed as a single, continuous orogenic belt that trends NE covering 1500km*400km from the Katanga region in the Democratic Republic of Congo (DRC) up to the Ankole region in SW Uganda (Brinckmann et al., 2001; Kokonyangi et al., 2006; Buchwaldt et al., 2008).

However, based on satellite imagery and derived products (Landsat, SRTM-DEM), Tack et al. (2010) confirmed the existence of a break in the continuity of the thus-defined “Kibara belt” materialized by the NW-trending Palaeoproterozoic Ubende belt of SW Tanzania extending along trend across Lake Tanganyika into the Kivu-Maniema region of the DRC which “cross-cut” the Kibaran belt (Figure 1.2). Various authors have confirmed this break including Tack et al. (2002a, 2002b, 2006) who showed earlier that the Kibaran belt was divided in two distinct but coeval segments: the Kibara belt s.s. of Katanga (DRC) and the North-eastern Kibara belt extended on Burundi, Rwanda, Kivu and Maniema provinces of DRC, SW Uganda and W Tanzania.

This discontinuity between the two segments has been mapped as Palaeoproterozoic “Rusizian” basement by various authors (e.g. Cahen and Snelling, 1966; Lavreau, 1985).

For the sake of clarity, Tack et al. (2010) proposed to use, henceforward, the name “Kibara belt” (“KIB”) only for the part occurring SW of the Ubende–Rusizian belt in the Katanga region of the DRC, which includes the Kibara Mountains type area. The part to the NE trending belt, and east of the western branch of the East-African Rift System has been assimilated by the same author as distinct from the KIB and was named “Karagwe-Ankole belt” (“KAB”). The latter name has been attributed based on historic uses of it for designating the Mesoproterozoic belt in the Karagwe (NW Tanzania) and the Ankole (SW Uganda) regions (Cahen, Delhal and Deutsch, 1972; Cahen et al., 1984).

Both Karagwe-Ankolean and Kibara belts have been assimilated to an intra-continental orogen developed and evolved during 1400-900 Ma time-period between Archean-Palaeoproterozoic Congo craton in the west and north and Archean-Palaeoproterozoic Tanzania craton and Banguéulu Block in the east and south and these underlying Archean-Palaeoproterozoic layers that were extensively

affected by the Eburnean events between 2.2 and 1.9 Ga (Pohl and Günther, 1991; De Waele et al., 2008; De Clerq et al., 2008).

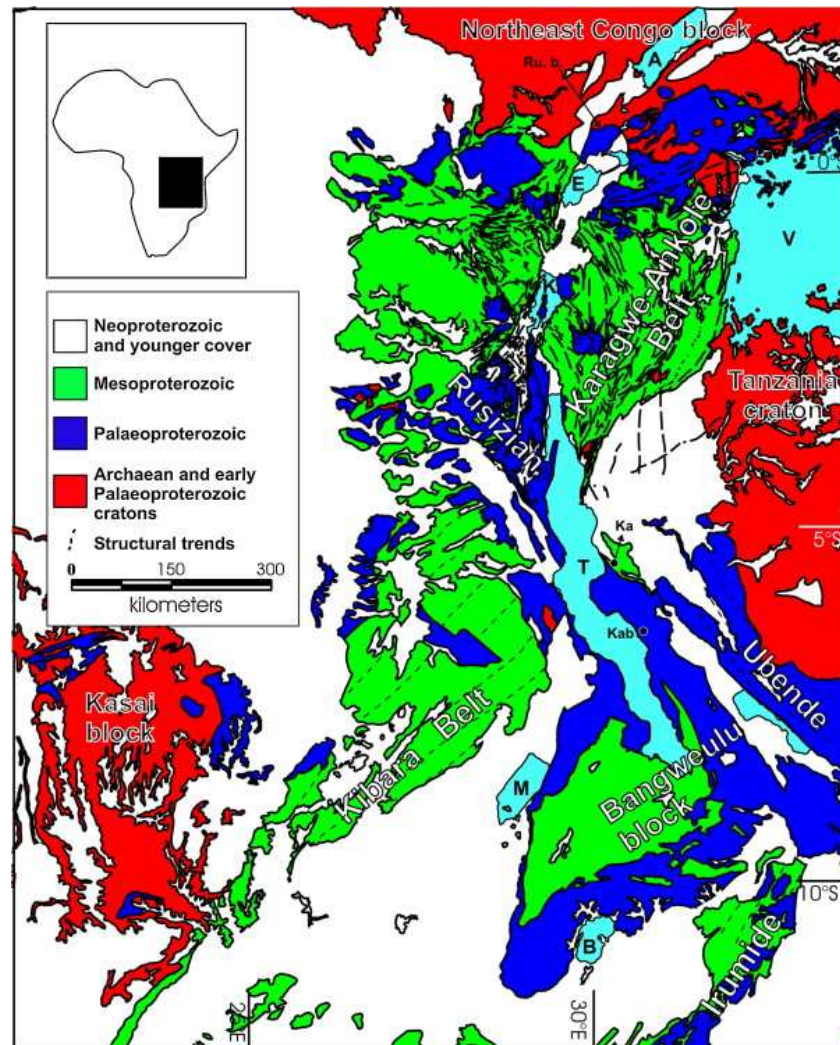


Figure 1.2: Map of the geological regional setting of the Karagwe-Ankole belt (KAB) in its Proterozoic and Archean framework (Fernandez-Alonso, 2007).

This belt forms a large metallogenic province hosting numerous granite-related ore deposits known for cassiterite, columbite / tantalite (so called “coltan”), wolframite, beryl, spodumene, amblygonite, monazite and gold mineralization (Pohl, 1994; Dewaele et al., 2010).

The origin and evolution of this Palaeo-Mesoproterozoic belt is up to now a matter of discussion: Pohl (1994), Pohl and Günther (1991) and Baudet et al. (1989) described the stratigraphy of the Kibaran belt as dominated by meta-sediments with intercalated volcanic rocks and rare carbonates. Baudet et al. (1989), Pohl and Günther (1991) reported lateral and vertical changes within the sedimentary sequences and realized that the sediments are composed of conglomerate fans

(characterizing the early phases of rifting), sheets passing into marine, clastic elements with quartzites, sandstones and shales with high content in organic matter.

Pohl and Günther (1991) described three groups of evolving sedimentary sequences and volcanic rocks as follow:

1. The lower group with dark laminated pelitic sedimentary rocks with intercalations of mature quartzites, conglomerates, sandstones and siltstones in which are reported inter-bedded acidic tuffs. The authors reported the presence of various sedimentary structures and estimated its thickness to attain the maximum in Burundi (1,000 m).
2. The middle group described as composed of arenaceous clastic rocks, banded fine-grained and occasionally conglomeratic white to pinkish quartzites. Here the authors mapped, on the top of this group in the west, the basaltic volcanic edifices and sills which were in association with thin sheets of dacitic, trachytic and rhyolitic rocks.
3. After the same authors and supported by Baudet et al. (1989), the upper group occurs only in major synclinoria with the lowest layers formed by immature sediments and the topmost by fine-grained white siltstones and shales with chert laminae indicating an environment of saline lakes.

For the evolution of this orogen, several models have been proposed: interpreted either as a collisional Orogeny (Kampunzu et al., 1986; Rumvegeri, 1991), or intra-continental orogen with different periods of extensions and compressions (Pohl and Günther, 1991; Klerkx et al., 1984, 1987) or intra-cratonic extensional detachment structure, conditioned by strike-slip reactivation of NW trending shear zones in the Palaeoproterozoic basements (Fernandez-Alonso and Theunissen, 1998).

Cahen et al. (1984) confirmed that the Palaeo and Mesoproterozoic rocks of the Kibaran belt have been intruded by different generations of granites but more recent investigations by Tack et al. (2006, 2008, 2010), using U-Pb SHRIMP datation identified only two generations: the barren G1-3 granites intruded at ca. 1380 \pm 10 Ma and G4 granites intruded at ca. 986 \pm 10 Ma. The crystallization of G4 granites has resulted in economically significant concentrations of rare metals (Dewaele et al., 2010).

The mineralization-bearing pegmatites which occurred at ca. 968 \pm 8Ma are associated with this G4 granite; the U-Pb ages of columbite/tantalite were estimated between 975 \pm 8 and 936 \pm 14 Ma in the Gatumba ore deposits (Dewaele et al., 2011). The latter author confirmed that the early ages of Nb-Ta

(975 to 966+/-8 Ma) overlap with the U-Pb ages of ca. 965+/-5Ma (962+/-2 Ma in Burundi) reported in Romer and Lehmann (1995) whereas the late Nb-Ta mineralization were interpreted as the result of later orogeny overprints and the entire set has been cut by cassiterite - mineralized quartz veins of ca. 951+/- 18 Ma age (Brinckman et al., 2001).

1.3 Exploration and Mining History of the study area

After the end of the First World War, Belgium sent a geological mission led by Chanone A. Salée of the University of Louvain to carry out geological mapping of Rwanda, Burundi and Kivu Province (Biryabarema, pers. comm.). This was done between 1922 and 1928 and resulted in a geologic map of Rwanda and neighbouring regions of Uganda and Tanganyika at a scale of 1/500,000.

Cassiterite was discovered for the first time in the Eastern Rwanda and in Gatumba and the mining activity started in 1930's dominated by Belgian companies such as MINETAÏN, SOMUKI and GEORWANDA.

Rwinkwavu was discovered in 1940's and has been exploited for tin and small amounts of tungsten mineralization since 1941.

In 1975, to enhance better organization and production increase, all the companies were grouped into SOMIRWA, "Société Minière du Rwanda" working in a joint-venture with the Government of Rwanda. In 1985, SOMIRWA went virtually bankrupt and was replaced by both the "Régie d'Exploitation et de Développement des Mines" (REDEMI) and the "Coopérative de Promotion de l'Industrie Minière Artisanale au Rwanda" (COPIMAR). The latter was a private structure supporting technically the artisanal miners.

The Geological Survey of Rwanda, assisted by several foreign technical and financial sponsors, has done a lot of geological reconnaissance surveys such as the geophysical exploration, geological mapping (since the 1960's) and the 1970's stream sediments geochemical exploration.

The year 2008 was marked by the privatization of around 20 mining concessions owned by REDEMI (Privatization Secretariat, oral communication). The main objectives of the privatisation of REDEMI were:

- To reduce the shares held by the government in public companies, thus alleviating the financial burden on its resources (through the elimination of subsidies and state investments) and reducing its administrative obligations in these enterprises;

- To generate revenues for the government through the sale or lease of state owned enterprises;
- To ensure better management and financial discipline in privatized companies;
- To attract foreign investment in Rwanda and the accompanying transfer of technology and knowhow; and
- To encourage Rwandan citizens to invest in the private sector and to stimulate their entrepreneurial spirit.

1.4 Previous work

The archives of OGMR-Kigali and RMCA-Brussels indicate only a few research projects in the eastern part of Rwanda. The first geologic map of eastern Rwanda was completed in 1967 by Petricec. In the 1970's, geophysical investigations which included the spectrometric and magnetometric data acquisition using helicopters were done successfully and identified geophysical anomalies.

In 1974-1981, the "Projet Recherches Minières" co-executed by the Government of Rwanda and the United Nations Development Program (UNDP) explored the whole country using "stream-sediment" techniques and geochemical anomalies were mapped. This geochemical exploration project identified in the eastern Rwanda a NE trending tungsten anomalous zone from Birenga (Gahombo) in the south to the Akagera National Park in the north (Rwagashayija, pers. comm.).

Dutu Stanchi et al. (1974), reported very low grades of copper, zinc, cobalt, nickel and chrome in the east but with high grades of Ni and Cr (between 1,000 and 2,000 ppm) in some places and for some specific altered rocks. They recommended further exploratory works. Bizimana (1982) reported economic reserves of mineralization between Bugarura-Kuluti and Akagera National Park.

During 1981, Sander & Geophysics Ltd, a Canadian Company carried out a geophysical campaign (gravimetric and radiometric survey) on the whole country and identified several geophysical anomalies.

The investigations on W- anomaly in the axis Kabarondo-Bare by Schipper (1987) did not reveal economically exploitable reserves. The geologic mapping of the whole country by a joint team from the Royal Museum for Central Africa-RMCA (Tervuren-Belgium) and the Geologic Survey of Rwanda, which resulted in a geologic map of Rwanda (1:250,000) and 12 map sheets (1:100,000), followed in 1987.

Paterson, Grant & Watson Ltd recently (2009) interpreted the 2009 New Resolution Geophysics (NRG-South Africa) airborne geophysical data on Rwanda and integrated the new data with existing geoscientific data. This identified 21 potential targeted mining areas in the country.

OGMR with the technical support of RMCA started to map the geology of the country on 1:50000 and two sheets have been so far completed during the year 2009 (Biryabarema, pers. comm.).

1.5 Objective of investigation

The geological and mining research on the Kibaran belt have been carried out since the colonial periods and a few recent metallogenetic studies to explain the formation and the origin of the mineralization using modern techniques and metallogenetic models were reported (Pohl and Günther, 1991; Pohl, 1994; Dewaele et al, 2007a, 2007b, 2008, 2010, 2011; De Clercq et al., 2008).

Most of the research, in Rwanda, was focused on the central NW trending “Tungsten Belt” extending from Nyakabingo to Bugarama via Gifurwe wolframite deposits (Günther and Pohl, 1991; Dewaele et al., 2010) and on the mines located in the western and central parts of the country. Only a few reports exist for the eastern part of Rwanda. The latter is known for its richness in cassiterite, wolframite and “coltan” and some of its mines are recorded among the oldest in the country, namely: Rwinkwavu, Musha-Ntungwa and Bugarura-Kuluti.

The aims of this study are mainly (disregarding the later orogenic and rifting events such as the Pan-African and the East-African Rift System which affected mechanically the study area):

1. To characterize the mineralogy and the geochemistry of the country rock for the Sn-, W- and Nb-/Ta- deposits of the study area;
2. To characterize the mineralogy, geochemistry and fluid properties of the hydrothermal Sn-W-Nb-/Ta- vein mineralization of the Rwinkwavu, Musha-Ntungwa and Bugarura-Kuluti deposits;
3. To investigate the mineral chemistry of ore minerals and argue the petrogenetic significance;
4. To identify a paragenetic scheme explaining the sequence of events, the fluid evolution and
5. To establish a metallogenetic model.

2. GEOLOGICAL SETTING

2.1 Stratigraphic units

The Rwanda Supergroup (also named Akanyaru Supergroup) is located in the Karagwe-Ankolean Mesoproterozoic Belt (KAB), part of the Central African Kibaran Belt (Tack et al., 2010).

The Geology of the country is dominated by Palaeo- and Mesoproterozoic rocks that were intruded by generations of granites which are reported in Tack et al. (2010) and Dewaele et al. (2010): G1-3 granites without Sn, W, Nb and Ta mineralization and G-4 granites associated with the previously mentioned mineralization.

The Palaeoproterozoic basement is recognized in south and south-west of Butare, Congo-Nile mountains range and south west of Ruhengeri (BRGM, 1987) where they comprise granitic – gneissic formations with quartzites forming N-S trending metamorphosed and faulted E-W mega-structures.

Radiometric age determinations applied to the samples of migmatites and gneisses from Butare region concluded that the oldest rocks are 2060 Ma old and therefore, associated to the paroxysm of the Ubendian metamorphism (Cahen et al., 1984).

Palaeoproterozoic outcrops are unknown in the east of Rwanda as is discussed in the present study. The stratigraphy of the latter consists of three principal lithological units: 1. Rare and sparsely distributed Mesoproterozoic magmatic complexes, 2. Mesoproterozoic sequences of meta-sediments deformed and folded during the Kibaran orogeny and 3. Quaternary thick alluviums present in valleys and terraces corresponding to a mixture of undifferentiated sediments of Holocene and Pleistocene ages (BRGM, 1987). These three units overlie directly the Precambrian rocks. A geological map of the study area is presented in Figure 2.1.

2.1.1 Mesoproterozoic magmatic complexes

The regional geology is dominated by two major parallel alignments of intrusive granites: Sake - Mugesera- Rwamagana-Rugarama-Nyagatare and Rusumo–Ihema granitic complexes (Figure 2.1). These granitic intrusions are complex and heterogeneous, syn- to post-Kibaran and comprise whitish granites, often pegmatitic and undifferentiated granites, granitoids and granites with two micas (BRGM, 1987).

Moreover, the study area exhibits, locally, sparse lenses of layered mafic to ultra-mafic sills and dykes composed of quartzite diorites, quartz and amphibole-rich diorites, amphibolites and gabbro-diorites (Dutu Stanchi et al., 1974; Uwizeye, 1987) out-cropping in the E of the Kibungo synclinerium neighbouring the lakes of Rwehikama and Nasho (S-E of Rwinkwavu anticline) where they consist of two elongated and parallel E-W trending units of mafic to ultra-mafic rocks separated by quartzitic layers.

Other intermediate to basic rocks occur further in the south and the south-east of the study area in Nyamiyaga and Musaza (Figure 2.1) as sill-shaped bodies hosted in the meta-sediments. The origin of these mafic to ultra-mafic suites is up to now unknown. Farther east of the study area, the Kabanga - Musongati greenstone belt (extended from Burundi in the S to Tanzania in the N) is the only regional structure which hosts mafic to ultra-mafic suites (Tack et al., 2010).

Economically exploitable Bushveld-type layered igneous complexes with anomalous contents of Ni-V-Ti-Fe-PGE-mineralization are reported in the Kabanga-Musongati greenstone belt, several kilometers far from the study area by Tack et al. (2010) and Mutima and Wei Li (2010).

2.1.2 Mesoproterozoic sequences of meta-sedimentary rocks

The sedimentary rocks have been affected by compressive and extensive events and thus, exposed to a regional metamorphism mostly of low grade (Fernandez and Theunissen, 1998) and in the sedimentary rocks of Rwanda supergroup, decreasing from the west to the east and from the granitic intrusions to other geologic formations (BRGM, 1987).

Based on Baudet et al. (1989) and Theunissen et al. (1991) three groups of geologic formations occur in the study area and are, from the most recent to the oldest (Figures 2.1 and 2.2):

- a) **Cyohoha group** comprising four formations which are from the recent to the oldest:
 1. **Birenga**: with clay-rich schists and alternation of schists and quartzites;
 2. **Kibungo**: the thickness of Kibungo formation is estimated to 100m. This geologic formation consists of medium to coarse grained sandstones or quartzites;

3. **Ndamira geologic formation:** Thick layers of laminated and zoned schists (1500m) and alternation of lenticular bodies of schists, isolated fine to coarse grained sandstones with local conglomerates;
 4. **Kibaya formation:** Its thickness is averaging 300m. It is formed by two types of rocks: quartzites or fine-grained sandstones in thin layers with very rare coarse-grained sandstones and black shales and alternation of lenticular layers of sandstones and schists.
- b) **Pindura group** represented by the **Bulimbi formation** (also called **Rukira** in the east) which is composed of metapelite-dominated schists with intercalation of thick layers of graphitic black shales and regular alternation of layers of sandstones and schists. The Bulimbi formation exhibits locally volcano-sedimentary rocks. The average thickness of this formation was estimated to be 1300m.
- c) **Gikoro group** comprising four lithologic units which are from the recent to the oldest:
1. **Gitwe formation:** It is 140m thick and represents the topmost geologic formation of this group, dominated by hard massive quartzites, sandstones and schists. This meta-sedimentary set is equivalent to Bwisige formation in the stratigraphic sequence of the central Rwanda (Baudet et al., 1989).
 2. **Musha formation:** A homogeneous series of schists locally intercalated with regular thick layers of fine-grained sandstones and schists. The fine-grained sandstones layers become rare on the top of the Musha formation.
 3. **Nyabugogo formation:** This constitutes the basic layer of the group and is composed of fine to coarse-grained quartzites, sandstones and schists.
 4. The Easternmost part area is dominated by the Rusumo geologic complex.

2.1.3 Quaternary laterites and alluviums

These comprise a 10m thick layer of undifferentiated eluviums and alluviums of holocene and pleistocene age as well as recent sediments located in the valleys and the terraces. Laterites are widespread with various thicknesses in the study area.

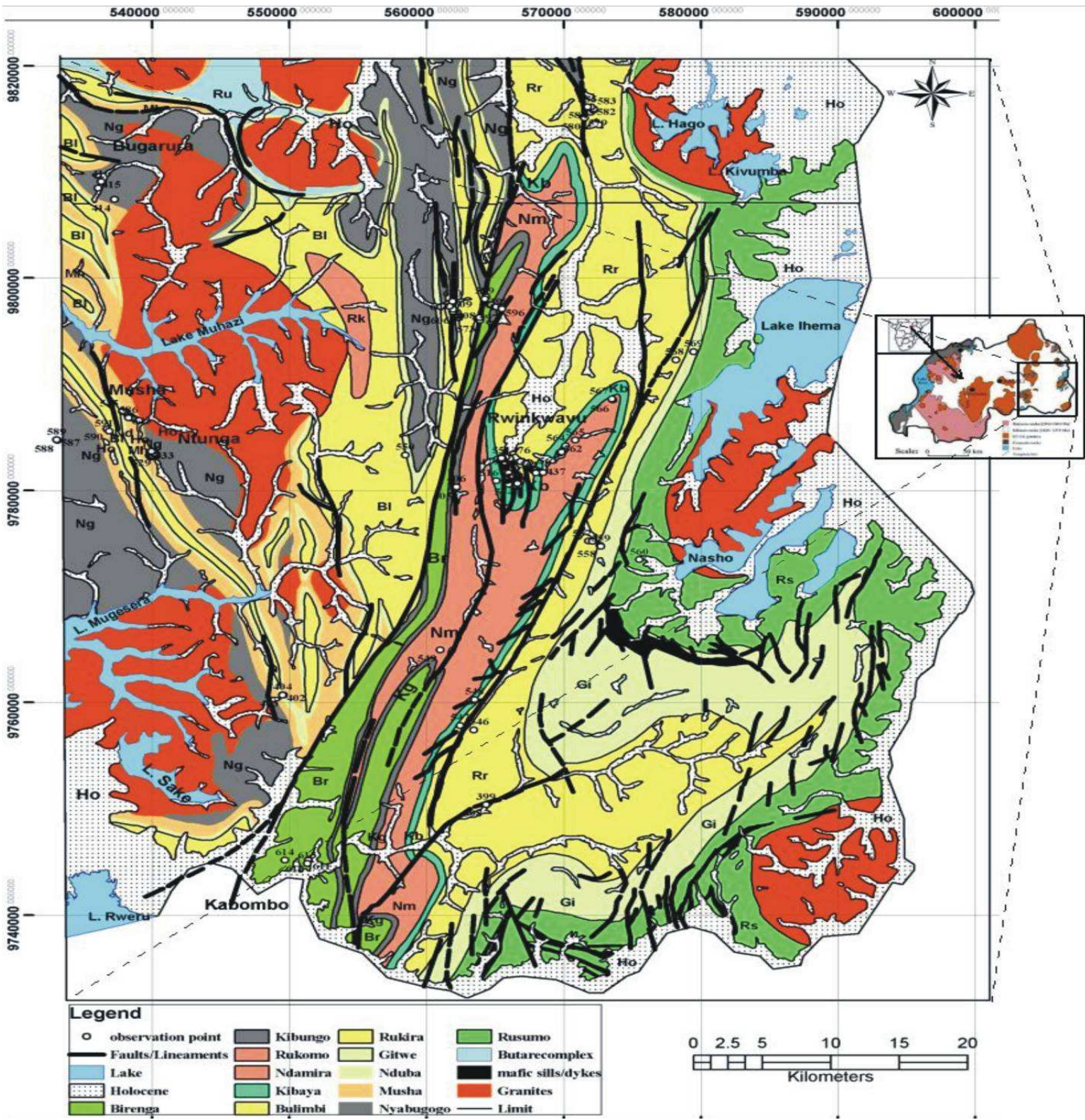


Figure 2.1: Geological map of south-eastern Rwanda (modified after Theunissen et al., 1991).

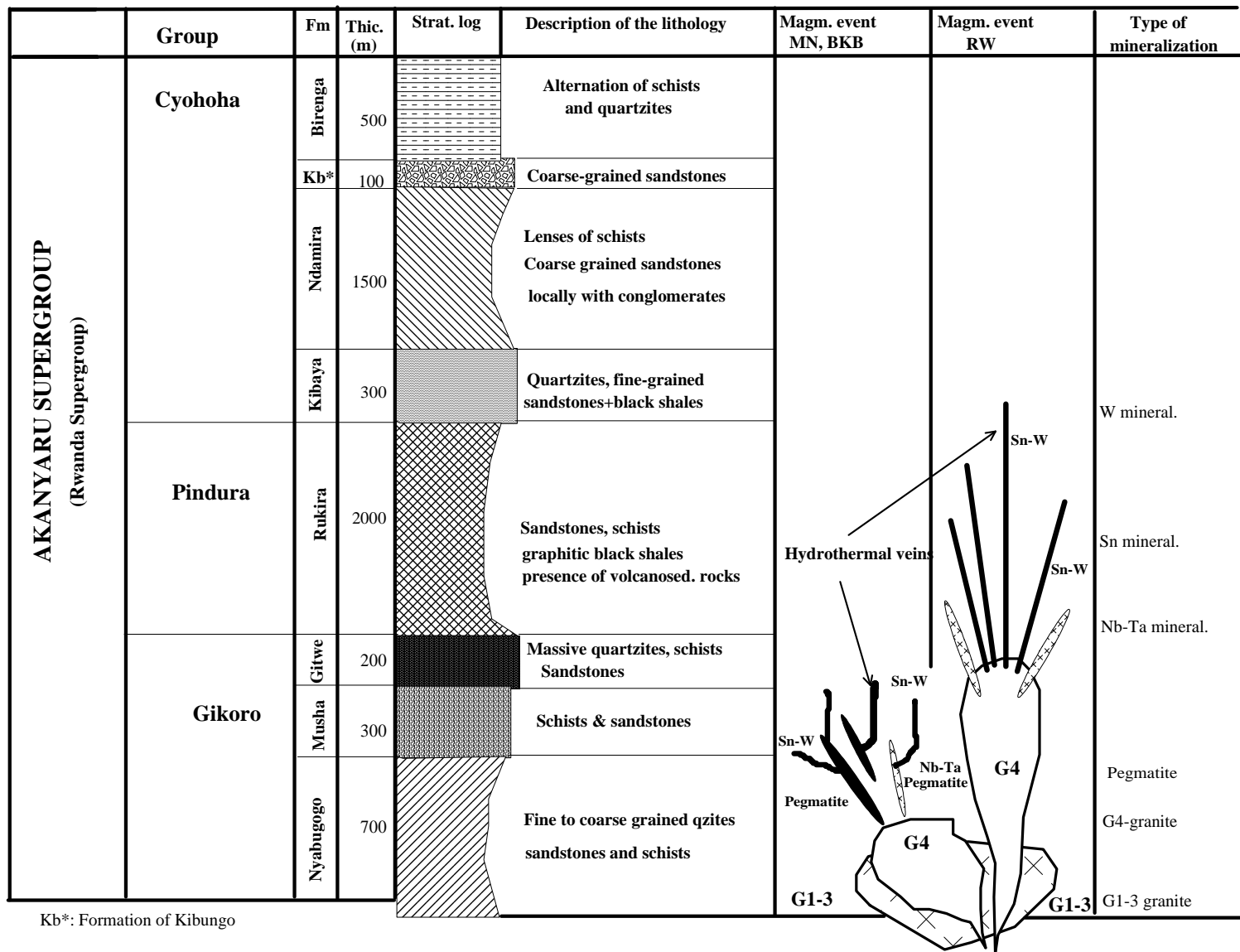


Figure 2.2: Simplified stratigraphic column combined with magmatic and metallogenic events in the study area adapted after Dewaele et al. (2011), Tack et al. (2010) and Baudet et al. (1989). MN-Musha-Ntunga; BKB-Bugarura-Kuluti-Bibare; Fm-formation; Bur.-Burundi; Gat.-Gatumba.

2.2 Structural Geology

Field observations and statistical analysis of field measurements (June-August 2010) were employed to understand the structural geology of the study area.

Stereograms and rose diagrams of the stratification planes (Figures 2.3, 2.4a and 2.4b) were prepared from field data (Table in Appendix 2) and plotted on the Schmidt net lower hemisphere projection.

Some models of structural evolution were proposed: Pohl (1988) and Pohl and Günther (1991) indicated that the geologic formations of the Rwanda Supergroup were deformed during the major folding phase of the Kibaran Orogeny at ca. 1200 Ma. This produced wide anticlinoria (as indicated in Figure 2.5). It also produced narrow synclinoria which were afterwards intruded by fertile granites. All of the aforementioned were later uplifted and eroded. The same authors confirmed that these events were followed by the initiation of intra-montane and foreland basins and the deformations were induced by regional shear zones and tensional tectonics.

The geology of eastern - Rwanda hosts similar fertile granites which probably generated the rare-metal related small bodies of felsic peraluminous pegmatites and their parent granites known in the literature as “G4” granites or “tin” granites of ca. 1,000 Ma.

The tectonic features of the study area are dominated by N-S, NE-SW and NW-SE faults and should be grouped into 3 principal shear zones. These are the arc-shaped Kibungo-Ntoma, the NE-SW Kibungo-Rusumo and the NW-SE South Byumba-Kibungo shear zones (Figure 2.6). The existence of these shear zones was confirmed by Paterson, Grant & Watson Ltd (2009) (Figure 2.6). The majority of the faults are normal but locally situated individual units of reverse and strike-slip faults were observed during the field investigations (Figure 2.7).

As shown in Figure 2.8 which is the structural map of the investigated area, major accidents are distributed in between two parallel N-S trending granites: Rusumo-Ihema in the east and Lake Sake-Nyagatare trend of granites in the west.

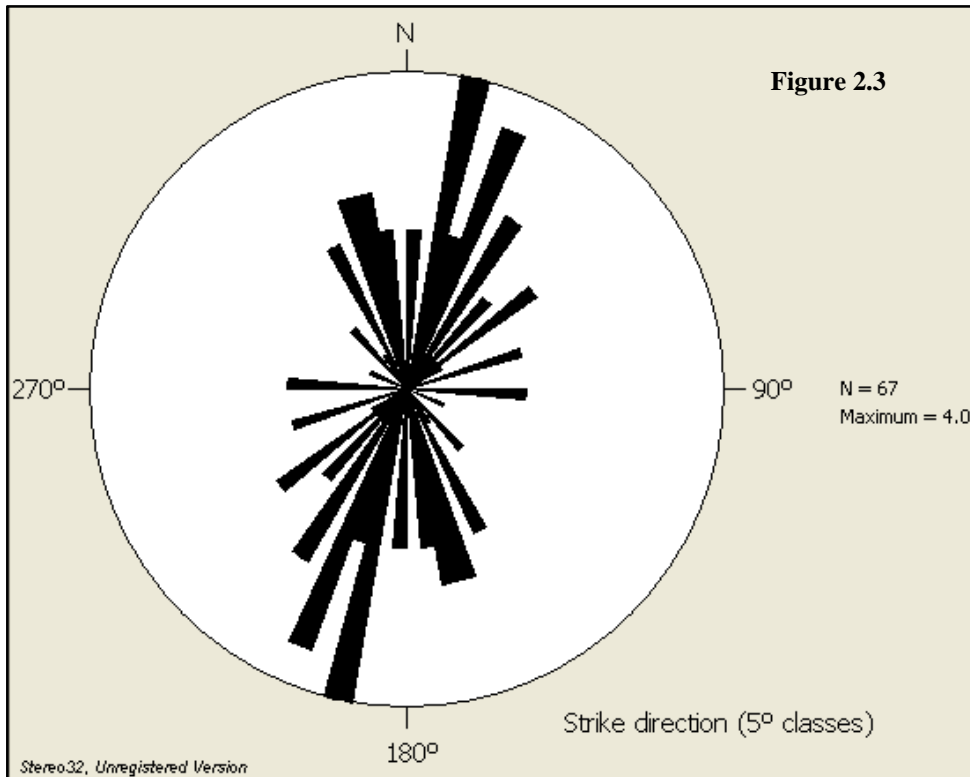


Figure 2.3

Rose diagram of the strike and dip direction of the bedding planes.

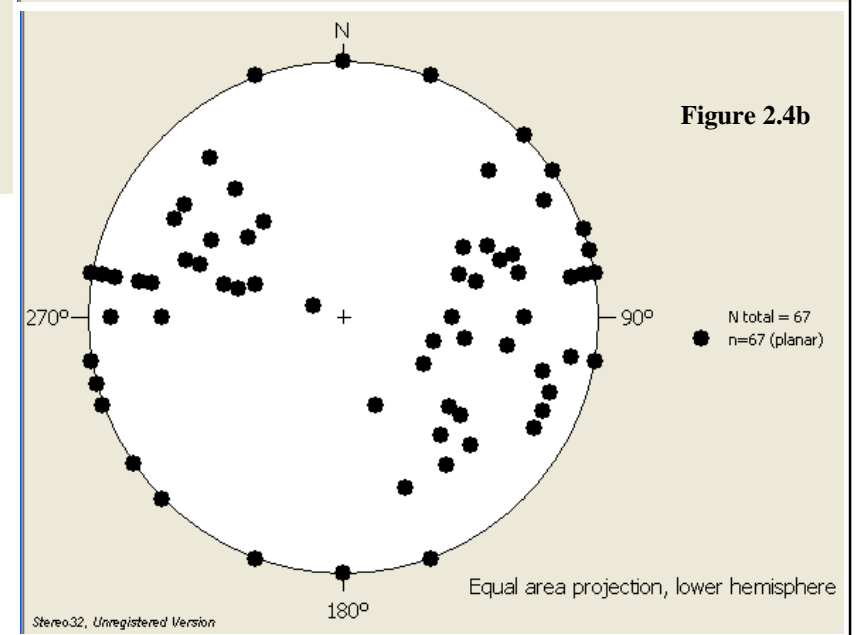
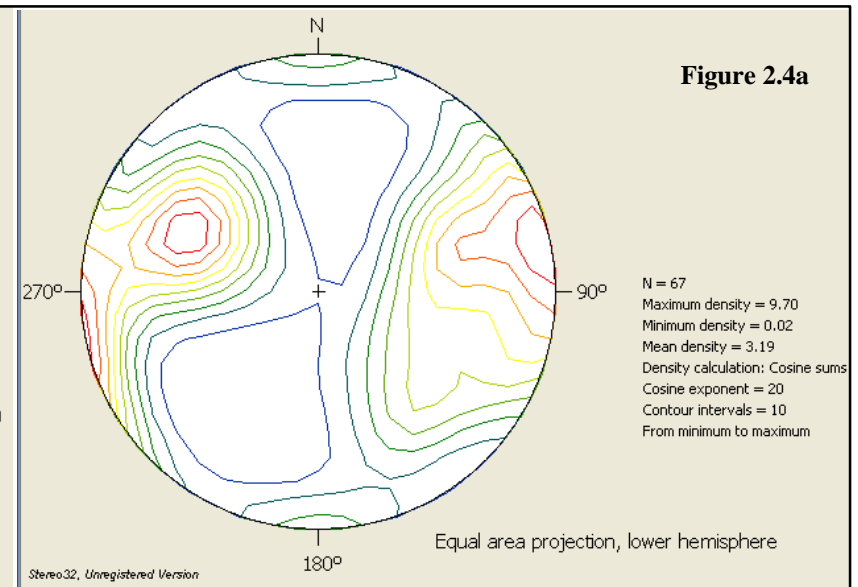
Figure 2.4a

Density equal area projection of strike and dip direction of the stratification planes in the study area.

Figure 2.4b

Equal area projection, lower hemisphere, strike and dip directions of the stratification planes in the study area.

(Field campaign, 2010)



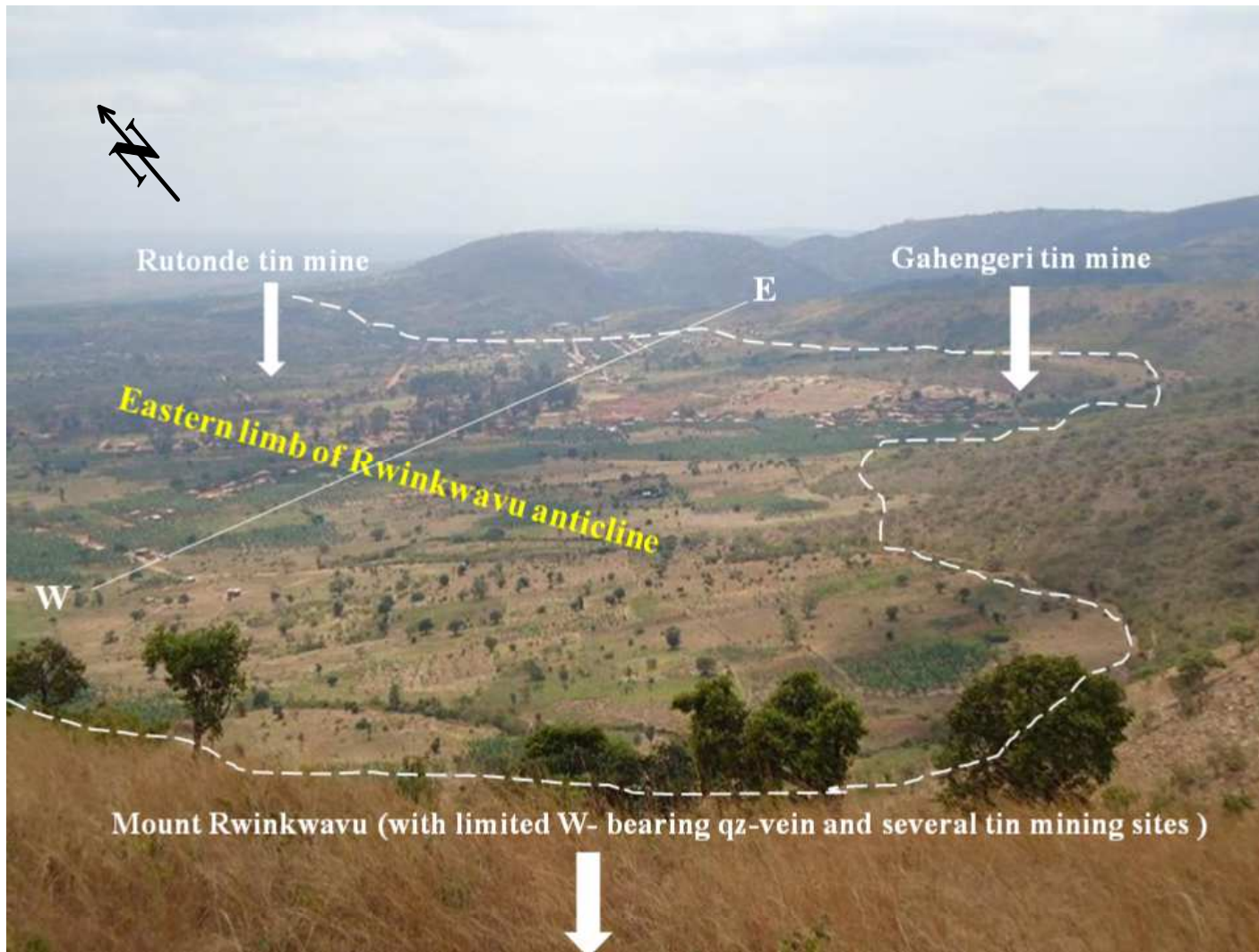


Figure 2.5: Photograph of Rwinkwavu anticline structure with some mining sites.

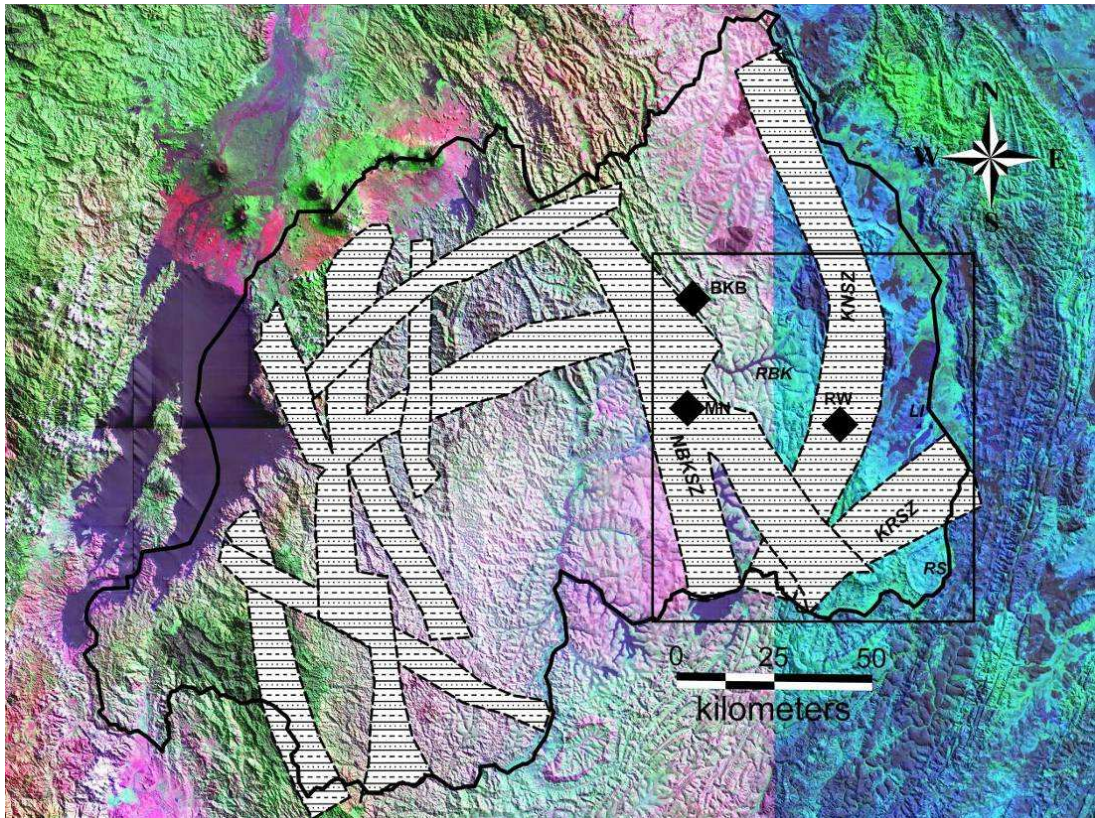


Figure 2.6: Interpreted shear zone map of Rwanda (Paterson, Grant & Watson Ltd, 2009) on a regional Landsat 3D-image (RTI, 2009). The square indicates the investigated area.

Abbreviations: KNSZ-Kibungo-Ntoma shear zone; NBKSZ-North Byumba-Kibungo shear zone; KRSZ-Kibungo/Rusumo shear zone; RBK- Rwamagana-Bugarura-Kuluti granite; RS- Rusumo granite; LI-Lake Ihema granite; RW-Rwinkwavu; MN-Musha-Ntunga; BKB-Bugarura-Kuluti-Bibare.

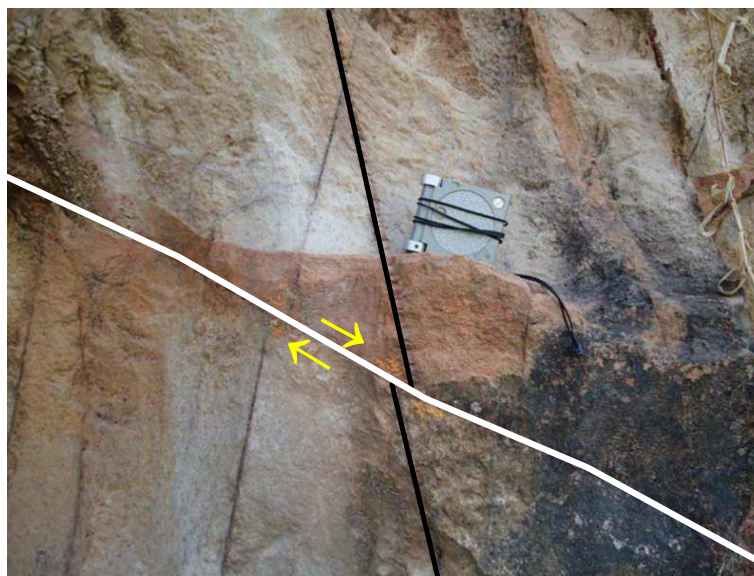


Figure 2.7: Right lateral strike-slip fault cross-cutting Kibaya sandstones.

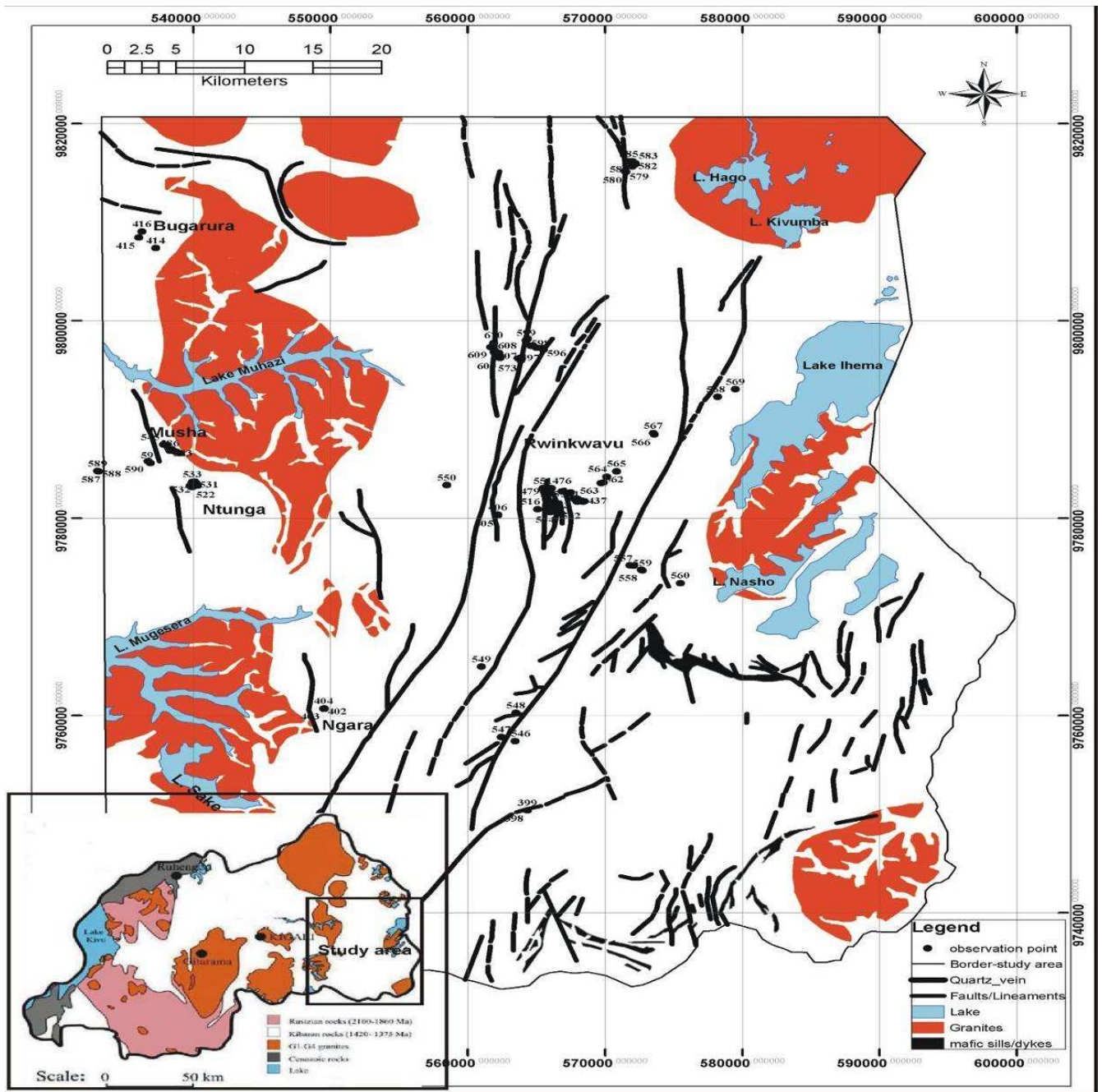


Figure 2.8: Structural map of the SE-Rwanda showing major faults and magmatic intrusions (modified after Theunissen et al., 1991).

3. COUNTRY-ROCK CHARACTERIZATION

A total of fifty four (54) samples representative of the country rock neighbouring the three investigated mining concessions were collected and analyzed using the light microscopy, SEM-EDX/WDX and XRF techniques (list of sampling sites in Appendix 3).

They include seventeen igneous rock samples, fourteen samples hand-picked from highly brecciated structures filled by hydrothermal muscovite, tourmaline, fragments of the host rock and quartz veins and seventeen meta-sedimentary rock samples. Table 3.1 shows the sample names, the locality names, their geographic coordinates, the type of rock samples and the principal forming minerals from the microscopic investigations.

Table 3.1: Overview list of country rock samples and gangue minerals of veins

Ref.	Sample	Locality	Easting	Northing	Rock-type	minerals (microscopy)
1	JC-1	Gashenyi	577498	9740345	BAS	Amp-plag-musc-qz-serp
2	JC-2	Musaza	572560	9736590	BAS	Amp-chl-tit. Magn.
3	JC-3	Kagera	567880	9739530	BAS	Amp-plag-fds
4	JC-10	Kibungo	557020	9767880	BAS	Plag-amp-biot
5	JC-13	East			BAS	Amp-qz-tit. Magn-chl
6	JC-14	East			BAS	Amp-epidotized micas
7	JC-4	Nkuri	446800	9825040	GN	Micr-biot-qz-plag-zir.
8	JC-5	Nyagatare	527400	9828000	GN	Plag-micr-biot-op. Min
9	JC-6	Mugonero	410875	9754757	GN	Plag-micr-biot-fds
10	JC-8	Kigoma			GN	
11	JC-11	Rusumo	584380	9746566	GN	Fds-qz-musc-biot-zir
12	JC-GRAN1	Nyagatare	537642	9849022	GN	micr.-biot.-epdt-qz-minor plag and op. min.
13	JC-GRAN2	Ngarama	526823	9830501	GN	microc.-qz-plag.-minor amount of biot.
14	JC-GRAN3	Nkuri	446800	9825040	GN	microc.-qz-musc.-biot.-blue colours (alteration?)
15	JC-6-1	Ntungwa	536911	9785351	MSD	qz-op. min.
16	JC-6-3	Ntungwa	537309	9784870	MSD	
17	JC-6-6	Ntungwa	539973	9783220	MSD	
18	JC-12	Kibungo			MSD	
19	JC-16	Ntungwa	536700	9785900	MSD	
20	JC-23*	Musha-Ntungwa	538350	9787020	MSD	
21	JC-26*	Musha-Ntungwa	537780	9788030	MSD	
22	JC-30*	Musha-Ntungwa	538170	9787160	MSD	
23	JC-31*	Kibungo	561260	9767440	MSD	op. min-qz
24	JC-37*	Nyarunazi	565700	9785200	MSD	musc.-tourm.-qz
25	JC-423	Rwinkwavu	567848	9781947	MSD	
26	JC-453	Rwinkwavu	566007	9780903	MSD	
27	JC-515	Rwinkwavu	566159	9781360	MSD	qz-tourm.-op. min
28	JC-520A	Ntungwa	539904	9783157	MSD	musc.-gart-qz-chl.
29	JC-521	Ntungwa	539897	9783166	MSD	Qz-op. min.
30	JC-25-6-4	Ntungwa	540266	9783325	MSD	
31	JC-26-6-1	Bugarama	473444	9847562	MSD	qz-micas-op. min

Abbreviations: V-hydrothermal veins; GN-granite; MSD-meta-sedimentary rocks; Dol-dolomite; PG-pegmatite; BAS- basic to intermediate igneous rocks, qz-quartz, tourm.-tourmaline, biot.-biotite, op. Min.-opaque minerals, musc-muscovite, andal-andalusite, micr.-microcline. (*) - Sample from the RMCA collection.

Table 3.1 (Continued).

Ref.	Sample	Locality	Easting	Northing	Rock-type	minerals (microscopy)
32	JC-HFLS	Gatore	564353	9750367	MSD	andal-garnet-op. min.
33	JC-6-7	Ntungwa	539969	9783228	PG	
34	JC-19	Cyubi (Muhanga)			PG	Qz-plag?
35	JC-24-6 LEP	Ngara	549567	9760661	PG	Short and platy sheets of micas
36	JC-24*	Musha-Ntungwa	540100	9782000	V	
37	JC-28*	Musha-Ntungwa	538950	9786380	V	qz-tourm.-op. min
38	JC-29*	Musha-Ntungwa	539890	9783340	V	qz-tourm.-op. min
39	JC-33*	Bujumu	545000	9813500	V	cass.-qz
40	JC-35*	Rwankuba	537100	9798400	V	mica-qz
41	JC-39*	Kizanye	566700	9783300	V	musc.-qz
42	JC-40*	Rwinkwavu	561800	9780400	V	musc.-qz
43	JC-392	Rwinkwavu	566250	9780950	V	tourm.-qz-op. min.
44	JC-435	Rwinkwavu	568373	9781691	V	pure qz
45	JC-457	Rwinkwavu	565894	9780928	MSD	tourm.-qz-op. min
46	JC-25-6-3	Ntungwa	540216	9783323	V	fractured and brecciated qz presenting resorbed rims
47	JC-26-6	Bugarama	473444	9847562	V	
48	JC-26-6-3	Bugarama	473651	9847561	V	Musc.-qz
49	JC-26-6-4	Bugarama	473651	9847561	V	qz tourm.
50	JC-23-6-4	Rwinkwavu	567380	9779860		
51	JC-24-6-2	Rwinkwavu	565532	9782943		
52	JC-24-6-3	Rwinkwavu	566427	9780708		Minor amount of tourm. hosted in qz matrix
53	JC-25-6-5	Ntungwa	540304	9783272		qz-altered micas-op. min.
54	JC-28-6-2	Bugarura	537734	9807824		

Abbreviations: V-hydrothermal vein; GN-granite; MSD-meta-sedimentary rock; Dol-dolomite; PG-pegmatite; BAS- basic to intermediate igneous rocks, qz-quartz, tourm.-tourmaline, biot.-biotite, op. min.-opaque minerals, musc-muscovite, andal-andalusite, micr.-microcline. (*)-Sample from the RMCA collection.

The meta-sedimentary rocks and the hydrothermal veins for each investigated mining concession will be described in chapter four and the present chapter is limited to the petrographic description of the igneous rocks originating from the melts which are the possible sources of the mineralizing fluids. In addition, the whole rock geochemistries of both igneous and meta-sedimentary rocks as well as the mineral chemistry of tourmaline in tourmalinite are discussed in this chapter.

3.1 Petrography and whole rock geochemistry of igneous rocks

3.1.1 Petrography

The macroscopic observations allowed us to distinguish a group of light coloured rocks which are the granites or granitic gneisses and the dark coloured rocks corresponding to the basic to intermediate rocks. The microscopic investigations show that the

investigated granites are composed of microcline, quartz, muscovite, plagioclases and a minor amount of biotite. Some of them show large crystals of plagioclase phenocrysts which are also identifiable by the naked eye (Figure 3.1).



Figure 3.1: Photograph of the coarse-grained granite of Ngarama area (2010 field work).

The primary minerals identified in the intermediate to basic rocks consist of amphiboles (hornblende), plagioclases, quartz and sometimes muscovite. The secondary minerals are chlorite, biotite and pale blue serpentines and in addition, opaque minerals occur as accessory minerals in several thin sections.

3.1.2 Whole rock geochemistry of igneous rocks

The whole rock geochemistry of thirteen igneous rock samples from south-eastern Rwanda has been investigated and compared to the major and trace element analyses of “tin”-granite from Les Chatelliers in the French Variscan Belt (Raimbault et al., 1995).

The samples were crushed, powdered and pressed to form pellets for trace element analysis. Fusion discs were prepared for major element analysis. The facilities of the laboratory of the Geology Department at the University of the Free State were used for conducting the analyses. The concentrations of 10 major elements and 30 trace elements were performed using XRF techniques. The resultant concentrations are presented in Appendix 6 and in Table 3.2.

Sample	JC-19*	JC-24-6-LEP	JC-6-7	JC-GRAN3*	JC-GRAN2	JC-GRAN1	JC-11	JC-6*	JC-5	JC-4*	JC-14	JC-13	JC-10	JC-3	JC-2	JC-1
Pros. Rock type	CY	NG	MN	NK	NGM	NT	RU	MU	NT	NK	East	East	KB	KG	MS	GS
	PEG	PEG	PEG	GRAN	GRAN	GRAN	GRAN	GRAN	GRAN	GRAN	BAS	BAS	BAS	BAS	BAS	BAS
P ₂ O ₅	0.16	0.02	0.02	0.22	0.22	0.01	0.13	0.11	0.10	0.15	0.06	0.19	0.13	0.12	0.16	0.06
SiO ₂	66.91	47.62	62.34	71.89	74.82	73.53	68.51	71.64	70.90	74.01	52.79	53.44	47.80	53.49	57.02	53.19
TiO ₂	0.00	0.05	0.00	0.26	0.48	0.14	0.38	0.31	0.21	0.12	0.57	1.90	1.23	0.98	2.28	0.80
Al ₂ O ₃	17.64	38.80	35.18	14.98	11.62	13.21	14.42	13.56	14.06	14.15	17.02	13.12	18.23	14.54	13.59	14.09
Fe ₂ O ₃	0.48	0.54	0.24	2.23	4.31	1.72	3.09	2.35	2.28	1.33	9.07	16.63	10.38	11.96	13.99	10.98
MnO	0.01	0.08	0.02	0.02	0.05	0.02	0.05	0.04	0.04	0.02	0.14	0.27	0.17	0.19	0.17	0.17
MgO	0.07	0.09	0.08	0.86	0.48	0.09	1.36	0.75	0.87	0.54	8.43	4.24	5.15	6.28	3.56	7.13
CaO	0.15	0.00	0.04	0.83	2.02	0.76	2.40	1.52	1.61	0.71	10.41	8.09	12.29	9.84	6.11	11.21
Na ₂ O	2.53	0.29	0.00	2.32	1.80	1.58	2.53	2.87	2.77	3.40	1.06	1.35	1.91	1.51	2.01	1.19
K ₂ O	11.36	10.57	0.93	5.37	3.77	7.94	4.18	4.94	5.62	4.95	0.58	0.36	0.32	0.12	0.20	0.75
LOI	1.8	2.8	1.1	1.11	0.41	0.22	0.8	0.44	0.42	0.68	0.3	0.1	0.8	1.6	1.16	2.21
A/CNK	1.24	3.57	34.74				1.25	1.25	1.21	1.45	0.76	0.73	0.68	0.68	0.94	0.58
Total	101.1	100.9	100	100.39	99.68	99.26	98	98	98.21	99.01	100.8	100.25	98.50	100.6	99.9	101.3
Sc	1	2	0	2	2	9	2	1	1	2	2	3	2	2	9	2
V	3	3	0	7	9	1	29	16	11	1	205	631	230	312	422	338
Cr	3	3	4	5	8	6	31	12	12	9	326	16	60	88	58	190
Ni	13	13	8	2	5	3	8	6	3	3	30	47	52	19	10	17
Cu	2	50	10	1	4	1	3	3	4	2	38	15	117	12	4	49
Zn	7	257	19	36	65	32	35	15	11	25	53	135	68	113	112	73
Ga	21	180	72	28	19	24	22	21	19	38	15	16	15	16	18	15
Ge	1	7	10	1	0	0	0	0	0	1	0	0	0	0	0	0
As	3	3	3	3	4	0	3	3	3	3	3	15	3	0	0	6
Se	0	0	0				0	0	0	0	0	0	0	0	0	0
Br	4	2	2	1	1	1	4	4	3	3	2	3	4	4	4	6

Table 3.2: Geochemical composition of the igneous rocks from various localities of the study area obtained using XRF techniques. **Abbreviations:** 1.localities: CY-Cyubi; NG-Ngara; MN-Musha-Ntungu; RU-Rusumo; MU-Mugonero; NT-Nyagatare; NK-Nkuri; KB-Kibungo; KG-Kagera; MS-Musaza; GS-Gashenyi, NGM-Ngarama. 2. Rock types: PEG-pegmatites; GRAN-granites; BAS-basic to intermediate igneous rocks. Samples with * are from other places and those without a star are from the study area.

Sample	JC-19*	JC-24-6-LEP	JC-6-7	JC-GRAN3*	JC-GRAN2	JC-GRAN1	JC-11	JC-6*	JC-5	JC-4*	JC-14	JC-13	JC-10	JC-3	JC-2	JC-1
Pros. Rock type	CY PEG	NG PEG	MN PEG	NK GRAN	NGM GRAN	NT GRAN	RU GRAN	MU GRAN	NT GRAN	NK GRAN	East BAS	East BAS	KB BAS	KG BAS	MS BAS	GS BAS
Rb	336	4500	404	373	153	328	197	190	217	361	30	8	16	4	4	41
Sr	74	14	9	156	101	80	196	123	154	166	87	96	201	114	133	70
Y	1	6	2	10	65	47	27	18	20	5	16	35	22	24	39	27
Zr	2	0	57	134	302	38	136	133	150	64	54	157	73	95	184	86
Nb	0	46	46	18	22	17	11	9	9	12	2	6	10	6	8	5
Mo	0	0	0	0	1	3	1	1	2	0	1	1	1	1	1	2
Cd	0	3	3	1	3	3	3	3	3	3	3	3	3	1	3	3
Sn	3	432	601	4	1	2	2	2	1	4	2	2	2	2	2	2
Sb	3	3	1	0	3	3	0	2	1	1	3	3	3	3	5	5
Ba	413	29	20	642	531	518	604	434	981	530	214	56	77	73	62	322
Hf	6	4	28	2	2	2	7	5	5	9	2	5	3	3	4	1
Ta	1	147	234	2	2	2	2	1	3	3	1	1	1	1	5	1
W	6	8	6	6	9	8	15	14	17	16	6	4	8	5	11	7
Tl	0	37	5	4	3	5	2	2	1	3	1	3	2	2	5	6
Pb	76	24	26	32	28	52	21	30	32	34	3	2	3	13	20	9
Bi	3	1	3	3	1	3	1	1	1	1	0	1	1	1	0	1
Yb	1	1	1	1	3	2	1	1	1	1	0	2	2	0	1	1
Th	0	1	2	28	20	30	14	26	35	10	1	6	1	5	7	4
U	1	1	2	8	6	13	5	13	9	5	1	2	2	1	4	2

Table 3.2 (Continued).

Abbreviations: 1.localities: CY-Cyubi; NG-Ngara; MN-Musha-Ntungwa; RU-Rusumo; MU-Mugonero; NT-Nyagatare; NK-Nkuri; KB-Kibungo; KG-Kagera; MS-Musaza; GS-Gashenyi, NGM-Ngarama. 2. Rock types: PEG-pegmatites; GRAN-granites; BAS-basic to intermediate igneous rocks. Samples with * are from other places and those without a star are from the study area.

According to Table 3.2, the rocks analyzed in this study show a wide range of chemical types from basic, intermediate to acidic compositions. The granites host between 68.51 and 74.82 wt. % SiO_2 . The intermediate to basic rocks have 47.80 to 53.49 wt. % SiO_2 . The latter show enrichment trends in the total Fe_2O_3 (9-16.63 wt. %), CaO (6-12.29 wt. %), TiO_2 (1-2.28 wt. %) and MgO (3.56-8.13 wt. %).

The light coloured rocks are depleted in the previously mentioned oxides and present low P_2O_5 but are enriched in K_2O with concentrations ranging from 4 to 5 wt. % for the eastern granites (Rusumo and Nyagatare) and maximum values of 10 to 11 wt. % for the fresh JC-19 pegmatite sample from Cyubi coltan mine (Muhanga district, Southern Province).

A chemical classification of the igneous rock samples has been done using the total alkalis versus silica discrimination diagram (TAS) (Le Maitre et al., 1989). The results are plotted in Figure 3.2. The results of the chemical composition and the TAS-discrimination diagram support the macroscopic observations in identifying two types of igneous rocks: acidic rocks (dacite and rhyolite) and intermediate to basic rocks (basalt and basaltic andesite classes).

The Al_2O_3 content of the analyzed samples is generally high ranging from 13 (JC-13) to 38.80 wt. % emphasizing the highly weathered nature of the regolith and therefore enrichment in clay minerals expressed in terms of Al_2O_3 contents in JC-24-6LEP (38.8 wt. %) and JC-6-7 (35.18 wt. %). The pegmatite sample JC-19 from Cyubi in Muhanga District is still fresh compared to the representative samples from east or from other parts of the country and this is shown by the high content in total alkalis [14 wt. % of ($\text{K}_2\text{O}+\text{Na}_2\text{O}$)]. This should indicate the presence of a high content of K-feldspars and muscovite in the pegmatite-forming minerals.

The intermediate to basic rocks are mostly confined to the easternmost zone of the study area which is the eastern limit of the western internal domain (WID) of the Kibara orogeny (Tack et al. 1994). This is in the vicinity of the transitional zone dominated by the Kabanga-Musongati greenstone belt which is located relatively far from the 3 investigated mining concessions and hence, has little or no direct implication in the Sn-W-Nb/Ta mineralizing processes.

The field work has shown that the mineralization occurs either within the granitic cupolas, in the direct environment of the granites or is hosted in hydrothermal veins cross-cutting the meta-sedimentary rocks. Henceforward the discussion will be limited to this latter group of country rock. In addition, the $\text{Al}_2\text{O}_3/(\text{Na}_2\text{O}+\text{K}_2\text{O}+2\text{CaO})$ ratios for all the felsic igneous rocks are above 1, ranging from 1.21 to 34.74 and thus, supporting the high peraluminous character of those granites (Fernandez-Alonso and Theunissen, 1998; Cerny et al., 2005).

Table 3.3: Sample/clarke values of selected trace-elements (ppm) of investigated felsite samples

Seq.	Sample	Prospect	Rock type	V	Cr	Ni	Cu	Zn	As	Rb	Sr	Y	Zr	Nb	Mo	Cd	Sn	Sb	Ba	Pb	Th	U
1	JC-19	CY	PEG	3	3	13	2	7	3	336	74	1	2	0	0	0	3	3	413	76	0	1
2	JC-24-6-LEP	NG	PEG	3	3	13	50	257	3	4500	14	6	0	46	0	3	432	3	29	24	1	1
3	JC-6-7	MN	PEG	0	4	8	10	19	3	404	9	2	57	46	0	3	601	1	20	26	2	2
4	JC-11	RU	GRAN	29	31	8	3	35	3	197	196	27	136	11	1	3	2	0	604	21	14	5
5	JC-6	MU	GRAN	16	12	6	3	15	3	190	123	18	133	9	1	3	2	2	434	30	26	13
6	JC-5	NT	GRAN	11	12	3	4	11	3	217	154	20	150	9	2	3	1	1	981	32	35	9
7	JC-4	NK	GRAN	1	9	3	2	25	3	361	166	5	64	12	0	3	4	1	530	34	10	5
8	JC-GRAN3	NK	GRAN	7	5	2	1	36	3	373	156	10	134	18	0	1	4	0	642	32	28	8
9	JC-GRAN2	NGM	GRAN	9	8	5	4	65	4	153	101	65	302	22	1	3	1	3	531	28	20	6
10	JC-GRAN1	NT	GRAN	1	6	3	1	32	0	328	80	47	38	17	3	3	2	3	518	52	30	13
11	GRAN26	CH	GRAN				9	44	12.5	1104	19	6	30	88	1		48	3	30	29	5	3
Clarke (*)				135	10	75	55	70	1.8	61	503	14	165	20	1.5	0.2	2	0.2	707	13	7.2	2.7
1	JC-19/ (*)	CY	PEG	0.0	0.3	0.2	0.0	0.1	1.9	5.5	0.1	0.0	0.0	0.0	0.0	0.1	1.4	14.0	0.6	5.8	0.0	0.4
2	JC-24-6-LEP/ (*)	NG	PEG	0.0	0.3	0.2	0.9	3.7	1.9	73.8	0.0	0.4	0.0	2.3	0.3	12.7	215.8	14.0	0.0	1.9	0.1	0.3
3	JC-6-7/ (*)	MN	PEG	0.0	0.4	0.1	0.2	0.3	1.9	6.6	0.0	0.1	0.3	2.3	0.2	16.4	300.4	5.3	0.0	2.0	0.3	0.6
4	JC-11/ (*)	RU	GRAN	0.2	3.1	0.1	0.1	0.5	1.9	3.2	0.4	1.9	0.8	0.5	0.6	15.5	1.0	1.3	0.9	1.6	2.0	1.8
5	JC-6/ (*)	MU	GRAN	0.1	1.2	0.1	0.1	0.2	1.9	3.1	0.2	1.3	0.8	0.5	0.4	15.5	1.0	10.3	0.6	2.3	3.6	4.9
6	JC-5/ (*)	NT	GRAN	0.1	1.2	0.0	0.1	0.2	1.9	3.6	0.3	1.5	0.9	0.5	1.3	15.5	0.3	4.0	1.4	2.5	4.9	3.4
7	JC-4/ (*)	NK	GRAN	0.0	0.9	0.0	0.0	0.4	1.9	5.9	0.3	0.4	0.4	0.6	0.2	15.5	1.9	5.7	0.7	2.6	1.4	1.7
8	JC-GRAN3/ (*)	NK	GRAN	0.1	0.5	0.0	0.0	0.5	1.9	6.1	0.3	0.7	0.8	0.9	0.2	5.7	2.1	0.9	0.9	2.5	3.9	2.9
9	JC-GRAN2/ (*)	NGM	GRAN	0.1	0.8	0.1	0.1	0.9	2.3	2.5	0.2	4.6	1.8	1.1	0.6	15.0	0.5	13.5	0.8	2.1	2.7	2.3
10	JC-GRAN1/ (*)	NT	GRAN	0.0	0.6	0.0	0.0	0.5	0.1	5.4	0.2	3.4	0.2	0.8	1.9	15.0	1.2	13.5	0.7	4.0	4.1	4.7
11	GRAN26/ (*)	CH	GRAN	0.0	0.0	0.0	0.2	0.6	6.9	18.1	0.0	0.4	0.2	4.4	0.3	0.0	24.0	16.0	0.0	2.2	0.8	1.0

(*) Clarke (Taylor, 1964; Wedepohl, 1969; Krauskopf and Bird, 1995), CH-Les Chatelliers rare element-bearing phosphorous poor granite, Vendée, France (Raimbault et al. 1995, Cerny et al. 2005). **Abbreviations:** 1.localities: CY-Cyubi; NG-Ngara; MN-Musha-Ntungwa; RU-Rusumo; MU-Mugonero; NT-Nyagatare; NK-Nkuri; NGM-Ngarama; CH-Les Chatelliers. 2. Rock types: PEG-pegmatites, GRAN-granites.

The enrichment in the same trace elements is noted for the pegmatite type samples which display high anomalous concentrations in Sn [215 and 300 times more than the Clarke (Taylor, 1964; Wedepohl, 1969; Krauskopf and Bird, 1995)]. The general trend for other granites from the study area shows enrichment in As, Rb, Y, Cd, Sb, Pb, Th and U, but are depleted in V, Ni, Cu, Zn, Sr, Ba, Zr, Nb, Mo and Sn. The same enrichment-depletion is distinguishable in JC-4 and GRAN3 from the Nkuri granite (Nyabihu District, Western Province) which are exceptionally enriched in Sn and in JC-6 from Mugonero (Karongi District, Western Province).

In addition, the enrichment-depletion diagram (Figure 3.3) plotted for selected trace elements and normalized to the French Variscan tin granite for the more or less fresh granites from the study area indicates that all those granites are enriched in Sc, Sr, Y, Zr, Mo, Ba, Hf, Pb, Th and U but depleted in Rb, Nb, Sn and Ta. Compared to the French Variscan granite, the south-eastern Rwandan granites showed a slight enrichment in W.

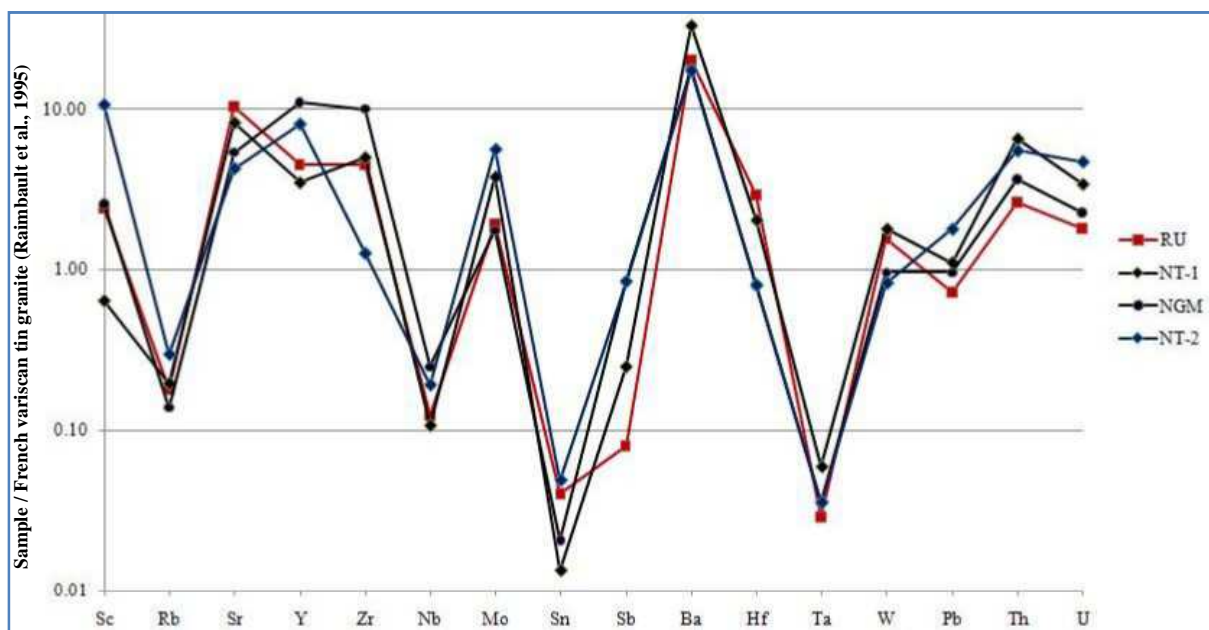


Figure 3.3: Selected trace elements for 4 granites from E-Rwanda normalized to the phosphorous poor “tin-granite” GRAN26 from Les Chateliers-French Variscan (Raimbault et al. 1995 in Cerny et al. 2005). **Abbreviations:** RU-Rusumo; NT-Nyagatare; NGM-Ngarama.

3.2 Chemical characterization of the meta-sedimentary rocks

A total of thirteen samples representative of the host rock for cassiterite and wolframite mineralization were collected from Rwinkwavu, Musha-Ntunga and Bugarura-Kuluti zones.

They consist of quartzite-sandstones and schist-dominated meta-sedimentary rocks. The concentrations of 10 major oxides and 30 trace elements were determined by XRF and the resultant concentrations are presented in Table 3.4.

Table 3.4: Chemical composition of meta-sedimentary rock samples from the study area.

Sample	JC-457	JC-521	JC-520A	JC-25-6-4	JC-30	JC-16	JC-6-1	JC-24-6-2	JC-515	JC-453	JC-423	JC-31	JC-HFLS	LLD
Locality	RW	MN	MN	MN	MN	MN	MN	RW	RW	RW	RW	RW	GAT	
P ₂ O ₅	0.07	0.04	0.01	0.16	0.02	0.06	0.08	0.08	0.02	0.03	0.02	0.37	0.04	17
SiO ₂	51.45	89.52	87.68	82.70	79.92	72.30	65.55	48.65	82.45	36.08	82.36	60.41	60.98	56
TiO ₂	0.51	0.36	0.37	0.53	0.69	1.36	1.00	0.95	0.57	2.26	0.56	1.06	1.22	57
Al ₂ O ₃	18.89	5.40	7.52	8.23	11.87	23.78	19.98	17.74	11.10	29.67	11.58	22.34	20.14	64
Fe ₂ O ₃	22.40	3.83	1.69	7.03	3.27	1.21	5.74	28.00	2.67	20.62	3.27	14.11	13.14	13
MnO	0.07	0.02	0.07	0.02	0.02	0.01	0.04	0.02	0.01	0.05	0.01	0.01	0.07	22
MgO	1.68	0.15	0.40	0.29	0.44	0.13	0.23	0.17	0.53	2.27	0.19	0.18	1.32	59
CaO	0.13	0.01	0.02	0.01	0.04	0.03	0.02	0.01	0.04	0.19	0.04	0.16	0.14	19
Na ₂ O	0.53	0.00	0.00	0.04	0.19	0.00	0.32	0.28	0.06	0.78	0.00	0.00	0.65	15
K ₂ O	0.01	0.25	1.88	1.69	2.47	0.01	4.21	2.59	2.49	0.08	0.00	0.04	2.08	15
LOI	1.98	1.24	1.65	0.43	2.38	1.21	3.5	2.48	1.32	3.15	3.57	1.72	1.60	
CIA	0.97	0.95	0.80	0.83	0.82	1.00	0.81	0.86	0.81	0.97	1.00	0.99	0.87	
Total	98.52	100.8	101	101	101	100.1	100.7	100.9	101	98.5	101	100.4	101	
Sc	34	6	1	10	7	8	17	60	7	51	8	32	43	3.9
V	337	19	16	59	49	55	95	452	37	553	43	192	256	4.4
Cr	239	19	18	55	45	79	78	336	30	899	40	309	229	2.7
Cu	19	9	1	22	11	7	5	34	5	29	24	22	16	1.2
Zn	102	6	45	14	23	5	38	22	32	88	19	19	25	0.9
Cd	3	3	3	3	3	3	3	1	3	5	3	3	38	6
Sn	12	13	96	128	26	6	4	2	93	21	7	2	81	3
Mo	50	0	0	1	0	2	0	2	0	5	0	9	18	0.5
Ni	7	4	7	5	6	7	13	17	4	20	7	49	1	1.2
As	893	16	3	173	184	3	11	762	72	1114	126	6	6	6.7
Br	1	0	0	1	2	3	2	2	0	0	3	5	0	1
Rb	2	23	1314	131	98	1	193	94	313	9	0	1	128	0.7
Sr	70	3	8	15	17	21	37	36	35	131	7	20	31	0.4
Y	11	13	0	18	17	9	17	22	10	89	7	60	25	0.9
Zr	33	304	256	287	227	317	219	160	320	294	636	154	169	0.7
Nb	2	6	12	18	15	18	19	8	8	12	7	8	10	0.7
Sb	2	3	3	3	3	1	3	3	1	4	2	3	0	5.7
Ba	33	66	155	500	447	56	753	624	500	253	5	72	3	nd
Tl	3	2	10	3	3	3	3	3	4	4	1	2	2	2
Bi	1	4	3	1	0	1	1	0	0	0	0	0	5	2.7
Ga	0	10	17	1	0	54	37	0	4	0	1	28	383	0.7
Ge	0	2	5	0	0	0	0	0	0	0	0	0	2	0.4
Se	0	0	0	0	0	0	0	0	0	0	0	0	2	0.8
Yb	0	0	1	0	1	1	1	0	0	1	1	4	2	1.6
Hf	2	14	10	0	0	21	11	2	2	2	1	2	2	3.7
Ta	0	2	6	0	0	4	3	0	0	0	0	4	13	2.5
W	1	16	20	0	0	9	9	1	13	1	0	31	1	1.4
Pb	51	8	5	19	13	38	19	25	15	31	9	31	4	2
Th	6	6	0	10	8	12	16	11	6	13	7	47	10	2
U	3	4	1	6	2	6	2	4	1	7	1	14	3	1.3

Abbreviations: RW-Rwinkwavu; MN-Musha-Ntunga; GAT-Gatore; LLD-low limit of detection; nd-not determined; LOI-loss on ignition. The major elements are in wt. % whereas the LLD values are in ppm.

3.2.1 Chemical composition based on major elements

The rock samples analyzed in this study have shown a wide range of chemical trends containing between 36.08 and 89.52 wt. % SiO₂.

Al₂O₃: The majority of the analyzed samples showed high concentrations of aluminium oxide ranging from 5.4 (JC-521) to 29.67 wt. % (JC-453).

Fe₂O₃ (tot.) concentrations were between 1.21 (JC-16) and 28 wt. % (JC-24-6-2) with three rocks displaying total iron oxide concentrations above 20 wt. %. They were sampled in the shear zones developed within the core of the anticline re-fractured by recent orogenies such as the Pan-African and EARS and therefore, the high Fe content is most likely the result of the weathering which originates laterites formation.

MnO, CaO and P₂O₅ contents were very low: <0.1 wt. % (MnO), <0.2 wt. % (CaO) and <0.4 wt. % (P₂O₅). **MgO** concentrations were in most cases below 0.5 wt. % but three samples showed high contents: respectively 2.27 (JC-453), 1.68 (JC-457) from Rwinkwavu and 1.32 wt. % for JC-HFLS from the quarry of Gatore.

Na₂O and K₂O also were low: below 1 wt. % for Na₂O and 6 out 13 meta-sedimentary rock samples showed K₂O content below 0.1 wt. %. However, seven samples showed K₂O concentrations between 1.69 and 4.21 wt. %.

TiO₂: The concentrations of TiO₂ of eight analyzed samples were below 1 wt. % while four of them were found to contain TiO₂ concentrations between 1 and 2 wt. %. In addition, one sample (JC-453) had the maximum TiO₂ content with a value of 2.26 wt. %.

3.2.2 Correlation coefficients-Discrimination plots (major elements)-Alteration estimate

The determination of the Pearson's correlation coefficient (r) is the method normally applied for a better understanding of the chemical components of the samples distribution based on geo-statistical studies. The formula for the Pearson correlation coefficient can be written as follows (Hartung, 1999):

$$r_{xy} = \frac{\sum x_i y_i - n \bar{x} \bar{y}}{(n-1) s_x s_y} = \frac{n \sum x_i y_i - \sum x_i \sum y_i}{\sqrt{n \sum x_i^2 - (\sum x_i)^2} \sqrt{n \sum y_i^2 - (\sum y_i)^2}}$$

A correlation is +1 in the case of a perfect positive correlation, -1 in the case of a perfect negative correlation and some value between -1 and +1 in all other cases, indicating the degree of linear dependence between the variables. As it approaches zero there is less of a relationship (closer to

uncorrelated). The closer the coefficient is to either -1 or +1, the stronger is the correlation between the variables. If the variables are independent each other, Pearson's correlation coefficient is zero.

	P ₂ O ₅	SiO ₂	TiO ₂	Al ₂ O ₃	Fe ₂ O ₃	MnO	MgO	CaO	Na ₂ O	K ₂ O
P ₂ O ₅ Pearson cor.	1	-.189	.068	.237	.228	-.299	-.240	.312	-.230	-.197
SiO ₂ Pearson cor.	-.189	1	-.744**	-.9**	-.875**	-.357	-.666*	-.69**	-.79**	.117
TiO ₂ Pearson cor.	.068	-.74**	1	.89**	.399	.151	.551	.616*	.628*	-.160
Al ₂ O ₃ Pearson cor.	.237	-.85**	.890**	1	.531	.195	.532	.698**	.631*	-.191
Fe ₂ O ₃ Pearson cor.	.228	-.87**	.399	.531	1	.311	.527	.524	.653*	-.111
MnO Pearson cor.	-.299	-.357	.151	.195	.311	1	.681*	.412	.685**	.152
MgO Pearson cor.	-.240	-.666*	.551	.532	.527	.681*	1	.770**	.885**	-.253
CaO Pearson cor.	.312	-.69**	.616*	.69**	.524	.412	.770**	1	.662*	-.457
Na ₂ O Pearson cor.	-.230	-.79**	.628*	.631*	.653*	.68**	.885**	.662*	1	.056
K ₂ O Pearson cor.	-.197	.117	-.160	-.191	-.111	.152	-.253	-.457	.056	1

** . Correlation is significant at the 0.01 level (2-tailed).

* . Correlation is significant at the 0.05 level (2-tailed), number of samples: 13.

Table 3.5: Pearson correlation matrix and coefficients for major elements (yellow colour: strong positive correlation r is $>+0.5$, blue colour: strong negative correlation r is <-0.5).

Table 3.5 summarizes the correlation coefficients for the major elements. Table 3.5 and the Harker diagrams of Figures 3.4a and b indicate that: TiO₂, Al₂O₃, Fe₂O₃, MgO, CaO and Na₂O show a strong to moderate negative correlation with SiO₂ (Figures 3.4a and b).

In addition, with the exception of K₂O ($r = -0.2$) and MnO ($r = +0.2$), all other major oxides show a positive correlation with Al₂O₃ suggesting the key role played by aluminous minerals in the alteration processes. The Fe₂O₃ correlates positively with Al₂O₃, MgO, CaO and Na₂O, as well as MnO and MgO and MnO and Na₂O.

Moreover, and with the aim to obtain an impression of the extent of alteration, a bivariate diagram of Al₂O₃ vs. Al₂O₃+Na₂O+CaO+K₂O (Nesbitt and Young, 1982 in Rollinson, 1993) was plotted and is shown in Figure 3.5. The latter indicates that the alteration processes are moderate to high based on the moderate to elevated values of the chemical index of alteration (CIA) which range between 80 and 100.

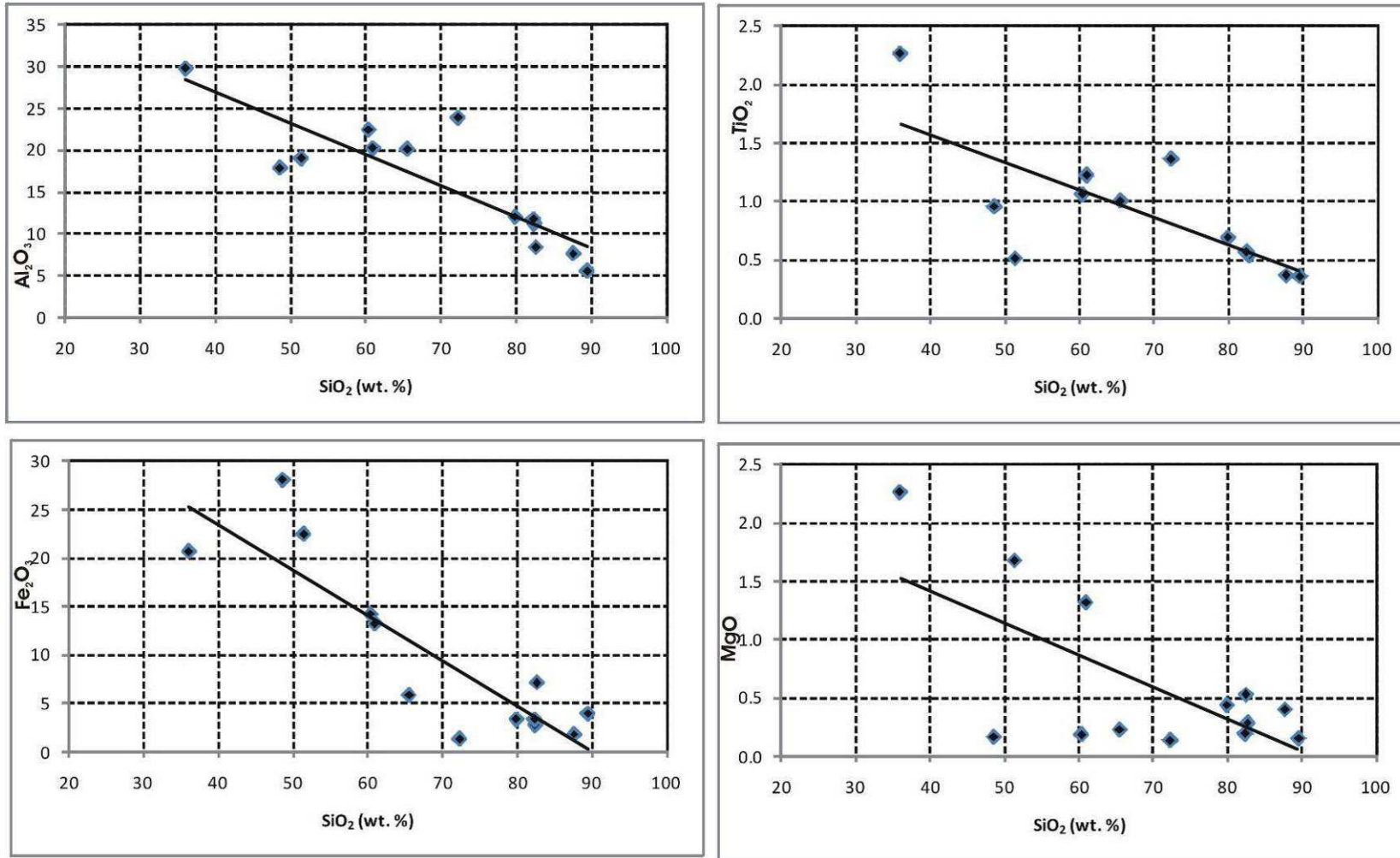


Figure 3.4a: Harker diagrams of SiO₂ vs. Al₂O₃, TiO₂, Fe₂O₃ and MgO of the meta-sedimentary rock samples from the study areas.

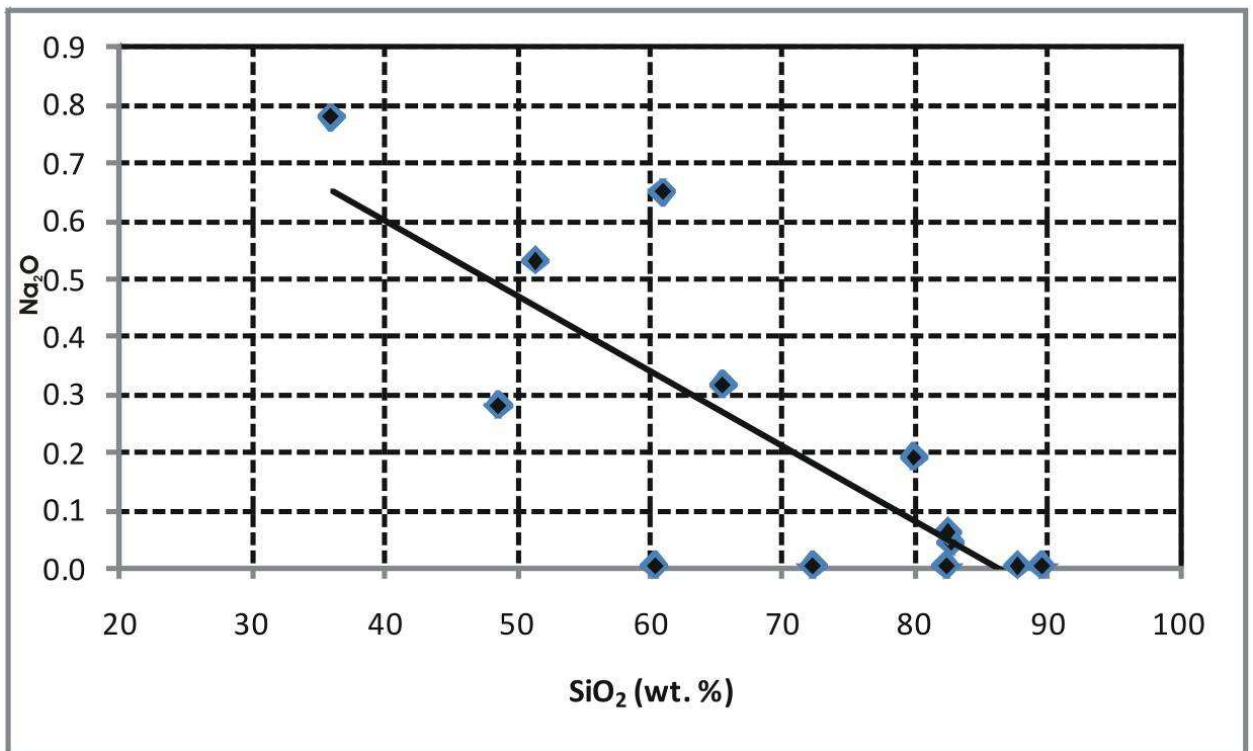
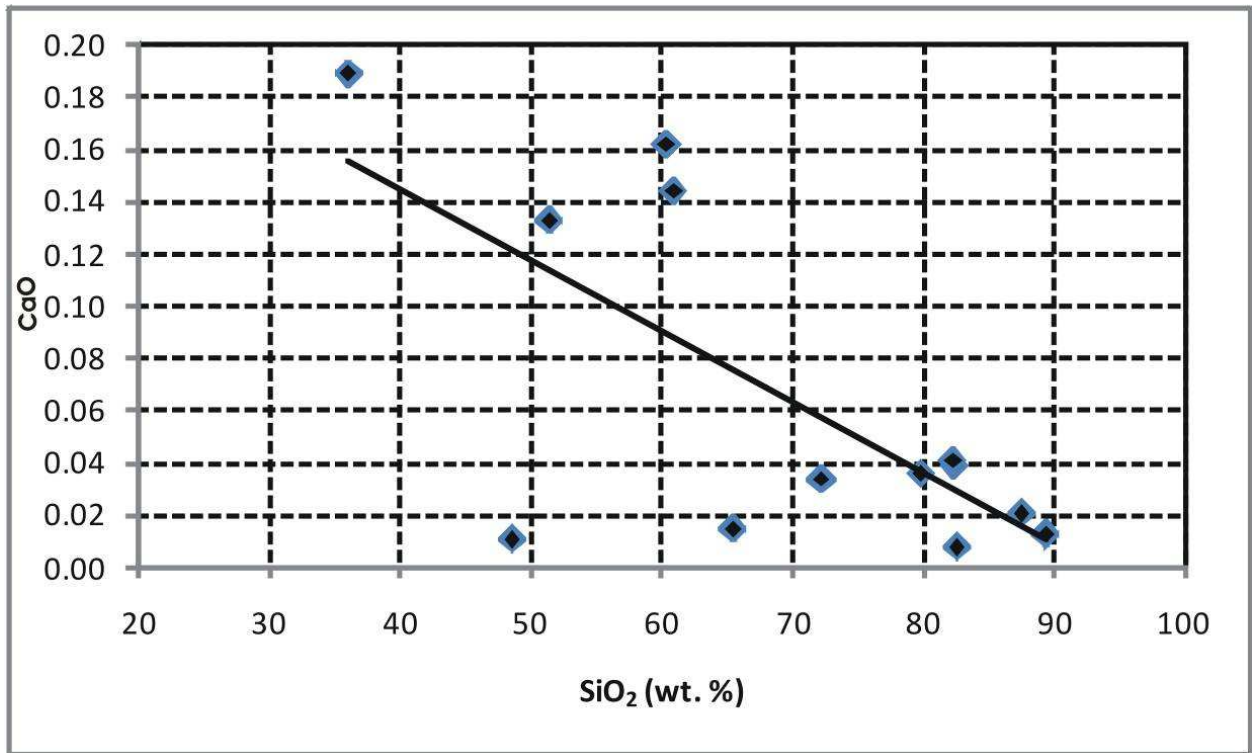


Figure 3.4b: Haker diagrams of SiO₂ vs. CaO and Na₂O of the meta-sedimentary rock samples from study area.

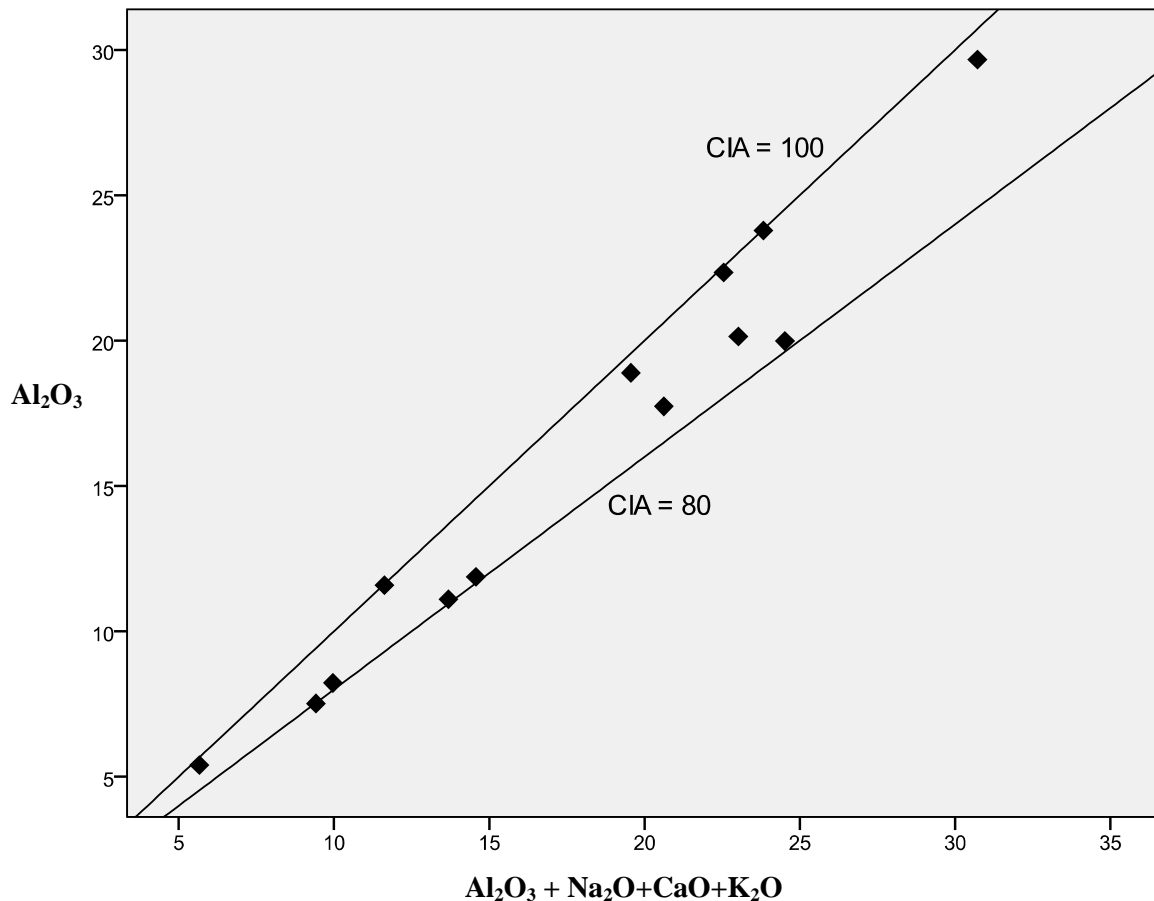


Figure 3.5: Al_2O_3 vs. $Al_2O_3 / (Al_2O_3 + Na_2O + CaO + K_2O)$ plot used to evaluate the extent of alteration of the meta-sedimentary rocks from the study area (after Nesbitt and Young, 1982). The data are from Table 3.4.

3.2.3 Depletion-enrichment trends based on trace element analyses

Using XRF techniques, measurements of trace elements were performed on meta-sedimentary rocks hand-picked from East-Rwanda.

Selected trace elements were normalized against the French Variscan “tin”- granite after Raimbault et al. (1995) and the diagram is shown in Figure 3.6. The investigated meta-sedimentary rock samples were depleted in Sn, Rb, Nb and Ta and enriched in Sc, Sr, Zr, Ba, Th and U. Apart from two meta-sedimentary rock samples from Rwinkwavu which showed slight enrichment in W, the remaining samples are depleted in this trace element.

However, the concentrations of Sn, W, Nb and Ta are low in the ordinary meta-sedimentary samples and increase from the latter to their contacts with the mineralized hydrothermal veins. This might indicate a contamination from the ascending mineralizing fluids (Table 3.4 and location map of the samples in Figure 2.1).

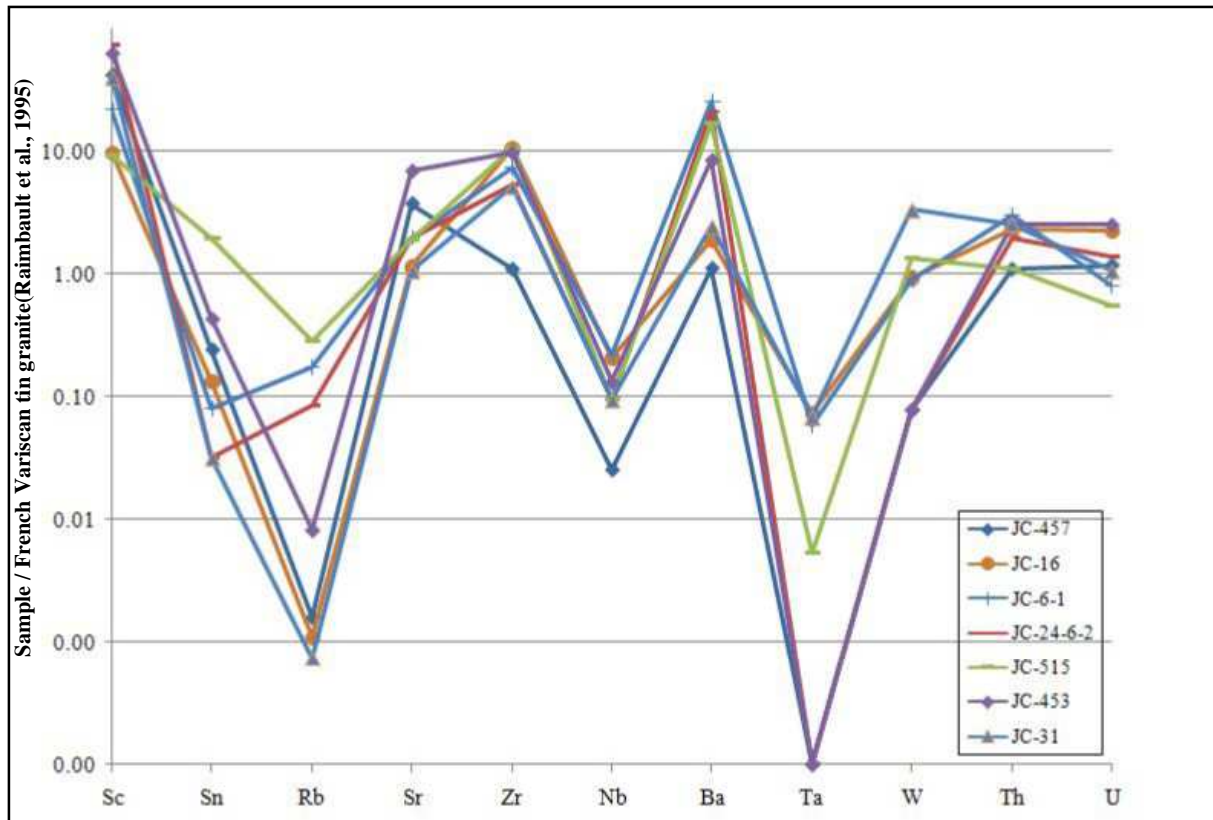


Figure 3.6: Multi-element normalized plot for some of the study area meta-sediments, normalized against the French Variscan tin granite (after Raimbault et al., 1995).

3.2.4 Classification of the meta-sedimentary rock samples from the study area.

Based on Herron (1988) who initially identified nine classes of terrigenous sandstones and shales (Fe-shale, Fe-sand, shale, wacke, arkose, litharenite, sublitharenite, subarkose and quartz arenite) indicating enrichment or depletion in total iron oxide or in quartz, the investigated meta-sedimentary rock samples were classified based on a $\log (\text{Fe}_2\text{O}_3 [\text{Total}]/\text{K}_2\text{O}) - \log (\text{SiO}_2/\text{Al}_2\text{O}_3)$ bivariate plot (Herron, 1988).

The results of the investigated samples are plotted in Figure 3.7: two samples out of thirteen are Fe-shales and two are Fe-sand. The rest of the analyzed rock samples show anomalous Fe contents (Table 3.4). They are probably lateritic weathering crusts. JC-30 and 515 are litharenite, JC-6-1 is shale and JC-520A is an arkose.

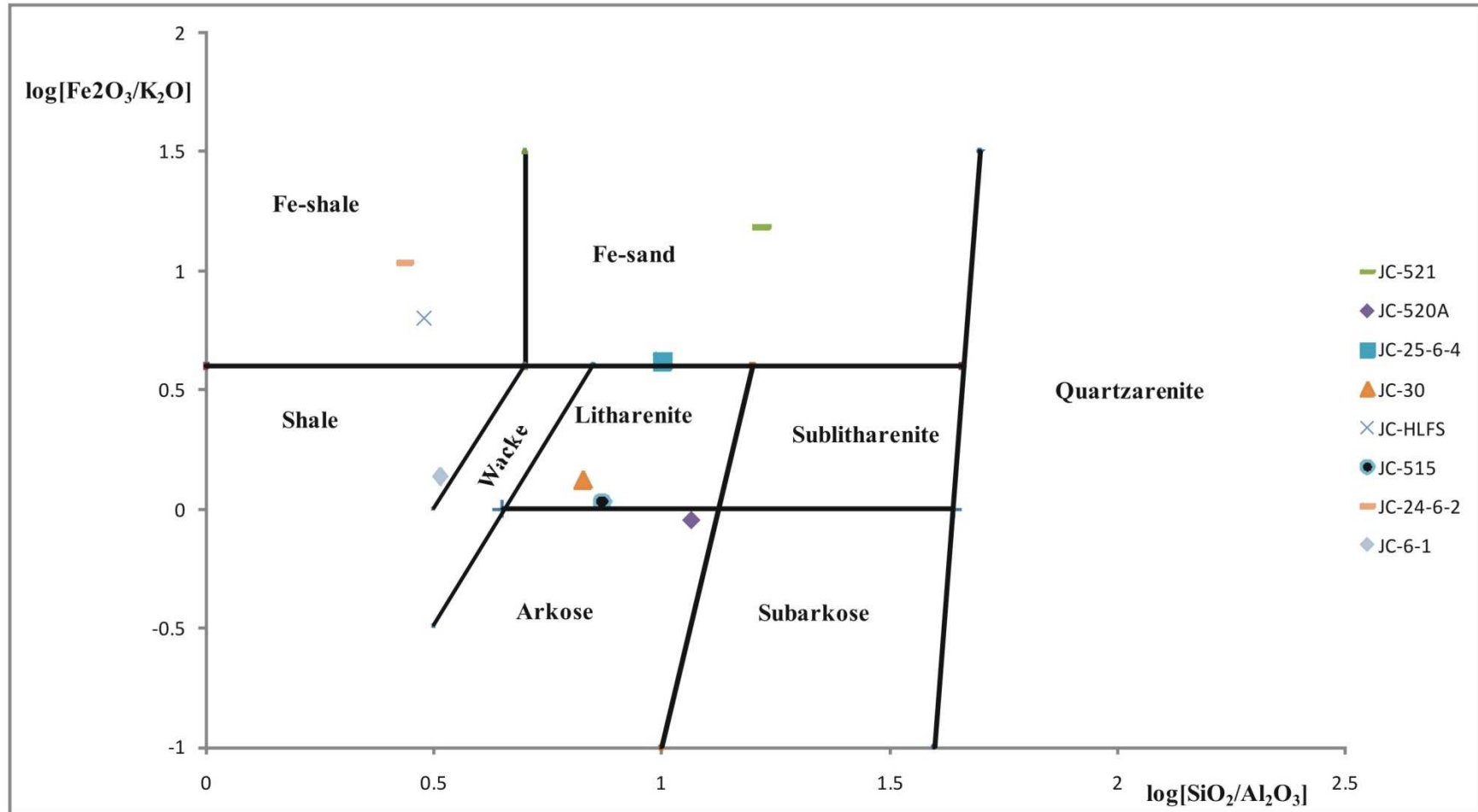


Figure 3.7: Chemical classification of meta-sedimentary rock samples from East-Rwanda based on Herron (1988). For the samples location, refer to Table 3.4.

3.2.5 Provenance of the sediments

With the principal aim of determination of the provenance of the sediments, as part of the main factors controlling the chemistry of the final meta-sedimentary rocks from East-Rwanda, a discriminant function diagram for the provenance signatures of the study area is plotted in Figure 3.8 using major elements (Roser and Korsch, 1988).

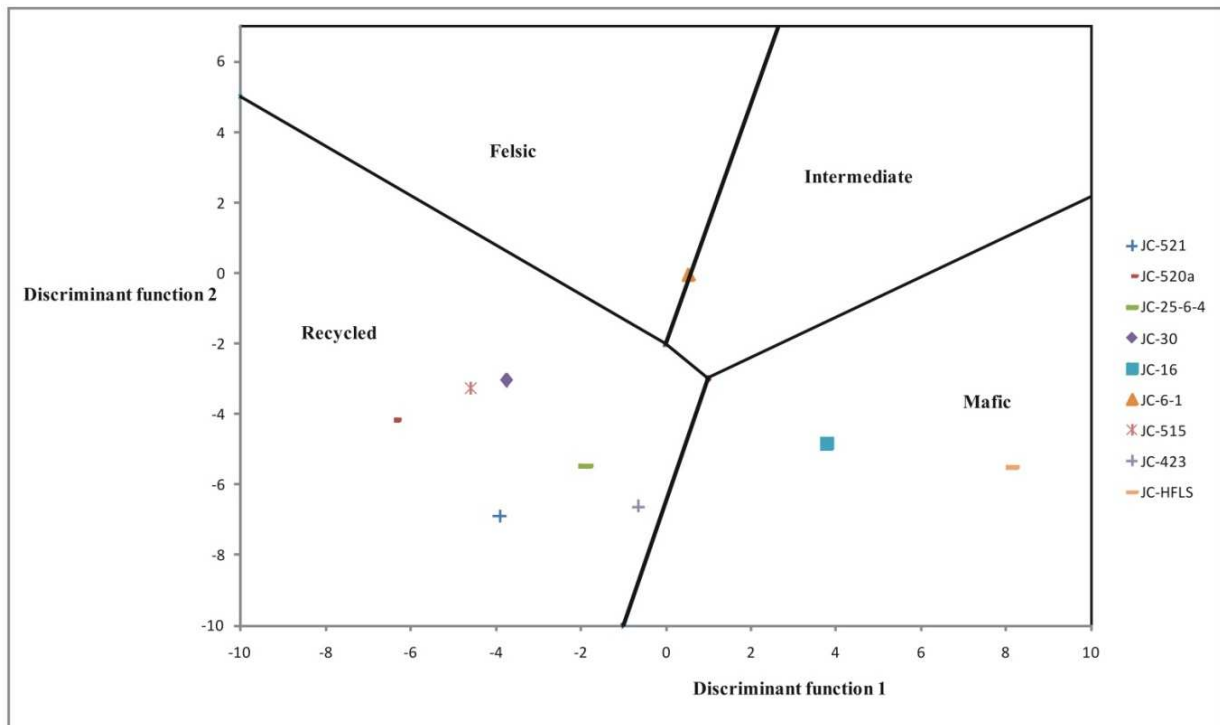


Figure 3.8: Discriminant diagram of sedimentary provenance signatures of studied samples after Roser and Korsch (1988).

Discriminant function 1 = $-1.773 \text{ TiO}_2 + 0.607 \text{ Al}_2\text{O}_3 + 0.76 \text{ Fe}_2\text{O}_3 \text{ (total)} - 0.5 \text{ MgO} + 0.616 \text{ CaO} + 0.509 \text{ Na}_2\text{O} - 1.224 \text{ K}_2\text{O} - 9.09$; Discriminant function 2 = $0.445 \text{ TiO}_2 + 0.07 \text{ Al}_2\text{O}_3 - 0.25 \text{ Fe}_2\text{O}_3 \text{ (total)} - 1.142 \text{ MgO} + 0.438 \text{ CaO} + 1.475 \text{ Na}_2\text{O} + 1.426 \text{ K}_2\text{O} - 6.681$.

Two samples from Rwinkwavu are plotting in the class of mafic provenance but only two will be considered as of mafic provenance (JC-16 and HFLS). The rest of the rock samples of the group which showed high Fe content (Table 3.4) are lateritic weathering crusts and were not considered as good indicators for the provenance signatures. 67% (from Musha-Ntungwa and surroundings) are of the recycled origin and only 1 sample (11%) from Ntungwa is of felsic to intermediate origin.

3.3 Mineral chemistry of tourmaline

The B-rich mineralizing fluids overprinted the meta-sedimentary rocks hosting the pegmatites/hydrothermal veins and originated a 20 to 40cm thick rim of tourmalinite around the intrusions. The chemistry of tourmaline of tourmaline-bearing rock samples from the study area was investigated for Fe and Mg.

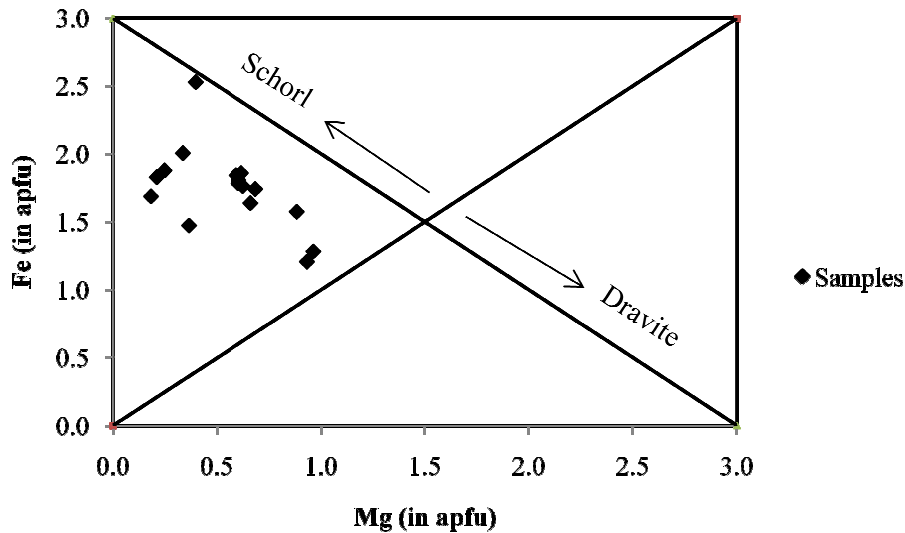


Figure 3.9: Fe vs. Mg discrimination diagram of tourmalines from the study area.

A discrimination diagram Fe-Mg (in apfu) for the tourmalines in the study area was plotted using the data from appendix 5 and is shown in Figure 3.9. The figure shows that the tourmalines in the tourmalinite samples are richer in Fe than in Mg and therefore, lie within the schorl field. They also showed high contents in Al_2O_3 (more or less 34 wt. %). The high Fe and Al contents are pointing towards magmatic rather than metamorphic or meta-sedimentary tourmalines (Henry and Guidotti, 1985).

4. PROSPECTS

4.1 RWINKWAVU TIN-TUNGSTEN DEPOSIT

The Rwinkwavu ore deposit is situated in Rwinkwavu Sector, Kayonza District, Eastern Province in the eastern part of Rwanda, between $30^{\circ}33'41''$ and $30^{\circ}37'16''E$ and $1^{\circ}50'41''$ and $2^{\circ}0'31''S$ and 25km west of Akagera river, the natural border between Rwanda and Tanzania. The total area of the concession has been estimated to be 6,472 ha. The mining concession currently belongs to Wolfram Mining Processing Ltd. and comprises 13 mining sites which are Kuyacumi, Gahushyi, Bwanika,

Gahengeri, Rutonde, Kizanye, Musumba, Kibaya, Nyarunazi, Migera, Nyaruhuru, Nyabimuri and Gihinga. This study also includes, Kirimbari as a representative of wolframite mines of the area.

Field work was carried out in Rwinkwavu area and surroundings during late June to late August 2010. The main goals were to record the lithology, to collect the samples for further investigations, to map the tectonic structures with the main focus on folds, faults, hydrothermal veins and fissure swarms within different geological formations of the study area. Furthermore, different mineralization scenarios of the mining concession have been located and described aiming at a better understanding of their genetic geodynamics.

4.1.1 Geological mapping (Figures 4.1 and 4.4)

The topography of the Rwinkwavu Sn (W) field is dominated by NE-SW Kizanye-Nyarunazi valley bordered by two NNE-SSW trending ridges composed mainly of different units of meta-sedimentary rocks. The core of the valley corresponds to a several tens of meters thick pile of soils, alluviums and laterites covering and thus, making inaccessible the outcrops. The elevations range from 1,350m (Kizanye valley) to 1,650m (Mount Rwinkwavu) (IGN and MINITRAPE, 1988).

Baudet et al. (1989) and Theunissen et al. (1991) attributed the rocks found in the Rwinkwavu area to the middle and upper part of the Rwanda Supergroup of Mesoproterozoic age (Pindura and Cyohoha Groups).

Based on Baudet et al. (1989) and Theunissen et al. (1991), the details of the stratigraphic units are described below, from the oldest to the youngest formation. A systematic verification of the stratigraphic units was made during the field work. Figure 4.4 shows a geological map of the Rwinkwavu area.

1. **Rukira formation:** Comprises metapelite - dominated packages of thinly stratified and laminated layers of schists with locally black shales: tourmaline chlorite schists and whitish to dark beige sericite schists underlying dark, ferruginous and silicified schist, fine-grained sandstones and siltstones.
2. **Kibaya formation:** Comprises 10m to 200m thick of continuous sandstones and hard layers of quartzite appearing along several outcrops. These latter are whitish in colour, well sorted medium to coarse grained and show sedimentary structures such as ripple marks, cross-stratification and oblique laminated beds.

3. **Ndamira formation:** Contains zoned clayish schists, siltstones and alternation of isolated lenses of schists, fine to coarse grained sandstones and lithic conglomerates. During the field work, two outcrops showing the volcano-sedimentary rocks have been identified respectively on the top of Mount Rwinkwavu (waypoint 555, Figure 2.1) and on the way to Akagera National Park before Nyankora commercial centre (waypoint 565, Figure 2.1).
4. **Kibungo formation:** sparsely distributed small outcrops of quartzite or medium to coarse grained sandstones have been identified further west of Rwinkwavu anticline on the left side of the main road Kayonza-Kibungo-Rusumo-Tanzania (waypoints 405 and 406, Figure 2.1).
5. **Birenga formation:** the silt-schist-dominated formation of Birenga with some quartzite is not found in the direct environment of Rwinkwavu anticline and overlies the formation of Kibungo. The outcrops of Birenga formation are rare and mostly found on the right side of the road Kayonza-Kibungo-Rusumo-Tanzania in the vicinity of Kabarondo town.
6. **Quaternary:** represented by undifferentiated Holocene and Pleistocene with several tens of meters of recent alluvial sediments deposited by rivers and/or erosion.

4.1.2 Deformation

According to Theunissen et al. (1991), structurally, the Rwinkwavu area is situated on an important NE-SW oriented anticline adjacent to the Kibungo syncline in the W and the Nyankora - Gashanda syncline together with the Nasho granite in the E. The Rwinkwavu anticline plunges to the south and has an eastward vergency. In the South-Eastern part of the anticline, the strike direction varies between N30E and N50E and the dip of the bedding planes ranges between 45° and 50° towards the E. In the south-western flank, the dip of the bedding planes is lower and attains 30°W in the westernmost valley near Kadiridimba (Figure 2.1 and Appendix 2). The anticline is symmetric in the northernmost part with steep-shaped angles of dip ranging from 70° to 80° for both the eastern and western limbs of the anticline.

The core of the anticline coincides with the Rutonde - Kizanye valley and is composed of ductilely deformed sub-horizontal layers of schists. Here the clay-rich metapelites have been folded, thrust-faulted, fissured, foliated and cracked. The foliation planes (S1) are well developed in the ductile metapelites of the Rukira formation and perpendicular to the stratification beddings in Rwinkwavu-Kirimbari anticlinal structure. Mylonitization is frequent in these meta-sedimentary formations.

The field observations showed that besides the folding structures, the Rwinkwavu area is cross-cut by a N-S to NW-SE network of open faults and fissures filled by quartz-muscovite-tourmaline veins with locally completely recrystallized and cemented lithic fragments of the host rocks. An important N30-40°E fissure swarm dipping 60°E - vertically is situated in the main axis of the anticline and hosts the most mineralized veins.

The cleavage planes are regularly observed and occur well developed in the metapelitic host rocks and within the quartzite. The same strike direction and dip are observed in both rock types.

During the field investigations, two types of hydrothermal veins were identified. This was done based on the relationship between their geometric emplacements (Figure 4.4):

- The first group of veins, possibly syn-deformational, is associated mostly with folding and displays high grades of tin/tungsten mineralization. The mineral assemblage here comprises cassiterite and/or wolframite, muscovite, sericite, tourmaline, zircon, fragments of the country-rock. A minor amount of quartz is sometimes included.
- The second group of veins cross-cut the previous one. This type of veins is mainly of milky quartz, Fe-rich minerals and fragments of the country-rock composition. They are hosted in fissures generated by late tectonic events (Pan-African? or recent East African Rift System? or both?) which have affected mechanically the eastern Rwanda.

The rocks in Rwinkwavu have been exposed to a regional metamorphism of low grade with greenschist facies (Baudet et al., 1989).

4.1.3 Mineralization

The samples were separated into three types: the ore mineral concentrates (11 samples), the hydrothermal veins (11 samples) and the host schists, sandstones and quartzite (8 samples), generally examined with the aim of determining their relationship to different types of hydrothermal veins.

A. Host Rocks

Some of the studied rocks were found within the Rwinkwavu anticline in the external periphery (Kibaya formation) either in the form of quartzite wherein silica makes up the matrix and is the principal component, or sandstone with fragments of quartz-clasts cemented by a clay-rich matrix. Others, located in the inner parts of the anticline, are fully schist-dominated (Rukira formation). Both

the sandstone to quartzite and schist host barren and/or mineralized quartz-muscovite - sericite-tourmaline veins, veinlets or networks of fracture fillings.

Quartzites and sandstones

The Kibaya formation (Figure 4.2) mainly crops out along the concentric wide layers of ca. 200 m width bordering the Rwinkwavu anticline following the arc-shaped Muganza - Rwinkwavu-Migera - Musumba trending series of highs.



Figure 4.2: Photograph of quartzite of Kibaya formation.

It comprises the quartzite and sandstones formed by quartz fragments hosted in a silici-clastic matrix. The main rock-forming minerals are quartz, tourmaline and Fe-minerals. Quartz is the dominant mineral and the grains are well sorted, fine to medium grained and equi-granular.

The quartz grains are pure, intensely compacted and recrystallized due to a low grade regional metamorphism. The quartzites often show a slight cleavage development around the main accidents and fractures. Quartz, muscovite and tourmaline can be found along these foliation planes. Massive blocks of iron minerals and fault breccias associated to recent weathering are found preferentially within fractures developed in the quartzitic apex of the Rwinkwavu anticline.

Schists

In the Rwinkwavu area, tin and tungsten ores occur as open-space hydrothermal vein fillings (primary mineralization) that produce a more or less thick halo of alteration. They also show several stages of vein growth. The mineralization also occurs as a secondary mineralization in alluvial and/or eluvial placers. The majority of hydrothermal vein deposits are hosted in the Rukira formation (Figure 4.3) or along the contact between Rukira and Kibaya formations. It is also the case of secondary ore deposits.



Figure 4.3: Boulders of schists from Rukira formation (hand-picked specimens).

The area is mainly characterized by cassiterite mineralization but one site, Nyamuyorwa, is known to host tungsten mineralization which, unfortunately, was not sampled during the field expedition.

Table 4.1.1 is an overview list of different mineral occurrences of the Rwinkwavu area (Kayonza District, Eastern Province):

Deposit	Zone	Minerals		Deposit type		Longitude	Latitude
		SnO ₂	WO ₃	Primary	Secondary		
Gahushyi	Mt Rwinkwavu	X		X	X	30°35'18"E	1°58'14"S
Gahengeri	Mt Rwinkwavu	X		X	X	30°36'40"E	1°58'23"S
Nyamuyorwa	Mt Rwinkwavu	X	X	X		30°36'16"E	1°59'08"S
Kuyacumi	Mt Rwinkwavu	X		X	X	30°35'31"E	1°58'21"S
Rutonde	Kizanye valley	X		X	X	30°36'15"E	1°57'45"S
Kizanye	Kizanye valley	X		X	X	30°35'29"E	1°55'43"S
Kibaya	Kizanye valley	X		X	X	30°35'25"E	1°55'32"S
Nyarunazi	Nyarunazi	X		X	X	30°35'29"E	1°55'43"S
Nyaruhuru	Nyaruhuru	X		X	X	30°38'31"E	1°51'11"S
Nyabimuli	Nyabimuli	X		X	X	30°37'59"E	1°53'57"S
Musumba	Musumba	X		X		30°34'43"E	1°55'43"S
Migera	Migera	X		X		30°35'51"E	1°54'23"S
Bwanika	Bwanika	X		X	X	?	?
Kirimbari	Kirimbari		X	X	X	30°38'28"E	1°40'34"S

Table 4.1.1: Overview of mineral deposits in the Rwinkwavu mining concession.

Kirimbari tungsten ore deposits will be described as part of Rwinkwavu mining sector. This is based on the fact that it is situated at ca. 20km from the main area where it is hosted in the same Rwinkwavu-Kirimbari anticlinal structure.

B. Setting of primary tin deposits

The primary deposits of Rwinkwavu are genetically hydrothermal vein-related. Based on the type of the host rock, three types of mineralized veins have been identified: the veins hosted in highly tourmalinized schists; concordant veins hosted in quartzite and veins which are crosscutting the schists and quartzite.

Mineralized veins hosted in schists

Economically exploitable vein-type tin deposits are those which are hosted in schists along the Kizanye-Rutonde valley at the lowest altitudes. However, veins with tin mineralization also are exploited in the highs of Nyarunazi, Nyabimuri, Bwanika and Nyaruhuru hills, but in this case, the mineralization is less rich and less important.

The Kizanye-Rutonde vein system is located underneath a thick layer of soils and alluvial sediments where the most important vein (the so called “vein n°7” by Wolfram Mining Processing Ltd) should be accessible via the underground galleries used for the tin exploitation works. This vein is more or less 700m long and the Kizanye-Rutonde stockwork is itself around 1km wide, where it comprises hundreds of veins of various lengths.

The mineral assemblages within the hydrothermal veins hosted in schists are mica-dominated and sometimes quartz may be present. The host rocks are intensively tourmalinized along their contacts with the hydrothermal veins. The tourmaline content decreases from the schists-vein contact to the inner parts of the host-rock.

The whitish or bluish quartz constitutes the core of the vein and it is surrounded symmetrically by two concentric layers: a cluster of reddish, platy and ferruginous muscovite followed by 10cm to 20cm of sericite. In addition to quartz, muscovite and sericite, several fragments of the host schist are part of the veins.

The contact sericitic wall/rocks are preferred sites for tin mineralization with average grades of 29.5 kg/m³ (Wolfram Mining Processing Ltd, pers. comm.).

Mineralized veins hosted in quartzite

Localized within the western flank of the Rwinkwavu anticline, the vein type which is quartz-dominated characterizes Mount Rwinkwavu, Musumba, Gahengeri and Migera tin deposits, hosted in ca. 300m thick quartzite of Kibaya formation. The cassiterite is here sparsely distributed in isolated grains of maximum size of 2cm in the quartz veins.

The contact between the quartz veins and surrounding host quartzite is marked by the presence of a thick (one to several cm) rim of tourmalinite.

Veins cross-cutting schists and quartzite

The veins which cross-cut both schists and quartzite beddings are rare and one of these veins (thickness: 0.8 m) in Nyamuyorwa mining site (Mount Rwinkwavu), has shown the co-existence of both tungsten and tin mineralization.

C. Alluvial/eluvial tin placers

The alluvial/eluvial tin deposits of Kizanye-Rutonde trend are the most important and generally, are composed of four layers of gravels/laterites separated by thin layers of clays. The artisan miners in Rutonde mining site confirmed that the cassiterite production per m³ ranges from 7kg to 30kg and the lowest layers are the most mineralized.

4.1.4. Petrography

A. Introduction

A total of 31 representative samples of the host rocks, barren veins and tin-, tungsten-bearing veins from Rwinkwavu mining concession and surroundings have been received from OGMR-Kigali-Rwanda and RMCA-Tervuren-Belgium or have been collected during the June-August 2010 field campaign for the petrographic analyses.

During the field investigations, the most important characteristics of sampled rocks were recorded. The map in Figure 4.4 displays the distribution of the samples in the area of the Rwinkwavu anticlinal structure and surroundings.

Petrographic analyses were conducted on a representative selection of samples from different locations, detailed descriptions of outcrops and sampled rocks are summarized for the whole set of samples in Appendix 2 and Table 4.1.2 is an overview list of the samples from Rwinkwavu. It indicates the samples examined, their geographic location and the type rock samples. Besides the macroscopic descriptions, petrographic investigations were carried out using light microscopy, the Scanning Electron microscope-Energy Dispersive Spectrometer/Wavelength Dispersive Spectrometer (SEM-EDX/WDX), fluid inclusion studies and X-Ray Fluorescence (XRF). The latter was done for a better understanding of the whole rock geochemistry (Appendix 1: Methodology).

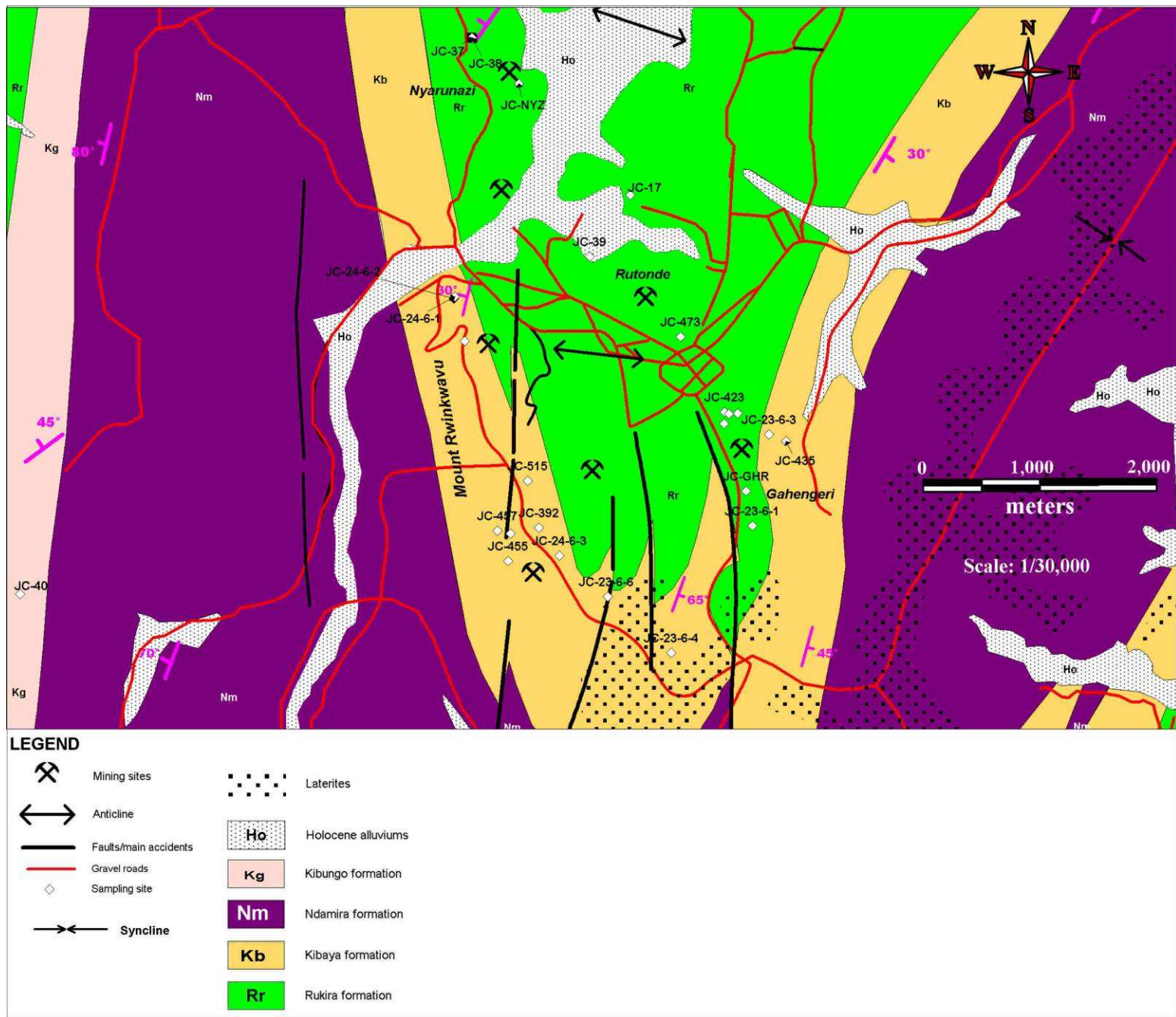


Figure 4.4: Geological and location map of the sampling sites in the Rwinkwavu area.

The thin sections were examined under a microscope in order to elucidate the textural characteristics, mineralogical content and cross-cutting relationships.

Table 4.1.2: Description of sampled rocks within the Rwinkwavu mining concession (Figure 4.4)

Ref	Sample	Locality	Easting	Northing	Elev.	Type of rock/minerals
-----	--------	----------	---------	----------	-------	-----------------------

1	JC-17	Rwinkwavu	567050	9783830	-	Cassiterite concentrate
2	JC-18	Mwiri	563570	9793640	-	Fe- ore
3	JC-31*	Kibungo	561260	9767440	-	Clay rich metamorphosed sedimentary rock
4	JC-37*	Nyarunazi	565700	9785200	-	Tourmaline-quartz-muscovite schists
5	JC-38*	Nyarunazi	565700	9785200	-	Cassiterite concentrate
6	JC-39*	Kizanye	566700	9783300	-	Quartz-muscovite vein with fragments
7	JC-40*	Rwinkwavu	561800	9780400	-	Quartz vein/greisens with host rock
8	JC-392	Rwinkwavu	566250	9780950	-	Quartzite: equi-granular quartz grains with tourmaline cemented by silico-clastic matrix and cross-cut by milky quartz veinlets
9	JC-423	Rwinkwavu	567848	9781947	1442	Metapelitic dominated sandstone
10	JC-424	Rwinkwavu	567842	9781844	1448	Cassiterite concentrate
11	JC-435	Rwinkwavu	568373	9781691	1553	Fe rich sandstone, rounded quartz phenocrysts within a matrix
12	JC-453	Rwinkwavu	566007	9780903	1574	Red Fe-rich quartzite
13	JC-455	Rwinkwavu	565986	9780667	1553	Cassiterite concentrate
14	JC-457	Rwinkwavu	565894	9780928	1556	Fe-minerals, quartz, tourmaline, lithic fragments.
15	JC-473	Rutonde	567474	9782600	1394	Quartz vein
16	JC-515	Rwinkwavu	566159	9781360	1568	Muscovite sericite schist
17	JC-23-6-1	Rwinkwavu	568080	9780960	-	Quartz vein
18	JC-23-6-3	Rwinkwavu	568230	9781750	-	Highly altered quartz veins
19	JC-23-6-4	Rwinkwavu	567380	9779860	-	Brecciated quartz vein
20	JC-23-6-6 638	Rwinkwavu	567885	9781929	1455	Cassiterite concentrate
21	JC-23-6-6	Rwinkwavu	566840	9780350	-	Quartz-muscovite vein
22	JC-24-6-1	Rwinkwavu	565543	9782960	1429	Milky quartz vein
23	JC-24-6-2	Rwinkwavu	565532	9782943	1436	Layered and zoned sandstone
24	JC-24-6-3	Rwinkwavu	566427	9780708	1618	tourmaline developed within quartz vein
25	JC-24-6-4 642	Rwinkwavu	565623	9782572	1499	Cassiterite concentrate
26	JC-GHR	Gahengeri	568030	9781260	-	Cassiterite concentrate
27	JC-KRM	Kirimbari	563706	9796148	1661	Ferberite concentrate
28	JC-KRM1-676	Kirimbari	563706	9796148	1661	Ferberite concentrate
29	JC-MGR	Migera	564900	9789800	-	Cassiterite concentrate
30	JC-NYZ	Nyarunazi	566100	9784800	-	Cassiterite concentrate
31	JC-HFLS	Gatore	564353	9750367	1359	Hornfels

(*)-Sample rock obtained from the RMCA collections.

B. Host rocks

The studied schists are located within the core of the Rwinkwavu anticline where they form the Rukira formation of Mesoproterozoic age, deformed and uplifted during the Kibaran Orogeny. Due to a thick pile of Quaternary alluviums and laterites, the outcrops are rare along the anticline but the number of outcrops increases further to the east and north-east in the vicinity of Kirimbari tungsten deposit and in the Akagera National Park. They are metamorphic rocks that have been deeply buried, heated, recrystallized and thus, showing preferred directions of schistosity planes.

Investigations carried out in the field have shown that during the recrystallization, the minerals (in many cases) have been segregated into dark and light layers (Figures 4.3 and 4.5) and in some outcrops, the schists are graphite - rich and form locally black shales between Rukira business centre and the hornfels quarry of Gatore.

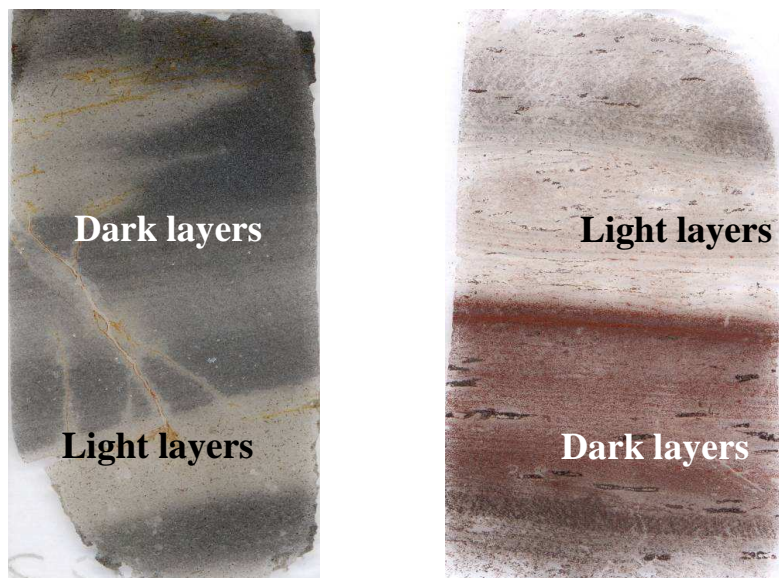


Figure 4.5: Scanned thin-sections of meta-pelites from the Rukira formation within the Rwinkwavu anticline showing alternation of light and dark layers.

The schists are mainly fine-grained, mica-dominated and show three modes of occurrence. These include:

- 1) Chlorite-muscovite schists
- 2) Quartz-sericite schists
- 3) Fe- rich and silicified schists

The chlorite-muscovite- quartz-sericite schists are tourmalinized at the contacts with the hydrothermal veins, thinly stratified (Figure 4.3) and light purple-grey to beige coloured while Fe- and/or graphite rich schists are dark coloured. This is supported by microscopic investigations (Figure 4.6) which

revealed a strong alignment of minerals with alternation of coarse-grained, white to light gray layers of quartz and fine-grained coloured layers with high content of mica.

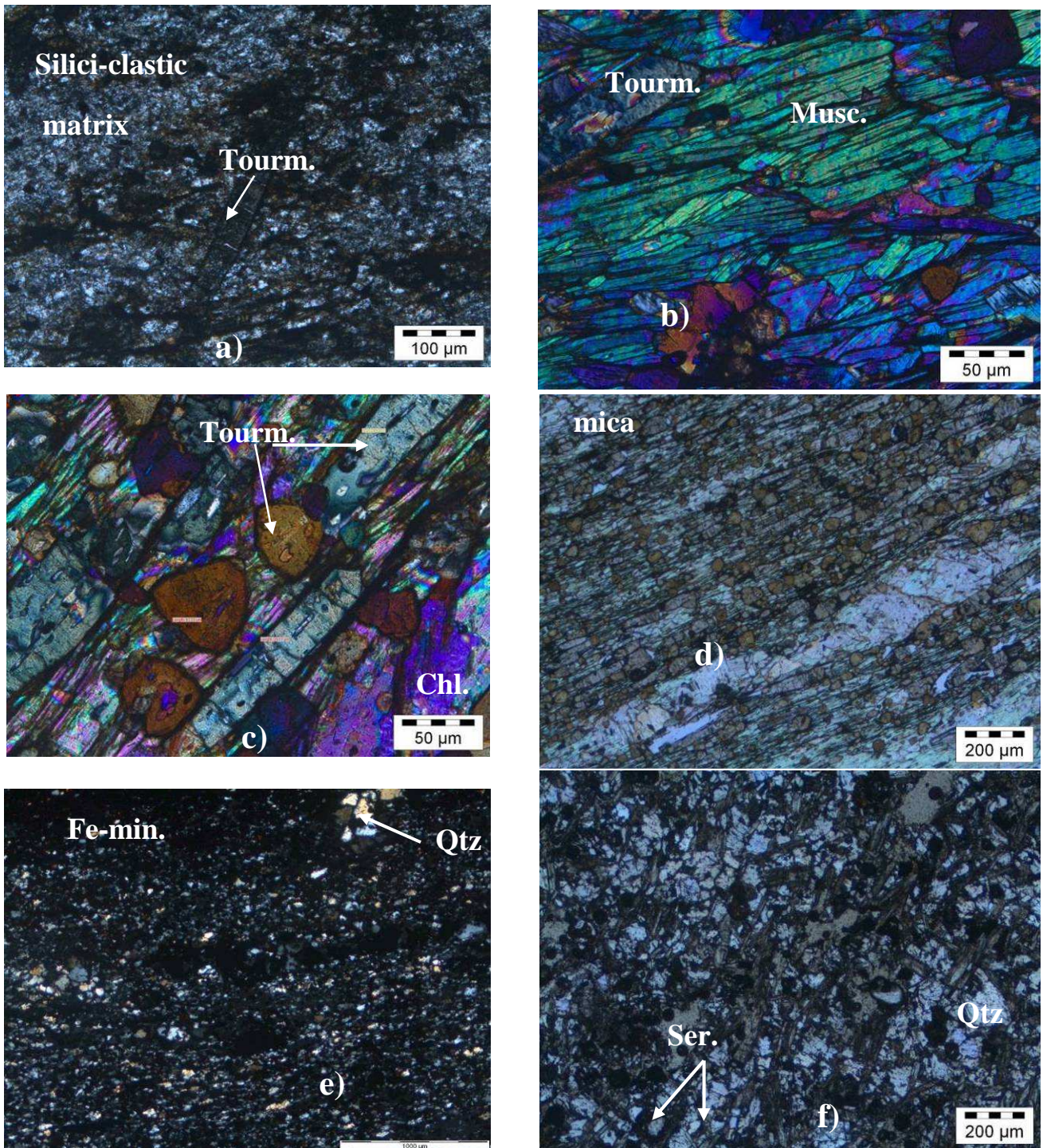


Figure 4.6: Microphotographs showing general characteristics of the studied tourmalinized schists; a) PPL, x10; b)XPL, x20; c)XPL, x20; d) PPL, x4; e) XPL, x2; f) PPL, x4 (Qtz: quartz, Fe-min.: iron minerals, Ser.: sericite, Chl.:chlorite, Tourm.: tourmaline, musc.: muscovite).

Besides the quartz and the group of mica (muscovite and chlorite), the thin sections analyzed under transmitted light display the tourmaline in variable elongated forms but also the aggregates of tiny flakes of sericite and a small amount of opaque minerals (possibly iron minerals such as hematite and/or goethite) distributed within a silici-clastic matrix.

C. Tin and wolframite ore-gangue minerals

The gangue minerals are an association of muscovite, quartz, tourmaline, sericite with accessory minerals like hematite, goethite and zircon.

The primary cassiterite in Rwinkwavu ore deposit is found in highly altered muscovite-quartz veins where it is associated with muscovite, sericite, quartz, fragments of the host rock, rutile, hematite/goethite and tourmaline. These hydrothermal veins are hosted within Mesoproterozoic meta-sedimentary suites which include quartzites, sandstones and metapelites. The host rocks were affected by several alteration processes including the sericitization, kaolinization, muscovitization, tourmalinization, hematitization and laterization. The hydrothermal alteration is evidenced by the presence of 3 concentric mineral zones around a core of quartz (from the inner to the outer): a muscovite zone, a sericite zone (which can be followed by a kaolinite zone) and a tourmaline zone. The cassiterite is mostly hosted in the sericite zone. The hematitization and lateritization are related to the weathering processes.

As mentioned in the section 4.1.3, the secondary mineral deposits occur as lateritic levels developed over Mesoproterozoic meta-sedimentary rocks and composed by a sequence of 4 horizons which show an increasing productivity with the depth. The cassiterite found in these laterites shows inclusions of quartz, ilmenite, rutile, hematite and zircon. The crystal size ranges from 2cm to less than 1mm facilitating the handpicking of tin-ore during the mining activities.

In both mineral occurrences, the crystals of cassiterite are either light yellow to red-brown (in the case of samples from Kuyacumi-Gahushyi-Mt Rwinkwavu) or brown to black in other cases. The crystals are euhedral, bi-pyramidal or prismatic and show adamantine or adamantine metallic luster, white streak, and twinning and often corroded edges.

In the direct vicinity of Rwinkwavu, the wolframite mineralization is exploited in the unique site of Nyamuyorwa (Mount Rwinkwavu) which was not operating during the field excursion. Further NE in the mine of Kirimbari, located in the Rwinkwavu anticline; two mining companies were exploiting wolframite from hydrothermal quartz veins (Figure 4.7).

The wolframite crystals are massive and/or euhedral, dark- gray to black-coloured with a sub-metallic to metallic luster and a dark brown streak.

The tungsten ore of Kirimbari shows unevenly distributed zones of alteration which are either white chalky or red coloured. The earlier zone may correspond to the anthoinite mineralization (Al [OH/WO₄]) while the later is possibly the oxidized Fe- rich mineral.



Figure 4.7: Mineralized quartz vein (Kirimbari tungsten mine)

The light microscopic and SEM-EDX/WDX investigations reveal that the gangue assemblage consists of quartz, micas, tourmaline and opaque minerals (Figure 4.8).

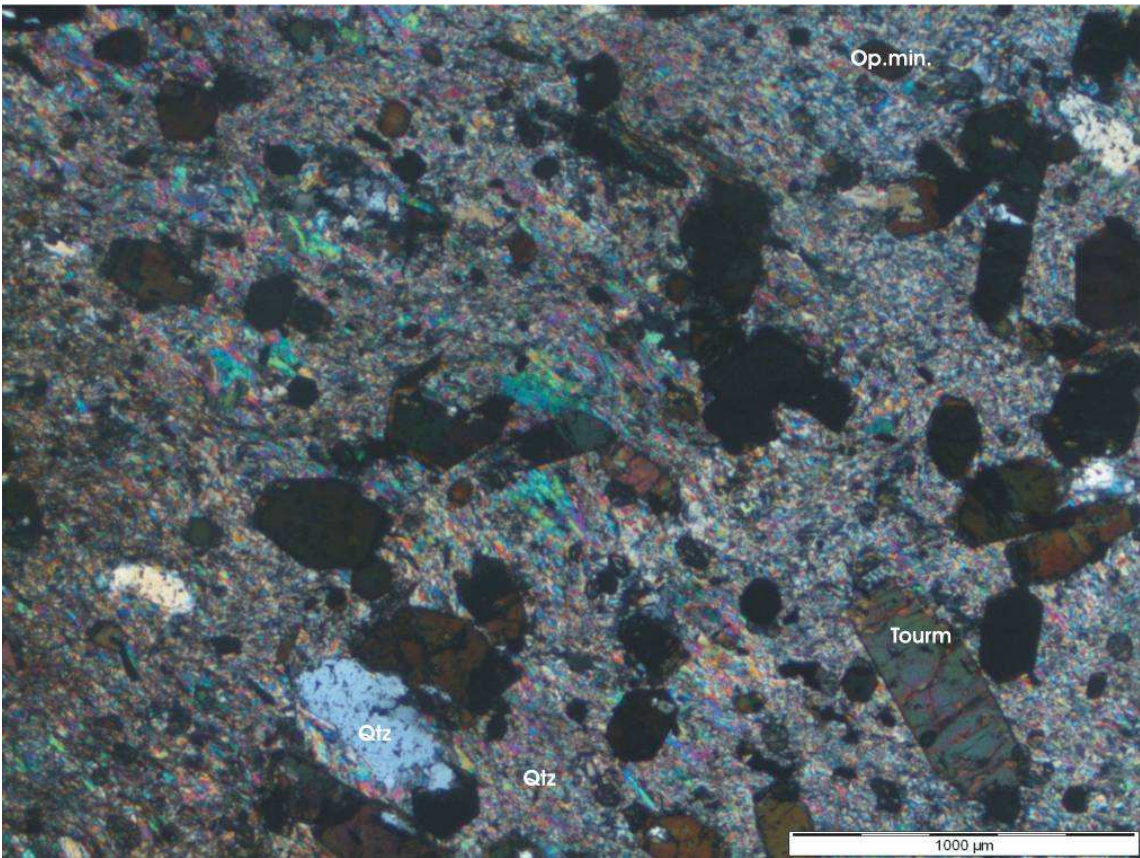
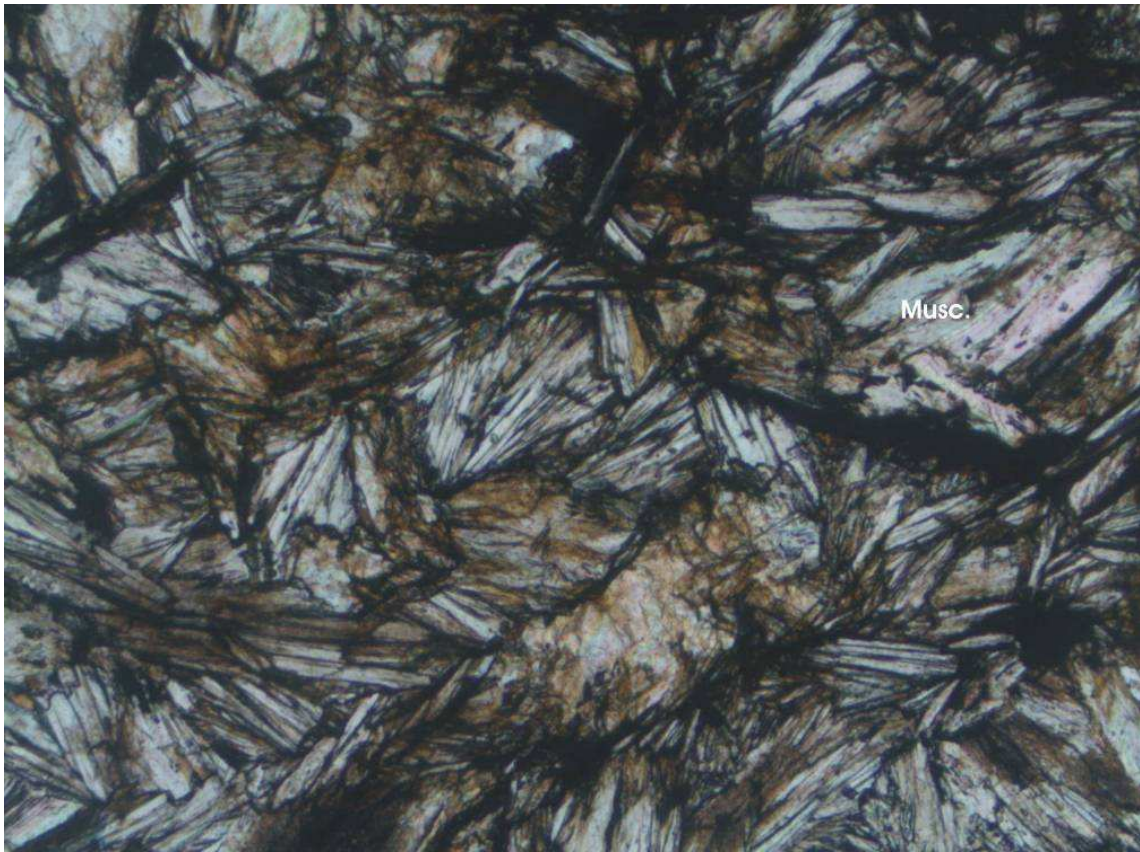


Figure 4.8: Microphotographs (XPL) of gangue minerals of mineralized nodes.
Abbreviations: Qtz: quartz, musc: muscovite, tourm: tourmaline, Op. min.: opaque minerals.

4.1.5 Mineral Chemistry of cassiterite and wolframite

Thirteen samples from the Rwinkwavu mining concession and surroundings were hand-picked, prepared and analyzed using the Scanning Electro-Microscopy JEOL JSM-6610 of the Department of Geology and the SHIMADZU SSX-550 Superscan SEM of the Department of Biology, University of the Free State in Bloemfontein, South Africa. The analyses were carried out on respectively thin and doubly polished thick sections and epoxy resin-embedded samples composed of cassiterite or wolframite grains. Eight (8) of them were cassiterite, two (2) were wolframite samples from Kirimbari tungsten ore mine (ca. 20km NE of Rwinkwavu but within the same Rwinkwavu-Kirimbari anticlinal structure) and three were representative of the gangue minerals and the host rocks.

Approximately 200 qualitative and quantitative SEM-EDX analyses were performed on the 13 representative samples from Rwinkwavu mining area and the results of element abundances in oxide minerals and cations are displayed in Tables 4.1.5, 4.1.6 and 4.1.7, as well as in Appendix 4. Back-scattered electron images (BSE) were taken prior to analysis to study the internal structure of individual mineral grains. The SEM-EDX/WDX investigations carried out on the representative of the host rocks reveal the presence of quartz grains, zircon, muscovite, tourmaline, ilmenite, rutile, Fe-minerals (hematite/goethite) and small amounts of phosphate minerals in the mineral association. Ore minerals (cassiterite and wolframite), as the primary target of this study, were mineralogically and chemically characterized. Below follows a summary of the main mineralogical and chemical characteristics of cassiterite and wolframite from Rwinkwavu.

A. Mineral Chemistry of cassiterite

Chemical composition

Average chemical concentrations per sample of eight element oxides in the cassiterite samples were measured. Those are SnO₂, Nb₂O₅, Ta₂O₅, Fe₂O₃ [tot.], MnO, TiO₂, WO₃ and ZrO₂.

Tin oxide-SnO₂: Is the most abundant oxide in the Rwinkwavu cassiterite samples and thus representing 69 (Mount Rwinkwavu) to ca. 99 (wt. %) (Kizanye). Tin oxide content in the cassiterite samples from Migera and Gahengeri appears high in the range of 95-97 (wt. %).

Niobium oxide-Nb₂O₅: The majority of investigated samples have Nb₂O₅ concentration values between 0 and 1.4 wt. %. However, the cassiterite samples of Mount Rwinkwavu mine show relatively high Nb₂O₅ contents while those from Nyarunazi tin mine are Nb₂O₅-poor.

Tantalum oxide as Ta₂O₅: The Ta₂O₅ content in the Rwinkwavu cassiterite ranges from 0.11 to 1.273 (wt. %). Three out of eight investigated cassiterite samples have shown Ta₂O₅ contents to be around 0.4 (wt. %). The maximum chemical concentrations of this oxide have been measured in the samples from Mount Rwinkwavu and Gahengeri with respectively 1.273 and 0.914 (wt. %).

Six (6) cassiterites out of eight (8) sampled in Rwinkwavu showed Nb/Ta ratio values above the unity extending on a wide range of 1.4-26.3 and thus, illustrating the dominant Nb chemical contents on Ta while the two remaining samples Nb/Ta ratios are below 1 (0.4 and 0.6 respectively).

Total iron oxide as Fe₂O₃: The total iron oxide content values measured in the cassiterite samples are within 0.2-2 (wt. %) interval with the maximum concentrations found in the samples from Gahengeri and Mt Rwinkwavu.

Manganese oxide-MnO: The concentrations of MnO in the analyzed cassiterite samples are within 0.053 - 0.148 (wt. %) interval. The highest MnO contents have been recorded in the samples from Gahengeri [0.148 (wt. %)] and Migera [0.117 (wt. %)].

Titanium oxide-TiO₂: The analyses performed on cassiterite samples from Rwinkwavu reveal that the maximum TiO₂ content is displayed in samples from Gahengeri mining site with an average concentration of 0.4 (wt. %).

Tungsten oxide as WO₃: WO₃ contents in the investigated cassiterites range from 0.05 (Nyarunazi) to 0.5 (wt. %) (Gahengeri).

Zirconium oxide-ZrO₂: The contents of ZrO₂ in the cassiterite samples vary from 0.05 (Gahengeri) to around 0.5 (wt. %) (Mount Rwinkwavu)

The average chemical contents of analyzed tin- ore from Rwinkwavu are summarized in Table 4.1.3. The table indicates the maximum, the minimum, the average, the standard deviation and the low limit of detection (LLD) of each oxide-abundance. The concentrations are given in wt. %. The maximum value of SnO₂ [99.6 (wt. %)] has been measured in Gahengeri mine and the minimum concentration in SnO₂ (56.5 wt. %) occurs in mineralized muscovite-quartz veins of Mount Rwinkwavu. Taking into account the most common accessory oxides associated with cassiterite (Fe-, W-, Mn-, Ti-, Ta- and Nb- oxides), Gahengeri mine displays the maximum in total Fe₂O₃ (12.5 wt%), WO₃ (3.03 wt. %), MnO (0.7 wt. %), TiO₂ [ca. 1.1 (wt. %)] and Ta₂O₅ [5.2 (wt. %)] content. The maximum of Nb₂O₅ [1.4 (wt. %)] and ZrO₂ [2.2 (wt. %)] content have been measured in Kuyacumi mining site (Mount Rwinkwavu) while the samples from Nyabimuli show the highest HfO₂ content [1.3 (wt. %)]. The F,

Cl and P average contents in the investigated cassiterite-samples are respectively 0.4, 0.05 and 0.07 (wt. %). The Br is in traces.

Oxide	Average	Maximum	Minimum	Standard deviation	LLD*
WO ₃	0.2	3.0	0.0	0.5	0.30
Nb ₂ O ₅	0.2	1.4	0.0	0.3	0.23
Ta ₂ O ₅	0.5	5.2	0.0	0.8	0.54
P ₂ O ₅	0.1	2.1	0.0	0.3	0.00
I ₂ O ₅	0.1	1.2	0.0	0.2	-
SnO ₂	93.1	99.6	56.5	8.8	2.63
SiO ₂	2.0	25.0	0.0	5.2	-
TiO ₂	0.3	1.1	0.0	0.3	0.25
ZrO ₂	0.1	2.2	0.0	0.3	0.19
HfO ₂	0.1	1.3	0.0	0.2	0.06
GeO ₂	0.0	1.1	0.0	0.1	0.03
AmO ₂	0.4	5.5	0.0	1.4	-
ThO ₂	0.0	0.6	0.0	0.1	-
Fe ₂ O ₃	1.1	12.4	0.0	2.0	0.38
Y ₂ O ₃	0.1	1.0	0.0	0.2	0.04
Sc ₂ O ₃	0.1	0.8	0.0	0.2	0.01
In ₂ O ₃	0.1	5.1	0.0	0.7	0.05
Ga ₂ O ₃	0.0	1.2	0.0	0.1	0.06
Al ₂ O ₃	1.2	15.3	0.0	2.3	0.12
As ₂ O ₃	0.0	1.1	0.0	0.1	0.02
Sb ₂ O ₃	0.1	1.6	0.0	0.2	0.03
Ce ₂ O ₃	0.1	3.8	0.0	0.5	-
SrO	0.0	0.5	0.0	0.1	0.02
BaO	0.0	0.9	0.0	0.1	0.02
MnO	0.1	0.7	0.0	0.1	0.08
CaO	0.2	4.7	0.0	1.0	0.04
Rb ₂ O	0.0	0.6	0.0	0.1	0.02
Na ₂ O	0.3	2.4	0.0	0.6	0.03

Table 4.1.3: Summary of oxide contents in the cassiterite samples from Rwinkwavu area (number of samples = 8).
LLD*: low limit of detection

Pearson's correlation coefficient of major oxides in the cassiterite samples from Rwinkwavu

	WO ₃	Nb ₂ O ₅	Ta ₂ O ₅	SnO ₂	TiO ₂	ZrO ₂	Fe ₂ O ₃	Al ₂ O ₃	MnO
WO ₃	1	-.112	.670**	-.136	.074	.021	.632**	-.089	.146
Nb ₂ O ₅	-.112	1	-.138	-.294*	.244	.539**	.104	.582**	.012
Ta ₂ O ₅	.670**	-.138	1	-.461**	.079	-.136	.698**	.040	.122
SnO ₂	-.136	-.294*	-.461**	1	-.124	-.247	-.454**	-.645**	.018
TiO ₂	.074	.244	.079	-.124	1	.579**	.453**	.502**	.047
ZrO ₂	.021	.539**	-.136	-.247	.579**	1	.333*	.753**	-.097
Fe ₂ O ₃	.632**	.104	.698**	-.454**	.453**	.333*	1	.363**	.138
Al ₂ O ₃	-.089	.582**	.040	-.645**	.502**	.753**	.363**	1	-.039
MnO	.146	.012	.122	.018	.047	-.097	.138	-.039	1

** . Correlation is significant at the 0.01 level (2-tailed). Number of analyzed spots: 59.

* . Correlation is significant at the 0.05 level (2-tailed).

 : Positive correlation

 : Negative correlation

Table 4.1.4: Pearson's correlation coefficients for samples of cassiterite from Rwinkwavu (n = 8).

Table 4.1.4 indicates the values of Pearson's correlation coefficients. From the table, it is clear that negative and positive correlations between the distributions of different element-oxides in the cassiterite from Rwinkwavu exist.

Table 4.1.4 shows that tin oxide (SnO₂) correlates negatively with Fe₂O₃, Ta₂O₅ and Al₂O₃ while WO₃ and respectively Fe₂O₃ and Ta₂O₅ positively correlate. This may indicate the co-existence of substitution processes of Sn- by Fe-, Ta- and W- contained in the hydrothermal fluids and mutual substitution between those cations in the cassiterite structure.

However, the mass-balance between Al₂O₃ and SnO₂ should be attributed to the water-rich hydrothermal fluids/wall-rock interaction expressed in multiple types of hydrothermal alterations of the minerals associated with the cassiterite which consist in sericitization, muscovitization, tourmalinization and kaolinization (in the study area).

There is a positive correlation between Nb₂O₅ and Al₂O₃. The correlation between SnO₂ and TiO₂; Fe₂O₃ and MnO respectively is poor or non-existent.

Geochemical trends in cassiterite

The diagrams displayed in Figure 4.9 show evolutionary trends of chemical components in cassiterite from Rwinkwavu: in the upper part, Fe_2O_3 and Ta_2O_5 contents increase when WO_3 is increasing. Moreover, the same figure, but in the lower part, indicates positive trends between Fe_2O_3 and respectively Ta_2O_5 and TiO_2 .

These variation trends in increasing-decreasing of oxide concentrations along cassiterite samples from Rwinkwavu illustrated by the discrimination diagrams below are possibly a consequence of geochemical variations which will be discussed in chapter 6.

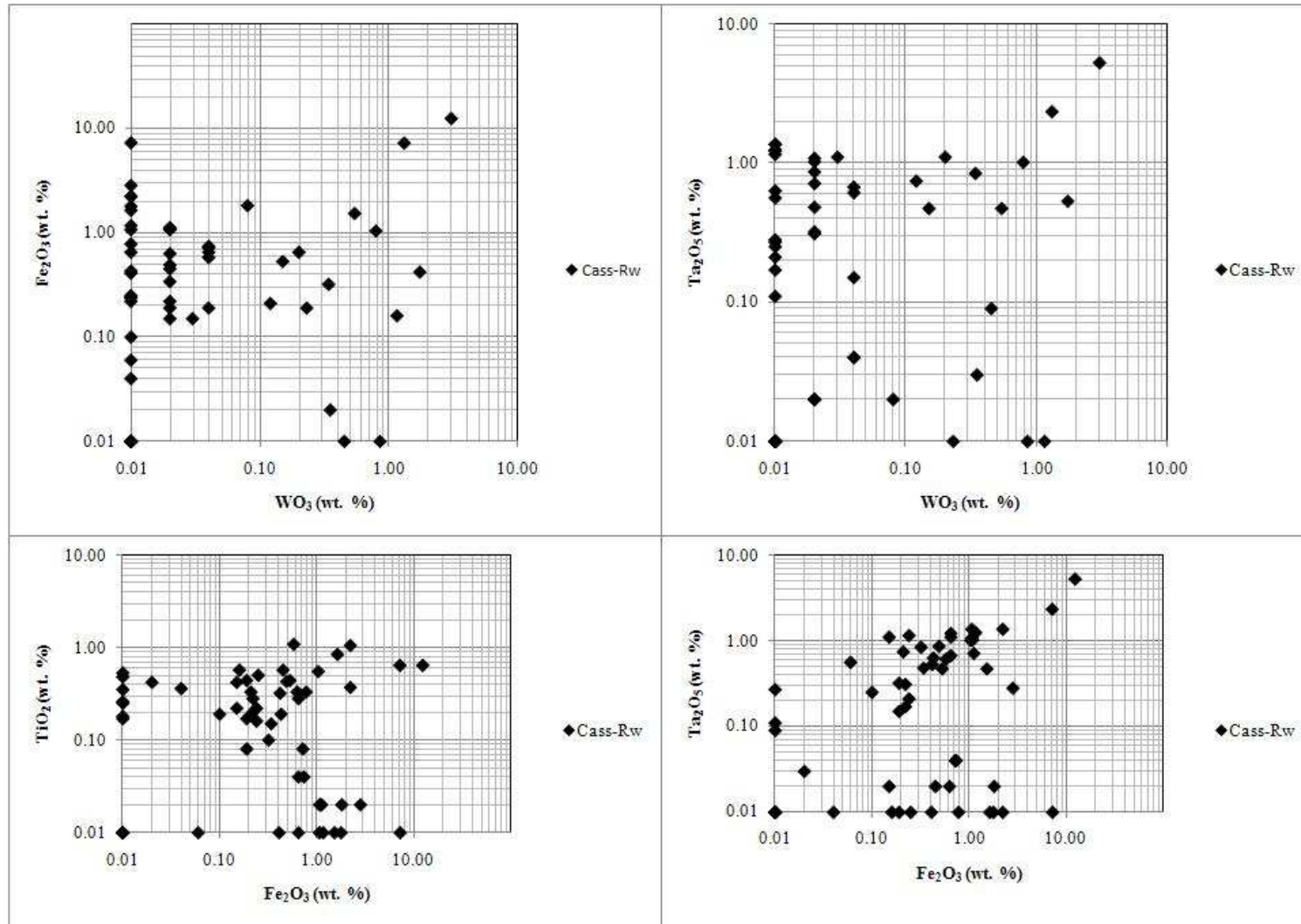


Figure 4.9: Discrimination diagrams of major element oxides in cassiterite from Rwinkwavu mines using WO_3 vs. Ta_2O_5 and Fe_2O_3 (upper 2 graphs) and Fe_2O_3 vs. Ta_2O_5 and TiO_2 correlations (lower 2 graphs).

Table 4.1.5: Chemical composition of selected cassiterite samples from Rwinkwavu.

Sample	JC-GHR					JC-NYZ					JC-38						JC-455
Spot	2	4	5	15	19	2	4	5	6	7	2	3	5	6	7	8	5
WO ₃	0.0	0.0	0.0	0.0	0.0	0.0	0.0	0.0	0.0	0.2	0.0	0.0	0.0	0.0	0.0	0.1	0.0
Nb ₂ O ₅	0.1	0.0	0.6	0.1	0.0	0.0	0.0	0.0	0.0	0.0	0.1	0.4	0.0	0.2	0.5	0.0	0.3
Ta ₂ O ₅	0.0	0.7	0.2	0.0	0.6	0.7	0.9	1.0	1.1	1.1	1.1	0.0	0.3	0.5	0.0	0.7	0.3
P ₂ O ₅	0.0	0.0	0.0	0.0	0.0	0.0	0.0	0.0	0.0	0.0	0.0	0.0	0.0	0.0	0.0	0.0	0.0
I ₂ O ₅	0.0	0.0	0.0	0.0	0.0	1.2	0.2	0.9	0.6	0.3	0.0	0.0	0.0	0.0	0.0	0.0	0.0
SnO ₂	97.5	96.9	98.9	99.1	96.7	82.8	90.3	90.2	91.2	80.7	98.2	98.5	99.3	98.6	98.4	98.6	98.9
SiO ₂	0.0	0.0	0.0	0.0	0.0	6.1	0.0	0.0	0.0	4.5	0.0	0.0	0.0	0.0	0.0	0.0	0.0
TiO ₂	0.0	0.0	0.2	0.1	1.1	0.0	0.4	0.0	0.0	0.3	0.4	0.6	0.1	0.2	0.2	0.3	0.2
ZrO ₂	0.1	0.0	0.0	0.0	0.0	0.0	0.0	0.0	0.0	0.0	0.0	0.0	0.0	0.0	0.0	0.0	0.0
HfO ₂	0.0	0.0	0.0	0.0	0.0	0.0	0.0	0.0	0.0	0.0	0.0	0.0	0.0	0.0	0.0	0.0	0.0
GeO ₂	0.0	0.0	0.0	0.0	0.0	0.0	0.0	0.0	0.0	0.0	0.0	0.0	0.0	0.0	0.0	0.0	0.0
AmO ₂	0.0	0.0	0.0	0.0	0.0	0.0	4.8	5.1	4.8	5.5	0.0	0.0	0.0	0.0	0.0	0.0	0.0
ThO ₂	0.0	0.0	0.0	0.0	0.0	0.6	0.0	0.0	0.0	0.0	0.0	0.0	0.0	0.0	0.0	0.0	0.0
Fe ₂ O ₃	0.7	0.7	0.2	0.7	0.6	1.1	0.5	1.1	1.1	0.7	0.2	0.5	0.2	0.3	0.2	0.2	0.2
Y ₂ O ₃	0.0	0.0	0.0	0.0	0.0	0.0	0.0	0.0	0.0	0.0	0.0	0.0	0.0	0.0	0.0	0.0	0.0
Sc ₂ O ₃	0.0	0.0	0.0	0.0	0.0	0.7	0.0	0.8	0.8	0.1	0.0	0.0	0.0	0.0	0.0	0.0	0.0
In ₂ O ₃	0.0	0.0	0.0	0.0	0.0	0.0	0.0	0.0	0.0	0.0	0.0	0.0	0.0	0.0	0.0	0.0	0.0
Ga ₂ O ₃	0.0	0.0	0.0	0.0	0.0	0.0	0.0	0.0	0.0	0.0	0.0	0.0	0.0	0.0	0.0	0.0	0.0
Al ₂ O ₃	1.5	1.7	0.0	0.0	1.0	2.9	1.6	0.8	0.5	0.4	0.0	0.0	0.0	0.0	0.7	0.0	0.0
As ₂ O ₃	0.0	0.0	0.0	0.0	0.0	0.0	0.0	0.0	0.0	0.0	0.0	0.0	0.0	0.0	0.0	0.0	0.0
Sb ₂ O ₃	0.0	0.0	0.0	0.0	0.0	0.0	0.0	0.0	0.0	0.0	0.0	0.0	0.0	0.0	0.0	0.0	0.0
Ce ₂ O ₃	0.0	0.0	0.0	0.0	0.0	3.8	1.1	0.0	0.0	0.0	0.0	0.0	0.0	0.0	0.0	0.0	0.0
SrO	0.0	0.0	0.0	0.0	0.0	0.0	0.0	0.0	0.0	0.0	0.0	0.0	0.0	0.0	0.0	0.0	0.0

(continued on page 62)

Table 4.1.5 (continued)

Sample	JC-GHR					JC-NYZ					JC-38						JC-455
Spot	2	4	5	15	19	2	4	5	6	7	2	3	5	6	7	8	5
BaO	0.0	0.0	0.0	0.0	0.0	0.0	0.0	0.0	0.0	0.0	0.0	0.0	0.0	0.0	0.0	0.0	0.0
MnO	0.0	0.1	0.0	0.0	0.0	0.0	0.0	0.0	0.0	0.0	0.0	0.1	0.1	0.2	0.0	0.0	0.1
CaO	0.0	0.0	0.0	0.0	0.0	0.0	0.0	0.0	0.0	0.0	0.0	0.0	0.0	0.0	0.0	0.0	0.0
Rb ₂ O	0.0	0.0	0.0	0.0	0.0	0.0	0.0	0.0	0.0	0.0	0.0	0.0	0.0	0.0	0.0	0.0	0.0
Na ₂ O	0.0	0.0	0.0	0.0	0.0	0.0	0.0	0.0	0.0	0.0	0.0	0.0	0.0	0.0	0.0	0.0	0.0
Au	0.0	0.0	0.0	0.0	0.0	0.0	0.2	0.0	0.0	0.0	0.0	0.0	0.0	0.0	0.0	0.0	0.0
Cl	0.0	0.0	0.0	0.0	0.0	0.0	0.0	0.0	0.0	0.0	0.0	0.0	0.0	0.0	0.0	0.0	0.0
F	0.0	0.0	0.0	0.0	0.0	0.0	0.0	0.0	0.0	6.3	0.0	0.0	0.0	0.0	0.0	0.0	0.0
Tot.	100.8	100.7	100.8	100.8	100.8	100.4	100.4	100.5	100.5	100.3	100.5	100.5	100.5	100.5	100.5	100.5	100.0

Number of cations based on 2 oxygens

W	0.00	0.00	0.00	0.00	0.00	0.00	0.00	0.00	0.00	0.001	0.00	0.000	0.00	0.00	0.000	0.001	0.000
Nb	0.001	0.000	0.006	0.001	0.000	0.000	0.000	0.000	0.000	0.000	0.001	0.004	0.000	0.003	0.006	0.000	0.004
Ta	0.000	0.005	0.001	0.000	0.004	0.005	0.006	0.007	0.007	0.007	0.007	0.000	0.002	0.003	0.000	0.005	0.002
P	0.001	0.001	0.001	0.001	0.001	0.000	0.000	0.000	0.000	0.000	0.000	0.000	0.000	0.000	0.000	0.000	0.000
I	0.000	0.000	0.000	0.000	0.000	0.012	0.002	0.009	0.006	0.003	0.000	0.000	0.000	0.000	0.000	0.000	0.000
Sn	0.967	0.960	0.981	0.982	0.959	0.821	0.895	0.894	0.904	0.799	0.973	0.977	0.984	0.977	0.975	0.977	0.980
Si	0.001	0.001	0.001	0.001	0.001	0.152	0.000	0.000	0.000	0.112	0.000	0.000	0.000	0.000	0.000	0.000	0.000
Ti	0.001	0.001	0.003	0.001	0.020	0.000	0.008	0.000	0.000	0.005	0.008	0.011	0.001	0.003	0.004	0.006	0.004
Zr	0.001	0.000	0.000	0.000	0.000	0.000	0.000	0.000	0.000	0.000	0.000	0.000	0.000	0.000	0.000	0.000	0.000
Hf	0.000	0.000	0.000	0.000	0.000	0.000	0.000	0.000	0.000	0.000	0.000	0.000	0.000	0.000	0.000	0.000	0.000
Ge	0.00	0.000	0.000	0.000	0.000	0.000	0.000	0.000	0.000	0.000	0.000	0.000	0.000	0.000	0.000	0.000	0.000
Am	0.000	0.000	0.000	0.000	0.000	0.000	0.026	0.028	0.026	0.030	0.000	0.000	0.000	0.000	0.000	0.000	0.000

Table 4.1.5 (continued)

Sample	JC-GHR					JC-NYZ					JC-38						JC-455
Spot	2	4	5	15	19	2	4	5	6	7	2	3	5	6	7	8	5
Th	0.000	0.000	0.000	0.000	0.00	0.003	0.000	0.000	0.000	0.000	0.000	0.000	0.000	0.000	0.000	0.000	0.000
Fe	0.014	0.012	0.004	0.013	0.01	0.021	0.009	0.020	0.020	0.012	0.003	0.008	0.004	0.006	0.003	0.004	0.004
Y	0.001	0.001	0.001	0.001	0.00	0.000	0.000	0.000	0.000	0.000	0.000	0.000	0.000	0.000	0.000	0.000	0.000
Sc	0.000	0.000	0.000	0.000	0.00	0.016	0.000	0.017	0.017	0.002	0.000	0.000	0.000	0.000	0.000	0.000	0.000
In	0.000	0.000	0.000	0.000	0.000	0.000	0.000	0.000	0.000	0.000	0.000	0.000	0.000	0.000	0.000	0.000	0.000
Ga	0.001	0.001	0.001	0.001	0.001	0.000	0.000	0.000	0.000	0.000	0.000	0.000	0.000	0.000	0.000	0.000	0.000
Al	0.044	0.050	0.001	0.001	0.030	0.085	0.045	0.024	0.013	0.010	0.001	0.001	0.001	0.001	0.020	0.001	0.000
As	0.001	0.001	0.001	0.001	0.001	0.000	0.000	0.000	0.000	0.000	0.000	0.000	0.000	0.000	0.000	0.000	0.000
Sb	0.000	0.000	0.000	0.000	0.000	0.000	0.000	0.000	0.000	0.000	0.000	0.000	0.000	0.000	0.000	0.000	0.000
Ce	0.000	0.000	0.000	0.000	0.000	0.035	0.010	0.000	0.000	0.000	0.000	0.000	0.000	0.000	0.000	0.000	0.000
Sr	0.001	0.001	0.001	0.001	0.001	0.000	0.000	0.000	0.000	0.000	0.000	0.000	0.000	0.000	0.000	0.000	0.000
Ba	0.000	0.000	0.000	0.000	0.000	0.000	0.000	0.000	0.000	0.000	0.000	0.000	0.000	0.000	0.000	0.000	0.000
Mn	0.001	0.002	0.001	0.001	0.001	0.000	0.000	0.000	0.000	0.000	0.000	0.001	0.002	0.004	0.000	0.000	0.002
Ca	0.000	0.000	0.000	0.000	0.000	0.000	0.001	0.001	0.001	0.001	0.001	0.001	0.001	0.001	0.001	0.001	0.000
Rb	0.001	0.001	0.001	0.001	0.001	0.000	0.000	0.000	0.000	0.000	0.000	0.000	0.000	0.000	0.000	0.000	0.000
Na	0.002	0.002	0.002	0.002	0.002	0.001	0.001	0.001	0.001	0.001	0.001	0.001	0.001	0.001	0.001	0.001	0.000
ΣCat.	1.038	1.039	1.006	1.010	1.034	1.155	1.008	1.006	1.000	0.988	1.000	1.008	1.001	1.003	1.015	1.001	0.995
Nb/Ta	4.988	0.074	6.319	4.988	0.109	0.047	0.039	0.033	0.031	0.030	0.151	33.256	0.104	0.831	44.895	0.045	1.824
Nb+Ta	0.002	0.005	0.007	0.002	0.005	0.005	0.006	0.007	0.008	0.008	0.009	0.005	0.002	0.006	0.006	0.005	0.006
Fe+Mn	0.015	0.014	0.004	0.014	0.012	0.021	0.010	0.021	0.020	0.013	0.003	0.009	0.006	0.010	0.003	0.004	0.006
(Nb+Ta)/Sn*	0.00	0.01	0.01	0.00	0.00	0.01	0.01	0.01	0.01	0.01	0.01	0.00	0.00	0.01	0.01	0.01	0.01
log(*)	-2.78	-2.30	-2.12	-2.78	-2.32	-2.21	-2.17	-2.10	-2.08	-2.02	-2.06	-2.32	-2.62	-2.22	-2.20	-2.27	-2.22
(Fe+Mn)/Sn**	0.02	0.01	0.00	0.01	0.01	0.03	0.01	0.02	0.02	0.02	0.00	0.01	0.01	0.01	0.00	0.00	0.01
log(**)	-1.82	-1.84	-2.35	-1.84	-1.91	-1.59	-1.97	-1.63	-1.65	-1.80	-2.48	-2.01	-2.24	-1.98	-2.48	-2.35	-2.23
W/Sn	0.00	0.00	0.00	0.00	0.00	0.00	0.00	0.00	0.00	0.00	0.00	0.00	0.00	0.00	0.00	0.00	0.00
log(W/Sn)	-3.57	-3.57	-3.58	-3.58	-3.57	-3.80	-3.84	-3.84	-3.85	-2.79	-3.70	-3.88	-3.88	-3.88	-3.88	-3.10	-3.88

Relationship among Ta, Nb, W, Fe, Mn distribution in cassiterite mineralization of Rwinkwavu

Table 4.1.5 summarizes the results from SEM-EDX analyses of selected cassiterite samples in atoms per formula unit (apfu) which have been used in (Fe+Mn) vs. (Ta+Nb) [Figure 4.10] and (Fe+Mn) vs. W [Figure 4.11] discrimination diagram after Möller et al. (1988).

In order to exclude various types of mainly siliceous impurities within the samples from various mineral occurrences, the ratio (Ta+Nb)/ (Fe+Mn) was used for the discussion and this is illustrated in Figure 4.10.

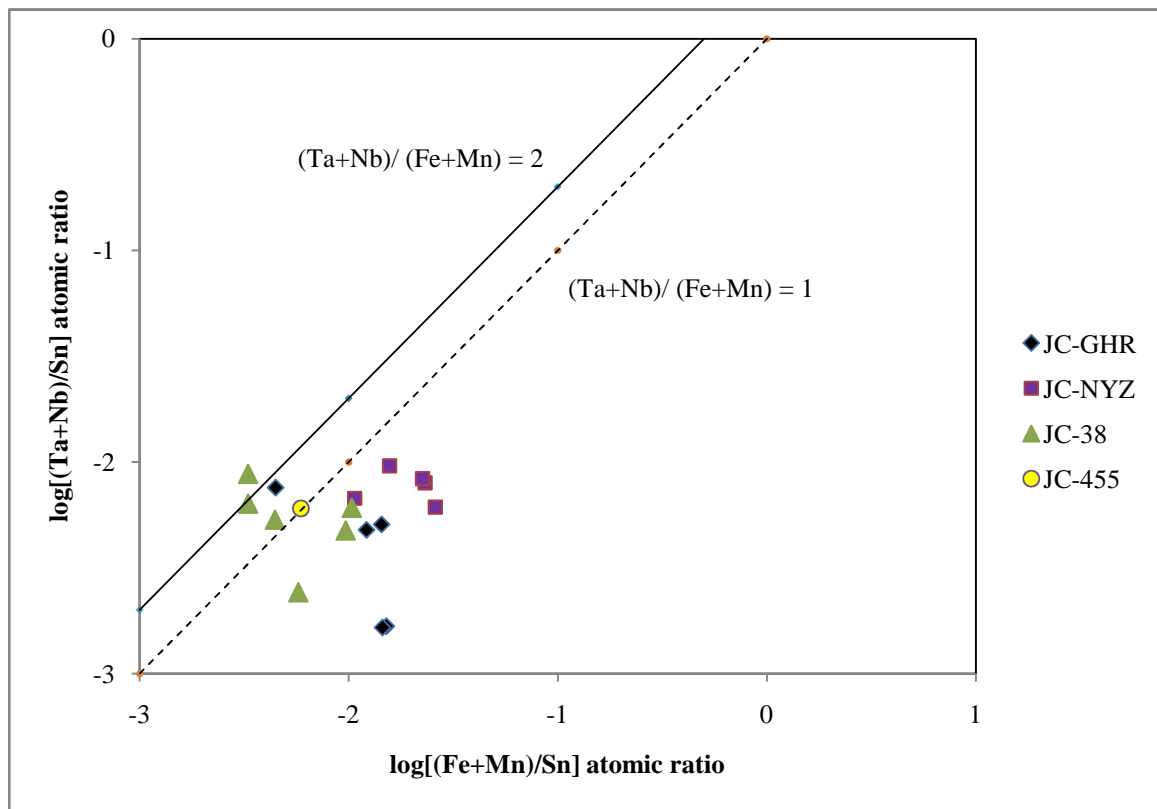


Figure 4.10: Correlation diagram of cassiterite samples of Rwinkwavu using $\log [(Ta+Nb)/Sn]$ vs. $\log [(Fe+Mn)/Sn]$ after Möller et al. (1988).

Figure 4.10 plotted and interpreted after Möller et al. (1988) shows the discrimination diagram of (Fe+Mn) vs. (Ta+Nb) for the selected investigated cassiterite samples from Rwinkwavu expressed in apfu. It shows a poor correlation between Ta+Nb and Fe+Mn. If the element contents are assumed to be due to contamination by mineral inclusions of the type (Fe, Mn) (Ta, Nb)₂O₆, then, a correlation along the line which indicates the atomic ratio (Ta+Nb)/(Fe+Mn) = 2 should be expected.

However, the majority of investigated spots fall below a line that indicates an atomic ratio (Ta+Nb)/(Fe+Mn) = 2. There is, thus, a clear excess of (Fe+Mn) content which could indicate the presence in

cassiterite crystals of an Fe-rich inclusion testifying to the possible substitution between Sn and Fe based on the $\text{Sn}^{4+} \leftrightarrow \text{Fe}^{3+} + \text{H}^+$ or $\text{Sn}^{4+} + \text{O}^{2-} \leftrightarrow \text{Fe}^{3+} + \text{OH}^-$ substitution law.

The remaining three spots are plotting along the line $(\text{Ta}+\text{Nb})/(\text{Fe}+\text{Mn}) = 2$ indicating that $(\text{Ta}+\text{Nb})$ content in cassiterite is controlled by the solid inclusions of the type $(\text{Fe}, \text{Mn})(\text{Ta}, \text{Nb})_2\text{O}_6$ and therefore, follows the substitution law of the type $3 \text{Sn}^{4+} \leftrightarrow 2 (\text{Ta}, \text{Nb})^{5+} + (\text{Fe}, \text{Mn})^{2+}$.

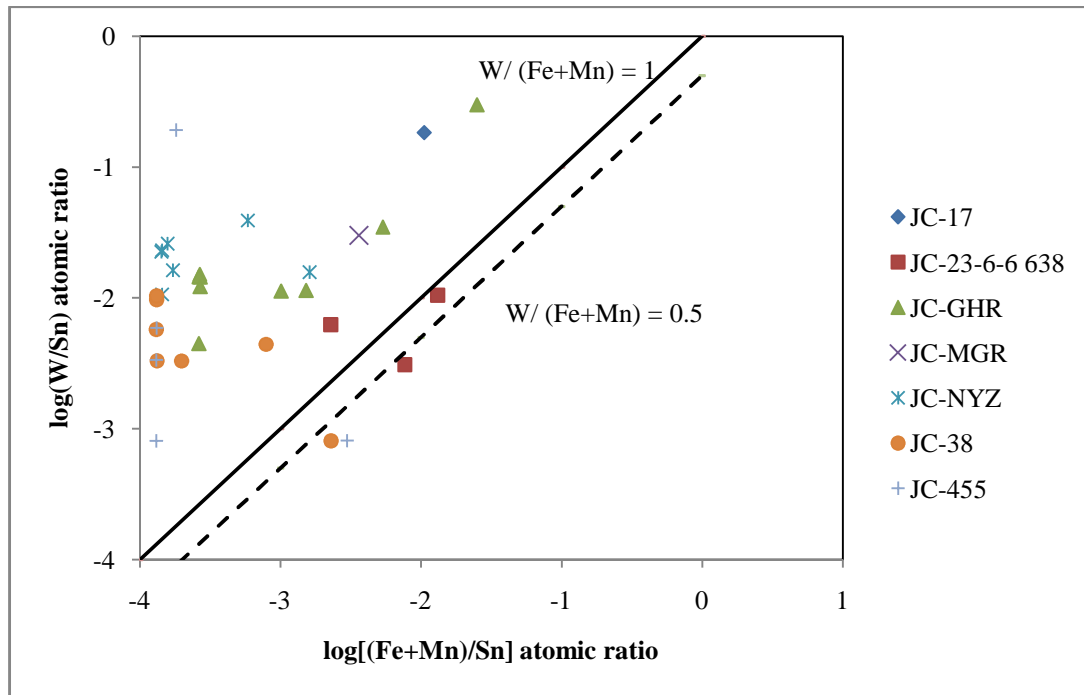


Figure 4.11: Correlation diagram for selected cassiterite samples using $\log [W/Sn]$ vs. $\log [(Fe+Mn)/Sn]$ after Möller et al. (1988).

The correlation diagram of Figure 4.11 shows a poor positive correlation of $(\text{Fe}+\text{Mn})$ with W . The field survey did not show any out-crop of felsic igneous rocks generating the rare element ores such as cassiterite and wolframite exploited in Rwinkwavu. Therefore, all the cassiterite samples were hand-picked from either muscovite-sericite-quartz veins originated from B-rich hydrothermal fluids (tourmalinization of the host meta-sedimentary rocks on 20cm to 40cm) or from placers and thus, may represent the cassiterites crystallized under hydrothermal conditions. Figure 4.11 was adapted from Möller et al. (1988) and reflects the data from Table 4.1.5 where the values of W/Sn and $(\text{Fe}+\text{Mn})$ taken into account are those which are above zero. Apart from the analyzed points of the only cassiterite sample JC-23-6-6 638 from Gahengeri which is plotted along the line of atomic ratio $W/(\text{Fe}+\text{Mn}) = 1$ and thus, indicating the presence of wolframite in solid inclusions, the all remaining samples fall above the diagonal line of equation $W/(\text{Fe}+\text{Mn}) = 1$. Contrarily to the previous correlation diagram (Figure 4.10) W content occurs in evident excess instead of $\text{Fe}+\text{Mn}$ and consequently, $(\text{Fe}+\text{Mn})$ seems to be independent from contamination of the type $(\text{Fe}, \text{Mn})\text{WO}_4$. This

might indicate that the substitution of the type $\text{Sn}^{4+} \leftrightarrow \text{W}^{4+}$ predominates in the cassiterite samples from Rwinkwavu.

B. Mineral Chemistry of Wolframite

As indicated in section 4.1.3, Nyamuyorwa is the only tungsten ore deposit in the nearby vicinity of Mount Rwinkwavu. Unfortunately, due to technical problems, the mining activities in the Nyamuyorwa tungsten ore deposit were stopped several months before the June-August field trip and hence, there is a lack of representative wolframite samples from the above mentioned site.

However, two wolframite samples from a primary quartz vein were hand-picked and analyzed using the SEM-EDX facilities of the Department of Geology, University of the Free State, Bloemfontein, South Africa. It is assumed that the chemical and mineralogical characteristics of both wolframite mineral deposits (Nyamuyorwa and Kirimbari) may show similarities, firstly based on the similar geological contexts of the quartz vein type ore deposits, the location in the same Rukira formation and within the same Kirimbari-Rwinkwavu anticlinal structure and secondary, the absence of outcrop of rare metal parental granite.

A summary of the 16 chemical analyses performed on JC-KRM and 13 cassiterite grains that were investigated on JC-KRM-1 676, is presented in Table 4.1.6. Appendix 4 is an overview of the mineral chemistry of the whole sample. It indicates that besides the tungsten ore, the paragenetic sequence also reveals inclusions of quartz, muscovite, biotite, tourmaline, garnets, ilmenite, Fe- minerals which may correspond to hematite and/or goethite and small amounts of apatite.

The 29 analyses of the wolframite samples show 3 dominant oxides:

1. **Tungsten oxide- WO_3 :** WO_3 contents range from 39 to 76.7 wt. %
2. **Total Iron oxide- Fe_2O_3 :** Fe_2O_3 ranges between 19.9 and 59.88 wt. %
3. **Manganese oxide- MnO :** measured contents are enclosed in 0.2-5.3 wt. % interval.

Additional to these 3 element oxides, small amounts of Br, P_2O_5 , Al_2O_3 , Ta_2O_5 , SnO_2 , CaO and MgO were identified and quantified in some of the selected spots of the investigated wolframite samples.

The bulk chemical formulae of selected analyses were calculated and are displayed in Table 4.1.7. The average formula for the wolframite sample from Kirimbari should be written as follows: $\text{Al}_{0.015}\text{Mg}_{0.114}\text{Ca}_{0.004}\text{Mn}_{0.094}\text{Fe}_{0.960}\text{W}_{0.843}\text{O}_4$ and Fe- content is dominant. Such results are indicating that the investigated wolframite samples are ferberites.

Table 4.1.6: Chemical composition of selected wolframite samples from Rwinkwavu – Kirimbari (Sample JC-KRM) using SEM-EDX/WDX.

Analysis	5	6	7	8	9	10	11	12	13	16	17	18	20	21	23	28
WO ₃	74.1	73.9	74.9	74.8	68.6	67.6	68.5	75.5	68.8	76.7	68.2	58.9	71.6	41.1	73.7	73.2
MnO	5.3	1.1	3.8	4.7	-	2.8	0.4	3.1	0.2	3.0	2.4	-	5.3	0.9	3.6	1.4
Fe ₂ O ₃	19.9	24.6	21.1	20.1	30.2	28.9	29.6	21.3	29.7	20.3	28.9	36.5	20.6	56.8	22.2	25.4
CaO	0.2	-*	-	-	-	0.3	-	0.1	0.1	-	0.2	-	0.2	-	0.2	-
MgO	0.3	0.3	0.2	0.1	0.2	0.3	0.0	-	0.3	-	0.2	-	0.4	-	0.3	-
Ta ₂ O ₅	-	-	0.0	0.3	1.0	-	1.2	-	0.9	-	0.2	-	1.9	0.3	-	-
SnO ₂	0.2	-	-	-	-	-	0.2	0.0	-	-	-	-	-	-	-	-
Al ₂ O ₃	-	-	-	-	-	-	-	-	-	-	-	4.5	-	-	-	-
Br	-	-	-	-	-	-	-	-	-	-	-	-	-	0.8	-	-
Number of cations based on 4 oxygens																
W	0.900	0.898	0.909	0.909	0.833	0.821	0.832	0.917	0.835	0.931	0.829	0.716	0.870	0.499	0.895	0.889
Mn	0.209	0.046	0.152	0.187	-	0.111	0.015	0.123	0.010	0.119	0.094	-	0.211	0.037	0.141	0.055
Fe	0.702	0.867	0.743	0.707	1.064	1.019	1.044	0.749	1.047	0.716	1.017	1.287	0.725	2.001	0.782	0.895
Ca	0.009	-	-	-	-	0.016	-	0.007	0.005	-	0.008	-	0.009	-	0.012	-
Mg	0.021	0.020	0.013	0.007	0.012	0.022	0.002	-	0.019	-	0.013	-	0.030	-	0.024	-
Ta	-	-	0.000	0.003	0.013	-	0.016	-	0.012	-	0.002	-	0.024	0.004	-	-
Sn	0.004	-	-	-	-	-	0.003	0.000	-	-	-	-	-	-	-	-
Al	-	-	-	-	-	-	-	-	-	-	-	0.249	-	-	-	-
∑Cat.	1.71	1.71	1.7	1.7	1.79	1.853	1.782	1.692	1.787	1.664	1.835	2.12	1.71	2.39	1.72	1.73

-*: Not detected.

Table 4.1.7: Determination of the bulk chemical formulae of selected wolframite samples from Kirimbari (JC-KRM and JC-KRM-1 676): **JC-KRM.**

Spot	W	Mn	Fe	Ca	Mg	Ta	Sn	Al	Bulk chemical formulae
5	0.90024	0.20913	0.70189	0.00906	0.02113	-	0.00355	-	Mn _{0.21} Fe _{0.7} W _{0.9} O ₄
6	0.89782	0.04563	0.86742	-	0.02043	-	-	-	Mn _{0.04} Fe _{0.87} W _{0.9} O ₄
7	0.90935	0.15159	0.74310	-	0.01338	0.00013	-	-	Mn _{0.15} Fe _{0.74} W _{0.9} O ₄
8	0.90874	0.18730	0.70682	-	0.00704	0.00344	-	-	Mn _{0.2} Fe _{0.7} W _{0.9} O ₄
9	0.83309	-	1.06429	-	0.01197	0.01275	-	-	Mg _{0.01} Ta _{0.01} Fe _{1.1} W _{0.8} O ₄
10	0.82143	0.11071	1.01850	0.01610	0.02184	-	-	-	Ca _{0.02} Mn _{0.11} Fe ₁ W _{0.8} O ₄
11	0.83224	0.01508	1.04421	-	0.00211	0.01555	0.00336	-	Ta _{0.01} Mn _{0.01} Fe ₁ W _{0.8} O ₄
12	0.91664	0.12301	0.74944	0.00654	-	-	0.00019	-	Mn _{0.12} Fe _{0.75} W _{0.9} O ₄
13	0.83515	0.00952	1.04668	0.00503	0.01902	0.01160	-	-	Ca _{0.005} Mg _{0.02} Ta _{0.01} Mn _{0.01} FeW _{0.8} O ₄
16	0.93109	0.11865	0.71633	-	-	-	-	-	Mn _{0.12} Fe _{0.7} W _{0.93} O ₄
17	0.82884	0.09365	1.01709	0.00805	0.01268	0.00217	-	-	Mn _{0.1} Fe ₁ W _{0.8} O ₄
18	0.71577	-	1.28722	-	-	-	-	0.24915	Al _{0.25} Fe _{1.29} W _{0.72} O ₄
20	0.86976	0.21111	0.72549	0.00906	0.02958	0.02384	-	-	Mn _{0.21} Fe _{0.7} W _{0.87} O ₄
21	0.49888	0.03730	2.00144	-	-	0.00370	-	-	Mn _{0.04} Fe ₂ W _{0.5} O ₄
23	0.89454	0.14127	0.78184	0.01207	0.02395	-	-	-	Mn _{0.14} Fe _{0.8} W _{0.9} O ₄
28	0.88907	0.05476	0.89524	-	-	-	-	-	Ca _{0.01} Mg _{0.02} Mn _{0.05} Fe _{0.9} W _{0.8} O ₄
	0.84267	0.09429	0.96044	0.00412	0.01145	0.00457	0.00044	0.01557	Avg bulk formulae for wolfr.*

*Bulk chemical formula of the tungsten ore in Kirimbari (JC-KRM):



JC-KRM-1 676

	14	15	16	17	19	21	22	23	26	27	28	29	34
Na ₂ O	-	-	-	0.62	-	-	-	-	-	-	0.69	-	-
Al ₂ O ₃	-	-	-	-	-	-	-	-	-	1.04	-	-	-
K ₂ O	-	-	-	0.23	-	-	-	-	-	-	-	-	-
CaO	1.03	0.33	5	0.44	-	0.29	-	-	-	-	-	-	-
MnO	5.24	3.55	-	3.88	2.32	3.14	2.01	-	2.07	-	0.99	0.79	2.95
Fe ₂ O ₃	26.56	26.5	38.07	26.82	33.64	31.66	28.9	31.29	28.34	59.88	42.22	25.57	26.9
WO ₃	64.62	68.71	56.93	66.21	62.82	63.14	69.09	68.71	68.62	39.08	52.88	72.56	68.75
P ₂ O ₅	2.18	0.92	-	1.57	1.22	1.05	-	-	0.97	-	1.03	1.08	1.41
Yb ₂ O ₃	0.36	-	-	0.24	-	0.74	-	-	-	-	-	-	-
Br	-	-	-	-	-	-	-	-	-	-	2.19	-	-
Number of cations based on 4 oxygens													
Na	-	-	-	0.053	-	-	-	-	-	-	0.059	-	-
Al	-	-	-	-	-	-	-	-	-	0.054	-	-	-
K	-	-	-	0.013	-	-	-	-	-	-	-	-	-
Ca	0.049	0.016	0.237	0.021	-	0.014	-	-	-	-	-	-	-
Mn	0.196	0.133	-	0.145	0.087	0.117	0.075	-	0.077	-	0.037	0.03	0.11
Fe	0.881	0.879	1.263	0.89	1.116	1.05	0.959	1.038	0.94	1.987	1.401	0.848	0.893
W	0.739	0.786	0.651	0.757	0.719	0.722	0.79	0.786	0.785	0.447	0.605	0.83	0.787
P	0.081	0.034	-	0.059	0.046	0.039	-	-	0.036	-	0.039	0.04	0.053
Yb	0.009	-	-	0.006	-	0.018	-	-	-	-	-	-	-
ΣCat.	1.955	1.848	2.151	1.944	1.967	1.961	1.824	1.824	1.839	2.488	2.14	1.748	1.842

The formula for wolframite is (Mn, Fe)WO₄. For the better chemical characterization of the two wolframite samples from Kirimbari-Rwinkwavu anticline, a discrimination diagram of Fe-ferberite (in apfu) on the x-axis, against Mn-huebnerite (in apfu) on the y-axis, was plotted (Figure 4.12).

This formula will be correct in the case of the distribution of the analyzed spots along the line which corresponds to $Mn/Fe = 1$. Contrarily, all the analyses are plotting far below the $Mn/Fe = 1$ line and most of them plot below the line $Mn/Fe = 0.25$, indicating that Fe- end members are highly dominant and therefore, indicates that the analysed wolframite is a ferberite. A negative trend exists which points towards the members of a solid solution with substitution scheme between Fe and Mn.

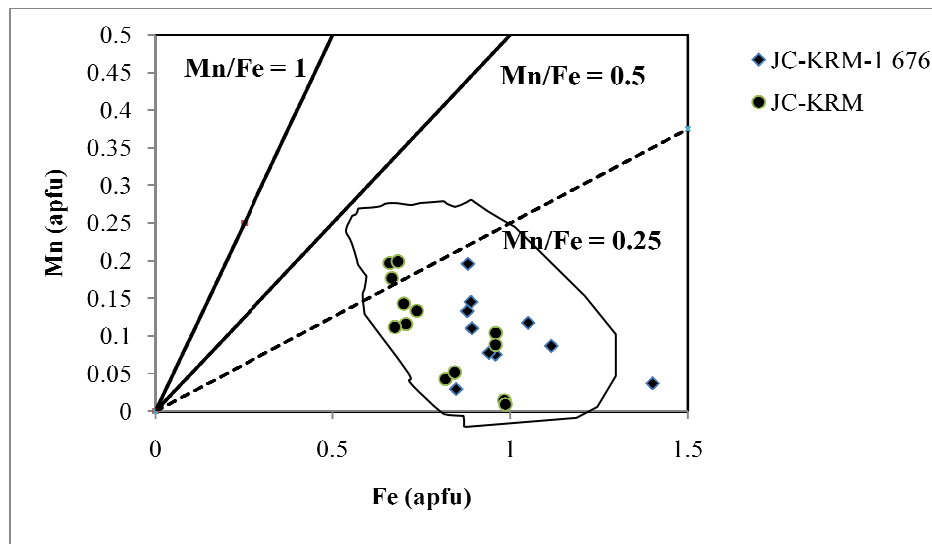


Figure 4.12: Binary plot of Fe vs. Mn (in apfu) for wolframite data from the study area.

4.2 MUSHA-NTUNGA PROSPECT

The Musha-Ntunga mining concession is located south of lake Muhazi, in the Rwamagana District, Eastern Province, between $30^{\circ}19'48''$ and $30^{\circ}25'20''E$ and $1^{\circ}52'46''$ and $1^{\circ}59'50''S$ and 7km west of Rwamagana, the capital city of the Eastern Province.

The concession is divided into two main zones: Ntunga cassiterite mine and Musha known for both cassiterite and coltan mineralization. The total area of the concession has been estimated to 5,272 ha (4,562 ha for Musha and 710 ha for Ntunga).

Since 2008, Rwanda Metals is carrying out intense exploratory works in Ntunga. Musha is owned by Rwanda Minerals Mining. The Musha-Ntunga mineral district is limited by four other mining districts: Bugarura-Kuluti (north) and Rwinkwavu (east) discussed in this study and Mugesera-Bugesera (south) and Rutongo (west).

Similar to the Rwinkwavu and Bugarura-Kuluti mining concessions, the field work was carried out in the Musha-Ntungwa mineral district from late June to late August 2010. Lithological units, intrusive bodies and tectonic features were mapped. In addition, samples were collected for petrographic and geochemical investigations using the preparation lab, XRF, fluid stage and SEM-EDX/WDX at the Department of Geology of the University of the Free State.

4.2.1 Geological setting

Baudet et al. (1989) and Theunissen et al. (1991) indicate that the rocks found in the Musha-Ntungwa area are of Mesoproterozoic age and belong to the lower and middle part of the Rwanda Supergroup (Gikoro and Pindura Groups). Weathered meta-sedimentary successions locally dominated by tourmaline muscovite schists and sandstones lie underneath a thick layer of lateritic cover with a thickness averaging 10m. Pegmatites and pegmatitic-type vein swarms, which are now highly kaolinized, intrude into those rocks. The details of the stratigraphic units are described below (in sequence from oldest to the youngest formation) after Baudet et al. (1989) and Theunissen et al. (1991). They have been verified during the June-August 2010 field campaign. Figure 4.13 shows a geological map of Musha-Ntungwa:

1. **Nyabugogo Formation** is the oldest geological formation in the investigated area and consists mainly of thick layers of fine to highly coarse grained quartzites alternating with fine grained layers of sandstones and schists.
2. **Musha Formation** comprises a meta-sedimentary thick homogeneous set of schists alternating with fine grained sandstones.
3. **Nduba Formation** on the top of the Musha formation has a constant thickness. The Nduba unit comprises hard layers of massive quartzites, sandstones and schists.
4. **Bulimbi Formation** consists of pelitic-dominated zoned thick piles of meta-sediments which display graphitic black shales and homogeneous thick layers alternating with sandstones and schists. The volcano-sedimentary suites were locally identified within the the Bulimbi Formation.
5. **Quaternary sequence** is well developed in both Musha and Ntungwa where it is represented by undifferentiated Holocene and Pleistocene sedimentary suites which may attain several

tens of meters of recent eluvial and alluvial piles of sediments deposited by local processes of leaching and/or erosion.

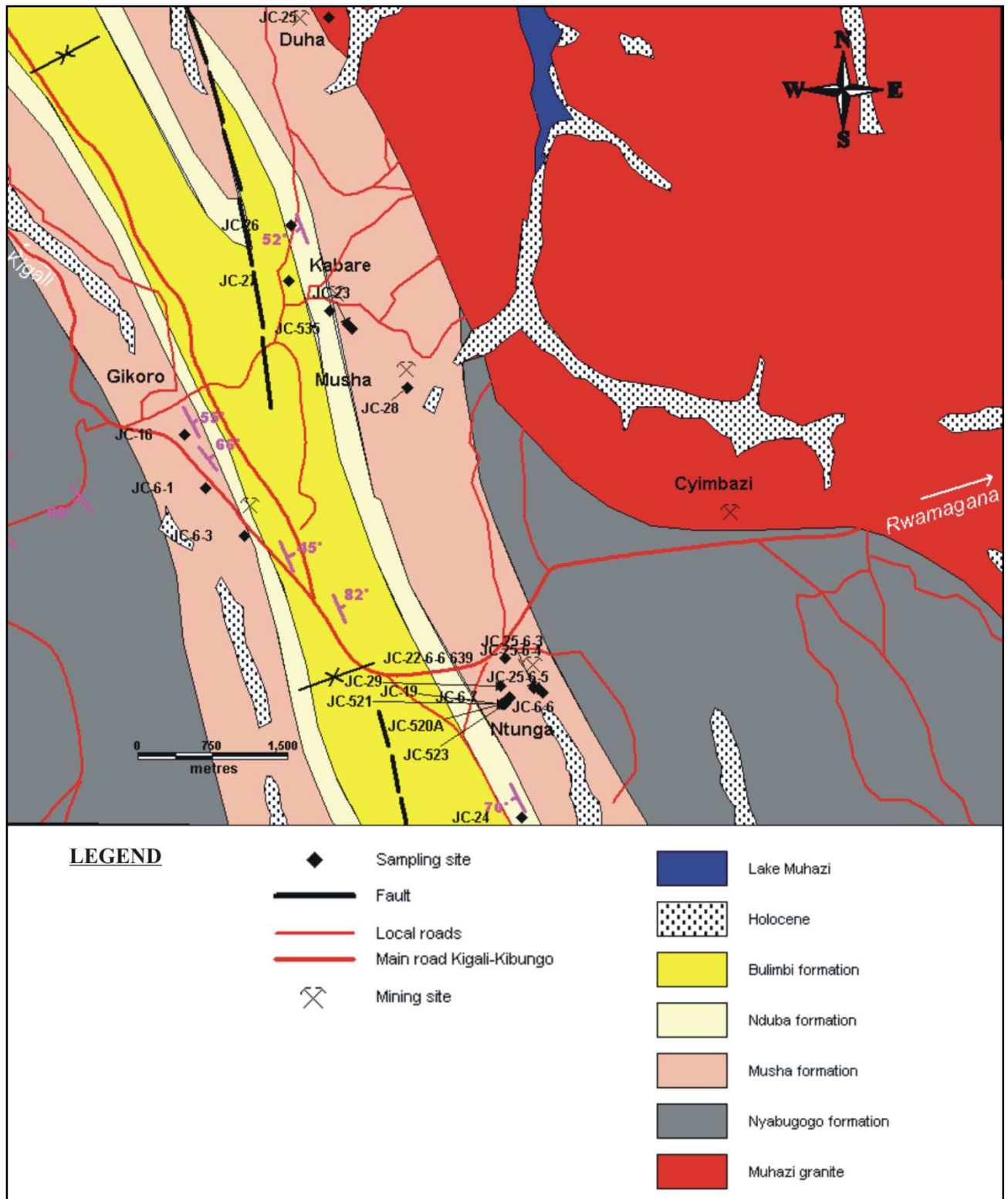


Figure 4.13: Geological map of Musha-Ntunga area with the location of the sampling sites.

4.2.2 Deformation

The Musha-Ntunga tin-coltan mines are hosted in a NW-SE oriented anticline extending from Gikomero hill (N) to Lake Rweru (S) and bordered in the NW and W by the Miyove syncline and by the Kibungo syncline in the E. The Musha-Ntunga anticline structure is plunging to the north (nearby Kigali Capital City), parallel to the Rutongo anticline and has a westward vergency.

The main tectonic event which has overprinted this mineral district is folding. Satellite images and field observations indicate that the main compressive events were of NE-SW direction and have built up perpendicularly, NW trending parallel ridges.

Besides the folding, a major fault was identified in the western part of the two mining concessions and includes two segments:

- The northernmost dissecting the geological formations between Lake Muhazi and the main road Kigali-Kibungo and is N-S oriented.
- The southernmost also with a N-S orientation is extended between the main road Kigali-Kibungo (N) and lake Mugesera towards the S.

In Ntunga area, the strike direction values of the stratification (S₀) vary between N160E and N240E and the dip of the bedding planes ranges from 50° to vertical towards the W.

In Musha sub-prospect, the strike directions measured were around N155E and the dip of the bedding planes was slightly lower than that of Ntunga and attained 45°W (Figure 4.13).

The meta-volcano-sedimentary rocks of Musha-Ntunga were intruded by small pegmatitic bodies which are cropping out in the zone, as well as by several pegmatite-type hydrothermal quartz veins (Figures 4.15, 4.17 and 6.1).

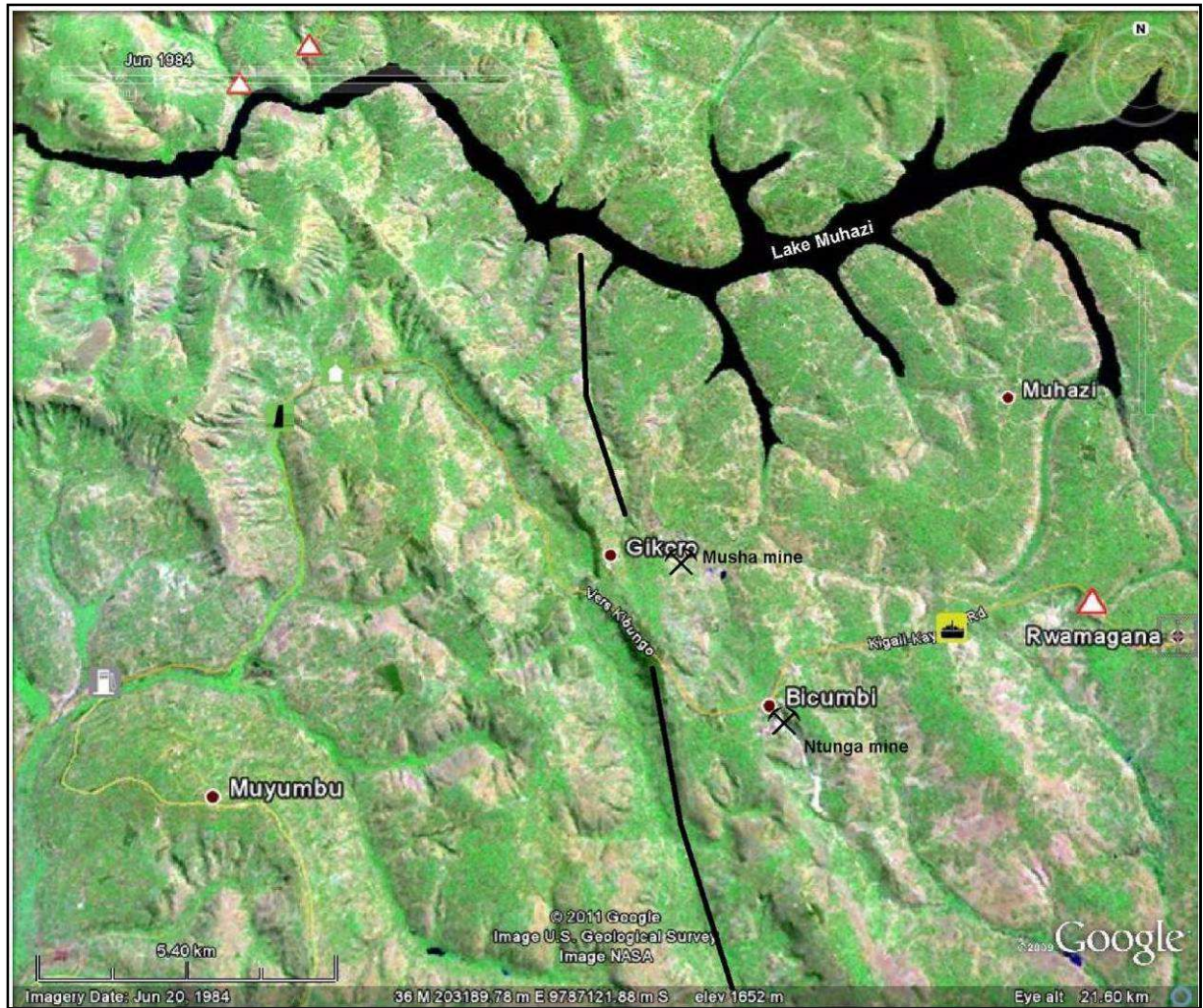


Figure 4.14: Satellite image of the Musha-Ntunga mining district. The image shows the NW-SE Janjagiro-Gikoro-Bicumbi ridge cross-cutting a N-S fault.

4.2.3 Mineral occurrence and mineralization

Ntunga, Cyimbazi, Shogo and Kabare mines of Musha-Ntunga are characterized by cassiterite mineralization while Duha mine is known to host coltan mineralization (see Figure 4.13 for the location).

The field investigations carried out in Musha-Ntunga showed that:

- On the one hand, the Musha Nb-/Ta- and Sn- ore deposits occur as primary deposit in kaolinized pegmatitic intrusions and in NW-SE pegmatite-type quartz veins underneath 30m to 40m of eluvial sediments and laterites (Figure 4.17). Sn- and Nb-/Ta- mineralization appear to be associated with pegmatites and hydrothermal veins. Besides the cassiterite, the mineral

association of the Sn-, Nb- and Ta- bearing quartz-veins comprise other major minerals such as quartz and muscovite in the near surface and deeper, they associate quartz and more or less albitized microcline becoming more pegmatitic and less mineralized in deeper areas. Wall-rocks are highly kaolinized, tourmalinized and sericitized (Figure 4.17).

- On the other hand, the secondary tin or coltan deposits in the form of alluvial/eluvial placers exist and are currently the most productive because of their easy exploitation.

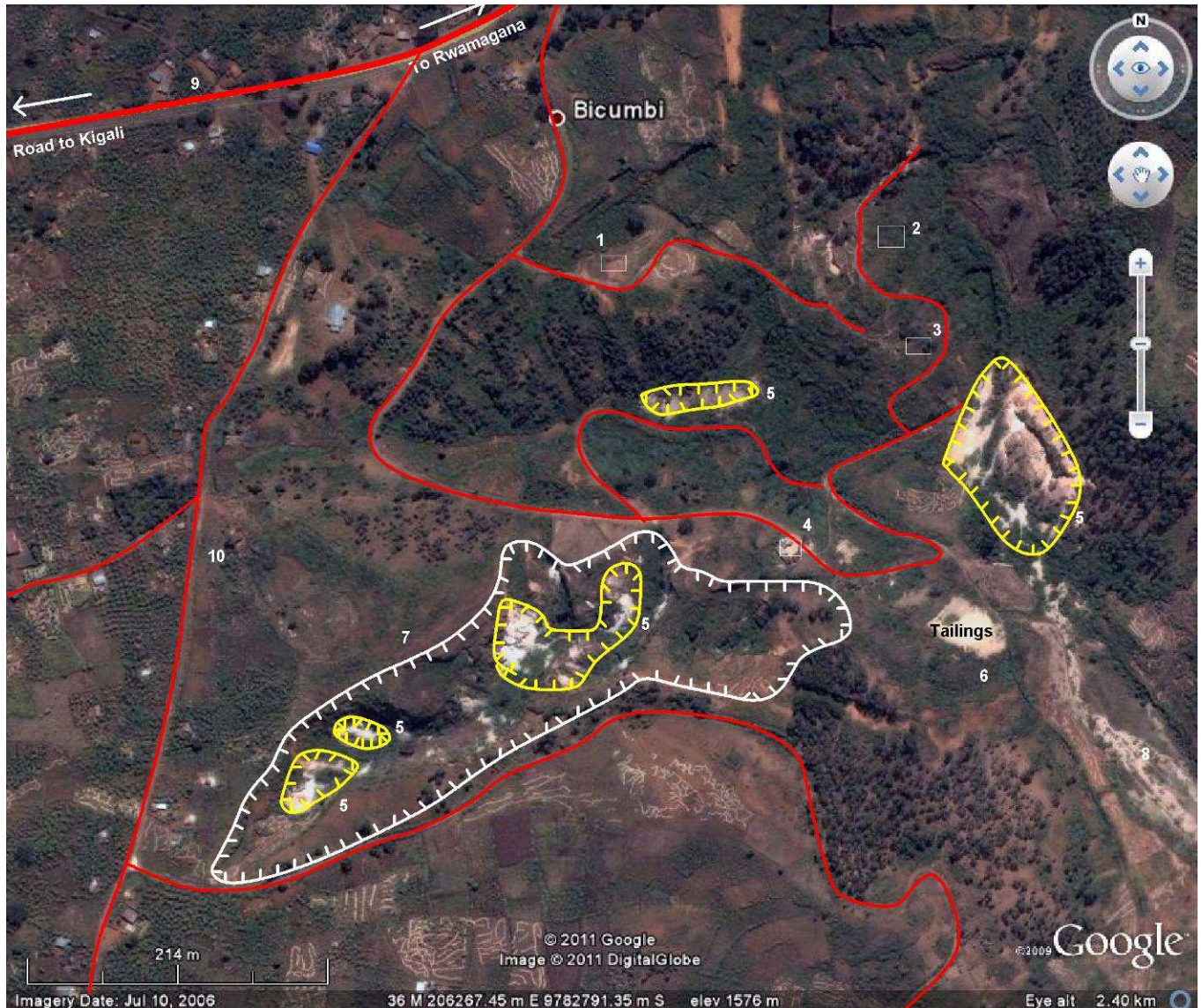


Figure 4.15: Mining operations at Ntungwa tin mine; 1 and 2- current mined places by artisan miners; 3- SOMIRWA gallery; 4- Rwanda Metals Office; 5- Small out-cropping pegmatitic bodies; 6- tailings; 7- Quarry exploited for kaolin; 8- ravine; 9- Main road; 10- local roads/pathways.

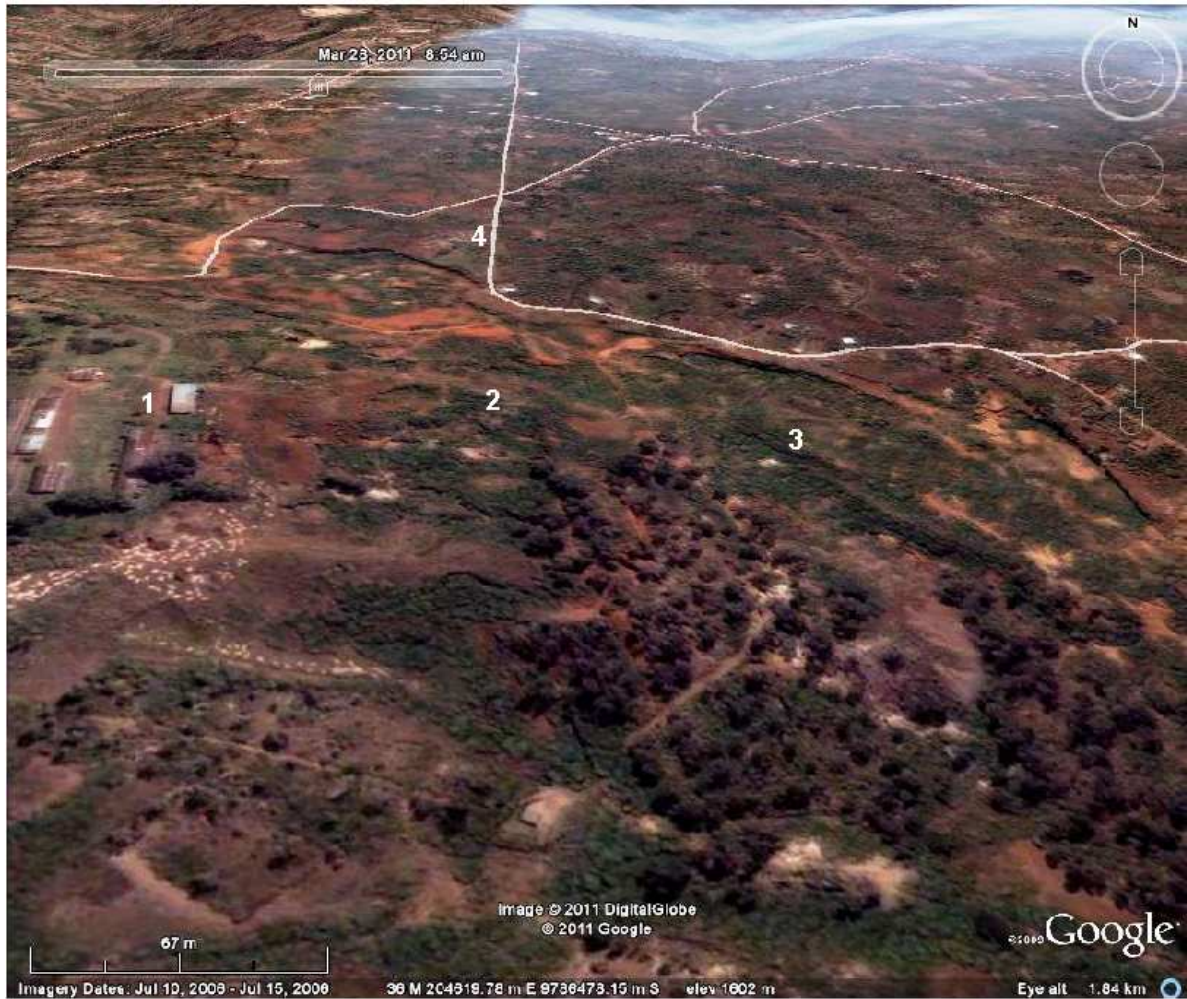


Figure 4.16: Mining operations at Musha mine; 1- Rwanda Mining Minerals Office; 2- Shogo I; 3- Shogo II; 4- Kabare.

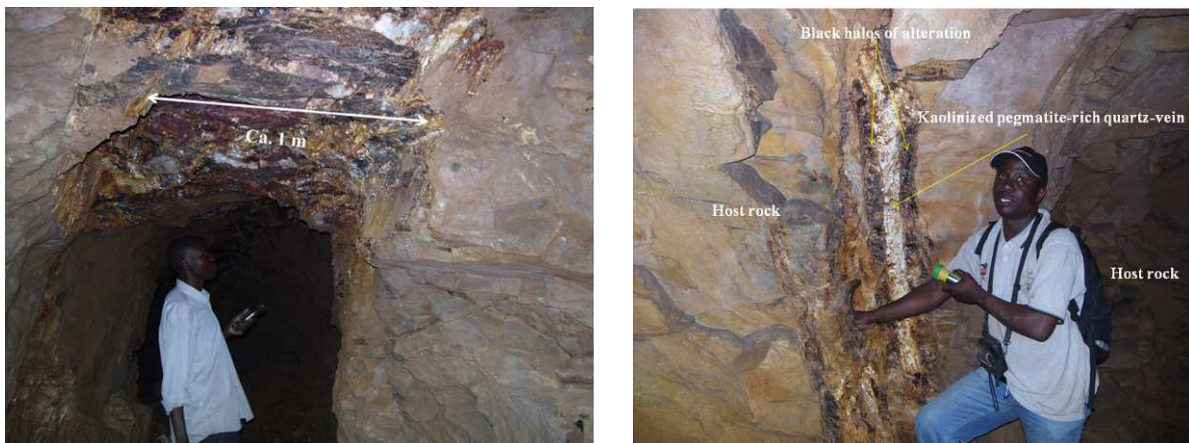


Figure 4.17: (left) NW-SE quartz-veins in Musha area (thickness: 1 m) and (right) pegmatite vein bordered by tourmaline-rich halos of alteration.

The mineral deposits in the Musha-Ntungwa area are hosted in the Nyabugogo and Musha formations.

Similar structures occur in the Ntunga tin deposit but pegmatites are thicker and kaolinization is there more pronounced than in Musha (Figure 4.15). Mineralized quartz veins have NE trends and N-S stockworks are visible. The veins/wall rock contacts are marked by halos of alteration.

The general characteristics of the cassiterite mineralization exploited in Musha-Ntunga are similar to those detailed in section 4.1.3 of the Rwinkwavu tin-tungsten deposit.

After the 1994 Genocide in Rwanda, the only coltan deposit of Musha-Ntunga, Duha, did not re-open and only one sample of “coltan” mineralization (JC-25) was obtained from the collection of the Royal Museum for Central Africa, Tervuren–Belgium for mineral chemistry investigation using SEM-EDX/WDX. This coltan mineralization associated with quartz is black and has sub-metallic to resinous lustre with a red brown streak.

4.2.4 Petrography

A total of 22 representative samples of the country rock, barren veins and mineralized veins from Musha-Ntunga were provided by OGMR-Kigali-Rwanda and RMCA-Tervuren-Belgium or were collected during the June-August 2010 field trip for petrographic analysis.

Figure 4.13 displays the location map of the samples in Musha-Ntunga (an overview of these will be given later) and their geographic location. The description of the rock-types is given in Table 4.2.1.

22 samples were investigated using macroscopic, light microscopic, SEM-EDX/WDX, XRF and fluid inclusion methods using the Laboratories of the Department of Geology. Macroscopic investigations indicate that the Musha-Ntunga rocks are of meta-sedimentary type: Schists, quartzites and sandstones. They have been intruded either by barren and/or fertile small bodies of pegmatites or fertile pegmatite-dominated hydrothermal quartz vein. The metamorphism here is of low to medium grade, generally greenschist and locally chlorite-biotite (direct contact with intrusive bodies) facies. Nine thin sections were prepared for petrographical investigations and analyzed using the transmitted light microscopy in plane polarized light or under crossed nichols.

The majority of them (8 samples) were from meta-sedimentary host rocks and only one sample was from highly fractured quartz. The latter showed in light microscopy intact continuous fragments presenting resorbed rims and separated by cracks filled by cemented quartz crystal grains. This, probably originated on original hydrothermal quartz veins by later compressive movements.

Table 4.2.1: Summary of the characteristics of sampled rocks in the Musha - Ntunga concession.

Sample	Locality	Easting	Northing	Elevation	Rock-type/macrosopic description
JC-6-7	MN	539969	9783228	-	Whitish, weathered and kaolinized pegmatite
JC-6-6	MN	539973	9783220	-	Quartzite
JC-6-3	MN	537309	9784870	-	Quartzite
JC-6-1	MN	536911	9785351	-	clayish blue schist
JC-535	MN	538390	9786974	1582	Concentrate of alluvial cassiterite from Shogo I tin deposit
JC-523	MN	539935	9783161	1658	Milky quartz
JC-521	MN	539897	9783166	1605	Highly altered mica schist (from the same area but 5 to 7 m away).
JC-520A	MN	539904	9783157	1515	Highly altered mica schist sampled in the zone of direct contact between the pegmatite and the meta-sediment.
JC-30*	MN	538170	9787160	-	Highly altered mica rich sandstone with empty cubic cavities (pyrite?)
JC-29*	MN	539890	9783340	-	Quartz tourmalinite vein
JC-28*	MN	538950	9786380	-	Tourmaline rich brecciated quartz vein, wolframite altered in anthoinite + scorodite and empty cubic cavities (pyrite?)
JC-27*	MN	537760	9787460	-	Cassiterite in quartz vein. The core of the quartz is dark colored (smoky) and the rim corresponds to the milky quartz.
JC-26*	MN	537780	9788030	-	Quartz biotite schist with a red part (presence of Fe-minerals) and a light blue zone. Its surface displays cubic empty cavities (pyrite?).
JC-25-6-5	MN	540304	9783272	1538	Quartz-mica schist showing strain-slip cleavages which affected more or less the whole sample. Accessory minerals include garnet and opaque minerals.
JC-25-6-4	MN	540266	9783325	1544	Tourmaline schist
JC-25-6-3 643	MN	562188	9780331	1661	Platy minerals of muscovite
JC-25-6-3	MN	540216	9783323	1535	Quartz with many cracks filled by cemented re-crystallized quartz grains associated with minor amounts of muscovite
JC-25*	MN	538160	9790140	-	Coltan-bearing quartz vein; quartz slightly smoky.
JC-24*	MN	540100	9782000	-	Quartzite completely fragmented, probably from greisens.
JC-23*	MN	538350	9787020	-	Medium grained sandstone with alternation of zebra-shaped dark (possibly black tourmaline and opaque minerals rich) and white (quartz-rich) layers.
JC-22-6-6 639	MN	539930	9783630	-	Concentrate of eluvial cassiterite from Ntunga artisanal mine.
JC-16	MN	536700	9785900	-	Altered blue schist

Abbreviations: MN-Musha-Ntunga. (*)-Samples from the RMCA collection.

The light microscopy of the meta-sedimentary suites revealed fine to coarse grains of minerals cemented by a silici-clastic matrix and from granoblastic to lepidoblastic textures with mineral associations including mostly quartz, muscovite, biotite, tourmaline, garnet, opaque minerals, clay minerals and accessory minerals like zircon.

4.2.5 Mineral Chemistry of cassiterite and columbite-tantalite

In order to examine the chemical and mineralogical variations in the Sn- and Nb-Ta- bearing minerals and their host-rocks in Musha-Ntungwa mining concession, seven (7) samples were prepared and analyzed using the SEM/EDX-WDX techniques. These include 3 samples from the country rocks, 2 samples of tin mineralization, one sample of columbite-tantalite and one sample of muscovite. A total of around 80 mineral grains were analyzed and the results are displayed in Tables 4.2.3 and 4.2.4 and in Appendix 4. Additional to the cassiterite and columbite-tantalite minerals, the SEM/EDX-WDX investigations revealed that the mineral associations in those investigated samples comprise also inclusions of quartz, biotite, muscovite, garnet, tourmaline, Fe-minerals, rutile, ilmenite, zircon and sulphides (chalcopyrite, arsenopyrite and pyrite). This section will focus specifically on the mineral chemistry of the economically exploited ore minerals found in Musha-Ntungwa: Cassiterite and coltan.

A. Mineral chemistry of cassiterite

Table 4.2.2 Average chemical compositions of cassiterite group minerals from Musha - Ntungwa (JEOL JSM-6610 SEM-EDX in wt. %).

	JC-22-6-6 639	JC-535	JC-25-6-3 639	Average	LLD
SnO ₂	97.4	95.19	98.27	96.95	1.95
Fe ₂ O ₃	0.3	2.32	<LLD	0.87	0.25
TiO ₂	0.5	<LLD	<LLD	<LLD	0.28
MnO	<LLD	<LLD	0.13	0.10	0.10
Nb ₂ O ₅	<LLD	0.32	0.11	0.20	0.11
Ta ₂ O ₅	0.6	<LLD	<LLD	<LLD	0.35
WO ₃	0.4	<LLD	ND	<LLD	0.20
ZrO ₄	0.1	0.10	<LLD	0.09	0.08
Al ₂ O ₃	0.3	1.04	1.11	0.81	0.06
MgO	0.0	0.00	ND	0.00	0.00
Na ₂ O	ND	0.00	ND	0.00	0.00
CaO	ND	0.00	ND	0.00	0.00
SiO ₂	0.84	<LLD	ND	<LLD	0.09
SO ₃	ND	0.09	ND	0.03	0.01
F	0.3	0.46	ND	0.24	0.09

Abbreviation: <LLD: Below the lower limit of detection; ND-Not detected;
LLD-Lower limit of detection.

Table 4.2.2 shows the average chemical composition per cassiterite sample and the average for the whole group minerals. The cassiterite group minerals of Musha-Ntungwa appear to be mainly composed of tin oxide (average of 96.95 wt. %), iron (0.87 wt. % of Fe₂O₃), 0.81 wt. % Al₂O₃ and minor amounts of MnO (0.1 wt. %), Nb₂O₅ (0.2 wt. %). Other oxides are less than 0.1 wt. % or are in

traces. Table 4.2.3 details the chemical composition of cassiterite for each investigated cassiterite grain and its structural chemical formula.

Table 4.2.3: Chemical composition of selected cassiterite samples from the Musha-Ntungwa.

Sample	JC-22-6-6 639						JC-535					JC-25-6-3 639			
Point	1	2	3	4	5	9	1	4	8	9	10	3	5	6	7
SO ₃	-	-	-	-	-	-	-	-	-	0.4	-	-	-	-	-
WO ₃	-	0.2	0.9	0.1	1.2	-	0.1	0.4	-	-	-	-	-	-	-
Nb ₂ O ₅	0.5	-	-	0.3	-	-	0.6	-	0.8	0.3	-	-	-	-	0.5
Ta ₂ O ₅	1.4	0.4	0.7	0.9	-	-	-	-	1.0	-	-	-	-	-	0.8
SiO ₂	-	-	-	-	-	-	-	-	-	-	-	-	-	-	-
TiO ₂	0.3	0.5	0.7	0.3	0.6	0.5	0.1	0.0	0.1	0.3	0.1	0.3	-	-	0.2
ZrO ₂	-	-	0.2	0.2	-	0.4	-	-	-	0.5	-	0.2	-	-	-
SnO ₂	95.9	97.8	96.1	97.9	98.0	98.6	99.1	99.6	95.9	86.2	95.2	98.3	100.0	98.3	96.4
Al ₂ O ₃	-	0.8	0.9	-	-	-	-	-	-	2.8	2.4	1.1	-	1.7	1.7
Fe ₂ O ₃	0.2	0.4	0.3	0.2	0.1	0.5	-	0.0	-	9.3	2.2	-	-	-	0.1
MgO	-	-	-	-	-	-	-	-	-	-	-	-	-	-	-
CaO	-	-	-	-	-	-	-	-	-	-	-	-	-	-	-
MnO	0.1	-	0.4	-	0.1	0.1	0.1	0.0	-	0.2	0.1	0.2	-	-	0.4
Na ₂ O	-	-	-	-	-	-	-	-	-	-	-	-	-	-	-
F	1.6	-	-	-	-	-	-	-	2.3	-	-	-	-	-	-
Tot	100.0	100.0	100.0	100.0	100.0	100.0	100.0	100.0	100.0	100.0	100.0	100.0	100.0	100.0	100.0
Number of cations based on 2 oxygens															
S	0.000	0.000	0.000	0.000	0.000	0.000	0.000	0.000	0.000	0.008	0.000	0.000	0.000	0.000	0.000
W	0.000	0.001	0.005	0.001	0.008	0.000	0.001	0.002	0.000	0.000	0.000	0.000	0.000	0.000	0.000
Nb	0.005	0.000	0.000	0.003	0.000	0.000	0.006	0.000	0.008	0.003	0.000	0.000	0.000	0.000	0.005
Ta	0.009	0.003	0.005	0.006	0.000	0.000	0.000	0.000	0.007	0.000	0.000	0.000	0.000	0.000	0.005
Si	0.000	0.000	0.000	0.000	0.000	0.000	0.000	0.000	0.000	0.000	0.000	0.000	0.000	0.000	0.000
Ti	0.005	0.009	0.012	0.006	0.011	0.008	0.002	0.000	0.001	0.005	0.001	0.005	0.000	0.000	0.004

Abbreviations: *-(Nb+Ta)/Sn; **-(Fe+Mn)/Sn; ***-W/Sn; -: not determined.

Table 4.2.3 (Continued).

Sample	JC-22-6-6 639						JC-535					JC-25-6-3 639			
Point	1	2	3	4	5	9	1	4	8	9	10	3	5	6	7
Zr	0.000	0.000	0.002	0.002	0.000	0.005	0.000	0.000	0.000	0.006	0.000	0.003	0.000	0.000	0.000
Sn	0.929	0.947	0.931	0.948	0.949	0.955	0.960	0.964	0.929	0.835	0.922	0.952	0.969	0.952	0.934
Al	0.000	0.022	0.026	0.000	0.000	0.000	0.000	0.000	0.000	0.080	0.069	0.030	0.000	0.049	0.048
Fe	0.004	0.007	0.005	0.004	0.002	0.008	0.000	0.001	0.000	0.170	0.041	0.000	0.000	0.000	0.001
Mg	0.000	0.000	0.000	0.000	0.000	0.000	0.000	0.000	0.000	0.000	0.000	0.000	0.000	0.000	0.000
Ca	0.000	0.000	0.000	0.000	0.000	0.000	0.000	0.000	0.000	0.000	0.000	0.000	0.000	0.000	0.000
Mn	0.001	0.000	0.007	0.000	0.003	0.001	0.002	0.000	0.000	0.004	0.001	0.003	0.000	0.000	0.007
Na	0.000	0.000	0.000	0.000	0.000	0.000	0.000	0.000	0.000	0.000	0.000	0.000	0.000	0.000	0.000
Σcat.	0.955	0.988	0.993	0.971	0.972	0.978	0.971	0.968	0.945	1.111	1.034	0.993	0.969	1.001	1.005
Nb/Ta	0.570	0.000	0.000	0.548	-	-	-	-	1.260	-	-	-	-	-	0.935
(Nb+Ta)/Sn*	0.016	0.003	0.005	0.009	0.000	0.000	0.006	0.000	0.016	0.004	0.000	0.000	0.000	0.000	0.011
log(*)	-1.806	-2.533	-2.286	-2.023	-	-	-2.193	-	-1.798	-2.418	-	-	-	-	-1.961
(Fe+Mn)/Sn**	0.006	0.008	0.013	0.004	0.005	0.010	0.002	0.001	0.000	0.209	0.045	0.003	0.000	0.000	0.009
log(**)	-2.248	-2.124	-1.898	-2.354	-2.342	-1.987	-2.669	-2.927	-	-0.681	-1.342	-2.490	-	-	-2.052
W/Sn***	0.000	0.001	0.006	0.001	0.008	0.000	0.001	0.002	0.000	0.000	0.000	0.000	0.000	0.000	0.000
log(***)	-	-2.899	-2.235	-3.064	-2.096	-	-3.069	-2.629	-	-	-	-	-	-	-

Abbreviations: *-(Nb+Ta)/Sn; **-(Fe+Mn)/Sn; ***-W/Sn; -: not determined.

The majority of investigated mineral grains are identified as almost pure tin oxide minerals with little amounts of trace elements or inclusions of other mineral phases.

Furthermore, two analyses of sample JC-22-6-6 639 (7 and 10) were Fe-rich cassiterite where the wt. % of total Fe as Fe₂O₃ is respectively 29.6 and 37.2 (without crystal water measurements) and corresponding possibly to the hydro-cassiterite (Sn, Fe)(O, OH)₂ as defined by Rösler (1983).

Bivariate diagrams of Sn- vs. Nb-, Ta-, Fe- and Ti- (Figure 4.18a to d) of selected cassiterite samples from Musha-Ntungwa showed poor correlations.

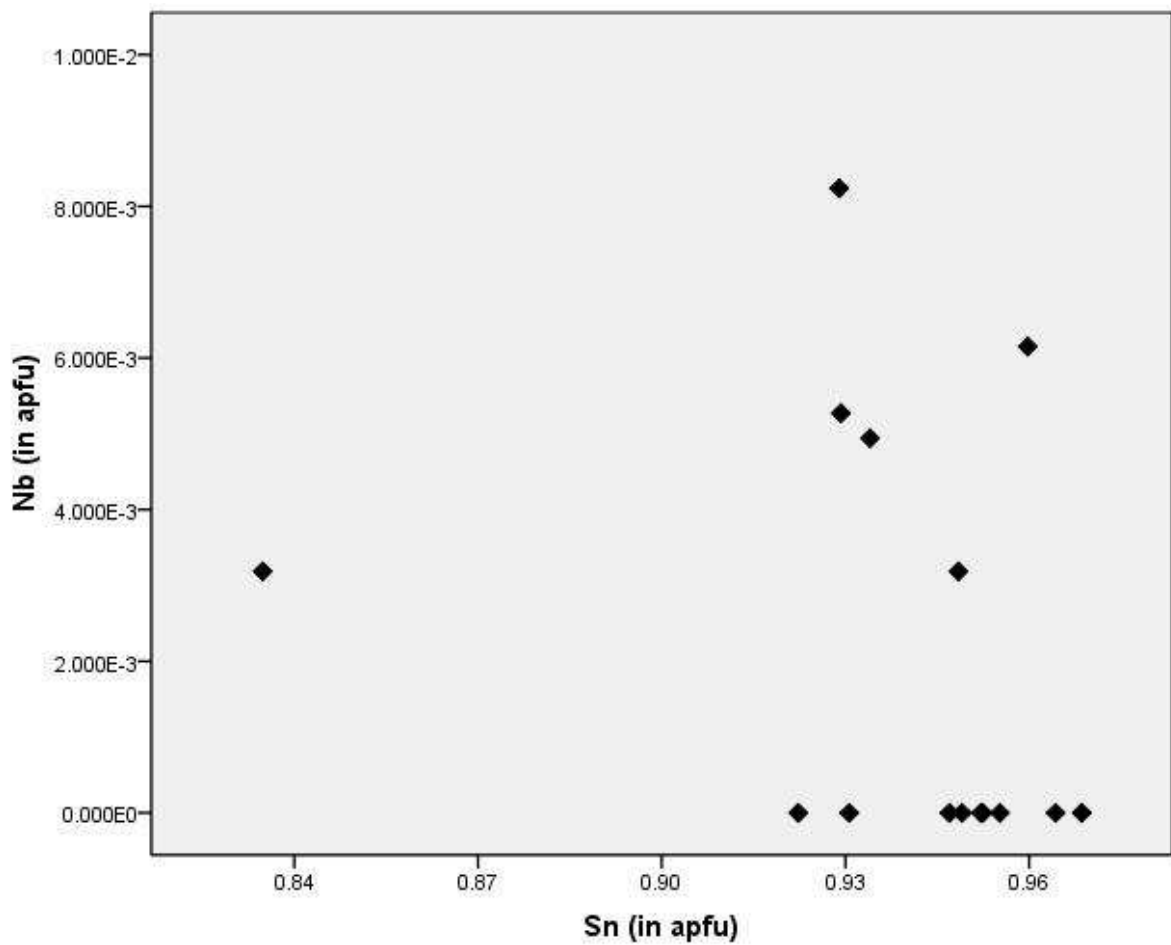


Figure 4.18a: Discrimination plot of Sn vs. Nb (in apfu) in cassiterite of Musha-Ntungwa.

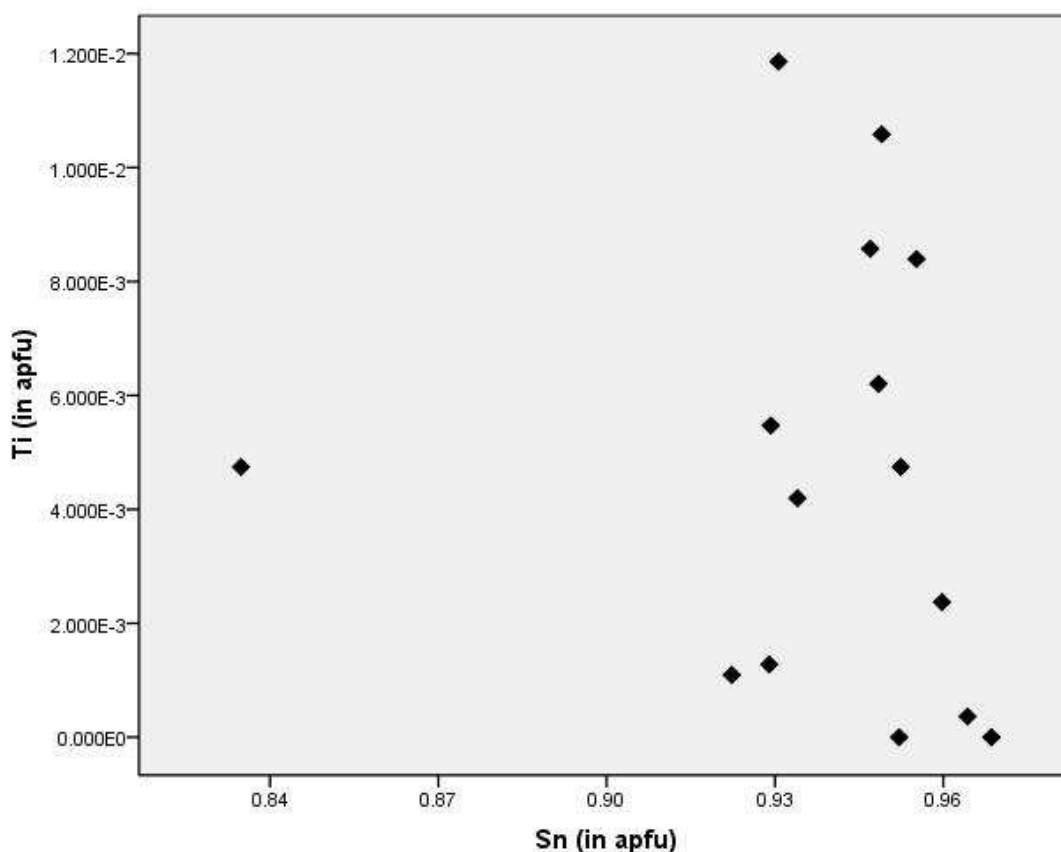


Figure 4.18d: Discrimination plot of Sn vs. Ti (in apfu) in cassiterite of Musha-Ntungwa.

With the aim to understand a systematic chemical variation of analyzed cassiterite samples, the results were plotted in variation diagrams of $\log [(Ta+Nb)/Sn]$ vs. $\log [(Fe+Mn)/Sn]$ and $\log [W/Sn]$ vs. $\log [(Fe+Mn)/Sn]$ after Möller et al. (1988) (Figures 4.19a and b). According to them, two types of compositions are distinguishable (Figure 4.19a): 4 analyses are distributed along the line $(Ta+Nb)/(Fe+Mn) = 2$ and therefore, reflecting a contamination by mineral inclusions of the type $(Fe, Mn)(Ta, Nb)_2O_6$ and 3 points falling below that line. This latter case presents an excess of $(Fe + Mn)$ content and indicates most likely the presence of Fe-rich mineral phases in the cassiterite.

Figure 4.19b shows that the two analyses of the cassiterite samples from Musha-Ntungwa plot above the line of equation $W/(Fe+Mn) = 1$ and therefore enriched in W indicating that the relationship between Sn and W in the cassiterite crystal is mostly guided by a substitution of the type $Sn^{4+} \leftrightarrow W^{4+}$.

The remaining analyses of these samples fall below $W/(Fe+Mn) = 0.5$ and according to Möller et al. (1988), this ratio suggests a high amount of Fe_2WO_6 in solid solution.

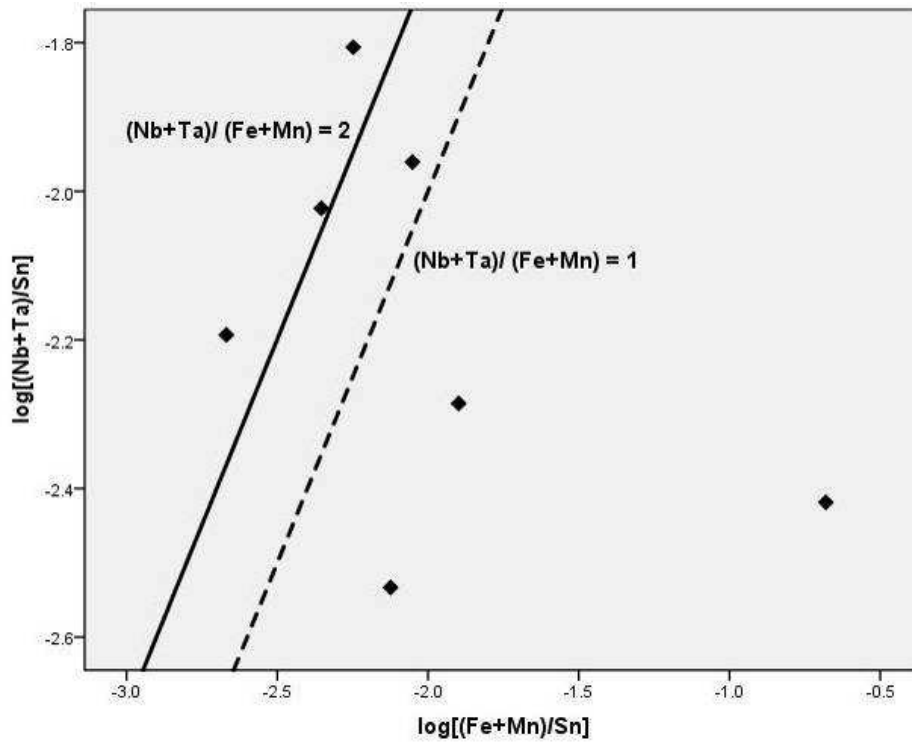


Figure 4.19a: Correlation diagram of selected cassiterite samples from Musha-Ntungwa using $\log [(\text{Ta}+\text{Nb})/\text{Sn}]$ vs. $\log [(\text{Fe}+\text{Mn})/\text{Sn}]$ after Möller et al. (1988).

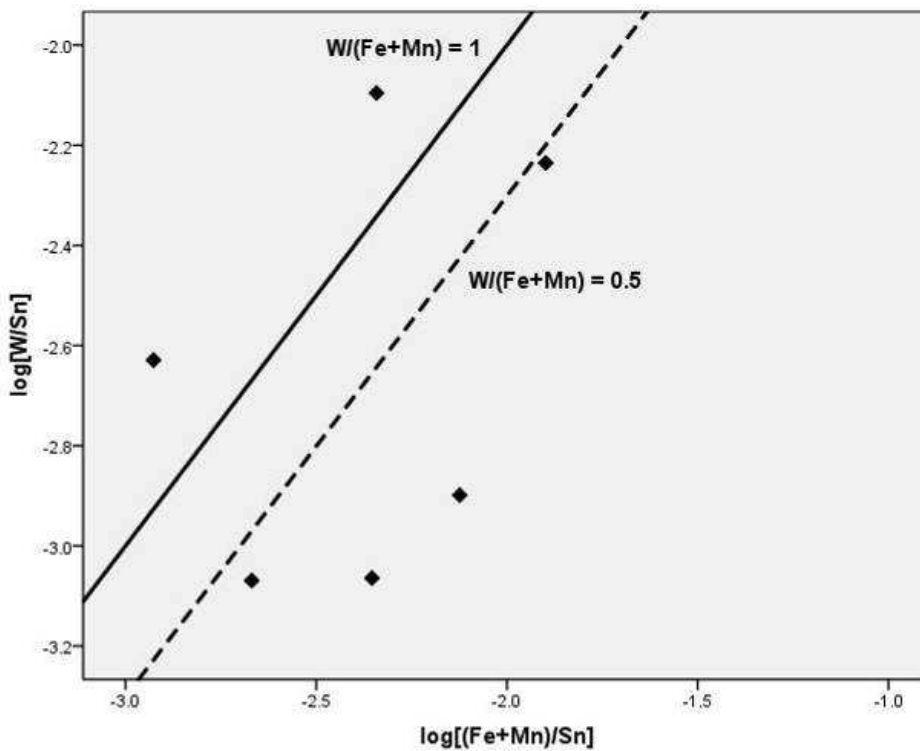


Figure 4.19b: Correlation diagram of selected cassiterite samples from Musha-Ntungwa using $\log [\text{W}/\text{Sn}]$ vs. $\log [(\text{Fe}+\text{Mn})/\text{Sn}]$ after Möller et al. (1988).

B. Mineral chemistry of columbite-tantalite

A systematic study of the columbite-tantalite mineralization from Musha-Ntungwa was carried out on a thick section. Investigated areas on the sample were photographed by back-scattered electron image (BSE), structural formulae were calculated and the results were plotted (per analysis) in the “columbite quadrilateral” after Beurlen et al. (2008). All the analytical data are displayed in Table 4.2.4.

The results of the analyses show that the “coltan” mineral is mostly composed of tantalum, averaging at 62.68 wt. % Ta₂O₅, niobium, with 19.53 wt. % Nb₂O₅ in average, calcium and manganese with equal amounts averaging at 3.80 wt. % of CaO and MnO.

Table 4.2.4: Chemical composition of analyses of coltan sample JC-25 from Musha-Ntungwa.

Spot	1	2	3	4	5	6	7	8	9	10	Avg
Nb ₂ O ₅	4.37	<DL	<DL	33.17	44.71	51.82	12.88	10.77	24.66	12.96	19.53
Ta ₂ O ₅	73.34	77.88	84.7	45.75	33.24	27.69	75.4	74.7	60.3	73.73	62.68
WO ₃	<DL	<DL	<DL	<DL	1.80	<DL	<DL	<DL	<DL	<DL	0.18
TiO ₂	<DL	<DL	<DL	<DL	0.19	<DL	<DL	<DL	<DL	<DL	0.02
SnO ₂	<DL	<DL	<DL	<DL	0.15	<DL	<DL	<DL	<DL	<DL	0.01
UO ₂	<DL	5.00	6.54	<DL	0.38	<DL	<DL	<DL	<DL	<DL	1.19
Fe ₂ O ₃	<DL	<DL	1.62	11.07	5.06	7.30	<DL	<DL	4.29	<DL	2.93
MnO	<DL	<DL	<DL	6.99	14.47	12.34	<DL	<DL	4.20	<DL	3.80
CaO	12.75	9.53	3.93	<DL	<DL	<DL	2.21	7.91	<DL	1.74	3.81
Na ₂ O	5.74	4.56	0.86	<DL	<DL	<DL	1.39	1.62	2.04	1.10	1.73
K ₂ O	<DL	<DL	<DL	<DL	<DL	<DL	<DL	<DL	0.90	<DL	0.09
BaO	<DL	<DL	2.32	<DL	<DL	<DL	8.10	4.97	3.58	10.48	2.94
SiO ₂	<DL	<DL	<DL	3.02	<DL	0.85	<DL	<DL	<DL	<DL	0.39
F	3.80	3.00	<DL	<DL	<DL	<DL	<DL	<DL	<DL	<DL	0.68
Tot.	100	100	100	100	100	100	100	100	100	100	100
Structural formula calculated based on 6 oxygen											
Nb	0.16	<DL	<DL	1.21	1.64	1.90	0.47	0.39	0.90	0.47	0.72
Ta	1.62	1.72	1.87	1.01	0.73	0.61	1.66	1.65	1.33	1.62	1.38
W	<DL	<DL	<DL	<DL	0.04	<DL	<DL	<DL	<DL	<DL	0.00
Ti	<DL	<DL	<DL	<DL	0.01	<DL	<DL	<DL	<DL	<DL	0.00
Sn	<DL	<DL	<DL	<DL	0.01	<DL	<DL	<DL	<DL	<DL	<DL
U	<DL	0.09	0.12	<DL	0.01	<DL	<DL	<DL	<DL	<DL	0.02
Fe	<DL	<DL	0.10	0.67	0.31	0.44	<DL	<DL	0.26	<DL	0.18
Mn	<DL	<DL	<DL	0.48	0.99	0.85	<DL	<DL	0.29	<DL	0.26
Ca	1.11	0.83	0.34	<DL	<DL	<DL	0.19	0.69	<DL	0.15	0.33
Na	0.90	0.72	0.13	<DL	<DL	<DL	0.22	0.25	0.32	0.17	0.27
K	<DL	<DL	<DL	<DL	<DL	<DL	<DL	<DL	0.09	<DL	0.01
Ba	<DL	<DL	0.07	<DL	<DL	<DL	0.26	0.16	0.11	0.33	0.09
Si	<DL	<DL	<DL	0.24	<DL	0.07	<DL	<DL	<DL	<DL	0.03
Σcations	3.79	3.35	2.63	3.62	3.73	3.87	2.80	3.14	3.31	2.76	3.30
Nb/Ta	0.10	0.00	0.00	1.21	2.24	3.11	0.28	0.24	0.68	0.29	0.52
Fe/Mn	-	-	-	1.4	0.3	0.5	-	-	0.9	-	0.7

<DL: Below detection limit.

Barium average content is 2.94 wt. % BaO, total Fe- as Fe₂O₃ forms 2.93 wt. % on average, whereas the average Na content corresponds to 1.73 wt. % Na₂O. U has been detected in high amounts in 3 analyses (2, 3 and 5) where its values are respectively 5.00, 6.54 and 0.38 wt. % UO₂ and 1.19 wt. % on average. The sum Nb + Ta is above 2*Ti and Ta>Nb (all in a.p.f.u) and using the classification of Hogarth (1977), the uranium mineral in this sample may correspond to the Uranmicrolite inclusion.

In other analyses, U has not been detected. It also contains F with average content of 0.68 wt. % and minor amounts of W- with 0.18 wt. % WO₃, K- with average content of 0.09 wt. % K₂O, Ti- with 0.02 wt. % TiO₂ and Sn- averaging 0.01 wt. % SnO₂.

The bulk structural formulae and the main group in which those analyzed Nb- and Ta- bearing minerals are found is compiled in Table 4.2.5.

Table 4.2.5: Structural chemical formula and nomenclature of selected “coltan” analyses from Musha-Ntungwa.

Spot	Structural formula	Other chemical components detected by SEM-EDX	Possible group
1	Na _{0.9} Ca _{1.1} Nb _{0.2} Ta _{1.6} O ₆	3.8 wt. % F	Tantalite
2	Na _{0.7} Ca _{0.8} U _{0.1} Ta _{1.7} O ₆	3.0 wt. % F	Tantalite
3	Na _{0.1} Ca _{0.3} Ba _{0.1} Fe _{0.1} U _{0.1} Ta _{1.9} O ₆	-	Tantalite
4	Si _{0.2} Mn _{0.5} Fe _{0.7} Nb _{1.2} Ta ₁ O ₆	-	Ferro-columbite
5	Mn ₁ Fe _{0.3} Ti _{0.01} W _{0.04} Ta _{0.7} Nb _{1.6} O ₆	0.15 wt. % SnO ₂ and 0.38 wt. % UO ₂	Mangano-columbite
6	Si _{0.1} Mn _{0.8} Fe _{0.4} Nb _{1.9} Ta _{0.6} O ₆	-	Mangano-columbite
7	Ba _{0.3} Na _{0.2} Ca _{0.2} Nb _{0.5} Ta _{1.7} O ₆	-	Tantalite
8	Ba _{0.2} Na _{0.3} Ca _{0.7} Nb _{0.4} Ta _{1.6} O ₆	-	Tantalite
9	Ba _{0.1} Na _{0.3} K _{0.1} Mn _{0.3} Fe _{0.3} Nb _{0.9} Ta _{1.3} O ₆	-	Columbite-tantalite
10	Ba _{0.3} Na _{0.2} Ca _{0.2} Nb _{0.5} Ta _{1.6} O ₆	-	Tantalite

The averages of Nb/Ta and Fe/Mn ratios of the columbite-tantalite sample are < 1 which means enrichment in both Ta and Mn. In addition, the Nb/Ta ratio < 1 allows classification of this sample in the tantalite group.

Based on Beurlen et al. (2008), the mineral chemical analyses are reported in the four-pole quadrilateral diagram representing the end-member species in Figure 4.20.

The columbite-tantalite sample from Musha-Ntungwa shows a Ta/(Ta+Nb) ratio varying between 0.243 and 1 and Mn/(Mn+Fe) ratio ranging between 0.0 and 0.78. In the Beurlen et al. (2008) diagram, there is a clear negative correlation between the Ta- and Nb- end members and the analyses are plotting between the Ta- (tantalite group), Fe-(ferro-tantalite and ferro-columbite groups) and Mn-(Mangano-columbite and mangano-tantalite groups) rich end-members.

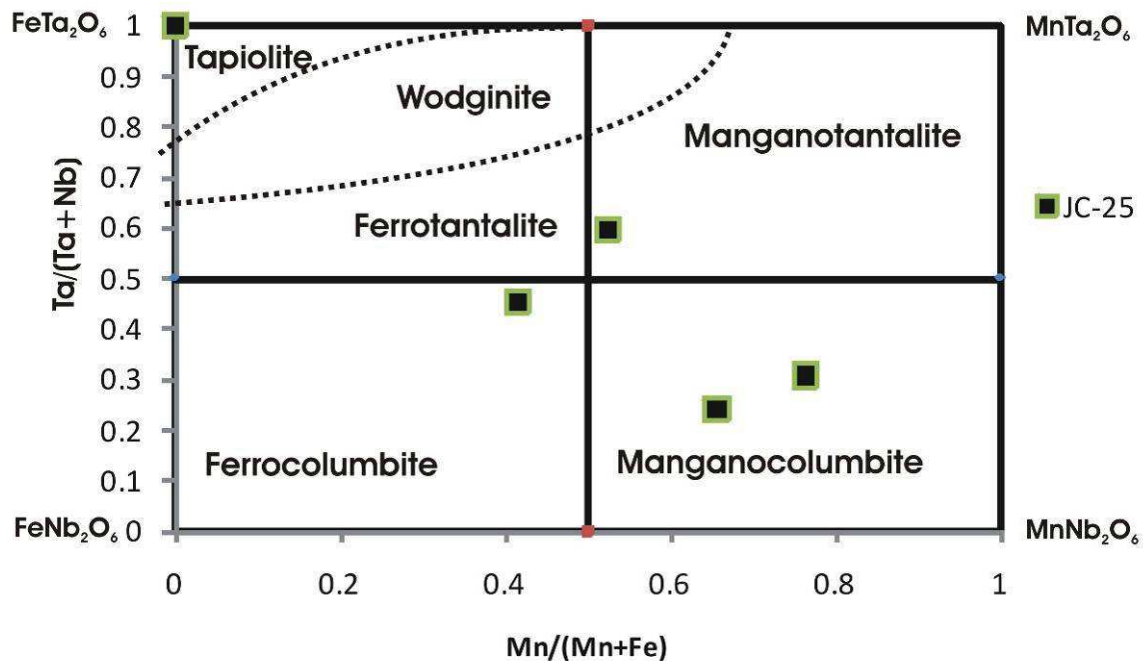


Figure 4.20: Chemical composition of selected columbite-tantalite analyses from Musha-Ntungwa represented in the FeTa-FeNb-MnNb-MnTa quadrilateral after Beurlen et al. (2008).

4.3 BUGARURA-KULUTI-BIBARE PROSPECT

The last prospect of the study area which is the Bugarura – Kuluti - Bibare mining district extends over ca. 17,000 ha between 30°14'8" and 30°29'40" long. E and 1°40'8" and 1°50'36" lat. S. in the Gatsibo District, Eastern Province. In this section, it will be called Bugarura-Kuluti.

This mineral district comprises three mining concessions which are Bugarura, Bibare and Kuluti. The Bugarura and Kuluti mining concessions are currently explored and exploited by Roka Rwanda. During the June-August 2010 field investigations, the Bibare mining concession was not exploited.

4.3.1 Geological setting

The geology of Bugarura-Kuluti has been described based on the field work carried out during the period of June-August 2010, Theunissen et al. (1991), MINETAIR (1965) in RMCA's archives and BRGM (1987). The local geology of Bibare is assumed to exhibit similar stratigraphy and tectonic structures as Bugarura or Kuluti mining concessions and will not be discussed in this study. The mineral district is hosted within Nyabugogo, Musha and Bulimbi meta-sedimentary formations (detailed descriptions in sections 4.1.1 and 4.2.1) affected by both contact metamorphism from the Muhazi-Gikoma - Kiziguro and Rugarama - Bujumu granites (Figure 4.21) and regional metamorphism which has affected the whole of eastern Rwanda.

The local geology structured, by sub-prospect, could be described as follows:

The **Bugarura tin** deposit is hosted by steep-dipping meta-sedimentary bed of quartzites, pelite-dominated sandstones and chlorite-sericite schists intruded by the Muhazi – Gikoma - Kiziguro granite.

The **Mamfu tin** prospect which is located west of Bugarura, separated from the latter by the Buhaza stream, shows a similar geological context.

The **Kuluti-Bujumu-Rugarama** tin mines displays three distinct meta-sedimentary formations in the surroundings of the Rugarama-Bujumu granite: a more or less metamorphosed, foliated clayish schist series and a mica schist suite separated by a 25-28m thick conglomeratic unit. The petrographical and mineralogical characteristics of each of these units, in sequence from the Rugarama - Bujumu granite to the most recent meta-sedimentary layers are the following:

- The Rugarama – Bujumu coarse-grained granitic intrusions are composed of rose feldspars, biotite, muscovite and quartz. These granitic cupolas are highly fractured and sealed by pegmatites consisting of quartz and big crystals of feldspar (size: ca. 15cm). The country rocks to these cupolas show a clear zoning from the contacts outwards: a 10m thick of biotite zone nearby the granite, a tourmaline-sericite-mica schist zone and finally, a shallow metamorphic schist zone intruded by multiple small bodies of pegmatites, greisens and hydrothermal quartz veins.
- A mica-schist suite covers the top of the above described granite and is underneath the first two uppermost meta-sedimentary formations. This layer comprises folded platy sericite and biotite schists.
- A conglomeratic layer between the two layers of schists with evenly distributed round-shaped lithic fragments within a reddish quartz-schist matrix and,
- A metamorphosed clay-dominated schist series of predominantly garnet, tourmaline, staurolite and sericite schists. In this series, the foliation is parallel to the stratification.

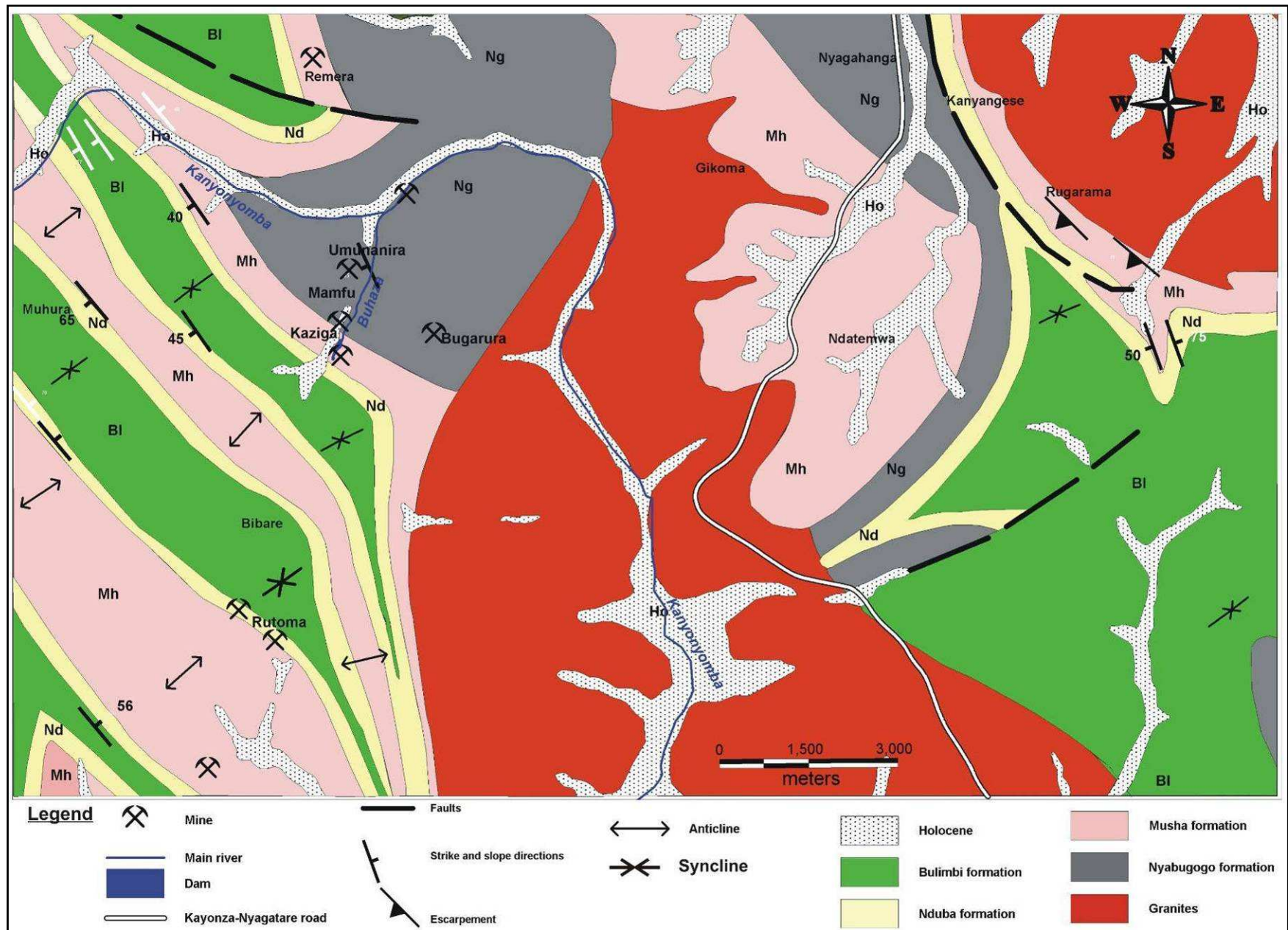


Figure 4.21: Geological map of Bugarura-Kuluti-Bibare prospect (adapted after Theunissen et al. 1991).

4.3.2 Deformation

The Bibare, Mamfu-Bugarura and Kuluti mining areas are located astride a succession of synclines and anticlines which form the SE extension of the NW-trending Byumba synclinorium. They comprise from the west to the east the Gahara-Rwankuba anticline, the Muhura-Bibare syncline, the Bwisige anticline, the Nyagahanga syncline, the Kabarore anticline and the Kiburara-Rubona syncline. The tectonic structures seem to be more complex in the Kuluti zone where they are influenced by the intrusion of the Bujumu-Rugarama, Muhazi and Kabarore granites.

A major NW-SE trending fault occurs in the south-eastern part of the Mamfu-Bugarura deposit; an additional NW-SE to N-S fault dissects the geological formations between Muhazi (W), Kabarore (NE) and Bujumu-Rugarama (E) granites (Figure 4.21).

4.3.3 Mineralization

Situated underneath a secondary dome-shaped tin alluvial placer consisting of a 50m to 60m thick layer of lateritized and brecciated old eluvial sediments, the richest tin deposit of Bugarura-Mamfu consists of two stockworks of quartz veins which, in the depths, become wide and are extended in the pegmatite body:

- In Bugarura, the mineralized quartz veins are E-W to NW-SE and N-S orientated and are extended over an area of approximately 1350m * 500m. Economically exploitable mineralization occurs in veins parallel to the quartzite layers and more than 20 of the latter (thickness range: 2-20 m) have been identified in the core of a lateritized dome. The greisens areas are the preferred zones for disseminated tin mineralization. The latter is sparsely distributed and genetically associated to network of milky quartz veins and veinlets which should become locally red in colour due to their amount of alkali-feldspar.
- The second stockwork of cassiterite-bearing quartz veins is located further south in Mamfu where they have NW - trends and host economically exploitable reserves. Here, the extension of tin placers is limited and thus of less economic significance.

The main commodity exploited in the Bugarura and Mamfu mining concessions is cassiterite which is, macroscopically, similar to the tin ores of the Rwinkwavu and Musha-Ntungwa types described in sections 4.1.3 and 4.2.3.

In Kuluti, the biotite zone is barren contrarily to the tourmaline-sericite-mica schist zone which may contain minor amounts of tapiolite $[(Fe, Mn)(Ta, Nb)_2O_6]$ -tetragonal and columbite/tantalite.

The pegmatites, greisens and quartz veins which intrude the metamorphic schist zone host economically exploitable tin mineralization and the average grades of 1.07kg/m³ (in placers) and 3kg/m³ (in quartz veins) were reported (BRGM, 1987).

Cassiterite is the principal ore mineral exploited in Kuluti, but in some mining sites such as Nyarunazi, Kivuba, Kayenzi and Nyagasiga, the coltan mineralization may co-exist with cassiterite mineralization.

Bibare concession is also known for tin mineralization which is mined in Bibare, Rutoma, Biniga and Gituza mining sites (BRGM, 1987; MINETAÏN, 1965) but also important quantities of wolframite have been exploited in Biniga and Rwankuba localities. The latter is the south-westernmost mining site of the Bibare concession and at the same time, the NE-extension of Gahengeri - Nyagasambu wolframite deposits (Roka Rwanda, pers. comm.).

4.3.4 Petrography

Eleven representative samples of barren veins and Sn-, Nb/Ta-, W-bearing ores were received from RMCA-Tervuren-Belgium or sampled during the June-August 2010 field trip for petrographic analyses and the most important characteristics of these rocks are shown in Table 4.3.1.

The country-rock in the three prospects (Rwinkwavu, Musha-Ntunga and Bugarura-Kuluti) does not show big differences amongst one another and they have been described in sections 4.1 and 4.2. They therefore, do not form an essential part of the currently investigated prospect. Only SEM-EDX and fluid inclusion studies were conducted on a representative selection of those specific samples.

The results for SEM-EDX/WDX analyses are shown in this section whereas the microthermometric investigations are discussed in chapter 5.

Table 4.3.1: List of geographic location and rock - types of samples from Bugarura-Kuluti-Bibare.

Ref.	Sample	Locality	Easting (m)	Northing (m)	Elevation (m)	Rock-type
1	JC-32*	Bujumu	544560	9813070	-	Quartz vein
2	JC-33*	Bujumu	545410	9813230	-	Cassiterite-bearing vein
3	JC-34*	Bugarura	537570	9807770	-	Concentrate of mixed cassiterite-coltan.
4	JC-35*	Rwankuba	537100	9798400	-	Concentrate of wolframite
5	JC-36*	Rwankuba	538690	9796320	-	Concentrate of cassiterite
6	JC-28-6-1 641	Bugarura	537261	9807353	1610	Quartz tourmalinite
7	JC-28-6-2	Bugarura	537734	9807824	-	Concentrate of cassiterite
8	JC-28-6-2 640	Bugarura	536300	9808950	-	Quartz vein
9	JC-28-6-3	Bugarura	536150	9808030	-	Concentrate of cassiterite
10	JC-28-6-4	Mamfu	536121	9808201	-	Quartz vein
11	JC-28-6-4 645	Bugarura	536279	9809024	1639	Concentrate of cassiterite

(*)-Samples from the RMCA Collection

4.3.5 Mineral Chemistry of cassiterite, columbite-tantalite and wolframite

Chemical and mineralogical variations in the Sn-, W- and Nb-Ta- bearing minerals in the Bugarura-Kuluti mining district were discussed based on the results from SEM-EDX/WDX analyses performed on six (6) ore mineral samples. These include JC-36 from Rwankuba tungsten mine, JC-34 with Sn-Nb-Ta and four Sn-bearing samples.

A total of around 70 analyses were completed and the results are displayed in Tables 4.3.2, 4.3.3, 4.3.5 and in Appendix 4. The cassiterite, wolframite and columbite-tantalite minerals in the investigated ore mineral samples are associated with silicate oxide and sulphide mineral phases such as quartz, biotite, muscovite, garnet, tourmaline, Fe-minerals, rutile, ilmenite, zircon and sulphides (chalcopyrite, arsenopyrite and pyrite). This section will focus specifically on the mineral chemistry of the economically exploited ore minerals found in Bugarura-Kuluti: cassiterite, coltan and wolframite.

A. Mineral chemistry of cassiterite

Table 4.3.2 indicates that the majority of analyses of cassiterite samples are identified as almost pure tin minerals but minor amounts of other mineral phases occur in inclusions.

Table 4.3.2 Average chemical compositions of cassiterite group minerals from Bugarura - Kuluti.

Elem/Samples	JC-33	JC-34	JC-28-6-1 641	JC-28-6-2 640	JC-28-6-4 645	LLD*
WO ₃	<DL	0.72+/-0.53	<DL	<DL	<DL	0.69
Nb ₂ O ₅	<DL	1.69+/-0.22	<DL	0.23+/-0.09	n.d.	0.16
Ta ₂ O ₅	<DL	3.34+/-1.10	<DL	<DL	n.d.	0.76
SnO ₂	92.89+/-1.18	91.52+/-1.73	95.90+/-1.25	90.50+/-1.30	99.08+/-1.29	2.70
TiO ₂	0.16+/-0.05	<DL	0.34+/-0.14	0.45+/-0.07	0.22+/-0.11	0.16
GeO ₂	0.21+/-0.07	n.d.	n.d.	n.d.	n.d.	0.03
HfO ₂	0.64+/-0.39	n.d.	n.d.	n.d.	n.d.	0.16
SiO ₂	2.08+/-0.04	0.91+/-0.05	n.d.	1.85+/-0.05	n.d.	0.06
ZrO ₂	<DL	<DL	<DL	0.14+/-0.06	<DL	0.06
Fe ₂ O ₃	<DL	0.37+/-0.06	2.38+/-0.14	5.91+/-0.21	n.d.	0.18
As ₂ O ₃	0.30+/-0.16	n.d.	n.d.	0.13+/-0.10	n.d.	0.10
Y ₂ O ₃	0.18+/-0.05	n.d.	n.d.	n.d.	n.d.	0.02
Al ₂ O ₃	0.11+/-0.01	1.02+/-0.03	0.47+/-0.03	0.33+/-0.02	n.d.	0.04
MgO	n.d.	0.03+/-0.02	n.d.	<DL	n.d.	0.01
MnO	<DL	0.17+/-0.04	n.d.	<DL	0.09+/-0.06	0.05
BaO	0.32+/-0.12	n.d.	n.d.	n.d.	n.d.	0.05
CoO	0.048+/-0.02	n.d.	n.d.	n.d.	n.d.	0.01
NiO	0.07+/-0.05	n.d.	n.d.	n.d.	n.d.	0.02
ZnO	0.12+/-0.04	<DL	n.d.	n.d.	n.d.	0.02
SrO	0.07+/-0.03	n.d.	n.d.	n.d.	n.d.	0.01
CdO	0.07+/-0.03	<DL	n.d.	n.d.	n.d.	0.02
Na ₂ O	0.51+/-0.04	0.07+/-0.01	n.d.	n.d.	n.d.	0.02
Cu ₂ O	0.13+/-0.09	n.d.	n.d.	n.d.	n.d.	0.03
Pt	0.22+/-0.13	n.d.	n.d.	n.d.	n.d.	0.05

Abbreviations: <DL-Below detection limit; LLD*-lower limit of detection, n.d.: not determined.

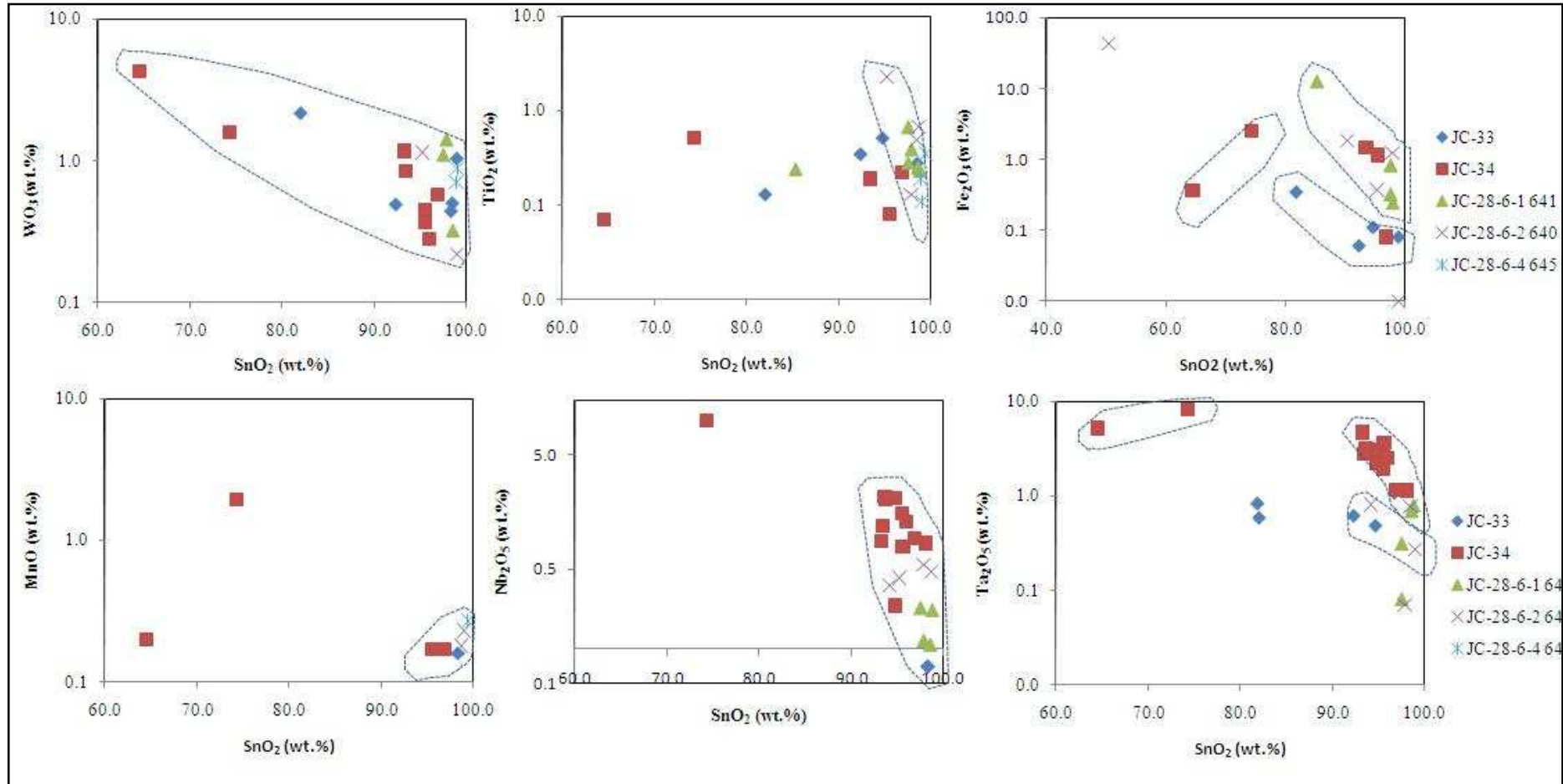


Figure 4.22: Bivariate diagrams of SnO₂ against WO₃, TiO₂, Fe₂O₃, Nb₂O₅, Ta₂O₅ and MnO for the cassiterite samples from Bugarura-Kuluti. SnO₂, WO₃, TiO₂, Fe₂O₃, Nb₂O₅, Ta₂O₅ and MnO contents are in wt. %.

The cassiterite mineralization is mostly composed of pure tin oxide – SnO₂ with average contents (per cassiterite sample) ranging between 90.50 and 99.08 +/-1.3 wt. %.

In addition to tin oxide, the SEM-EDX/WDX analyses showed other major oxides for which respective average content values are: 0.11 to 1.67+/- 0.23 wt. % Nb₂O₅, 0.24 to 3.34+/-1.1 wt. % Ta₂O₅, 0.07 to 0.45+/-0.07 wt.% TiO₂, 0.37 to 5.9+/-0.2 wt.% Fe₂O₃ and 0.05 to 0.17+/-0.03 wt.% MnO.

The discrimination diagrams plotted in Figure 4.22 indicate that tin oxide correlates poorly or negatively with other element-oxides.

With the aim to understand the chemical variation of analyzed cassiterite samples, the results of analyses also were plotted in two variation diagrams which are log [(Ta+Nb)/Sn] vs. log [(Fe+Mn)/Sn] and log [W/Sn] vs. log [(Fe+Mn)/Sn] after Möller et al. (1988) (Figures 4.23 and 4.24).

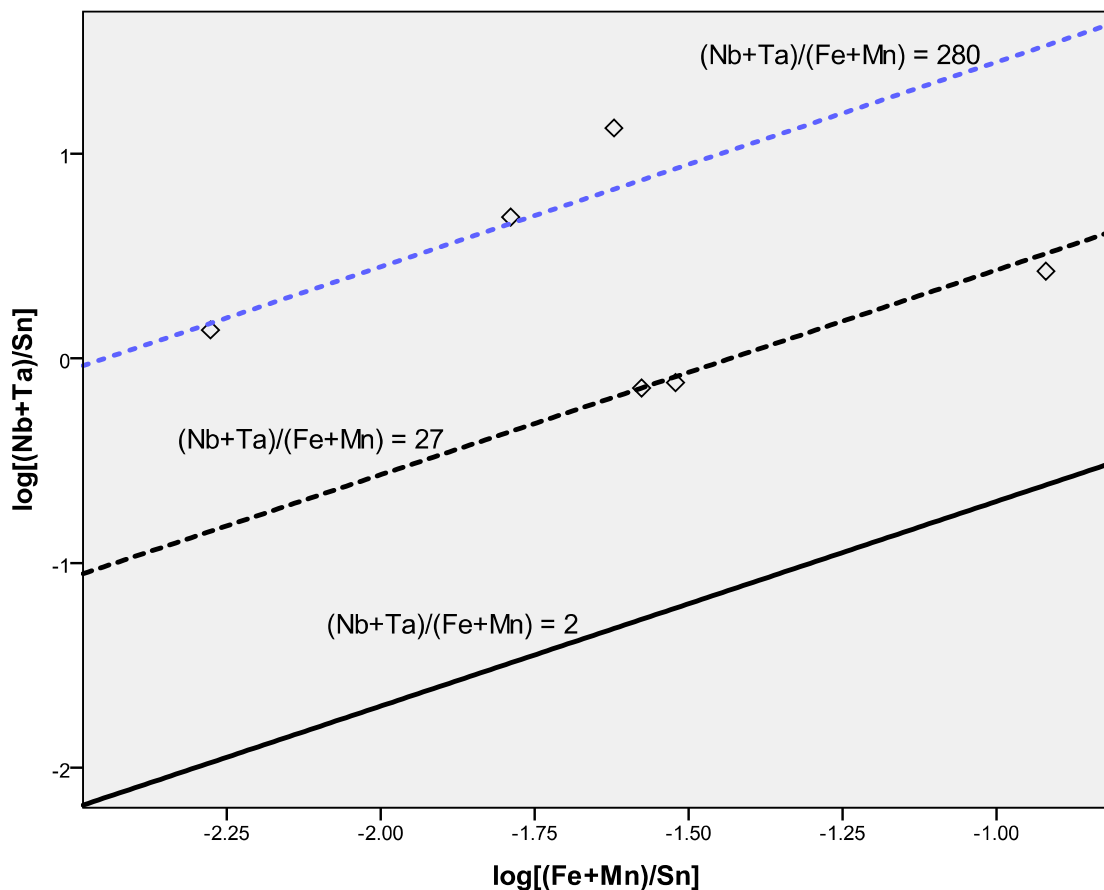


Figure 4.23: Correlation diagrams of analyses for cassiterite samples from Bugarura using $\log[(\text{Ta}+\text{Nb})/\text{Sn}]$ vs. $\log[(\text{Fe}+\text{Mn})/\text{Sn}]$ after Möller et al. (1988). Ta, Nb, Fe, Mn and Sn contents are in apfu.

On the one hand, the value distribution shows two types of samples (Figure 4.23): those which are plotting along $(\text{Nb}+\text{Ta})/(\text{Fe}+\text{Mn}) = 27$ and others which are along $(\text{Nb}+\text{Ta})/(\text{Fe}+\text{Mn}) = 280$. All analyzed samples plot above the line $(\text{Ta}+\text{Nb})/(\text{Fe}+\text{Mn}) = 2$ (proportion 1:2) and therefore, indicate that the cassiterite contamination is not controlled by $(\text{Fe}, \text{Mn})(\text{Ta}, \text{Nb})_2\text{O}_6$ mineral phase.

The excess of $(\text{Nb}+\text{Ta})$ content may point towards the existence of a simple substitution mechanism in the solid solution of $(\text{Nb}, \text{Ta})\text{O}_2$ in SnO_2 .

On the other hand, Figure 4.24 shows that three types of substitution mechanisms in the Bugarura-Kuluti cassiterite occur in the W/Sn vs. $(\text{Fe}+\text{Mn})/\text{Sn}$ discrimination diagram (Möller et al., 1988; Abdalla et al., 2008):

- Type: $\text{Sn}^{4+} \leftrightarrow \text{W}^{4+}$ concerns mainly the samples of the first group (indicated in Figure 4.24 as cass1) displaying excess of W over Fe+Mn. This should therefore compose with a solid solution of WO_2 in SnO_2 based on a simple substitution mechanism Sn-W.
- Type: $\text{Sn}^{4+} \leftrightarrow \text{Fe}^{3+} + \text{H}^+$ or $\text{Sn}^{4+} + \text{O}^{2-} \leftrightarrow \text{Fe}^{3+} + \text{OH}^-$ is associated with the group of cassiterite samples indicated as cass2 with a clear excess of Fe+Mn over the W content and according to Möller et al. (1988), this may indicate the presence of a component such as Fe_2WO_6 in a solid solution or Fe-rich phases within cassiterite mineralization.
- Type: $2 \text{Sn}^{4+} \leftrightarrow \text{W}^{6+} + (\text{Fe}, \text{Mn})^{2+}$ related to the samples of a group named cass3 in the same figure plotting along the line $\text{W}/(\text{Fe}+\text{Mn}) = 1$ (proportion 1:1 on atomic level) which indicates that the contamination within these cassiterite samples seems to be likely controlled by solid inclusions of type $(\text{Fe}, \text{Mn})\text{WO}_4$.

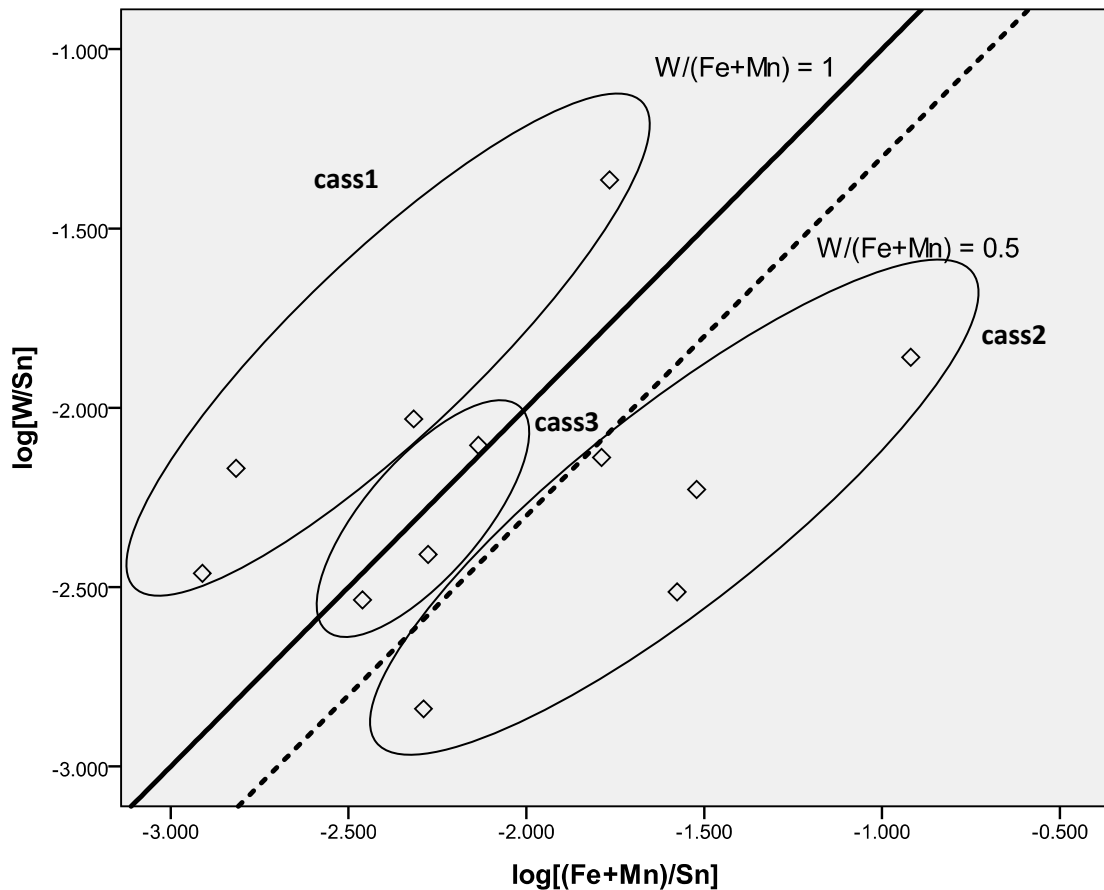


Figure 4.24: Correlation diagrams of analyses for cassiterite samples from Bugarura using $\log [W/Sn]$ vs. $\log [(Fe+Mn)/Sn]$ after Möller et al. (1988). Fe, Mn and Sn contents are in apfu.

B. Mineral chemistry of columbite-tantalite

A study of chemical mineralogy of the columbite-tantalite mineralization from Bujumu was carried out on the only coltan sample JC-34. Investigated areas on the sample were photographed by back-scattered electron image (BSE), structural formulae calculated and the results per analyses were co-plotted with the results of investigated samples from Rwanda after Melcher et al. (2009) in the “columbite quadrilateral” after Beurlen et al. (2008). All the analytical data are reflected in Table 4.3.3.

The results of the analyses (Table 4.3.4) show that the “coltan” mineral is mostly composed of tantalum, averaging 41.10 ± 2.5 wt. % Ta_2O_5 , niobium, with 36.50 ± 0.9 wt. % Nb_2O_5 in average, Fe_2O_3 with 9.93 ± 0.7 wt. % and manganese with averages of 7.90 ± 0.66 wt. % of MnO .

Table 4.3.3: Chemical composition of coltan analyses of sample JC-34 from Bugarura-Kuluti (this study) compared to those of the Cyubi, Ruhanga and Gasasa mines (Melcher et al.; 2009).

	Bugarura-Kuluti*			Cyubi**				Ruhanga **			Gasasa**	
	1	2	3	LLD*	6	8	10	1	100	102	20	21
WO ₃	2.55	1.08	0.89	2.02	n.d.	n.d.	0.114	0.128	n.d.	n.d.	0.236	0.161
Nb ₂ O ₅	34.4	39.72	35.38	1.84	19.32	5.57	5.54	59.09	14.01	4.37	47.96	26.07
Ta ₂ O ₅	44.68	40.88	37.74	5.83	62.93	77.19	63.96	19.45	68.69	80.02	32.46	56.36
TiO ₂	1.18	n.d.	n.d.	0.12	0.18	0.229	2.54	0.654	0.255	n.d.	0.253	0.205
SnO ₂	0.79	n.d.	1.28	0.52	n.d.	0.586	13.1	0.17	0.218	n.d.	n.d.	n.d.
Fe ₂ O ₃	9.09	10.16	10.54	1.43	11.2	14.32	7.09	3.65	8.53	1.97	12.75	13.56
In ₂ O ₃	n.d.	n.d.	1.16	0.35	n.d.	n.d.	n.d.	n.d.	n.d.	n.d.	n.d.	n.d.
Tl ₂ O ₃	n.d.	n.d.	0.53	0.32	n.d.	n.d.	n.d.	n.d.	n.d.	n.d.	n.d.	n.d.
MnO	7.31	8.16	8.24	1.32	5.54	1.48	6.52	15.69	7.05	12.34	6.82	4.09
Total	100	100	100		99.17	99.37	98.86	98.83	98.753	98.7	100.48	100.4
Structural formula calculated on the basis of 6 oxygens												
W	0.044	0.019	0.015	n.d.	0.000	0.000	0.002	0.002	0.000	0.000	0.004	0.003
Nb	1.036	1.196	1.065	n.d.	0.582	0.168	0.167	1.780	0.422	0.132	1.444	0.785
Ta	0.810	0.741	0.684	n.d.	1.141	1.399	1.159	0.353	1.245	1.450	0.588	1.021
Ti	0.059	0.000	0.000	n.d.	0.009	0.011	0.127	0.033	0.013	0.000	0.013	0.010
Sn	0.021	0.000	0.034	n.d.	0.000	0.016	0.347	0.005	0.006	0.000	0.000	0.000
Fe	0.455	0.509	0.528	n.d.	0.561	0.717	0.355	0.183	0.427	0.099	0.638	0.679
In	0.000	0.000	0.033	n.d.	0.000	0.000	0.000	0.000	0.000	0.000	0.000	0.000
Tl	0.000	0.000	0.009	n.d.	0.000	0.000	0.000	0.000	0.000	0.000	0.000	0.000
Mn	0.412	0.460	0.465	n.d.	0.313	0.083	0.368	0.885	0.398	0.696	0.385	0.231
Σcat.	2.837	2.925	2.834	n.d.	2.005	2.394	2.525	3.23	2.510	2.377	3.072	2.729
Nb/Ta	1.279	1.615	1.558	n.d.	0.510	0.120	0.144	5.048	0.339	0.091	2.455	0.769
Nb+Ta	1.846	1.937	1.749	n.d.	1.722	1.567	1.326	2.132	1.667	1.582	2.033	1.807
Ta/(Ta+Nb)	0.439	0.38	0.391	n.d.	0.662	0.893	0.874	0.165	0.747	0.917	0.289	0.565
Mn/(Fe+Mn)	0.475	0.475	0.468	n.d.	0.358	0.104	0.509	0.829	0.482	0.876	0.376	0.254

*Present study, LLD-lower limit of detection; **Melcher et al. (2009) with LLD (in wt. %) of 0.03 (WO₃), 0.15 (Nb₂O₅), 0.12 (Ta₂O₅), 0.04 (TiO₂), 0.03 (SnO₂), 0.03 (Fe₂O₃) and 0.04 (MnO); n.d.-not determined.

The W- average content is 1.51+/-0.7 wt. % WO₃ whereas the average Ti content corresponds to 0.39 +/-0.06 wt. % TiO₂.

The bulk structural formulae and the main group in which those Nb-, Ta- bearing minerals of the analyses are compiled in Table 4.3.4

Table 4.3.4: Structural chemical formula and nomenclature of selected “coltan” analyses from Bugarura-Kuluti.

Spot	Structural formula	Other chemical elements detected by SEM-EDX	Possible group
1	$Mn_{0.412}Fe_{0.455}Nb_{1.036}Ta_{0.81}O_6$	W, Ti and Sn	Ferro-columbite
2	$Mn_{0.46}Fe_{0.509}Nb_{1.196}Ta_{0.741}O_6$	W, Ti and Sn	Ferro-columbite
3	$Mn_{0.465}Fe_{0.528}Nb_{1.065}Ta_{0.684}O_6$	W, Sn, In ? and Tl ?	Ferro-columbite

The averages of Nb/Ta ratios of the columbite-tantalite sample from the study area are > 1 which indicates enrichment in Nb. In addition, the Nb/Ta ratio > 1 allows us classifying this sample in the columbite group (Pohl, 2011).

Lastly, and based on Beurlen et al. (2008), the results of each analysis were reported in the quadrilateral diagram representing the end-member species in Figure 4.25. The columbite-tantalite sample from Bugarura-Kuluti shows Ta / (Ta+Nb) ratio varying between 0.382 and 0.439 and a constant value of Mn/ (Mn+Fe) ratio which is 0.47. In the Beurlen et al. (2008) diagram, they are plotting in the ferro-columbite group rich end-members. In comparison with Melcher et al. (2009), the Bugarura-Kuluti coltan is enriched in Fe and Nb compared to the samples from Cyubi and Gasasa (enriched in Ta and Fe) or from Ruhanga (enriched in Mn).

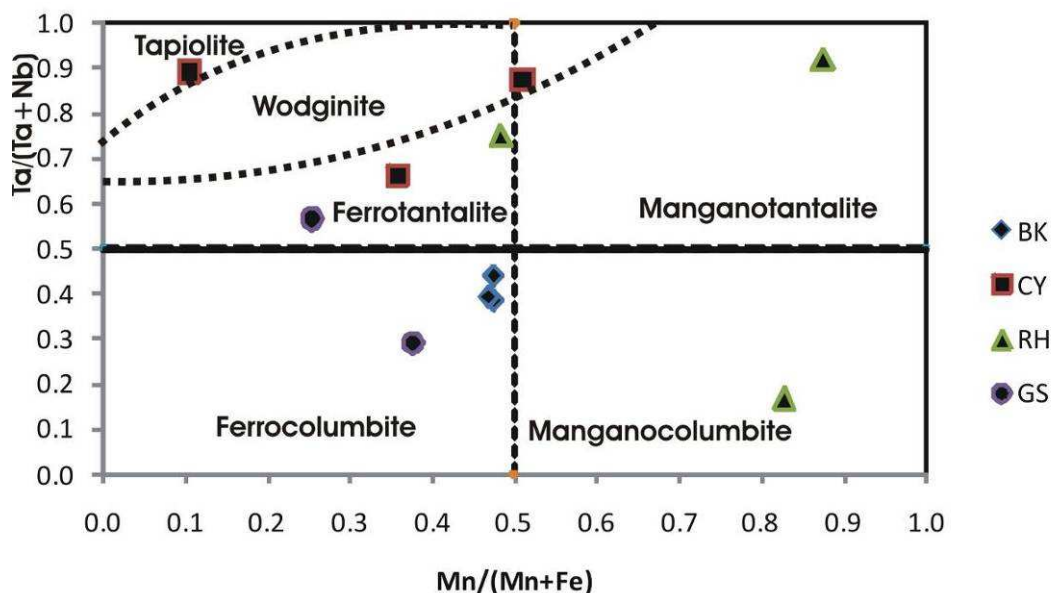


Figure 4.25: Chemical composition of selected analyses of columbite-tantalite samples from Bugarura-Kuluti (BK) (this study) and from Cyubi (CY), Ruhanga (RH) and Gasasa (GS) (Melcher et al., 2009) plotted in FeTa-FeNb-MnNb-MnTa quadrilateral after Beurlen et al. (2008).

In spite of the more or less sparse distribution of the complete data set in this columbite quadrilateral, the general trends begin with Nb-rich compositions for less fractionated pegmatites and evolve to the

Ta-rich series and according to Linnen and Keppler (1997) and Beurlen et al. (2008) this increase in Ta/(Ta+Nb) ratio with the degree of felsic magmatic melts fractionation should be explained as a consequence of the lower solubility of Nb-rich columbite group members in peraluminous granite/pegmatite melts in comparison with the Ta-rich members.

C. Mineral chemistry of wolframite

One ferberite ore sample, JC-36 from Rwankuba (Bibare concession) has been obtained from the collection of RMCA and analyzed using SEM-EDX/WDX facilities of the Department of Geology, University of the Free State, Bloemfontein, South Africa.

Table 4.3.5: Summary of the chemical composition of investigated tungsten-bearing ore samples from Bibare mining concession (Rwankuba mine).

Sample JC-36									
Spots:	1	2	3	4	5	9	10	11	LLD*
WO ₃	71.3	74.2	72.5	70.2	70.8	71.9	75.3	67.0	3.6
Fe ₂ O ₃	24.7	24.4	25.2	26.4	25.6	23.7	19.8	32.3	0.7
MnO	1.4	1.1	0.5	3.0	0.9	0.9	3.9	<DL	0.3
SnO ₂	n.d.	n.d.	n.d.	n.d.	n.d.	0.0	0.1	n.d.	0.0
MgO	0.4	0.2	0.2	0.2	0.2	n.d.	n.d.	0.5	0.1
Nb ₂ O ₅	n.d.	n.d.	n.d.	n.d.	n.d.	0.2	0.9	n.d.	0.0
Ta ₂ O ₅	0.9	n.d.	<DL	<DL	<DL	1.2	n.d.	<DL	0.7
P ₂ O ₅	1.2	n.d.	1.5	n.d.	2.1	2.1	n.d.	n.d.	0.1
Total	100.0	100.0	100.0	100.0	100.0	99.9	100.0	100.0	
Structural formula calculated based on 4 oxygens									
W	0.84	0.87	0.85	0.82	0.83	0.84	0.88	0.79	-
Fe	0.84	0.83	0.86	0.90	0.87	0.81	0.67	1.10	-
Mn	0.05	0.04	0.02	0.11	0.04	0.03	0.15	0.00	-
Sn	0.00	0.00	0.00	0.00	0.00	0.00	0.00	0.00	-
Mg	0.02	0.02	0.01	0.01	0.01	0.00	0.00	0.03	-
Nb	0.00	0.00	0.00	0.00	0.00	0.00	0.02	0.00	-
Ta	0.01	0.00	0.00	0.00	0.00	0.01	0.00	0.00	-
P	0.05	0.00	0.06	0.00	0.08	0.08	0.00	0.00	-
∑Cat.	1.82	1.76	1.80	1.85	1.84	1.78	1.73	1.92	-

Abbreviations: n.d.-not determined; <DL-below detection limit; LLD-lower limit of detection.

A summary of the chemical compositions of 8 analyses performed on JC-36 is presented in Table 4.3.5 while Appendix 4, which is an overview of the mineral chemistry of the whole sample, shows that besides the tungsten ore, the paragenetic sequence also reveals the existence of quartz and Fe-

minerals which may possibly correspond to hematite and/or goethite. The sample seems likely to contain minor amounts of phosphate minerals. Cassiterite and coltan are in traces.

The 8 analyses of the wolframite samples show three dominant oxides:

1. **Tungsten oxide- WO_3 :** WO_3 contents range from 67 to 75.3 wt. %.
2. **Total iron oxide- Fe_2O_3** ranges between 19.8 and 32.3 wt. %.
3. **Manganese oxide- MnO :** The measured contents are from below 1 up to 3.9 wt. %.

The structural chemical formula calculated is almost the same for all the analyses and can roughly be written as follows: **FeWO_4** which indicates that the investigated wolframite sample is a ferberite.

5. Fluid inclusion investigations

5.1 Introduction

The preliminary fluid inclusion microthermometric analyses on quartz crystals within various Sn-, W- and Nb-/Ta- mines of East-Rwanda were completed to constrain the temperature, salinity and general composition of the fluid reservoir from which they crystallized with the aim of having a clear understanding of the evolution of the mineralizing fluids.

Ten hydrothermal quartz vein crystals were sampled during the June-August 2010 field work from the study area and investigated for fluid inclusions. Five samples were from Rwinkwavu, two from Musha-Ntungwa and three from Bugarura-Kuluti-Bibare mining concession (Appendix 3).

In addition and in order to compare, one quartz vein sample from Bugarama tungsten mine (Burera District-Northern Province) which is the north-westernmost mine of the central Rwandan “Tungsten Belt” (Dewaele et al., 2010), one quartz sample from Cyubi coltan mine (Muhanga District, Southern Province) and one cassiterite sample from Rutongo tin mine (Rulindo District, Northern Province and located 25km far from Kigali City) also have been investigated. The expected comparison based on the present study, was however not possible due to a limited number of investigated fluid inclusions for these samples and because the above mentioned prospects were not the priority for the current research.

5.2 Mineralizing fluid properties and evolutionary trends

Doubly polished thick sections have been prepared and the transmitted light microscopy techniques using an OLYMPUS BX51 microscope were used for the first fluid inclusions mapping at room temperature (19-21°C).

In addition to the microscopic investigations, the freezing and heating microthermometric methods (Shepherd et al., 1985) were applied to the fluid inclusions with the size above 10 µm (Figure 5.2a) using the LINKAM TMSG 600 stage. Around one hundred heating-freezing measurements were made. Pure CO₂ inclusions in quartz were used for the calibration of the instrument at the triple point of CO₂ (-56.6°C).

The selected fluid inclusions were first of all cooled down to between -70°C and -100°C at the rates of 10 to 20°C/minute, then stepwise, heated up at the rates of 0.5 to 5°C/minute and the changes along the time of the heating were recorded.

Among the fluid inclusion properties recorded and compiled in Table 5.2 were the eutectic temperatures (T_e), the total melting temperatures of ice ($T_{m_{ice}}$), the homogenization temperatures for CO₂ ($T_{h_{CO_2}}$) and the total homogenization temperatures (T_h).

The mapping showed that the fluid inclusions in the samples from the study area are present in various numbers, shapes, sizes (Figure 5.2a) and categories per thick section. Therefore, the identification of fluid inclusion generations was not done during the present study. The isolated and relatively large inclusions (with diameter above 10 µm), probably of primary origin, were considered for this study and will be discussed. The mapping also shows how primary and secondary lode alike fluid inclusions are aligned along healed micro-fractures or micro-cracks. Figure 5.1 shows microphotographs of representative fluid inclusions which were investigated.

Most of the investigated inclusions were two phase (liquid + vapour). They were liquid – dominated. The remaining ones were formed by clusters of very small inclusions with sizes below 10µm and were often monophasic. The existence of two phases in most of the investigated fluid inclusions might indicate the immiscibility between the two phases at the time of trapping (Van den Kerkhof, 1988).

Some of the fluid inclusions of quartz crystal sample JC-19 from the Cyubi coltan mine showed three phases: liquid, vapour and solid phase composed of cubic daughter mineral (possibly halite) and/or other unidentified solid phases. Table 5.2 indicates that two inclusions from Bujumu (Bugarura-Kuluti) were vapour-dominated.

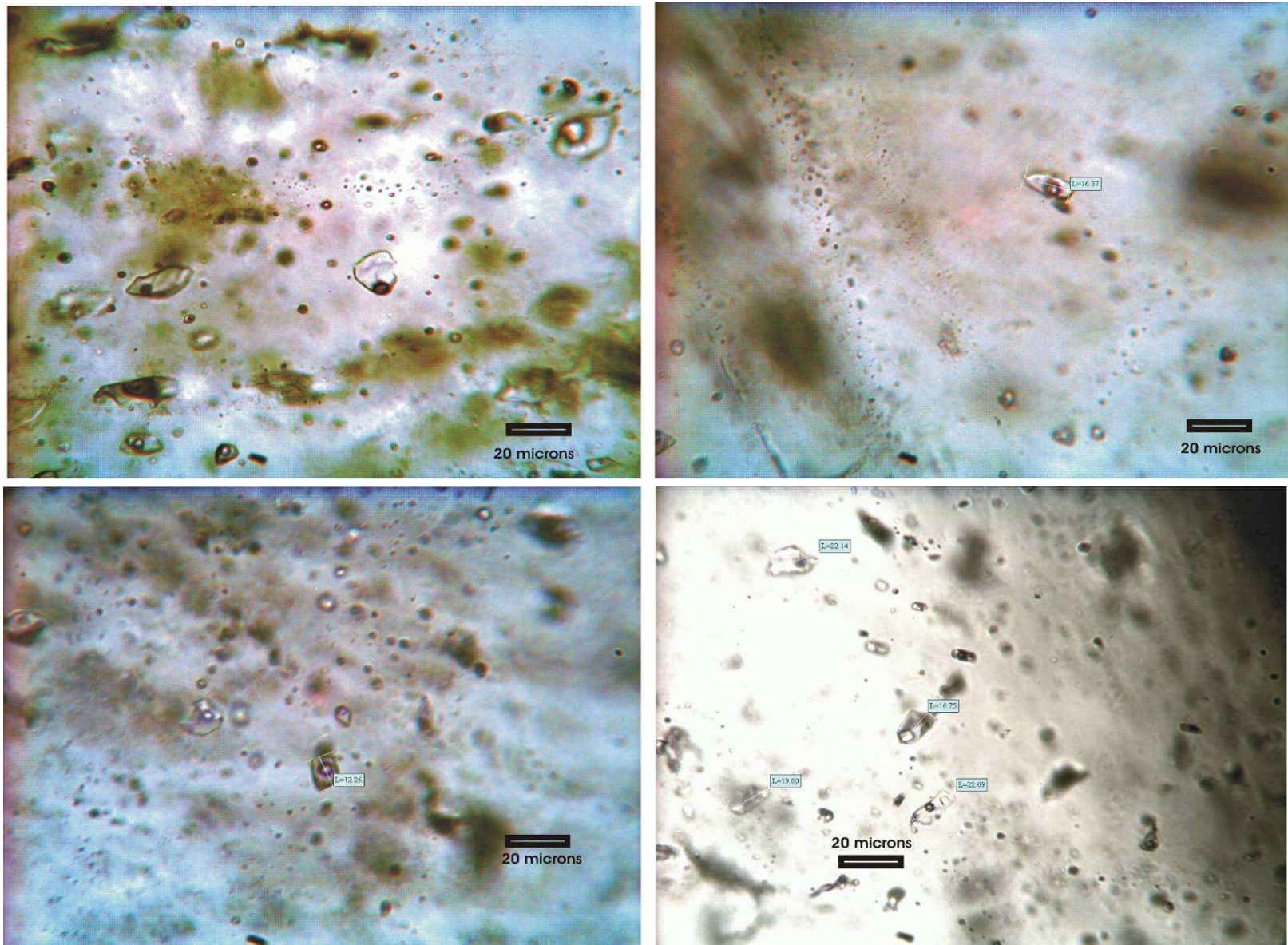


Figure 5.1: Microphotographs showing fluid inclusions in the selected thick sections from quartz crystal samples from the study area. Up-left: monophasic small inclusions with bi- to tri-phase inclusions. Up-right and down-left: trails and single two phase inclusions. Down-right: two phase inclusions and multi-phase inclusion with daughter mineral (possibly halite).

The results from different measurements are summarized in Table 5.2 and the histograms of $T_{m_{ice}}$ and T_h frequency distributions for the two phase fluid inclusions are shown in Figures 5.2b and 5.2c.

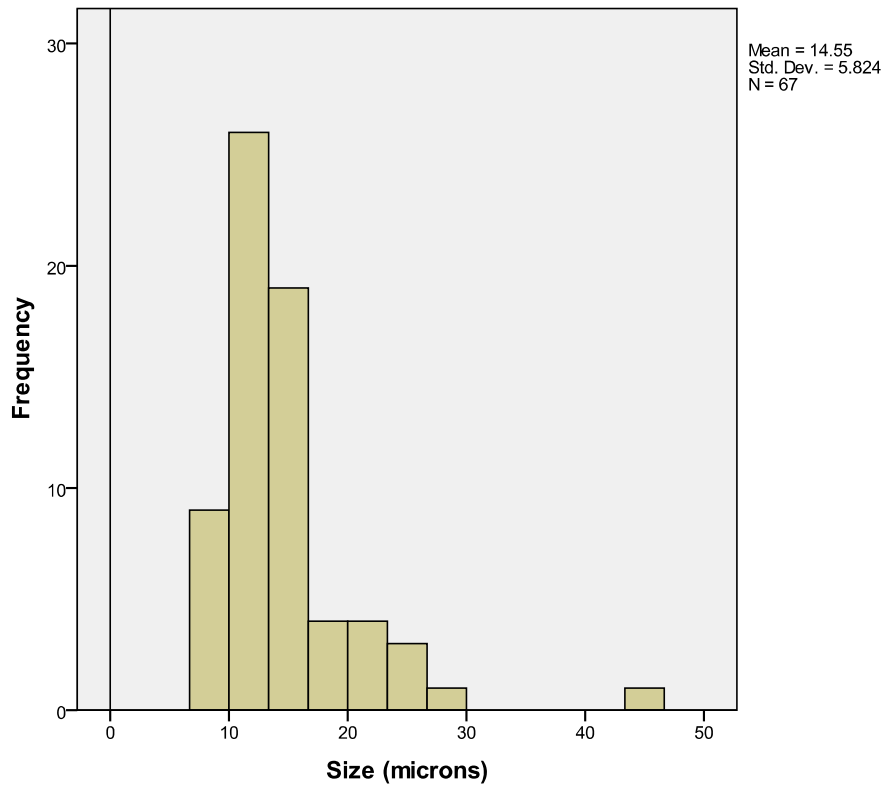


Figure 5.2a: Frequency distribution of investigated fluid inclusions sizes (in μm) from the study area.

The first melting temperature of ice or eutectic temperature (T_e) was very difficult to be accurately observed and therefore complicating the identification of the nature of cations in the studied fluid inclusions. The recorded T_e values in most of the samples from Rwinkwavu and Musha-Ntungwa were very low (between -74°C and -50°C). According to Crawford (1981), Mumm (2008) and Leeder et al. (1986) in Huizenga (2010), the low T_e might indicate the co-existence of various and multiple cations such as Ca^{2+} , Fe^{2+} , Mg^{2+} , ..., (Li and/or Br in some cases) in the chemical composition of the studied fluid inclusions. For the better determination of the chemical composition, further studies such as additional microthermometric investigations and Raman or FT-IR studies are recommended. Also, apart from the lowest value of T_e (-37.10°C) indicating the possible existence of $\text{CaCl}_2\text{-NaCl}$ in the system, most of inclusions of the samples from Bugarura-Kuluti-Bibare display the values of T_e between -20°C and -13°C . This indicates that the NaCl-KCl compositions dominate (Dewaele, pers. comm.).

Most of the recorded final melting temperatures of ice ($T_{m_{ice}}$) for the investigated fluid inclusions of quartz samples are between -13.5°C and -0.3°C . Such values of $T_{m_{ice}}$ indicate low to moderate salinities.

The values of homogenization temperatures of the investigated inclusions range between about 103°C and 360°C. (Figure 5.2c).

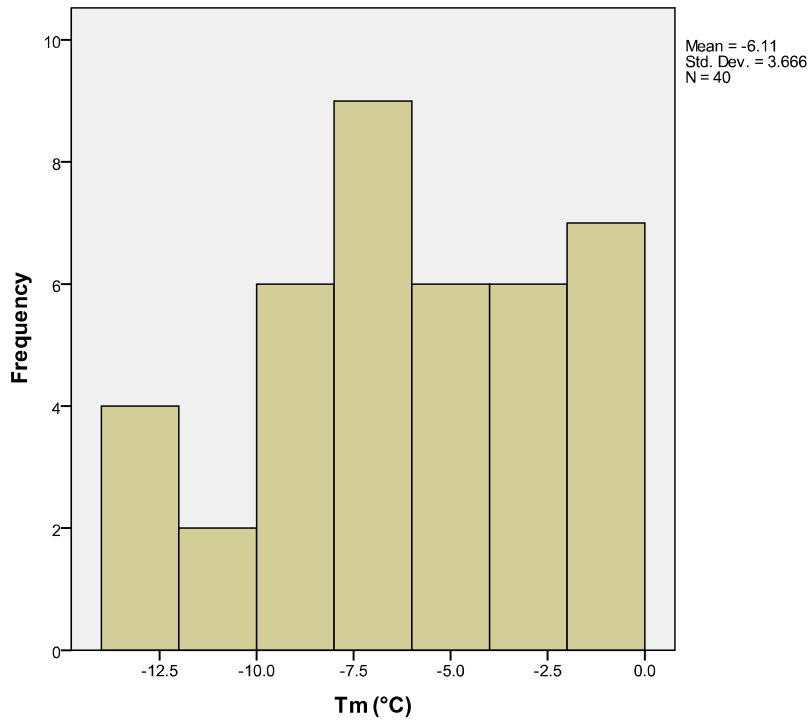


Figure 5.2b: Frequency distribution of the total melting temperature of ice-Tm (°C).

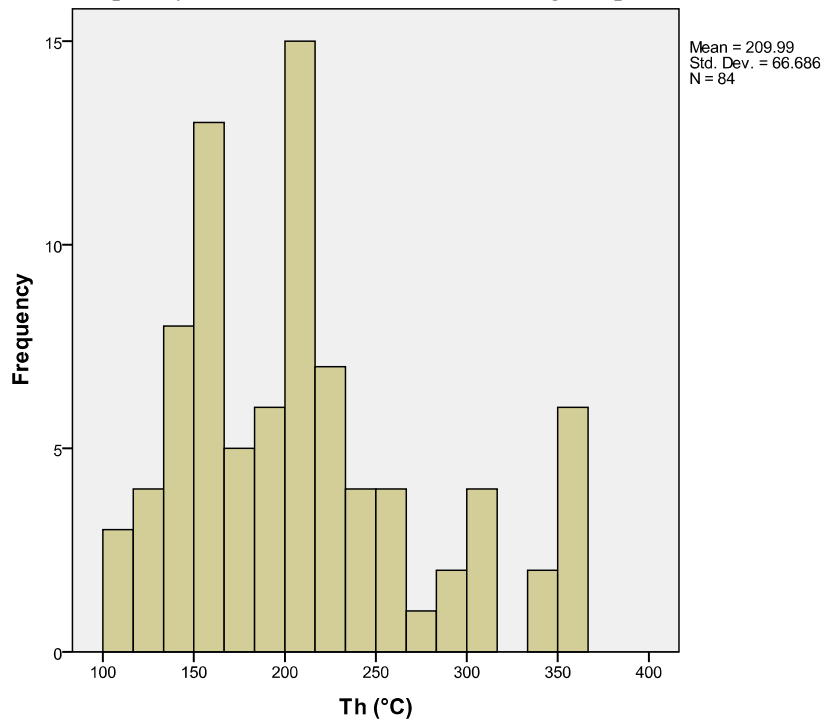


Figure 5.2c: Frequency distribution of homogenization temperatures of fluid inclusions of investigated samples from the study area.

The salinities of fluid inclusions were calculated after the Bodnar and Vityk equation (1994). The same methods were applied for the two phase fluid inclusions where clathrate were observed because the CO₂ was never appearing as a separate phase and thus, its amount was too small to influence the

ice melting temperatures of the fluid inclusions. Table 5.2 shows the salinity estimates and Figure 5.2d shows the distribution frequency. The values range from about 0.5 to 17.3 wt. % NaCl equivalents.

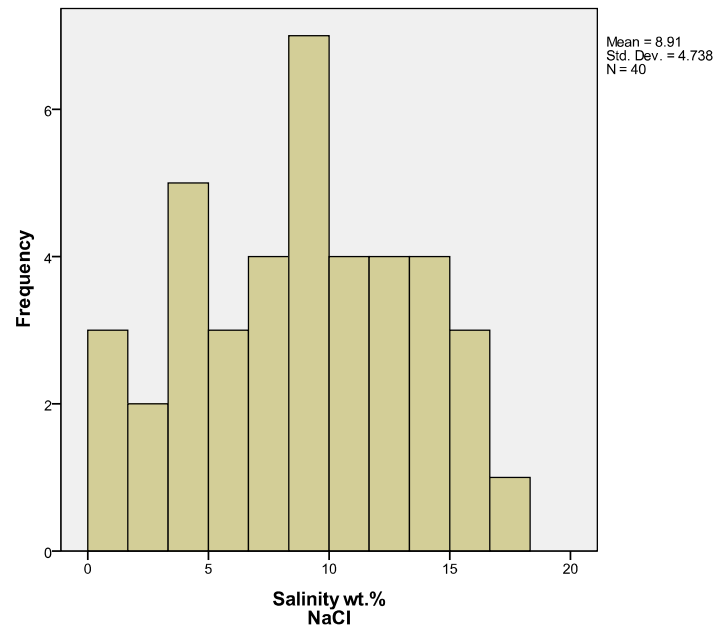


Figure 5.2d: Histogram showing the frequency distribution of salinities.

Using Bodnar and Vityk (1994), the trapping temperatures of investigated inclusions have been estimated and are shown in Table 5.1. The estimated depth of the Rugarama granite cupolas is 7.5km to 8km (MINETAİN, 1965 in the archives of the RMCA) equivalent to lithostatic pressures of more or less 2kbars and therefore those values are only valid for the formation lithostatic pressure of 2kbars. The calculated trapping temperatures range between 150°C and 560°C.

With the aim of understanding the mineralizing fluid evolution, a discrimination diagram of the salinities against the temperatures of homogenization was plotted in Figure 5.3. The latter shows one cluster of inclusions for Rwinkwavu prospect (RW-1) with T_h between 150°C and 250°C and salinities <10 wt. % NaCl equivalent. It also shows two types of fluid inclusions for Musha-Ntunga prospect: MN-1 with T_h between 250°C and 300°C and salinities < 6 wt. % NaCl equivalent and MN-2 with $T_h \approx 150^\circ\text{C}$ and salinity of 13 wt. % NaCl equivalent. The discrimination diagram also shows four types of inclusions for the Bugarura-Kuluti-Bibare samples: BKB-1 with T_h between 250°C and 300°C and salinities >12 wt. % NaCl equiv., BKB-2 with $T_h \approx 350^\circ\text{C}$ and very low salinities, BKB-3 with $T_h < 150^\circ\text{C}$ and salinities between 8 and 16 wt. % NaCl equiv. and BKB-4 with $T_h \approx 200^\circ\text{C}$ and salinity ≈ 8 wt. % NaCl equiv.).

Figure 5.3 shows a wide range of salinities and homogenization temperatures. Such distributions showing the contrast of salinities and homogenization temperatures between the populations of inclusions from the study area indicate various types of fluids inclusions generations of mineralizing fluids with external influences such as a mixing of magmatic solutions with fluids from different sources such as meteoric, connate and/or metamorphic waters. However, to confirm this hypothesis, it would be necessary to carry out additional investigations such as the H, O stable isotope studies on quartz-cassiterite mineral pairs.

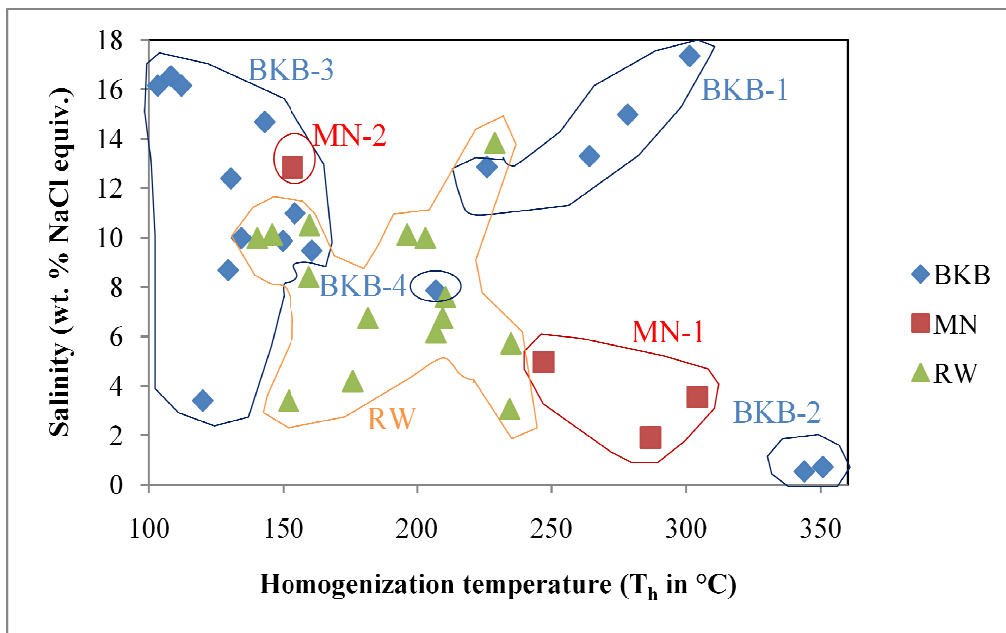


Figure 5.3: Bivariate diagram of homogenization temperatures (T_h in $^{\circ}\text{C}$) vs. salinities (in wt. % NaCl equivalent) for the two phase fluid inclusions in the studied samples.

Abbreviations: BKB-Bugarura-Kuluti-Bibare; MN-Musha-Ntunga; RW-Rwinkwavu.

Table 5.1 Estimated temperatures of hydrothermal ore formation using the equation of inclusion isochores at $P = 2\text{kbars}$ (Bodnar and Vityk, 1994). Yellow: Rwinkwavu, turquoise: Musha-Ntunga; blank: Bugarura-Kuluti and gray: Rutongo, Cyubi and Bugarama.

Salinity[wt. %NaCl]	1.4	8.4	10.1	4.2	10	10.1	10	7.6	6.7	3.1
T_h [$^{\circ}\text{C}$]	140	159.7	145.8	176.1	140.2	196.3	203.1	210.5	209.5	234.4
T_f ($^{\circ}\text{C}$)	220	220	220	250	220	280	280	285	285	320
Salinity[wt. %NaCl]	10	14.7	8.7	12.4	13.9	12.9	7.9	3.4	17.3	0.5
T_h [$^{\circ}\text{C}$]	134.3	143	129.4	130.4	229	226	207	120	301.2	343.8
T_f ($^{\circ}\text{C}$)	190	200	190	190	300	300	280	190	400	550
Salinity[wt. %NaCl]	5.7	5	12.9	3.5	1.9	16.5	16.1	16.1	9.9	9.5
T_h [$^{\circ}\text{C}$]	257.6	247	153.5	304.1	286.7	108.2	112.1	103.3	149.8	160.8
T_f ($^{\circ}\text{C}$)	340	340	200	420	400	160	160	150	220	220
Salinity[wt. %NaCl]	11	13.3	15	0.7	3.4	10.5	6.7	6.2	13.8	5.7
T_h [$^{\circ}\text{C}$]	154.5	264	278.2	350.8	152	160	181.7	207	228.8	234.9
T_f ($^{\circ}\text{C}$)	220	330	360	560	220	220	260	280	300	320

Table 5.2: Microthermometric data from aqueous fluid inclusions in the studied samples.

Sample	Loc.	RT	phase	T _e	T _m	T _{mCO2}	T _{mCL}	T _{hCO2}	T _h	T _d	Salinity NaCl equiv.	Size [μm]	V	L	Observations
JC-15	E	qv	L+V+S	-	-	-	-	-	352.0	-	-	13.60	30	70	-
JC-15	E	qv	-	-	-	-	-	-	352.0	-	-	16.30	45	55	-
JC-15	E	qv	-	-	-	-	-	-	349.2	-	-	10.80	50	50	-
JC-15	E	qv	-	-	-	-	-	-	356.4	-	-	11.80	-	100	-
JC-19	CY	pegm	-	-	-	-	-	-	212.0	-	-	15.00	5	95	-
JC-19	CY	pegm	-	-	-	-	-	13.60	248.0	-	-	26.00	-	100	-
JC-19	CY	pegm	-	-51.40	-	-	-	-	263.5	-	-	11.40	42	58	-
JC-19	CY	pegm	-	-	-	-	-	-	-	-	-	21.10	7	93	-
JC-19	CY	pegm	L+V	-7.50	-0.80	-	-	-	140.0	-	1.40	43.82	13	87	-
JC-19	CY	pegm	L+V+S	-12.50	-	-	-	-	308.3	-	-	13.06	70	30	-
JC-23-6-1	RW														
JC-23-6-3	RW	qv	L+V						164.0						
JC-23-6-3	RW	qv							174.1						
JC-23-6-3	RW	qv	L+V						172.4						
JC-23-6-3	RW	qv	L+V+S						206.7						dark brown to black thick rim around the bubble at 188.3°C

Abbreviations: E-East, CY-Cyubi, RW-Rwinkwavu, BGM-Bugarama, BGR-Bugarura, MN-Musha-Ntunga, BUJ-Bujumu, RUT-Rutongo, RT-rock-type, qv-quartz vein, pegm-pegmatite, cass-cassiterite, L-liquid, V-vapour, S-solid, -: not measured.

Table 5.2 (Continued)

Sample	Loc.	RT	phase	T _e	T _m	T _{mCO₂}	T _{mCL}	T _{hCO₂}	T _h	T _d	Salinity NaCl equiv.	Size [μm]	V	L	Observations
JC-23-6-3	RW	qv	L+V	-	-5.20	-	-	-	159.7	-	8.4	-	29	71	-
JC-23-6-3	RW	qv	L+V	-	-6.70	-	-	-	145.8	-	10.11	-	40	60	-
JC-23-6-3	RW	qv	L+V	-	-2.50	-	-	-	176.1	-	4.18	-	29	71	-
JC-23-6-3	RW	qv	L+V	-	-6.60	-	-	-	140.2	-	9.98	-	36	64	-
JC-23-6-3	RW	qv	S+V	-	-	-	-	-	-	230.1	-	-	-	-	crystal inclusion hosting a gas phase; decrepitation at 230.1°C
JC-23-6-3	RW	qv	L+V+S	-	-6.70	-	-	-	196.3	-	10.11	-	35	65	-
JC-23-6-3	RW	qv	L+V+S	-	-	-	-	31.90	215.6	-	-	-	-	-	-
JC-23-6-3	RW	qv	L+V	-	-6.60	-	-	-	203.1	-	9.98	-	25	75	-
JC-23-6-3	RW	qv	-	-	-	-	-	-	-	162.9	-	-	-	-	dark brown bubble, blue crystal and liquid phase (162.9°C is the T _d)
JC-23-6-3	RW	qv	L+V+S	-	-	-	-	-	-	162.2	-	-	-	-	-
JC-23-6-3	RW	qv	L+V	-	-	-	-	-	207.0	-	-	-	-	-	-

Abbreviations: E-East, CY-Cyubi, RW-Rwinkwavu, BGM-Bugarama, BGR-Bugarura, MN-Musha-Ntungwa, BUJ-Bujumu, RUT-Rutongo, RT-rock-type, qv-quartz vein, pegm-pegmatite, cass-cassiterite, L-liquid, V-vapour, S-solid, -: not measured.

Table 5.2 (continued)

Sample	Loc.	RT	phase	T _e	T _m	T _{mCO2}	T _{mCL}	T _{hCO2}	T _h	T _d	Salinity NaCl equiv.	Size [μm]	V	L	Observations	
JC-23-6-3	RW	qv	L+V	-	-	-	-	-	200.0	-	-	-	-	-	-	
JC-23-6-3	RW	qv	L+V	-	-	-	-	-	156.4	-	-	-	-	-	-	Bubble surrounded by a black rim
JC-24-6-1	RW	qv	L+V	-	-	-	-	-	181.0	-	-	11.68	30	70	-	
JC-24-6-1	RW	qv	L+V	-	-	-	-	-	200.7	-	-	12.26	43	57	-	
JC-24-6-1	RW	qv	L+V	-	-4.8	-	-	-	210.5	-	7.59	17.66	38	62	-	Presence of two immiscible phases of gas?
JC-24-6-1	RW	qv	L+V+S	-	-4.2	-	-	-	209.5	-	6.74	16.37	35	65	-	
JC-24-6-1	RW	qv	L+V	-	-	-	-	-	254.9	-	-	11	36	64	-	
JC-24-6-1	RW	qv	L+V	-	-1.8	-	-	-	234.4	-	3.06	13.97	37	63	-	
JC-26-6-6	BRM	qv	L+ V	-	-3.5	-	-	-	257.6	-	5.71	14.19	41	59	-	dark vapour phase FI near multiple trails of very small FI cross- cutting each other
JC-26-6-6	BRM	qv	L+V	-	-	-	-	-	155.4	-	-	12.36	34	66	-	
JC-27	MN	qv	-	-	-	-	-	-	154.0	-	-	12.00	30	70	-	
JC-27	MN	qv	-	-	-	-	-	-	155.0	-	-	10.50	25	75	-	
JC-27	MN	qv	-	-	-	-	-	57.00	151.0	-	-	20.40	20	80	-	
JC-27	MN	qv	-	-	-	-	-	20.00	146.0	-	-	12.00	35	65	-	

Abbreviations: E-East, CY-Cyubi, RW-Rwinkwavu, BGM-Bugarama, BGR-Bugarura, MN-Musha-Ntungwa, BUJ-Bujumu, RUT-Rutongo, RT-rock-type, qv-quartz vein, pegm-pegmatite, cass-cassiterite, L-liquid, V-vapour, S-solid, -: not measured.

Table 5.2 (continued)

Sample	Loc.	RT	phase	T _e	T _m	T _{mCO₂}	T _{mCL}	T _{hCO₂}	T _h	T _d	Salinity NaCl equiv.	Size [μm]	V	L	Observations
JC-27	MN	qv	-	-	-	-	-	-	-	-	-	8.00	-	100	-
JC-27	MN	qv	-	-	-3.00	-	-	-	247.0	-	4.96	26.00	20	80	-
JC-27	MN	qv	-	-	-	-	-	-	-	-	-	16.00	20	80	-
JC-27	MN	qv	-	-40.00	-	-	-	-	152.5	-	-	-	-	100	-
JC-27	MN	qv	-	-	-9.00	-	-	-	153.5	-	12.85	-	-	100	-
JC-27	MN	qv	-	-	-	-	-	-	200.0	-	-	15.30	40	60	-
JC-27	MN	qv	L+V	-	-	-	-	-	132.5	-	-	18.32	35	65	FI in a crack: secondary FI
JC-27	MN	qv	L+V	-	-2.10	-	-	-	304.1	-	3.55	11.32	25	75	show two immiscible gas phases
JC-27	MN	qv	L+V	-	-	-	-	-	206.7	-	-	10.81	33	67	-
JC-27	MN	qv	L+V	-	-1.10	-	-	-	286.7	-	1.91	12.52	40	60	-
JC-28-6-3	BGR	qv	-	-	-12.60	-	-	-	108.2	-	16.53	-	-	-	-
JC-28-6-3	BGR	qv	-	-	-12.20	-	-	-	112.1	-	16.15	-	-	-	-
JC-28-6-3	BGR	qv	-	-	-12.20	-	-	-	103.3	-	16.15	-	-	-	-
JC-28-6-3	BGR	qv	-	-	-	-	-	-	231.1	-	-	-	-	-	-
JC-28-6-3	BGR	qv	-	-	-	-	-	-	188.2	-	-	-	-	-	-
JC-28-6-4	BGR	qv	L+V	-	-6.5	-	-	-	149.8	-	9.86	16.64	21	79	secondary trails
JC-28-6-4	BGR	qv	L+V	-	-6.2	-	-	-	160.8	-	9.47	14	21	79	two immiscible gas phases

Abbreviations: E-East, CY-Cyubi, RW-Rwinkwavu, BGM-Bugarama, BGR-Bugarura, MN-Musha-Ntunga, BUJ-Bujumu, RUT-Rutongo, RT-rock-type, qv-quartz vein, pegm-pegmatite, cass-cassiterite, L-liquid, V-vapour, S-solid, -: not measured.

Table 5.2 (continued)

Sample	Loc.	RT	phase	T _c	T _m	T _{mCO₂}	T _{mCL}	T _{hCO₂}	T _h	T _d	Salinity NaCl equiv.	Size [μm]	V	L	Observations
JC-28-6-4	BGR	qv	L+V	-	-	-	-	-	230.0	-	-	14	21	79	-
JC-28-6-4	BGR	qv	L+V	-	-6.6	-	-	-	134.3	-	9.98	9.83	32	68	-
JC-28-6-4	BGR	qv	L+V+S	-	-10.7	-	-	-	143.0	-	14.67	16.5	26	74	triangle shaped FI
JC-28-6-4	BGR	qv	L+V+S	-	-5.6	-	-	-	129.4	-	8.68	29.98	21	79	two immiscible gas phases
JC-28-6-4	BGR	qv	L+V	-	-8.6	-	-	-	130.4	-	12.39	12.33	31	69	-
JC-30-6-2	RUT	cass	-	-	-	-	-	-	193.0	-	-	19.90	-	100	-
JC-30-6-2	RUT	cass	-	-	-	-	-	-	195.0	-	-	21.00	-	100	-
JC-30-6-2	RUT	cass	-	-25.50	-	-	-	-	308.0	-	-	22.00	18	82	-
JC-30-6-2	RUT	cass	-	-67.00	-10.00	-	-	-	229.0	-	13.94	10.00	15	85	-
JC-30-6-2	RUT	cass	-	-	-37.00	-	-	-	149.0	-	-	12.00	10	90	-
JC-32	BUJ	qv	-	-	-9.00	-	-	-	226.0	-	12.85	-	20	80	-
JC-32	BUJ	qv	-	-	-5.00	-	-	-	207.0	-	7.86	-	20	80	-
JC-32	BUJ	qv	-	-	-2.00	-	-	-	120.0	-	3.39	-	20	80	-
JC-32	BUJ	qv	-	-	-13.50	-	-	-	301.2	-	17.34	12.00	60	40	-
JC-32	BUJ	qv	-	-	-0.30	-	-	-	343.8	-	0.53	13.40	48	52	-
JC-32	BUJ	qv	-	-	-	-	-	-	352.6	-	-	14.00	40	60	-
JC-32	BUJ	qv	-	-16.50	-	-	-	-	220.0	-	-	25.00	-	-	-

Abbreviations: E-East, CY-Cyubi, RW-Rwinkwavu, BGM-Bugarama, BGR-Bugarura, MN-Musha-Ntungwa, BUJ-Bujumu, RUT-Rutongo, RT-rock-type, qv-quartz vein, pegm-pegmatite, cass-cassiterite, L-liquid, V-vapour, S-solid, -: not measured.

Table 5.2 (continued)

Sample	Loc.	RT	phase	T _e	T _m	T _{mCO2}	T _{mCL}	T _{hCO2}	T _h	T _d	Salinity NaCl equiv.	Size [μm]	V	L	Observations
JC-32	BUJ	qv	-	-20.00	-	-	-	-	354.8	-	-	13.90	27	73	-
JC-32	BUJ	qv	-	-37.10	-7.40	-	-	-	154.5	-	10.98	10.00	30	70	-
JC-32	BUJ	qv	-	-13.80	-9.40	-	-	-	264.0	-	13.29	17.53	20	80	-
JC-32	BUJ	qv	-	-19.30	-11.00	-	-	-	278.2	-	14.97	13.30	36	64	-
JC-32	BUJ	qv	-	-	-0.40	-	-	-	350.8	-	0.71	10.76	35	65	-
JC-32	BUJ	qv	-	-17.30	-	-	-	-	288.3	-	-	12.00	40	60	-
JC-457	RW	qv	-	-	-	-	-	-	200.0	-	-	15.30	-	-	-
JC-457	RW	qv	-	-11.40	-	-	-	-	197.0	-	-	8.00	-	-	-
JC-457	RW	qv	-	-	-	-	-	-	212.0	-	-	14.00	-	-	-
JC-457	RW	qv	-	-	-	-	-	-	-	-	-	15.00	30	70	-
JC-457	RW	qv	-	-	-	-	-	-	-	-	-	11.00	45	55	-
JC-457	RW	qv	-	-34.20	-	-	-	15.00	227.0	-	-	10.00	25	75	-
JC-473	RW	qv	-	-	-	-	-	-	-	-	-	8.00	30	70	-
JC-473	RW	qv	-	-8.00	-2.00	-	-	-	152.0	-	3.39	10.80	15	85	-
JC-473	RW	qv	-	-74.00	-7.00	-	-	-	160.0	-	10.49	12.60	25	75	-
JC-473	RW	qv	-	-36.00	-4.20	-	-	-	181.7	-	6.74	9.70	50	50	-
JC-473	RW	qv	-	-52.00	-	-	-	-	191.3	-	-	10.30	40	60	-
JC-473	RW	qv	-	-	-3.80	-	-	-	207.0	-	6.16	11.70	45	55	-
JC-473	RW	qv	-	-	-	-	-	-	-	-	-	10.70	60	40	-
JC-473	RW	qv	-	-53.80	-9.90	-	-	-	228.8	-	13.83	14.40	30	70	-
JC-473	RW	qv	L+V	-	-3.50	-	-	-	234.9	-	5.71	8.00	37	63	-

Abbreviations: E-East, CY-Cyubi, RW-Rwinkwavu, BGM-Bugarama, BGR-Bugarura, MN-Musha-Ntungwa, BUJ-Bujumu, RUT-Rutongo, RT-rock-type, qv-quartz vein, pegm-pegmatite, cass-cassiterite, L-liquid, V-vapour, S-solid, -: not measured.

6. Discussion

6.1 Metamorphism and hydrothermal mineral alteration

The lithology of the study area comprises the meta-sediments consisting of quartzites, sandstones and schists of Mesoproterozoic age. The meta-sedimentary rocks have undergone low to moderate regional metamorphic overprint which is characterized by the greenschist facies (Baudet et al., 1989; Pohl and Günther, 1991).

During the present study, the major and trace element compositions were investigated. The amount of SiO₂ was between 36 and 90 wt. % but the samples showed very low amounts of Na₂O (<0.8 wt. %), CaO (< 0.2 wt. %), MnO (< 0.07 wt. %) and P₂O₅ (< 0.4 wt. %).

More than half of the investigated rock samples had more than 2 wt. % of K₂O and Al₂O₃ contents were between around 6 and 30 wt. %. Both compositions may indicate the richness of the meta-sediments in feldspars, muscovite and/or clay minerals. The microscopic investigations confirmed the presence of feldspar and muscovite in variable amounts. The muscovite was then altered into kaolinite in the contacts between pegmatite or hydrothermal veins and the host sedimentary rocks.

Such interactions have been reported by several authors (e.g. Meyer and Hemley, 1967; Rose and Burt, 1979; Reed, 1997 and Deer et al., 1992) showing that the muscovite is originated from the weathering or the low-temperature hydrothermal alteration of the K-feldspars after the following chemical reaction: $3/2 \text{KAlSi}_3\text{O}_8 + \text{H}^+ \leftrightarrow 1/2 \text{KAl}_3\text{Si}_3\text{O}_{10}(\text{OH})_2 + 3 \text{SiO}_2 + \text{K}^+$ (muscovitization) and further hydration may produce the kaolinite (kaolinization). The latter is mostly under the weathering control.

The moderate to high values of the chemical index of alteration-CIA (80-100) [Figure 3.5 in 3.2.2] are in favour of an advanced alteration and support the existence of such types of alteration minerals.

Apart from K₂O and MnO, Al₂O₃ correlates positively with other oxides indicating the key-role of this oxide in the mineral alteration.

6.2 Contact metasomatism of country rocks by ore elements (Sn, W, Nb-Ta, B)

Considering the trace element analyses, the investigated meta-sedimentary rocks were poor in Sn, W, Nb and Ta (Figure 3.6) but showed increasing trends in these elements with the decreasing distances

to their contacts with the pegmatites and/or hydrothermal veins. This could indicate a possible mineralization from ascending hydrothermal solutions and could therefore, lead to Sn-, W-, Nb and Ta- enrichments. Similar contaminations were noted for the boron which reacted with the meta-sedimentary host-rocks and formed a 20cm to 40cm thick tourmaline-rich rim around the intrusions observable in the three investigated mining areas (Figure 4.17).

6.3 Origin of fertile pegmatite melts - possible sources for Sn, W and Nb - Ta

As reported in the literature, the meta-sedimentary rocks of the Kibaran orogeny have been intruded by two generations of granites: the so-called G1-3 granites of ca. 1380 +/- 10 Ma which are not mineralized in Sn-W (Nb-Ta) and the G4-granites also called “tin” granites of 986 +/- 10 Ma (Tack et al. 2010, Dewaele et al. 2010). The latter are known to be associated with the Sn-, W- and Nb-Ta- and other rare element mineralization characterizing the Kibaran metallogenic province.

Most of the mineral deposits in Rwanda occur in the vicinity of S-type and peraluminous granites which were qualified as “parental granites for rare element pegmatites” (Cerny et al., 2005; Dewaele et al., 2010) and acted as the source of the mineralizing fluids.

In Rwinkwavu, Musha-Ntungwa and Bugarura-Kuluti, the primary mineralization is of pegmatite and/or hydrothermal vein types. Moreover, the secondary deposits exist in the form of alluvial/eluvial placers which are overlying mineralized pegmatites or hydrothermal veins and are exploited for Sn-, W-, Nb-/Ta- mineralization. The pegmatites outcrop mainly in the Musha-Ntungwa and Bugarura-Kuluti mining concessions in the form of small (between tens of cm and several m thick) intrusive bodies (Figure 6.1).



Figure 6.1: Photograph of one of the small intrusive kaolinized pegmatites exposed in the Ntungwa Sn-mine (The scale is the artisan miner in right corner).

Microscopic analyses of Rusumo, Nyagatare and Ngarama granites (location map in Figure 2.1) showed that the rock-forming minerals are microcline, plagioclase and quartz with variable amounts of water-rich minerals such as biotite and muscovite.

The major element analyses showed enrichment in K_2O (4 to 5 wt. %) and Al_2O_3 (above 13 wt. % and the maximum value of 38.8 wt. % in pegmatites) and depletion in Fe_2O_3 , CaO , TiO_2 , MgO and P_2O_5 .

The Musha-Ntungwa and Ngara pegmatites are mica-dominated but entirely altered and thus it was not possible to get fresh pegmatite samples from them for the light microscopy study. Similar pegmatites are also common in the Bujumu and Kuluti localities.

For the granite and pegmatite samples, the $Al_2O_3/[Na_2O+K_2O+2CaO]$ ratios were between 1.21 and 34.74 indicating their high peraluminosity (Fernandez-Alonso and Theunissen, 1998, Cerny et al., 2005).

The excess of aluminium in the granites and pegmatites confirms the presence of the common peraluminous minerals such as K-feldspar, garnet, muscovite and biotite shown by the light microscopy and the SEM-EDX/WDX investigations in the granite/pegmatite structure.

The trace element normalized against the French Variscan tin granite (Figure 3.3) showed enrichment trends in Sc, Sr, Y, Zr, Mo, Ba, Hf, Pb, Th and U for the south-eastern Rwandan granites. The latter were depleted in Rb, Nb, Sn and Ta and compared to the French Variscan granite, the south-eastern Rwandan granites showed a slight enrichment in W.

Furthermore, and in comparison with the average continental crust abundances (Clarke) [Table 3.3] of Sn, Nb and Ta which are respectively 2, 20 and 2 ppm (Taylor, 1964; Wedepohl, 1969; Krauskopf and Bird, 1995), the results from trace element analyses indicated that the Sn, Nb and Ta concentrations are below or slightly above the Clarke and are 1-4 ppm for Sn, 9-22 ppm for Nb and 2-3 ppm for Ta and in the most cases, the Nb is higher than the Ta content. The latter may indicate the crystallization of granites from less fractionated magmatic melts (compared to the pegmatites) and based on Cerny (2005) and Lehmann and Lavreau (1988), the analyzed granites are geochemically different from the "tin" granites.

However, the pegmatite samples showed enrichment in As-, Rb-, Nb-, Sn-, Sb- and Pb and some of them host economically exploitable quantities of coltan, tin and tungsten mineralization (Rusanganwa,

pers. comm.). Also, the Nb/Ta ratios are very low (enrichments in Ta) and therefore, indicates that the pegmatites crystallized from highly fractionated felsic magmas (Beurlen et al., 2008).

Raimbault et al. (1995) and Cerny (2005) identified similar enrichment trends in the “Les Chatelliers” peraluminous low phosphorous rare metal granites of the French Variscan which were exploited for the kaolin with the cassiterite, wolframite and coltan as its by-products.

Based on these similarities, it can be concluded that the pegmatites of the study area may be equivalent to the late to post-Kibaran G4-granites defined by several authors (e.g.: Pohl and Günther, 1991; Tack et al., 2006, 2008, 2010; Dewaele et al., 2010). In terms of the model of Cerny et al. (2005), the Sn-W- rich residual melts could have been evolved from felsic magmas enriched in rare elements such as Ta, Sn, W and Rb and therefore, highly fractionated and were pre-enriched in Sn and W from the partial melting of crustal material possibly in the middle to lower crust.

6.4 Deformation control on emplacement of pegmatitic to quartz veins

The mineral deposits of Musha-Ntungwa and Bugarura-Kuluti are hosted in the Nyabugogo and Musha formations of Lower Mesoproterozoic age which overlay the Rwamagana-Rugarama-Kuluti granite (G4?). As evidenced by the 2010 field work, the latter is coarse - grained and composed of feldspars, biotite, muscovite and quartz and often with a preferential orientation of cleavage and cooling joints.

The relatively large size of the granite-forming minerals indicates clearly that the magmatic crystallization was initiated from a low to moderate cooling rate and the orientation of some of the minerals testifies that the granite crystallization might have been syn-deformational or contemporaneous to the end of the folding phases. The granitic cupolas (described in section 4.3.1) are fractured in a complex system of fissure swarms filled with a barren mixture of quartz, pegmatites and white feldspars. These were also observed further north in the Ngarama granite (Figure 3.1) and in both cases, the size of the minerals could be above ten (10) centimetres.

In accordance with Stevens et al. (1997), the multiple small anomalous pegmatites intruding the low grade metamorphic formations of the Musha-Ntungwa and Bugarura-Kuluti-Bibare mining concessions which are spatially associated with the cupola zones of the Rwamagana-Rugarama-Kuluti granite, might be genetically related to the most highly differentiated and water-saturated portions of the earlier mentioned G4-granites. The fractures filled with mineralized veins (Figure 4.17) show steep dips. According to Burnham (1979), the latter might be the result of mechanical effects of hydro-

fracturing caused by over-pressuring in the apical parts of the shallow seated late phases of the G4-granite and therefore causing a brittle explosive failure of the surrounding rocks.

6.5 Stratigraphic position of the mineralization

As an example, the Rugarama area (Figure 4.21) is characterized by a mineral zoning in accordance with the three types of pegmatite facies found around the granite (MINETAÏN in RMCA's archives, 1965). Therefore, comprising from the contact with the granite to the outer parts the following mineral zones are identified:

1. The most proximal zone consists of granitic pegmatites and pegmatites which are not mineralized (in Nb, Ta, Sn and W) and are hosted in the ca. 10m thick biotite zone in direct contact with the granite.
2. Then follows a zone which is muscovite-sericite rich and hosts a complex system of pegmatites, greisens and muscovite-quartz-tourmaline veins. The columbite group minerals exploited in some of the mines such as Duha, Nyarunazi, Kivuba, Kayenzi and Nyagasiga are likely associated with these types of intrusions.
3. The most surficial layer hosts the Sn- (W-) bearing pegmatites and greisens which intruded the meta-sedimentary suites. The mineralized hydrothermal quartz veins are cross-cutting the latter. In some cases, the quartz is dark coloured. The transparent but milky types of quartz also exist indicating the variation from the high dark quartz to the low milky quartz temperatures of crystallization. The hydrothermal veins also host the tin and tungsten mineralization.

The position of the tin and tungsten mines of the Rwinkwavu area seems to be different and more complex for two reasons:

1. There is no granite outcrops in the area hosting the mineral deposits and
2. Analyzing the mineral deposits map of Rwanda (Baudin et al., 1982; OGMR, 2009), the nearest granites which should have contributed to the mineralization genesis in the mineral deposits of Rwinkwavu are the Rwamagana and Lake Ihema granites. However, the most productive tin mines (Kizanye-Rutonde trend) which occur in the core of Rwinkwavu-Kirimbari anticlinal structure are located at more than 10km distance from both granites (Figure 2.6). The earlier originated the Musha-Ntunga and Bugarura-Kuluti-Bibare mineral districts whereas for the latter there is no known associated mine.

6.6 Paragenetic scheme and precipitation model of the mineralization

Based on the model of Cerny et al. (2005), the Sn and W mineralization may have been crystallized from the late to post felsic magmatic and residual melts rich in volatiles and circulating along the open fractures within the upper crust. The passage of the hydrothermal fluids through these open spaces of the host-rock followed a gradient of decreasing pressure and temperature; simultaneously to various forms of the host rock alterations such as greisenization, muscovitization, tourmalinization, phyllic alteration and kaolinization, the precipitation of the cassiterite and/or ferberite occurred; this process depends on the specific stability conditions for each type of metal-ligand complex in the fluid (Wood and Samson, 1998).

However, the presence of shallow-seated granite from which the late to post magmatic melts originated multiple mineralized muscovite-sericite-tourmaline-quartz veins through either open fractures or filling the cracks produced by the hydro-fracturing, is not excluded. Another proof of the existence of the buried granite is that the mineralization is occurring in the Rwinkwavu anticline and showing a zoning in mineral concentrations with decreasing contents from the lowest altitudes of Kizanye-Rutonde trend (ca. 1,350m) where the grades are more than 30kg/m³ to the highest levels of Mount Rwinkwavu in the western limb of the anticline (1,600m) with grade-values decreasing to between 7 kg/m³ and 3kg/m³ and from the inner to the outer parts of the anticline (Basigayabo, pers. comm.).

This observation is in accordance with Slatkine (1965) who estimated the extension of the mineralization on a height of ca. 400 m and linked the anomalous contents of cassiterite in the core of the Rwinkwavu anticline to a probable existence of buried fertile granite. The presence of the underlying granite, source for the mineralization in Rwinkwavu, was also reported on the basis of the results from interpretation of airborne geophysical data for Rwanda with its probable location underneath the Kibungu-Ntoma shear zone [Paterson, Grant & Watson Ltd., 2009 (Figure 2.6)]. For the confirmation of this hypothesis, further exploratory work is needed.

The paragenetic sequence of cassiterite, ferberite and columbite-tantalite has been constructed in the Musha-Ntungwa, Bugarura-Kuluti-Bibare and Rwinkwavu (Figure 6.2).

Based on mineral associations, in Musha-Ntungwa and Bugarura-Kuluti-Bibare, three types of pegmatites and hydrothermal quartz veins are overlying their parental granite which is composed of K-feldspar, biotite, muscovite and quartz crystals. The pegmatites occurring in the biotite zone are not mineralized and are composed of quartz, biotite, muscovite and garnet whereas the hydrothermal

veins are composed of K-feldspar, quartz, muscovite and the fragments of the host rocks. The hydrothermal quartz veins located at this level are not mineralized in Nb, Ta, Sn and W.

The coltan mineralization is limited on the pegmatites intruding the muscovite-sericite zone where it is associated with muscovite, quartz and tourmaline. This observation is in accordance with Linnen (1998) who favoured the late-magmatic crystallization of the columbite group minerals from evolved silicate melts over hydrothermal crystallization from fluids. The cassiterite and ferberite mineralization are found in the pegmatites, greisens and hydrothermal quartz veins which are intruding the most surficial layers of schists and where they are associated with quartz, greisens and tourmaline.

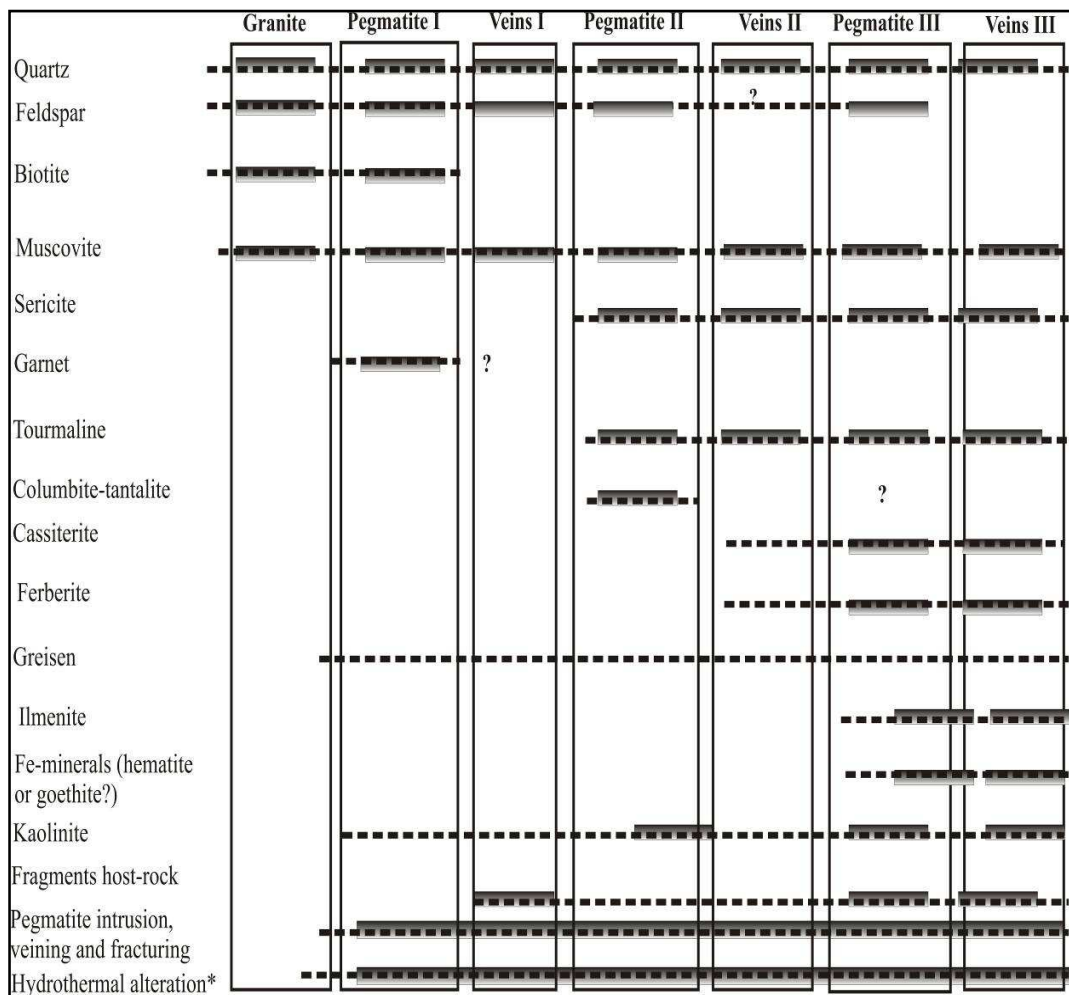


Figure 6.2: Paragenetic scheme of Bugarura-Kuluti-Bibare/Musha-Ntungwa and Rwinkwavu mineralization.

In Rwinkwavu, the primary mineralization is of hydrothermal vein type. The cassiterite is mostly associated with the sericite, muscovite and very often with the fragments of the host-schists (Rukira formation) in lower parts and at the highest altitudes it is associated with quartz and minor amounts of muscovite which disappear in the western limb of the anticline and where the cassiterite occurs

associated with quartz in hydrothermal quartz veins cross-cutting the quartzitic layers of the Kibaya formation.

The primary tungsten deposits of Nyamuyorwa and Kirimbari are hydrothermal quartz vein-types and hosted in the schists of Rukira formation. Some zones of the latter are enriched in carbonaceous matter and are locally transformed in black shales. The ferberite is associated with minor amounts of huebnerite, quartz, muscovite, garnet, ilmenite and intergrowths of Fe-minerals such as hematite or goethite (SEM data in Table 4.1.7 and Appendix 4).

The precipitation of Sn, W, Nb-Ta minerals in pegmatitic veins of the study area might have been caused by the pressure decrease, temperature decrease and the decrease in solute content (Burnham, 1967). The reducing properties of the metasedimentary strata of the study area may have played an important role in the mineral precipitation during the hydrothermal fluids-wall rock interaction (Figure 7.1).

6.7 Mineral chemistry of Sn, W and coltan pointing towards precipitation conditions.

On the one hand, it is confirmed that the cassiterite of the study area is associated with the late and post magmatic water and volatile-rich residual melts (e.g.: this study; Tack et al., 2010 and Dewaele et al., 2010) and in hydrothermal solutions, tin is mostly transported as reduced Sn^{2+} chloro-complexes (for ex. SnCl_2^0) rather than as Sn^{4+} hydroxy-chloro-complexes and the precipitation of cassiterite involves an oxidation to Sn^{4+} (Heinrich, 1995). This latter author also showed that three possible mechanisms were responsible for the cassiterite deposition:

- Vapour separation which removes HCl and hence causes the precipitation of cassiterite as illustrated by the following chemical equation: $\text{SnCl}_2 + \text{H}_2\text{O} + 0.5\text{O}_2 = \text{SnO}_2 + 2\text{H}^+ + 2\text{Cl}^-$,
- Mixing of hot saline magmatic melts with non magmatic fluids during emplacement of granites and subsequent metasomatic process and
- Acid neutralization by feldspar hydrolysis that takes place during the greisenization process after $[\text{Sn}^{2+} + 3(\text{Na}, \text{K}) \text{AlSi}_3\text{O}_8 + 2\text{H}_2\text{O} = \text{SnO}_2 + \text{KAl}_3\text{Si}_3\text{O}_{10}(\text{OH})_2 + 6 \text{SiO}_2 + 2\text{Na} + \text{H}_2]$ equation.

On the other hand, $\log [(\text{Fe}+\text{Mn})/\text{Sn}]$ vs. $\log [(\text{Nb}+\text{Ta})/\text{Sn}]$ (upper part of Figure 6.3) and $\log [(\text{Fe}+\text{Mn})/\text{Sn}]$ vs. $\log [\text{W}/\text{Sn}]$ (lower part of the same Figure) discrimination plots (Möller et al., 1988) for the cassiterite samples from the study area together with the cassiterite samples from Egyptian Pan-African Orogeny (data from Abdalla et al. 2008) may give indication of petrogenetic conditions.

Figure 6.3 shows that some of the cassiterite samples from Rwinkwavu, Musha-Ntungwa (this study) and all the samples from Egypt are showing roughly a positive trend plotting along the line $(\text{Nb}+\text{Ta})/(\text{Fe}+\text{Mn}) = 2$ in the first diagram, indicating a contamination by mineral inclusions of the type $(\text{Fe}, \text{Mn})(\text{Ta}, \text{Nb})_2\text{O}_6$ but the rest of the samples from the study area show enrichment trends in $(\text{Fe}+\text{Mn})$ which may indicate the existence of Fe-rich phases by simple substitution of Sn by Fe.

Contrarily, all the samples from Bugarura-Kuluti (part of this study) plot above $(\text{Nb}+\text{Ta})/(\text{Fe}+\text{Mn}) = 2$ and thus are $(\text{Nb}+\text{Ta})$ -dominated. This chemical trend may indicate that there is a substitution of the type $\text{Sn}^{4+} \leftrightarrow (\text{Ta}, \text{Nb})^{4+}$ in the cassiterite crystals.

In the second diagram of Figure 6.3, some cassiterite samples from the study area (Bugarura-Kuluti, BK; Musha-Ntungwa, MN) are plotting together with the Egyptian cassiterite samples along the line $W/(\text{Fe}+\text{Mn}) = 1$ and according to Möller et al. (1988), such ratio points towards the presence of wolframite in cassiterite as solid inclusions. The rest of the samples, including the whole set from Rwinkwavu, show excess in Fe and are therefore indicating the presence of Fe-rich mineral phases.

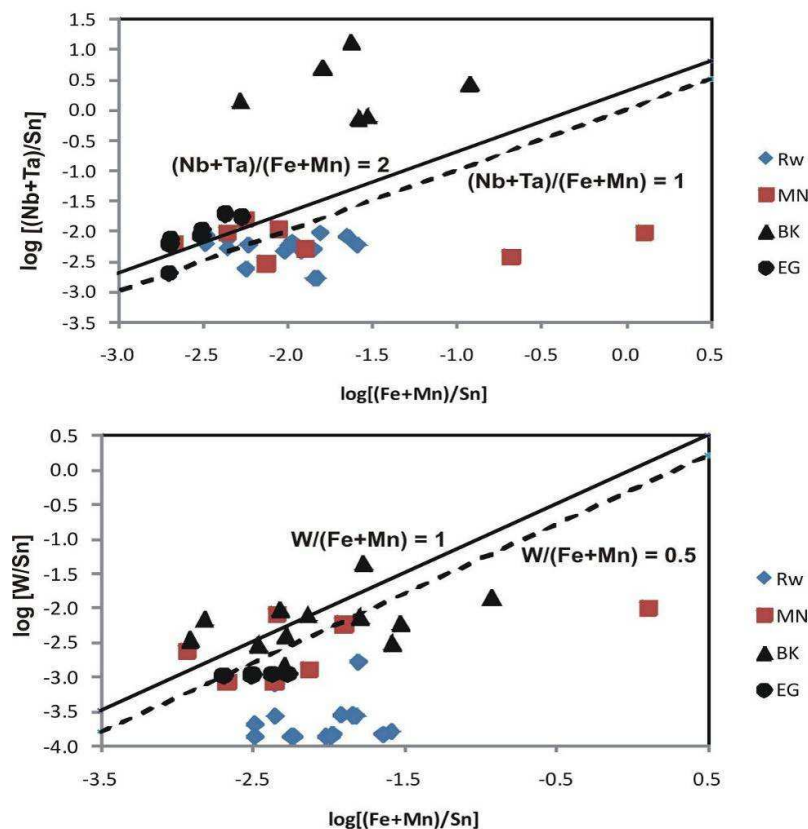


Figure 6.3: Discrimination plots of selected cassiterite samples from the study area using $\log[(\text{Nb}+\text{Ta})/\text{Sn}]$ vs. $\log[(\text{Fe}+\text{Mn})/\text{Sn}]$ (upper) and $\log[W/\text{Sn}]$ vs. $\log[(\text{Fe}+\text{Mn})/\text{Sn}]$ (lower) (after Möller et al., 1988) in comparison with cassiterite samples from granites of the Egyptian Pan-African Orogeny (Abdalla et al., 2008). **Abbreviations:** Rw-Rwinkwavu, MN-Musha-Ntungwa, BK-Bugarura-Kuluti, EG-Egypt. The concentrations are in apfu.

With regard to the tungsten mineralization, the W- is a hard metal existing in nature in the form of W^{6+} or W^{5+} and therefore, complexing with hard bases. In hydrothermal solutions, W species are transported in the form of tungstates (Wood and Samson, 1998). The stability of tungstates is Eh and pH-dependent and therefore, the W- ore precipitates in reducing conditions rather than the oxidizing ones.

The chemical analysis of the wolframite samples indicates that it is in a pure ferberite type with the chemical formula $FeWO_4$ and other chemical constituents are in small amounts or in traces.

The mineral chemistry of coltan mineralization was investigated and the results plotted (Figure 6.4) in columbite quadrilateral (Beurlen et al., 2008) binary plot of $Mn / (Fe+Mn)$ vs. $Ta / (Ta+Nb)$ together with the coltan samples from other deposits of Rwanda such as Ruhanga, Cyubi and Gasasa (Melcher et al. 2009) and of Podlesi-Czech Republic Variscan (Breiter et al., 2007). The samples from Rwanda show enrichment trends in Ta and Mn: Musha-Ntunga (MN) and Bugarura-Kuluti (BK)-trend 2 (this study) and other deposits-trend 3 (Melcher et al., 2009) whereas the ones from the Variscan orogeny are dominated by the Nb composition (ferro-columbite) but also characterized by a slight enrichment in Ta-trend 1 (Breiter et al., 2007). Based on Pohl (2011), these enrichment trends in Ta and Mn are an indication that the coltan samples from Rwanda have crystallized from more evolved felsic magmas than the ones from the Czech Republic Variscan.

According to Linnen (2004a, b), the solubility of Fe-rich members of the columbite group minerals in the melts is larger than that of Mn-rich end members and the enrichment in Mn over Fe might be likely controlled by other Fe-bearing minerals crystallized during the pegmatite evolution such as tourmaline or biotite (London et al., 2001). The more Fe-rich minerals are in paragenesis, the poorer in Fe the columbite is. In normal conditions, Fe-rich columbites represent the late stage of magmatic evolution and the increasing of Mn in this case might be dictated by a competition for Fe between the present minerals.

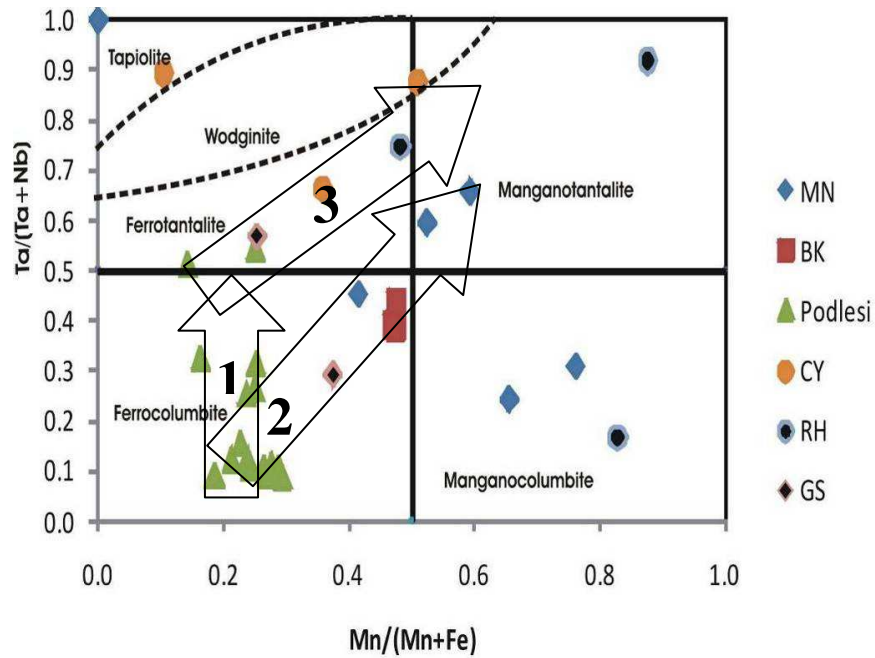


Figure 6.4: Columbite quadrilateral binary plot of Mn/ (Fe+Mn) vs. Ta/(Ta+Nb) in a.p.f.u (Beurlen et al., 2008) for the coltan samples of the study area, of selected mines in Rwanda (Melcher et al., 2009) and of Podlesi in Czech Republic (Breiter et al., 2007). **Abbreviations:** MN-Musha-Ntungwa, BK-Bugarura-Kuluti, CY-Cyubi, RH-Ruhanga and GS-Gasasa, 1, 2 and 3-evolution trends.

6.8 Fluid evolution

The results from the fluid inclusion studies show that:

- Most of the investigated inclusions are two phase (liquid-vapour). They are liquid-dominated but few of them are vapour-dominated indicating that the boiling phase traces were overprinted by later tectonic events or the phase itself was less important. In addition, monophasic and a limited number of multiphase inclusions were also identified.
- Total melting temperatures of ice range between -0.3°C and -13.5°C (Figure 5.2b) representing the salinities between 0.5 wt. % NaCl equivalent and 17.3 wt. % NaCl equivalents.
- The homogenization temperatures recorded were between 103°C and 360°C (Figure 5.2c).

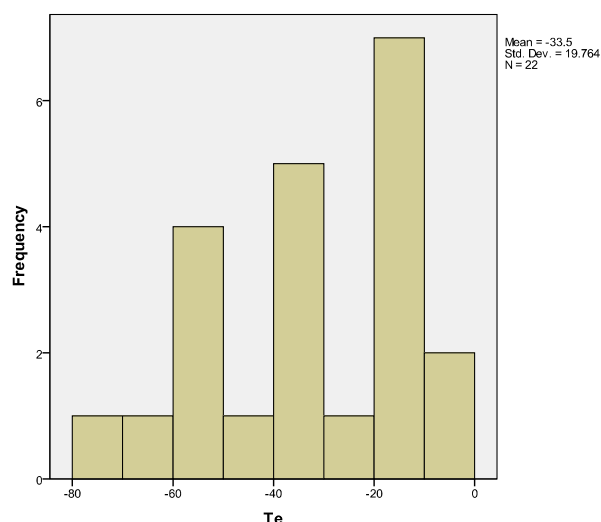


Figure 6.5: Frequency distribution of the eutectic temperatures T_e (°C).

Insofar as the depth of the Rugarama granite is estimated to be 7.5-8km, indicating lithostatic pressure values of more or less 2kbars (MINETAİN, 1965) and using the equation of Bodnar and Vityk (1994), the trapping temperature estimates in accordance with these previously mentioned conditions were between 150°C and 560°C for the quartz samples from Bugarura-Kuluti, 220°C and 320°C for the Rwinkwavu quartz samples and between 200°C and 420°C for the samples from Musha-Ntungwa (Table 5.1). The high values of pressure-corrected temperatures obtained by fluid inclusion microthermometry on quartz samples from Musha-Ntungwa (this study) overlap with the formation temperature of cassiterite ($\approx 400^\circ\text{C}$) based on the isotopic equilibrium between cassiterite and quartz from Musha (Dewaele et al., 2010).

In summary, the results of fluid inclusion investigations show a wide range of salinities and homogenization temperatures (Figure 5.3). There should be only two possible explanations to this: either by the presence of different hydrothermal populations which overlap or this might be due to a mixing of magmatic solutions with non-magmatic fluids. The latter can be composed of meteoric, connate and/or metamorphic waters. The stable isotope study on mineralized quartz by Dewaele et al. (2010) confirmed that the mineralizing fluids of Musha are from interaction between primary magmatic fluids and metamorphic waters. To extend this hypothesis on the origin and evolution of the mineralizing fluids in the Bugarura-Kuluti-Bibare and Rwinkwavu prospects, further stable isotope investigations are recommended.

The fluid-inclusions homogenizing at low temperatures may represent the younger generation of secondary inclusions. The fluid-inclusions which homogenize at moderate to high temperatures might be older and could be similar to the primary inclusions which have all disappeared due to a long-lived magmatic and tectonic history in the Kibaran metallogenetic province.

7. Development of a conceptual metallogenetic model

South-eastern Rwanda is located within the Karagwe - Ankolean Belt which is part of the Kibaran Belt and composed of meta-sedimentary rocks of the Mesoproterozoic age which were intruded by two granite generations: the G1-3 of 1380 \pm 10 Ma and the G4- granites of 986 \pm 10 Ma (Tack et al., 2010). The latter have been documented as the possible source for the Sn-W (Nb-Ta) mineralization (e.g.: Dewaele et al., 2011, 2010).

The above mentioned meta-sedimentary suites have undergone a low grade regional metamorphic overprint characterized by the greenschist facies (Baudet et al., 1989; Pohl and Günther, 1991).

Major element analyses of meta-sedimentary rock samples showed the decrease in abundance of TiO₂, Al₂O₃, Fe₂O₃, MgO, CaO and Na₂O as SiO₂ increases (Figures 3.4a and b). This is an indication of the maturity of the sediments resulting in a combined action of weathering processes which, in removing the most mobile elements (such as the ferromagnesian and alkalis), produce aluminous clay minerals from primary silicates. Subsequent hydraulic sorting separates finer-grained clays from the more silica-rich residual minerals (Young et al., 1998). The moderate to high value of CIA, as indicated in Figure 3.5 (Nesbitt and Young, 1982), supports the high maturity of the investigated meta-sediments.

Some anomalous Fe - enriched meta-sediments from shear zones of the Rwinkwavu anticline were not considered for the provenance signature. The reason for this is that they were lateritic weathering crusts. Furthermore, the major element investigations on felsic rocks, which are the possible source of Sn-, W- and Nb-/Ta-mineralization, showed enrichment trends in SiO₂, K₂O and Al₂O₃. These are characterized by the presence of mineral phases enriched in the previously mentioned oxides such as feldspars, muscovite, biotite and quartz. The presence of the latter minerals was confirmed during the present study by the light microscopy and the SEM-EDX/WDX analyses and confirmed the results reported in Fernandez-Alonso and Theunissen (1998). Moreover, they showed depletion trends in Fe₂O₃, CaO, MgO, TiO₂ and P₂O₅. The values of Al₂O₃/ (Na₂O+K₂O+2CaO) ratios were above 1.2 and this may allow those granites to be qualified as low phosphorous and strongly peraluminous granites (Fernandez-Alonso and Theunissen, 1998; Romer and Lehmann, 1995; Cahen et al., 1984; White and Chappell, 1977).

In addition, the trace element analysis showed two groups of felsic rock samples:

- The granites which were enriched in Sc, Sr, Y, Zr, Mo, Ba, W, Pb, Th and U and depleted in Rb, Nb, Sn and Ta when normalized against the French Variscan “tin” granite. In comparison with the Clarke values (Taylor, 1964; Wedepohl, 1969; Krauskopf and Bird, 1995), they

showed that the Sn, W, Nb and Ta concentrations were below or slightly above the Clarke values and hence, are geochemically different from the so-called “tin” granites mentioned in the literature. They possibly correspond to the G1-3 granites (e.g. Cerny, 2005; Lehmann and Lavreau, 1988; Tack et al., 2010 and Dewaele et al., 2010).

- The pegmatites show higher concentrations in As, Rb, Nb, Sn, Sb and Pb than the Clarke values (Taylor, 1964; Wedepohl, 1969; Krauskopf and Bird, 1995) and are hosting the currently exploited Sn-, W- and Nb-Ta ore deposits. Such enrichment trends have been reported for the low phosphorous rare-metal pegmatites in the French Variscan by several authors (e.g. Cerny et al., 2005; Raimbault et al., 1995). Therefore, the fertile pegmatites that out-crop in the Musha-Ntungwa and Bugarura-Kuluti mineral districts may be called the “tin” granites derived from “parental granite for rare element pegmatites” of Rwamagana (Dewaele et al., 2010). Both are definitely equivalent to the young generation-G4 granites commonly known in the Kibaran Belt (Tack et al., 2010).

The buried Rwinkwavu granite which is overlain and surrounded by economically exploited mineral deposits may be the possible source for the mineralizing fluids which originated the tin and tungsten-bearing hydrothermal veins. Evidence for this are the anomalous concentrations of Sn and W in their contacts with the host-rocks is most likely the “tin” (or G4) granite.

The origin of the mineral deposits of eastern Rwanda can be explained using the model of Cerny et al. (2005) which states that the Sn, W, Nb and Ta-rich residual melts would have been evolved from highly fractionated felsic magmas which were pre-enriched in Nb, Ta, Sn and W from partial melting of undepleted middle to lower crustal protoliths. This model is suitable for this case for two main reasons: 1. The distribution patterns of Sn, W, Nb and Ta anomalies in and around the fertile intrusions and their parental granites (Chapter 3). 2. The chemical trends of the columbite group which showed an increase of Ta and Mn with advanced fractional crystallization (Figure 6.4).

This study revealed the frequent occurrence of Fe-rich tourmalines, schorl (Mineral chemistry of tourmaline in section 3.8), in concentric tourmalinite rims along the pegmatite/vein intrusions. This indicates that the B-enriched parent fluids were of magmatic origin (Henry and Guidotti, 1985). The key role of B in the lowering of the granite solidus temperatures and increasing the range of temperatures over which magmatic crystallization may occur was documented in Dingwell (1988). London (1996) and Pollard et al. (1987) noted that B and other fluxing elements such as F, Li and P were responsible for the increase of H₂O-solubility in the magmas causing the decrease of viscosity and the solidus temperatures of the magmatic melts which is in favour of crystal-melt separation. This

therefore, promotes rare metal enrichments in residual melts. In the Bugarura-Kuluti and Musha-Ntunga prospects, the assumed simultaneous increase of the water- solubility in the residual melts and the enrichment of hydrothermal solutions in Sn, W and probably other incompatible elements, might have generated an increase of a vapour-dominated phase with relatively high salinities and possibly richer in Nb and Ta than in Sn and W. The results of fluid inclusion investigations on quartz samples from Bujumu (BKB-1 in Figure 5.3) showed that a few inclusions, possibly equivalent to the remnants of the early generation of inclusions, are vapour-dominated, more saline than others, with relatively high T_h (250°C - 300°C) and thus, tend to have a “pneumatolytic” character. These conditions are likely in favour of pegmatite-type coltan-dominated mineral precipitation in some known mining sites of Bugarura-Kuluti and Musha-Ntunga. This hypothesis is consistent with Linnen (1998) who showed that the Nb and Ta were more associated with silicate melts rather than hydrothermal aqueous fluids. Fetherston (2004) showed in experiments that the Ta starts to react mostly with other chemical components at temperatures above to 300°C-400°C and remains immune to chemical attacks on the temperatures below 150°C.

Cerny et al. (2005) supported by Burnham (1979), considered the fluid saturation as a consequence of hydrous melts precipitating anhydrous minerals such as quartz and feldspars. The decrease in water solubility may be considered as a consequence of decreasing pressure as the granite magmas rise through the crust during the late stages of fractional crystallization.

The Sn might have been mobilized and transported by the residual ascending Cl-bearing and water-rich aqueous fluids exsolved at shallow crustal levels (Taylor and Wall, 1992; Heinrich, 1995). The fluid oversaturation in Sn and precipitation of cassiterite in hydrothermal veins might have been derived from combined processes of decrease in temperature and/or the chloride activity. The influx of cold meteoric waters in the ascending hydrothermal fluids influenced the increase of oxygen fugacity and/or pH. This is evidenced by a wide spectrum of T_h (103°C-360°C) of fluid inclusions. The mixing of fluids from different sources is also supported by the contrasts of salinities (0.5-17.3 wt. % NaCl equiv.) between various investigated inclusions from the study area. Moreover, as shown by extensive wall-rock alteration (Figure 4.17), the active role of the interaction between the resulting fluids and the host-rocks causing destabilization of complexes and the cassiterite precipitation may not be excluded (Jackson et al., 1982).

In the study area the cassiterite precipitated possibly either according to the $\text{SnCl}_2 + \text{H}_2\text{O} + 0.5\text{O}_2 = \text{SnO}_2 + 2\text{H}^+ + 2\text{Cl}^-$ equation which is Eh and pH-dependent and is followed by acidification or the acid neutralization by hydrolysis of feldspars of the wall - rocks as follow: $\text{Sn}^{2+} + 3(\text{Na, K})\text{AlSi}_3\text{O}_8 +$

$2 \text{H}_2\text{O} = \text{SnO}_2 + \text{KAl}_3\text{Si}_3\text{O}_{10}(\text{OH})_2 + 6 \text{SiO}_2 + 2\text{Na} + \text{H}_2$ (Heinrich, 1995). For this latter reaction, the final products include not only cassiterite, but also muscovite and quartz.

The W might have been concentrated and transported in the form of tungstates such as WO_4^{2-} or HWO_4^- (Wood and Samson, 1998).

The Eh-pH diagram of Fe-Mn-W-C-H₂O system at 25°C, 100°C, 300°C and 400°C was constructed in HSC-V5-software after Haung et al. (2002). The aim was to determine the stability field of FeWO_4 and MnWO_4 and the probable conditions of ferberite precipitation (Figure 7.1).

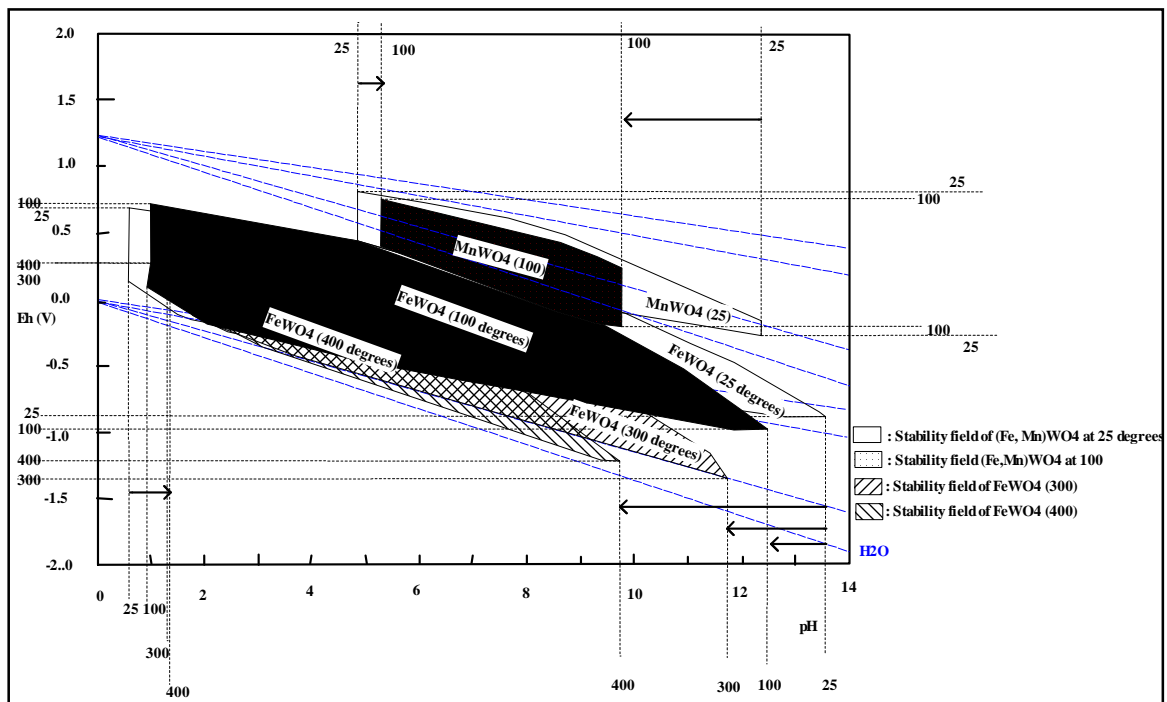


Figure 7.1: Eh-pH diagram for the W-C-Fe-Mn-H₂O system at 25°C, 100°C, 300°C and 400°C (Haung et al., 2002).

As shown in Figure 7.1, the results obtained by the software from pre-defined parameters indicate that the stability fields of FeWO_4 and MnWO_4 decrease to decreasing of Eh and pH during an increase of temperatures. The precipitation of ferberite was possibly caused by oversaturation in Fe of the resulting fluids from the mixture between the W-rich and Fe-bearing hydrothermal fluids of magmatic origin. This is confirmed by the fluid inclusion investigations (Section 5.2) as well as meteoric (connate/ metamorphic) waters with high Fe content (leached from the host meta-sediments). The Fe of magmatic origin together with the Fe dissolved in the surface cold waters might have reacted together with W to form the ferberite.

Reducing conditions caused by carbonaceous matter in the meta-sediments played a key-role in the ferberite deposition. This is confirmed by the results of investigations carried out on meta-

sedimentary samples and using Herron (1988) which showed that some, among them, were plotting in Fe-shales and Fe-sands types (Figures 3.7 and 3.8). In addition, the whole rock chemistry investigations on the same meta-sedimentary rock samples showed also enrichment trends in Al_2O_3 , Fe_2O_3 and TiO_2 (Section 3.2.1). When normalized against the French Variscan “tin” granite, they showed low contents of Sn, W, Ta and Nb (Section 3.2.3) and cannot, therefore, be the source for the above mentioned mineralization. However, due to the metasomatism processes from pegmatites into country rock, the Sn, W, Nb and Ta contents were increasing with the decreasing distances to the contacts between the pegmatites/veins and the host rocks.

The anomalous distribution patterns of meta-sedimentary rocks in the study area (Table 3.4 and Figure 2.1) might have been originated by rare elements - rich ascending hydrothermal fluids. Similar cases were noted by Beer and Ball (1986) in the pelitic rocks extended around the contact zones of granites and in mineralized areas of SW-England introducing metasomatic fluids in the host rocks and causing Sn and W enrichments. As illustrated by Table 5.2 and shown in Figure 5.3 (case of fluid inclusions of samples from Rwinkwavu), the cassiterite and ferberite mineralization is more abundant in aqueous, less saline and low temperature hydrothermal fluids.

Using the data from the mining exploitation reports (MINETAİN in the archives of the RMCA, 1965), Varlamoff (1948, 1972), Cerny (1993b), Cerny et al. (2005), Tack et al. (1990, 1994 and 2010) and based on the results from fluid inclusion in samples from the June-August 2010 field campaign, a conceptual model was developed and is presented in Figure 7.2.

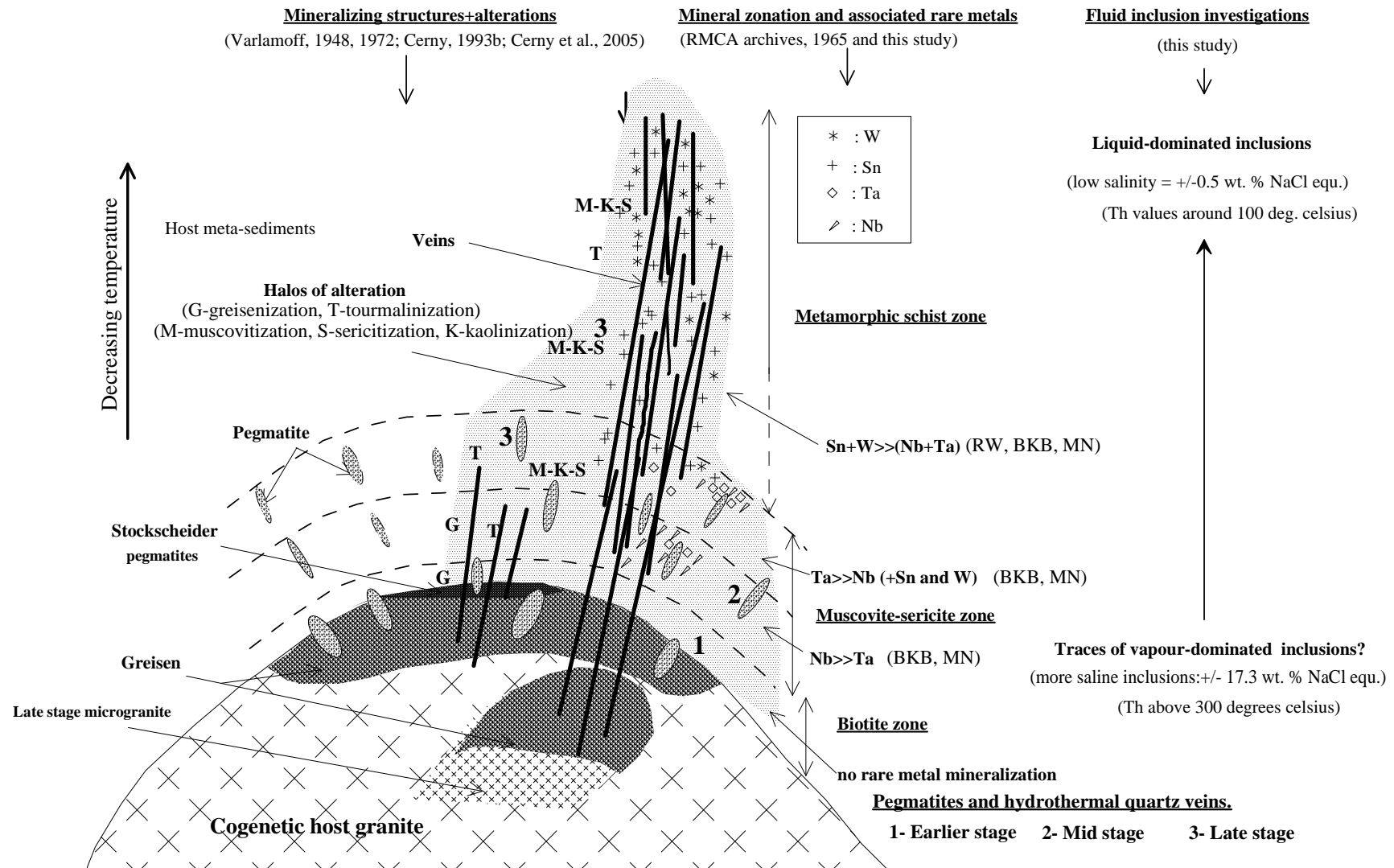


Figure 7.2: Conceptual metallogenic model for eastern Rwanda [modified and adapted after Varlamoff (1948, 1972), MINETAİN in RMCA's Archives (1965); Cerny (1993b); Cerny et al. (2005) and Tack et al. (1990, 1994 and 2010)]. **Abbreviations:** BKB-Bugarura-Kuluti-Bibare; RW-Rwinkwavu and MN-Musha-Ntungwa.

The conceptual model indicates a metallogenetic evolution of the mineralization in six (6) successive events which can be summarized as follows:

1. Deposition of the meta-sedimentary rocks;
2. Intrusion of G1-G3 granites in an extensional context;
3. Deposition of the sediments;
4. Deformation of ca. 1000Ma;
5. Syn- to post-folding Rwamagana-Rugarama-Kuluti granite intrusion (G4 granite of ca. 985Ma) and development of granitic cupolas which were later healed or intruded by pegmatites and veins (Figure 7.2);
6. Intrusion of mineralized pegmatites and quartz veins (Figure 7.2). This was done in only one generation of successive stages. The earlier stage is barren in Nb-Ta-Sn-W (named earlier stage in Figure 7.2); the following stage (indicated as mid stage in Figure 7.2) is associated more with the coltan than the Sn and W mineralization while the later stage is more enriched in Sn and W than in Nb and Ta mineralization. The intrusion of the pegmatites and hydrothermal quartz-muscovite-sericite-tourmaline veins caused intense hydrothermal alterations (of the wall-rocks) such as tourmalinization, greisenization, muscovitization, sericitization and kaolinization. The latter processes combined with the weathering influenced the precipitation of Sn and W mineralization.

Compared to other Sn-, W- and coltan deposits found in the Central and Western - Rwanda, the southeastern deposits occur in the same geological and metallogenetic settings and do not show major differences from the previous ones. They are all granite-related, hosted in Mesoproterozoic meta-sediments, tectonically controlled and the primary deposits are, in both cases, of pegmatite and/or hydrothermal veins types. The fluid inclusion studies showed that the mineralizing fluids in the south-east were hosting more than one cation in their chemical composition and presented a wide range of formation temperatures (150°C to above 500°C). This indicates the influence of meteoric waters whereas the west/central deposits had a H₂O-CO₂-CH₄-N₂-NaCl composition and a formation temperature between 300°C [Nyakabingo and Gifurwe tungsten mines (Pohl and Günther, 1991; De Clerq et al., 2008)] and 400°C [Rutongo and Musha (Günther, 1990 in Dewaele et al., 2010)] with active metamorphic processes (De Clerq et al., 2008; Dewaele et al., 2010). Also, both zones were dominated by similar types of hydrothermal alterations: greisenization, muscovitization, sericitization, kaolinization and tourmalinization.

8. Conclusions

From the present research project, it can be concluded that:

- South-eastern Rwanda is composed of meta-sedimentary rocks of the Mesoproterozoic age which were intruded by two granite generations: the oldest G1-3 of roughly 1380+/-10 Ma age and the younger G4- granites of 986+/-10 Ma age (Tack et al., 2010). The latter is associated with the Sn-W-Nb-Ta- mineralization which occurs in the three investigated mineral deposits (Rwinkwavu, Musha-Ntungwa and Bugarura-Kuluti) [Tack et al., 2010; Dewaele et al., 2011, 2010].
- The primary mineralization is pegmatite/hydrothermal quartz veins type and tectonically controlled. In addition, the secondary deposits exist in the form of alluvial/eluvial placers. The salinities of the mineralizing fluids are between 0.5 and 17.3 wt. % NaCl-equivalent. The trapping temperatures are extending from 150°C to above 500°C. The contrast of salinities and the wide range of formation temperatures between various investigated inclusions might be due to a mixing of magmatic fluids with metamorphic to meteoric waters.
- The mineral associations in the eastern Rwandan ore deposits are coltan-muscovite-quartz-tourmaline, cassiterite-sericite-muscovite-tourmaline and ferberite-huebnerite-quartz-muscovite-garnet-ilmenite-hematite-goethite.
- In the cassiterite samples from Bugarura-Kuluti, the dominant substitution is Sn^{4+} replaced by $(\text{Ta}, \text{Nb})^{4+}$. In the cassiterites from Musha-Ntungwa and Rwinkwavu prospects, the 3 Sn^{4+} is replaced by $2(\text{Ta}, \text{Nb})^{5+} + (\text{Fe}, \text{Mn})^{2+}$ and/or $\text{Sn}^{4+} + \text{O}^{2-}$ is replaced by $\text{Fe}^{3+} + \text{OH}^-$. The cassiterite samples also show intergrowths with W-rich mineral phases.
- The coltan samples from Rwanda show increased incompatible element contents (Pohl, 2011; Melcher et al., 2009 and this study) compared to the Czech Republic variscan coltan mineralization (Breiter et al., 2007). This is an indication that the earlier have crystallized from more evolved felsic magmas than the latter.
- The dominant wolframite mineral is ferberite.
- There are different generations of fluid inclusions, ore mineral zoning and various types of hydrothermal alterations. This indicates that the metallogenetic evolution in the eastern Rwandan mineral deposits took place in multi-phases involving multi-stage circulation of hydrothermal fluids.

9. References

- Abdalla, H.M., Matsueda, H., Obeid, M.A. and Takahashi, R. (2008). Chemistry of cassiterite in rare-metal granitoids and the associated rocks in the Eastern Desert, Egypt. *Journal of Mineralogical and Petrological Sciences*, **103**, 318-326.
- Baudet, D., Hanon, M., Lemonne, E. and Theunissen, K. (1989). Lithostratigraphie du domaine sédimentaire de la chaîne kibarienne au Rwanda. *Annales de la Société Géologique de Belgique*, **112**, 225-246.
- Baudin, B., Zigirababiri, J., Ziserman, A. and Petricec, V. (1982). *Carte des gîtes minéraux du Rwanda au 1: 250 000*.
- Beer, K.E. and Ball, T.K. (1986). Tin and tungsten in pelitic rocks from S.W. England and their behavior in contact zones of granites and in mineralized areas. *Proceedings of the Ussher Society*, **6**, 330-337.
- Beurlen, H., Da Silva, M.R.R., Thomas, R., Soares, D.R. and Olivier, P. (2008). Nb-Ta-(Ti-Sn) oxide mineral chemistry as tracer of rare-element granitic pegmatite fractionation in the Borborema Province, Northeastern Brazil. *Mineralium Deposita*, **43**, 207-228.
- Bizimana, E. (1982). *Aperçu géologique de la zone Akagera Sud (IVa)*. Unpublished report, Geological Survey of Rwanda, pp.11.
- Bodnar, R.J., Vityk, M.O. (1994). Interpretation of microthermometric data for H₂O-NaCl fluid inclusions, *In: Fluid inclusions in Minerals, Methods and Applications*, B. De Vivo and M.L./ Frezzotti, eds. by Virginia Tech, Blacksburg. VA, 117-130.
- Breiter, K., Skoda, R. and Uher, P. (2007). Nb-Ta-Ti-W-Sn oxide minerals as indicators of a peraluminous P- and F-rich granitic system evolution: Podlesi, Czech Republic. *Mineralogy and Petrology*, **91**, 225-248.
- BRGM (1987). *Plan minéral du Rwanda*, Orléans, France, pp.580.
- Brinckmann, J., Lehmann, B., Hein, U., Hohndorf, A., Mussallam, K., Weiser, T. and Timm, F. (2001). La géologie et la minéralisation de l'or de la chaîne Kibarienne, Nord-Ouest du Burundi,

Afrique Orientale. *Geologisches Jahrbuch Reihe D*, **101**, pp.195.

Buchwaldt, R., Toulkeridis, T., Todt, W., Ucauwun, E.K. (2008). Crustal age domains in the Kibaran belt of SW-Uganda: combined zircon geochronology and Sm-Nd isotopic investigation. *Journal of African Earth Sciences*, **51**, 4-20.

Burnham, C.W. (1967). Hydrothermal fluids in the magmatic stage. *In: Barnes, H.L., (ed.), Geochemistry of hydrothermal ore deposits. Holt, Rinehart and Winston*, 34-76.

Burnham, C.W. (1979). Magmas and hydrothermal fluids, *In: Barnes, H.L., (ed.), Geochemistry of hydrothermal ore deposits, 2nd ed., New York, John Wiley*, 71-136.

Cahen, L., Delhal, J. and Deutsch, S. (1972). A comparison of the ages of granites of SW Uganda with those of the Kibaran of central Shaba (Katanga, Rep. Zaire) with some new isotopic and petrogenetical data. *Annales-serie IN-8- Sciences Géologiques*, **73**, 1-67.

Cahen, L. and Snelling, N.J. (1966). *The geochronology of equatorial Africa*, North-Holland Publishing Company, Amsterdam.

Cahen, L., Snelling, N.J., Delhal, J., Vail, J.R., Bonhomme, M. and Ledent, D. (1984). *The geochronology and evolution of Africa*, Clarendon Press Oxford, pp.512.

Cerny, P. (1993b). Rare-element granitic pegmatites. Part II: Regional to global environments and petrogenesis, in *Ore deposit models*, vol. II edited by P.A. Sheahan and M.A. Cherry, Geoscience Canada, Reprint series, **6**, 49-62.

Cerny, P., Blevin, P.L., Cuney, M. and London, D. (2005). Granite - related ore deposits. *Economic Geology*, **100**, 337-370.

Crawford, M.L. (1981). Phase equilibria in aqueous fluid inclusions. *In: short course in Fluid Inclusions: Applications to Petrology* (L.S. Hollister & M.L Crawford eds.), *Mineral Assoc. Can., Short course Handbook*, **6**, 75-100.

De Clerq, F., Muechez, P., Dewaele, S. and Boyce, A. (2008). The tungsten mineralization at Nyakabingo and Gifurwe (Rwanda): Preliminary results. *Geologica Belgica*, **11**, 251-258.

De Waele, B., Johnson, S.P., Pisarevsky, S.A. (2008). Palaeoproterozoic to Neoproterozoic growth and evolution of the eastern Congo Craton: its role in the Rodinia puzzle. *Precambrian Research*, **160**, 127-141.

Dewaele, S., De Clerq, F., Muchez, P., Schneider, J., Burgess, R., Boyce, A. and Fernandez-Alonso, M. (2010). Geology of the cassiterite mineralization in Rutongo area, Rwanda (Central Africa): Current state of knowledge. *Geologica Belgica* **13/1**, 91-112.

Dewaele, S., Henjes-Kunst, F., Melcher, F., Sitnikova, M., Burgess, R., Gerdes, A., Alonso-Fernandez, M., De Clerq, F., Muchez, P. and Lehmann, B. (2011). Late Neoproterozoic overprinting of cassiterite and columbite – tantalite bearing pegmatites of the Gatumba area, Rwanda (Central Africa). *Journal of African Earth Sciences*, www.elsevier.com/locate/jafrearsci, 1-17.

Dewaele, S., Tack, L., Fernandez-Alonso, M., Boyce, A. and Muchez, P. (2007a). Cassiterite and columbite - tantalite mineralization in pegmatites of the northern part of the Kibaran orogen (Central Africa): the Rutongo area (Rwanda). In: Andrew, C.J., et al (eds), *Proceedings of the 9th biennial SGA meeting. Mineral exploration and research: digging deeper 20th-23rd August 2007, Dublin, Ireland, 1489-1492.*

Dewaele, S., Tack, L., Fernandez-Alonso, M., Boyce, A. and Muchez, P. (2007b). Cassiterite mineralization in vein-type deposits of the Kibaran orogen (Central Africa): Nyamyumba (Rutongo area, Rwanda). In: Andrew, C.J., et al (eds), *Proceedings of the 9th biennial SGA meeting. Mineral exploration and research: digging deeper 20th-23rd August 2007, Dublin, Ireland, 1007-1010*

Dewaele, S., Tack, L., Fernandez-Alonso, M., Boyce, A., Muchez, P., Schneider, J., Cooper, G. and Wheeler, K. (2008). Geology and mineralization of the Gatumba area, Rwanda: present state of knowledge. *Etudes Rwandaises*, **16**, 6-24.

Dingwell, D.B. (1988). The structures and properties of fluorine-rich magmas: A review of experimental studies. *Canadian Institute of Mining and Metallurgy, Special volume*, **39**, 1-12.

Dutu Stanchi, I., Cardoso da Fonseca, E. and Ferrand, A. (1974). *Rapport sur les recherches géologiques-géochimiques dans la zone de Rusumo (SE-Rwanda)*. Unpublished report, UNDP-Projet Recherches Minières, pp.35.

Fernandez-Alonso, M. and Theunissen, K. (1998). Airborne geophysics and geochemistry provide new insights in the intra - continental evolution of the Mesoproterozoic Kibaran belt (Central Africa). *Geological Magazine*, **135**, 203-216

Fetherston, J.M. (2004). Tantalum in Western Australia, Geological Survey of Western Australia. *Mineral Resources Bulletin*, **22**, pp.161.

Günther, M.A. (1990). *Flüssigkeitseinschlüsse und geologisches Umfeld zentralafrikanischer Sn-, W- und Au-Lagerstätten (Rwanda und Burundi)*, Unpublished PhD thesis, Naturwissenschaftlichen Fakultät der technischen Universität Carolo-Wilhelmina zu Braunschweig, pp.144.

Hartung, J. (1999). A note on combining dependent tests on significance. *Biometrical Journal*, **41**, 7, 845-855.

Haung, H.H., Anttila, K. and Roine, A. (2002). Eh-pH diagram, *Outokumpu HSC Chemistry for Windows: chemical reaction and equilibrium software with extensive thermochemical database*, Research Oy, Pori, Finland.

Heinrich, C.A. (1995). *Geochemical evolution and hydrothermal mineral deposition in Sn (-W-base metal) and other granite-related ore systems: some conclusions from Australian examples: Mineralogical Association of Canada, Short course Handbook*, **23**, 203-220.

Henry, D.J. and Guidotti, C.V. (1985). Tourmaline as a petrogenetic indicator mineral: an example from staurolite grade metapelites of New Maine. *American Mineralogist*, **70**, 1-15.

Herron, M.M. (1988). Geochemical classification of terrigenous sands and shales from core or log data. *Journal of sedimentary petrology*, **58**, 820-829.

Hogarth, D.D. (1977). Classification and nomenclature of the pyrochlore group. *American Mineralogist*, **62**, 403-410.

Huizenga, J.M. (2010). *Short course in fluid inclusions*, Short course handbook, pp.46.

Institut Géographique National de Belgique and MINITRAPE (1988). *Carte topographique du Rwanda à 1:50 000*, 43 feuilles, Service de cartographie du Rwanda.

Jackson, N.J., Halliday, A.N., Sheppard, S.M.F. and Mitchell, J.G. (1982). Hydrothermal activity in the St. Just mining district, Cornwall, *In: A.M. Evans (Editor), Metallization associated with acid magmatism*, 6, Wiley, London, 137-179.

Kampunzu, A.B., Rumvengeri, B.T., Kapenda, D., Lubala, R.T. and Caron, J.P.H. (1986). Les Kibarides d'Afrique Centrale et Orientale: une chaîne de collision. *UNESCO, Geology for Development Newsletter* 5, 125-137.

Klerkx, J., Liegeois, J.P., Lavreau, J. and Theunissen, K. (1984). Granitoïdes Kibariens précoces et tectonique tangentielle au Burundi: magmatisme bimodal lié à une distension crustale, *In: Klerkx, J., Michot, J. (Eds), African Geology*, a volume in honour of Cahen, Royal Museum for Central Africa, Tervuren, 29-46.

Klerkx, J., Liégeois, J.P., Lavreau, J. and Claessens, W. (1987). Crustal evolution of the Northern Kibaran Belt, eastern and Central Africa, *In: Kroner, A., (Ed), Proterozoic Lithospheric evolution*, vol. 17. *American Geophysical Union and the Geological Society of America*, 217-233.

Kokonyangi, J.W., Kampunzu, A.B., Armstrong, R., Yoshida, M., Okudaira, T., Arima, M. and Ngulube, D.A. (2006). The Mesoproterozoic Kibaride Belt (Katanga, DR Congo). *Journal of African Earth Sciences*, 46, 1-35

Krauskopf, K.B. and Bird, D.K. (1995). *Introduction to Geochemistry*, McGraw-Hill, pp.647.

Lavreau, J. (1985). Le groupe de la Rusizi (Rusizien du Zaire, Rwanda et Burundi) à la lumière des connaissances actuelles. Royal Museum for Central Africa, Tervuren (Belgium), Dpt Géologie-Minéralogie, *Ann. Rep. 1984*, 111-119.

Leeder, O., Thomas, R. and Kemm, W. (1986). *Einschlüsse in Mineralen*. Dt vgl Grundstoffind, 1. Aufl., Leipzig, pp.180.

Lehmann, B. and Lavreau, J. (1988). Geochemistry of tin granites from Kivu (Zaire), Rwanda and Burundi. *IGCP n°255 Newsletter / Bulletin* 1, 43-46.

Le Maitre, R.W. (1989). *A classification of igneous rocks and glossary of terms. Recommendations of the IUGS Commission on the Systematics of igneous rocks*. Oxford: Blackwell.

Linnen, R.L. and Keppler, H. (1997). Columbite solubility in granitic melts: consequences for the enrichment and fractionation of Nb and Ta in the Earth's crust. *Contributions to Mineralogy and Petrology*, **128**, 213-227.

Linnen, R.L. (1998). The solubility of Nb-Ta-Zr-Hf-W in granitic melts with Li and Li + F: constraints for mineralization in rare metal granites and pegmatites. *Economic Geology*, **93**, 1013-1025.

Linnen, R.L. (2004a). PIG Comments and questions, reply: http://www.minsocam.org/MSA/Special/Pig/Pig_CQ/PIG_CQ/Kjellman.html

Linnen, R.L. (2004b). Ferrocolumbite-manganotantalite trends in granites and pegmatites: experimental and natural constraints. *Geol Soc Amer Progr Abstr* 36.

London, D. (1996). Granitic pegmatites. *Transactions of the Royal Society Edinburgh, Earth Sciences*, **87**, 305-19.

London, D., Evensen, J.M., Fritz, E., Icenhower, J.P., Morgan, G.B. and Wolf, M.B. (2001). Enrichment and accommodation of manganese in granite - pegmatite systems. *11th An. Goldschmidt Conference Abstract 3369*. CDR PDF version.

Melcher, F., Graupner, T., Sitnikova, M., Oberthür, T., Gäbler, H.E., Bahr, A. and Henjes-Kunst, F. (2009). *Herkunftsnachweis von Columbit-Tantalit-Erzen –Status-quo-Bericht*, BGR open file report no. 11082/09

Meyer, C. and Hemley (1967). Wall rock alteration. In: Barnes (ed.), *Geochemistry of hydrothermal Ore deposits*. Holt, Rinehart and Winston, 166-235.

MINETAİN (1965). *Géologie de Bugarura-Kuluti*. Unpublished report in RMCA Archives-Tervuren.

Möller, P., Dulski, P., Szacki, W, Malow, G. and Riedel, E. (1988). Substitution of tin in cassiterite by tantalum, niobium, tungsten, iron and manganese. *Geochimica et Cosmochimica Acta*, **52**, 1497-1503.

Mumm, A.S. (2008). *Introduction to fluid inclusion research*, Short course handbook, pp.53.

Mutima, J. and Wei Li, J. (2010). Au, Sn, W and Nb/Ta Mineralization in Northern and North-eastern Burundi. *Academia Arena*, **2(2)**, 55-65.

Nesbit, H.W. and Young, G.M. (1982). Early Proterozoic climates and plate motions inferred from major element chemistry of lutites. *Nature*, **299**, 715-717.

OGMR (2009). *Mineral deposits map of Rwanda 1:250 000*.

Paterson, Grant and Watson LTD (2009). *Interpretation of the New Resolution Geophysics (NRG) airborne geophysical survey, Rwanda and integration with existing geosciences data*, Toronto-Canada, 47 figures, pp.65.

Pohl, W. (1988). "Post-orogenic" events within and nearby the Kibara belt in Central Africa. *IGCP Project N°255 Newsletters* **1**, 47-50, TU Braunschweig – MRAC Tervuren.

Pohl, W. (1994). Metallogeny of north-eastern Kibara belt, Central Africa-Recent perspectives, *Ore Geology Reviews*, **9**, 105-130.

Pohl, W. (2011). *Economic Geology, Principles and Practice: Metals, Minerals, Coal and hydrocarbons — Introduction to Formation and Sustainable Exploitation of Mineral Deposits*, Wiley-Blackwell, pp.663.

Pohl, W. and Günther, M.A. (1991). The origin of Kibaran (late Mid-Proterozoic) tin, tungsten and gold quartz vein deposits in Central Africa: a fluid inclusions study. *Mineralium Deposita*, **26**, 51-59.

Pollard, P.J., Pichavant, M., and Charoy, B. (1987). Contrasting evolution of fluorine- and boron-rich tin systems. *Mineralium Deposita*, **22**, 315-321.

Radar Technologies International (2009). Landsat image (3D) of Rwanda, Paris, France.

Raimbault, L., Cuney, M., Azencott, C., Duthou, J.L. and Joron, J.L. (1995). Multistage magmatic genesis of Ta-Sn-Li mineralized granite at Beauvoir, French Massif Central: a geochemical study, *Economic Geology*, **90**, 548-576.

Reed, M.H. (1997). Hydrothermal alteration and its relationship to ore fluid composition. *In: H.L. Barnes (ed.), Geochemistry of hydrothermal Ore deposits*. John Wiley&Sons, pp. 303-66.

Rollinson, H.R. (1993). *Using geochemical data: evaluation, presentation, interpretation*. United Kingdom, Longman, pp.352.

Romer, R.L. and Lehmann, B. (1995). U-Pb Columbite age of Neoproterozoic Ta-Nb mineralization in Burundi. *Economic Geology*, **90**, 2303-2309.

Rose, A.W. and Burt, D. (1979). Hydrothermal alteration. In: H.L. Barnes (ed.), *Geochemistry of hydrothermal ore deposits*. John Wiley & Sons, 173-235.

Roser, B.P. and Korsch, R.J. (1988). Provenance signatures of sandstone-mudstone suites determined using discriminant function analysis of major-element data. *Chemical Geology*, **67**, 119-139.

Rösler, H.J. (1983). *Lehrbuch der Mineralogie*, VEB Deutscher Verlag für Grundstoffindustrie, Leipzig, pp.833.

Rumvengeri, B.T. (1991). Tectonic significance of Kibaran structures in Central and Eastern Africa. *Journal of African Earth Sciences*, **13**, 267-276.

Sander and Geophysics LTD (1981). *Aeromagnetic survey of Rwanda*. Unpublished report, Geological Survey of Rwanda, pp.139.

Schipper, N. (1987). *Prospection de tungstène dans le Sud - Est du Rwanda: Résultats des travaux de follow-up dans les secteurs Kabarondo-IA et Bare*. Unpublished report, UNDP-Projet Recherches Minières, pp.43.

Shepherd, T.J., Rankin, A.H. and Alderton, D.H.M. (1985). *A practical guide to fluid inclusion studies*, Blackie, Glasgow and New York, pp.239.

Slatkine, A. (1965). Sur la minéralisation en étain de la région de Rwinkwavu. *Bulletin du Service Géologique du Rwanda*, **2**, 15-31.

Stevens, G., Boer, R. and Gibson, R.L. (1997). Metamorphism, fluid flow and gold remobilization in the Witwatersrand Basin: towards a unifying model. *South African Journal of Geology*, **100**, 363-75.

Tack, L., Liegeois, J.P., Deblond, A. and Duchesne, J.C. (1994). Kibaran A-type granitoids and mafic rocks generated by two mantle sources in a late orogenic setting (Burundi). *Precambrian research*,

Tack, L., Baudet, D., Chartry, G., Fernandez-Alonso, M., Lavreau, J., Liegeois, J.P., Tahon, A., Theunissen, K., Tréfois, P. and Wingate, M. (2002a). The Northeastern Kibaran Belt (NKB) reconsidered: evidence for ca. 1370 Ma-old, repeatedly reactivated Kibara mobile belt, preceding the c.a. 1.0 Ga Rodinia Supercontinent assembly. *Abstract for the 19th Colloquium of African Geology, El Jadida, Morocco, 19-23 March 2002, Special Abstracts volume.*

Tack, L., Fernandez-Alonso, M., De Waele, B., Tahon, A., De Waele, S., Baudet, D. and Cutten, H. (2006). The Northeastern Kibaran Belt (NKB): a long-lived intraplaque history. *Extended Abstract of oral communication submitted to session 1 (“Geodynamics of Africa”) of the 21st Colloquium of African Geology (CAG21) at Maputo (Mozambique), 3-5 July 2006, 149-151.*

Tack, L., Fernandez-Alonso, M., Tahon, A., Wingate, M. and Barritt, S. (2002b). The “Northeastern Kibaran Belt” (NKB) and its mineralization reconsidered: New constraints from a revised lithostratigraphy, a GIS-compilation of existing geological maps and a review of recently published as well as unpublished igneous emplacement ages in Burundi. *Abstract for the 11th Quadrennial IAGOD Symposium and Geocongress, Windhoek (Namibia), 22-26 July 2002.*

Tack, L., Wingate, M., Dewaele, B., Meert, J., Griffin, B., Belousova, E.A., Tahon, A., Fernandez-Alonso, M., Cutten, H. and Dewaele, S. (2008). The Proterozoic Kibaran Belt in Central Africa: intra-cratonic 1375 Ma emplacement of a LIP, *Abstract for the 22nd Colloquium African Geology (CAG 22), 04-06.11.2008, Hammamet, Tunisia, Abstract volume, pp.89.*

Tack, L., Wingate, M.T.D., De Waele, B., Meert, J., Belousova, E., Griffin, B., Tahon, A. and Fernandez-Alonso, M. (2010). The 1375 Ma “Kibaran event” in Central Africa: Prominent emplacement of bimodal magmatism under extensional regime. *Precambrian research*, **180**, 63-84.

Taylor, S.R. (1964). Abundance of chemical elements in the continental crust: a new table. *Geochimica et Cosmochimica Acta*, **28**, 1273-85.

Taylor, S.R. and McLennan, S.M. (1985). *The continental crust: its composition and evolution*, Blackwell.

Taylor, J.R. and Wall, V.J. (1992). The behavior of tin in granitoids magmas. *Economic Geology*, **82**, 403-420.

Theunissen, K., Hanon, M. and Fernandez-Alonso, M. (1991). *Carte géologique du Rwanda, 1/250000*, Service Géologique, Ministère des Mines, de l'Industrie et de l'Artisanat, République Rwandaise.

UNCTAD and the Ministry of Trade and Industry of Rwanda (2010). *Rwanda's development-Driven trade policy*, pp.81.

Uwizeye, F. (1987). *Les roches mafiques et ultramafiques de Kibungo*. Unpublished report, Service Géologique, Ministère des Mines, de l'Industrie et de l'Artisanat, République Rwandaise, pp.60.

Van den Kerkhof, A.M. (1988). *The system CO₂-CH₄-N₂ in fluid inclusions: Theoretical modelling and geological applications*, PhD Thesis, Free University Press, pp.206.

Varlamoff, N. (1948). Gisements de cassitérite de la région de Kalima (Maniema, Congo Belge). *Annales de la Société Géologique de Belgique*, **71**, 194-237.

Varlamoff, N. (1972). Central and West African rare-metal granitic pegmatites, related aplites, quartz veins and mineral deposits. *Mineralium Deposita*, Springer-Verlag, **7**, 202-216.

Wedepohl, K.H. (1969). *Handbook of Geochemistry*, Volume **2**. Springer-Verlag, loose leaf.

White, A.J.R. and Chappell, B.W. (1977). Ultra - metamorphism and granite genesis. *Tectonophysics*, **43**, 7-22.

Williamson, B.J., Spratt, J., Adams, J.T., Tindle, A.G. and Stanley, C.J. (2000). Geochemical constraints from zoned hydrothermal tourmalines on fluid evolution and Sn mineralization: an example from fault breccias at Roche, SW England. *Journal of Petrology*, **41**, 9, 1439-1453.

Wood, S.A. and Samson, I.M. (1998). Solubility of ore minerals and complexation of ore metals in hydrothermal solutions. *Reviews in Economic Geology*, **10**, 33-80

Young, G.M., von Brunn, V., Gold, D.J.C. and Minter, W.E.I. (1998). Earth's oldest reported glaciations: physical and chemical evidences from the Archean Mozaan Group (≈ 2.9 Ga). *South African Journal of Geology*, **106**, 523-538.

APPENDIX 1: METHODOLOGY

1. Field investigations: The field investigations have been carried out during the June-August 2010 field campaign and were facilitated by the materials and tools provided jointly by the Department of Geology, University of the Free State (UFS)-Bloemfontein and Rwanda Geology and Mines Authority (OGMR)-Kigali. More than 240 observation points were recorded and more or less 50 rock samples collected for further analyses. Each rock sample was cut into three pieces: one for the preparation of the thin/doubly polished thick section, one for XRF analysis and one kept for the reference at the Department of Geology, University of the Free State, Bloemfontein.

2. Optical microscopy: The mineral identification using the reflected and the incident light from the polarized microscopy were used on polished thin sections. The transmitted-light microscopy served as a tool to identify for each rock sample detailed information on its mineralogical composition. For this purpose, an OLYMPUS BX51 microscope (Department of Geology, University of the Free State) was used for optical reconnaissance.

3. SEM-EDX/WDX:

The samples of ore minerals were coated using a carbon coating machine, QUORUM/Q150T. The SEM-E/WDX analyses were completed on ore mineral concentrates and rock samples for the mineral chemistry determination with a SHIMADZU SSX-550 Superscan SEM of the Department of Biology and a JEOL JSM-6610 SEM machine (photo on the right side) was made available by the Department of Geology, University of the Free State/ Bloemfontein for this purpose. The SEM-EDX data were measured with internally calibrated

standards and the results were automatically normalized to 100%.



4. Whole rock chemistry: Whole rock major and trace element analyses were completed, and mass balance calculations were carried out to determine which elements were concentrated in each of the identified mineralogic zones. The samples were crushed, using Retsch KG 5657 Haan BB 100 jaw crusher with steel carbide plates and milled using a Giebertechnik Labor-Scheibenschwingmuhle (T1400) to obtain a homogenized powder.



Photo of Axios XRF (on the left) (<http://www.panalytical.com>)

For the trace elements quantification and analyses, pressed pellets consisting of 8 g sample and 3 g Hoechst wax were produced. For the major elements analyses, fusion discs were made using roasted powder, that consist of 0.28 g of the sample and 1.52 g of mixture of lithium-meta and tetra borate. The powders were weighed and dried at 110°C for 24 hours, weighed again for the determination of quantity of percolated water, roasted for another 4 hours at 1000°C in the furnace and weighed again to determine the loss on ignition (LOI). The major and trace elements analyses were carried out at the Department of Geology, UFS Bloemfontein using the PAN

analytical WD-XRF Axios spectrometer with the following technical parameters: accelerating voltage (60 kV), beam current (160 mA) and the power (4 kW). The operations on Axios spectrometer were facilitated by the Super Q software. The following standards were used for XRF investigations:

Item	Standard names
Major elements	G-1, W-1, AGV-1, BCR-1, DST-1, G-2, GSP-1, PCC-1, BHVO-1, MAG-1, SY-2, SY-3, MRG-1, ASK-1, ASK-2, GR, GA, GH, BR, MICA-FE, MICA-MG, DR-N, UB-N, BX-N, DT-N, VS-N, GS-N, FK-N, GL-O, AN-G, BE-N, MA-N, AL-I, IF-G, AC-E, JG-1, JG-1A, JG-2, JG-3, JB-1, JB-1A, JB-2, JB-3, JR-2, JA-1, JA-2, JA-3, JF-1, JF-2, JP-1, JGB-1, JCH-1, JDO-1, JLK-1, JLS-1, JSD-1, JSD-2, JDS-3, JSI-1, JSI-2, JR-3, JGB-2, JH-1, NIM-D, NIM-G, NIM-L, NIM-N, NIM-P, NIM-S, SARM-39, SARM-40, SARM-41, SARM-42, SARM-43, SARM-44, SARM-45, SARM-46, SARM-47, SARM-48, SARM-49, SARM-50, SARM-51, SARM-52
Trace elements	AC-E, AGV-1, AL-I, AN-G, ASK-1, ASK-2, BCR-1, BE-N, BHVO-1, BR, BX-N, DR-N, DT-N, DTS-1, FK-N, G1, G2, GA, GH, GL-O, GR, GS-N, GSP-1, IF-G, JA-1, JA-2, JA-3, JB-1, JB-1A, JB-2, JB-3, JCH-1, JDO-1, JF-1, JF-2, JG-1, JG-1A, JG-2, JG-3, JGB-1, JGB-2, JH-1, JLK-1, JLS-1, JP-1, JR-1, JR-2, JR-3, JSD-1, JSD-2, JSD-3, JSI-1, JSI-2, MAG-1, MA-N, MICA-FE, MICA-MG, MRG-1, NIM-D, NIM-G, NIM-L, NIM-N, NIM-P, NIM-S, PCC-1, SARM-39, SARM-40, SARM-41, SARM-42, SARM-43, SARM-44, SARM-45, SARM-46, SARM-47, SARM-48, SARM-49, SARM-50, SARM-51, SARM-52, SY-2, SY-3, UB-N, VS-N, W-1

The following 29 trace elements: V, Cr, Ni, Cu, Zn, As, Br, Rb, Sr, Y, Zr, Nb, Mo, Sr, Sn, Sb, Ba, Tl, Pb, Th, U, Ga, Ge, Se, Yb, Hf, Ta, W and Bi and 10 major elements: SiO₂, Al₂O₃, Fe₂O₃, MnO, MgO, CaO, Na₂O, K₂O, TiO₂, P₂O₅ were determined. For each major and trace element the spectrometer calculated the specific detection limit. Due to the presence of sodium in the fusion discs, the Na₂O was measured on the pressed pellets.

5. Microthermometry (detailed in section 5.2).

APPENDIX 2: LIST OF OBSERVATION POINTS (OP) FROM THE FIELD INVESTIGATIONS OF JUNE-AUGUST 2010

OP	Easting	Northing	Elevation	Description	Stratification (S0)	Cleavages: S1/S 2
370	567988	9781648	1480	Quartz veins of 40cm (thickness)	-	-
371	567985	9781645	1479	Continued quartz vein	-	-
372	567885	9781929	1455	Eluviums (grade: 30 kg/T)	-	-
373	565523	9783059	1402	Sandstones (30cm) cut by mky qz veins//to S0, locally perpendicularly to S0	-	-
374	565543	9782960	1429	Milky quartz vein	-	-
375	565535	9782947	1435	Continuation of the milky quartz vein	-	-
376	565532	9782943	1436	Continuation of the milky quartz vein	-	-
377	565530	9782943	1436	Continuation of the milky quartz vein	-	-
378	565573	9782901	1446	Continuation of the milky quartz vein	-	-
379	565569	9782864	1452	Changing orientation of the quartz vein in sandstones	-	-
380	565569	9782864	1453	Quartz vein	-	-
381	565579	9782843	1458	Exploration trench	-	-
382	565574	9782841	1456	Exploration trench	-	-
383	565583	9782825	1460	Quartz vein+old mining road	-	-
384	565623	9782622	1489	Schists (west); iron-quartz-schists	-	-
385	565617	9782612	1490	Gossan (laterites)	-	-
386	565623	9782572	1499	Exploitation of eluviums at Gahushyi hill, 4 kg/200 l/day	-	-
387	565696	9782380	1521	Exploitation of eluviums at Gahushyi hill	-	-
388	565740	9782322	1531	Exploitation of eluviums at Gahushyi hill	-	-
389	565735	9782301	1532	1 m milky ferruginous qz vein NNE-SSW/80°ENE, Nyamuyorwa wolframite expl	-	-
390	566427	9780708	1618	Quartz vein with tourmaline	-	-
391	566435	9780726	1615	Quartz vein with tourmaline	-	-
392	566450	9780773	1595	Quartz vein with tourmaline plus wolframite	-	-
393	566450	9780773	1597	-	-	-
394	566456	9780793	1588	-	-	-
395	566457	9780792	1588	-	-	-
398	564353	9750367	1359	-	-	-
399	564355	9750367	1357	Gatore	-	-
400	549567	9760661	1439	Ngara SnO2-Coltan mine (kaolinized pegmatite)	-	-
401	549521	9760677	1430	Ngara SnO2-Coltan mine with a high concentration of micas	-	-
402	549529	9760702	1430	Exploitation pit in Ngara	-	-
403	549520	9760687	1428	Exploitation pit in Ngara	-	-
404	549516	9760677	1417	Exploitation pit in Ngara	-	-
405	562181	9780273	1657	Gasetza WO3 mine in sandstones+quartzites of 1 m thick, medium to fine grained pinkish sandstones	-	-

406	562188	9780331	1661	Small quartz vein (Ntunga), schists with mineralization of tourmaline	240N/060, 219/047	-
407	540216	9783323	1535	Schists and underground exploitation (gallery) in Ntunga tin mine	-	-
408	540266	9783325	1544	Pegmatite of appr. 5 m of thickness in Ntunga mine	-	-
409	540304	9783272	1538	Schists with tourmaline	244/053, 256/060	-
410	473626	9847458	1913	Wolframite exploitation in Bugarama concession	-	-
411	473651	9847561	1970	Former box-sluicing	-	-
412	473444	9847562	1929	Sample of black shales	-	-
413	446801	9824733	2265	-	-	-
414	537261	9807353	1610	Quartz vein hosted in quartzitic rocks/Bugarura East	-	-
415	536054	9808414	1628	Underground exploitation in Mamfu mine	-	-
416	536279	9809024	1639	Gallery in Mamfu II concession	-	-
417	537642	9849022	1336	-	-	-
418	526823	9830501	1466	Granite of Ngarama anatectic xenoliths and cracks filled with quartz veins	-	-
419	567740	9781985	1422	NS mineralized qz vein (mineralized trainee)	-	-
420	567853	9781970	1443	vein of sericite within schists/no qz	-	-
421	567851	9781964	1442	-	-	-
422	567852	9781954	1443	qtz vein	-	-
423	567848	9781947	1442	cntd qtz vein	-	-
424	567842	9781844	1448	mineralized qz vein2	-	-
425	567843	9781854	1449	mineralized qz vein2	-	-
426	567955	9781878	1459	mineralized qz vein1	-	-
427	567961	9781935	1455	mineralized qz vein1	-	-
428	568002	9781897	1467	mineralized qz vein	-	-
429	568003	9781908	1467	mineralized qz vein	-	-
430	568002	9781908	1468	sample of the host rock (hard quartzitic sandstone)	-	-
431	568018	9781901	1475	-	N70E/60°NW	-
432	568167	9781775	1492	soil occupied by several plantations	-	-
433	568241	9781744	1514	Fissure swarm (fractured zone)	-	-
434	568281	9781759	1538	hard and very thick layers of sdst	-	-
435	568373	9781691	1553	Thick layers of sdst (pronounced levels of alteration mainly oxidation)	-	-
436	568396	9781657	1554	-	N0/subvert.	-
437	568494	9781687	1500	Quartzites	-	-
438	566508	9780578	1556	Quartz vein 1	-	-
439	566526	9780585	1548	Quartz vein 1	-	-
440	566475	9780602	1605	limit of fractured zone filled by qz veins, altered sandstones with multiple veinlets	-	-
441	566473	9780599	1620	-	Stratification N15/35°E	-
442	566427	9780710	1611	Quartz vein 2	-	-

443	566441	9780751	1597	Quartz vein 2	-	-
444	566158	9780743	1600	Pit (old exploitation)	-	-
445	566159	9780748	1598	Pit (old exploitation)	-	-
446	566148	9780783	1590	Pit (old exploitation)	-	-
447	566148	9780793	1595	Pit (old exploitation)	-	-
448	566151	9780800	1598	Pit (old exploitation)	-	-
449	566154	9780820	1587	Pit (old exploitation)	-	-
450	566013	9780908	1585	Quartz vein 3	-	-
451	566013	9780908	1582	Quartz vein 3	-	-
452	566008	9780900	1581	Quartz vein 4	-	-
453	566007	9780903	1574	Sample	-	-
454	565980	9780753	1563	Very hard and massive quartzites	-	-
455	565986	9780667	1553	Eluvial SnO ₂ exploitation (Gahushyi, Kuyacumi), exploitation pit of 8-10 m deep	-	-
456	565995	9780581	1562	17 m deep exploitation pit (production: 200 kg/day)	-	-
457	565894	9780928	1556	Mineralized quartz vein 1	-	-
458	565905	9780939	1562	Mineralized quartz vein 1	-	-
459	565910	9780954	1558	Mineralized quartz vein 1	-	-
460	565845	9781039	1549	Mineralized quartz vein 2	-	-
461	565854	9781065	1553	Mineralized quartz vein 2	-	-
462	565864	9781121	1563	Mineralized quartz vein 2	-	-
463	565859	9781160	1564	Tailings concentrated in a quarry	-	-
464	565902	9781219	1570	Host rock	-	-
465	565912	9781242	1574	Host rock	N10E/70°E	-
466	565934	9781211	1573	Mineralized quartz vein 3	-	-
467	565947	9781228	1577	Mineralized quartz vein 3	-	-
468	565981	9781246	1578	Old quarry exploited before (primary mineralizations in NS quartz veins)	-	-
469	565980	9781511	1587	Road	-	-
470	565994	9781516	1589	Water reservoir	-	-
471	565541	9782954	1446	45-50cm thick quartz vein	-	N60E/70°E
472	565522	9783060	1404	-	S0 N30E/30°W	-
473	567474	9782600	1394	Rutonde tin mine	-	-
474	567287	9782498	1394	Road to Nyankora	-	-
475	566868	9782705	1395	Stadium/road	-	-
476	566096	9783006	1359	road	-	-
477	565814	9783112	1368	Kadiridimba bridge	-	-
478	565536	9783022	1407	-	S0 N70E/30°SW	-
479	565537	9782996	1416	Exploration trench	-	-

480	565561	9782885	1445	Mineralized quartz vein 4	-	-
481	565561	9782864	1444	Mineralized quartz vein 4	-	-
482	565615	9782613	1487	-	S0 NS/35°W	-
483	565631	9782574	1495	path	-	-
484	565684	9782382	1508	Quartz vein with mineralized pockets	-	-
485	565691	9782394	1518	Quartz vein with mineralized pockets	-	-
486	565700	9782411	1512	Quartz vein with mineralized pockets	-	-
487	565752	9782131	1536	Quartz vein with mineralized pockets 1	-	-
488	565775	9782129	1533	Quartz vein with mineralized pockets 2/3	-	-
489	565748	9782097	1538	Quartz vein with mineralized pockets 1	-	-
490	565759	9782096	1538	Quartz vein with mineralized pockets 2	-	-
491	565759	9782059	1538	Quartz vein with mineralized pockets 3	-	-
492	565759	9782050	1538	quarry	-	-
493	565781	9782004	1542	Quartz vein 4	-	-
494	565781	9781993	1542	Quartz vein 4	-	-
495	565786	9781949	1547	Quartz vein 5	-	-
496	565788	9781926	1549	Quartz vein 5	-	-
497	565793	9781932	1544	Old tin exploitation of quartz vein	NS/80°E	-
498	565778	9781901	1551	Old tin exploitation of quartz vein	-	-
499	565753	9781848	1550	Old tin exploitation of quartz vein	-	-
500	565800	9781813	1550	Thick mineralized quartz vein (50-60cm)	-	-
501	565796	9781785	1553	Thick mineralized quartz vein (50-60cm)	-	-
502	565803	9781772	1554	Quartz vein 6	-	-
503	565816	9781794	1553	Quartz vein 6	-	-
504	565820	9781785	1551	Quartz vein 7/8	-	-
505	565816	9781776	1555	Quartz vein 7	-	-
506	565823	9781773	1551	Quartz vein 8 (80cm thick)	-	-
507	565833	9781721	1558	Quartz vein 9 (80cm thick)	-	-
508	565836	9781734	1562	Quartz vein 9 (80cm thick) swarm of veins hosted in sandstones and quartzites	-	-
509	565850	9781735	1560	Quartz vein 10	-	-
510	565843	9781714	1566	Quartz vein 10	-	-
511	565993	9781520	1580	Water reservoir	-	-
512	566077	9781546	1566	Quartz vein cross cutting S0, host rock=schists	-	-
513	566074	9781531	1564	Quartz vein cross cutting S0, host rock=schists	-	-
514	566191	9781475	1554	Mineralized quartz vein ; tot. production around 20 T	N70E/20°W	-
515	566159	9781360	1568	Mineralized quartz vein ; tot. production around 20 T	N70E/20°W	-
516	565097	9780893	1435	Rusave village (Gahushyi-Rwinkwavu)	-	-

517	539912	9783541	1536	Ntunga pathway	-	-
518	539875	9783447	1528	Joint between two roads	-	-
519	539788	9783280	1530	road	-	-
520	539904	9783157	1515	quarry pegmatites of 4 m thick	-	-
521	539897	9783166	1605	pegmatitic intrusion	-	-
522	539942	9783136	1662	Pegmatite within the host rocks	S0 N160/vertical	-
523	539935	9783161	1658	pegmatitic extension	-	-
524	539981	9783240	1574	possible end of the pegmatite (extended in the deep geologic formations)	-	-
525	540018	9783250	1563	-	N165/60°NW	-
526	540055	9783246	1561	Qz vein, 70cm thick, N195/65°NW parallel to S0 (sill)	-	-
527	540220	9783355	1532	-	N160/60°NW	-
528	540206	9783411	1543	Gallery entrance	-	-
529	540207	9783415	1547	Gallery entrance	-	-
530	540225	9783485	1565	well of 5 to 8 m in exploitation	-	-
531	540209	9783521	1587	exploitation of a qz vein	-	-
532	540113	9783691	1628	road	-	-
533	539957	9783664	1622	Ntunga road to the concession	-	-
534	538239	9787031	1608	Musha	-	-
535	538390	9786974	1582	JC-535, exploitation of cassiterite in the eluviums but SnO ₂ -bearing quartz veins	-	-
536	538386	9787000	1581	Highly sericitized and kaolinized quartz vein	-	-
537	538468	9786885	1563	Alluvial/eluvial tin mineral exploitation	-	-
538	538515	9786838	1556	Pit (eluvial/alluvial cassiterite exploitation)	-	-
539	538538	9786814	1553	Pit (eluvial/alluvial cassiterite exploitation)	-	-
540	538576	9786786	1547	Pit (eluvial/alluvial cassiterite exploitation)	-	-
541	538778	9786688	1523	road limit between Shogo I and Shogo II	-	-
542	539049	9786568	1496	Shogo tin exploitation (alluviums)	-	-
543	538290	9786812	1559	Entrance of a gallery ("bouveau")	stratification NS/60°W	-
544	538003	9787359	1597	New exploitations in Kabare site	-	-
545	537832	9787436	1596	Vein highly muscovitized	-	-
546	563465	9757389	1413	Mesozonal metamorphism with garnet facies, Rukira fm; levels of black shales underneath Kibaya fm	N10E/80°W	-
547	562451	9757812	1423	Sedimentary structures, tens of black levels (high concentrations of volcanic ash)	-	-
548	563518	9760252	1473	Kibaya quarry	N55E/60°N, N45E/60°N,N30E/75°N, N40E/45°N, N20E/75°N	-
549	561004	9764917	1648	Syncline of Kibungo, sericito-schists	N15E/40°SE	-
550	558464	9783330	1583	Rurambi, brechiated zone formed by elongated qtzites ; parallel oriented qz veins	-	-

551	565474	9783018	1384	Medium-grained quartzites of dmtric layers	N35E/65°E	-
552	566574	9780457	1611	Wolfram-bearing quartz vein/tourmaline	-	-
553	566779	9780505	1601	Cross stratification, light quartzites of Kibaya fm	N20E/50°SE	-
554	566635	9780655	1550	Upper Rukira fm and lower Kibaya fm: quartzophyllades	N50E/10°NW	-
555	565992	9781651	1575	Volcano-sedimentary rocks	N160E/30°SW	-
556	571824	9775190	1497	Metapelites of Rukira fm	N20E/90°	-
557	572102	9775159	1502	Black shales, S0//S1	N15E/70°W	-
558	572654	9774750	1615	Gitwe fm	-	-
559	572732	9774668	1621	Fine grained and massive quartzites/Bwatantama	N25E/75°NW	-
560	575502	9773407	1391	Gitwe quartzites?	-	-
561	567984	9781646	1382	-	N20E/55°E	-
562	569715	9783533	1421	Mineralized veins, limit between Ndamira and Kibaya fms	NS/Subvertical, N30E/50°E	-
563	569864	9783592	1457	Axial plan of the syncline S0 perpendicular to S1	-	-
564	570143	9784188	1544	-	N50E/50°NW	NS/70°W
565	570857	9784737	1551	Volcanosedimentary rocks?Ndamira fm?	-	-
566	573591	9788487	1470	Sandstones Kibaya?	N40E/50°NW	-
567	573517	9788595	1497	Quartzites, Kibaya?	N50E/40°SE	-
568	578195	9792273	1500	Metapelites of Rukira fm?	-	N15E/45°SE
569	579490	9793048	1610	Akagera Game Lodge	-	-
570	563706	9796148	1661	-	N50E/70°S, N60E/55°SE, N40E/40°S	N10W/70°N, N80E/60°N
571	563869	9796131	1619	-	N10E/80°S	-
572	563891	9796130	1622	-	N20E/50°S	-
573	563886	9795998	1635	rocks completely recrystallized, quartz veins with tourmaline, light quartzites with locally conglomerates(Kibungo fm)	N20E/50°S	-
574	563388	9796233	1624	-	N15E/30°N	-
575	563919	9796255	1630	-	NS/90°	-
576	563867	9796254	1634	-	N10E/90°	-
577	571469	9815159	1382	Zoned quartzophyllades of Rukira fm	-	-
578	571484	9815145	1372	Mineralized vein (depth: 100 m)	-	-
579	571526	9815070	1365	Walls mineralized in ferberite (Mucucu hill). 2 possible explanations: wolframite or the scheelite crystallized in ferberite? Schists with garnet (volcanosediments?)	-	-
580	571528	9815072	1365	-	N35W/subvertical	-
581	571962	9815614	1426	-	N10W/80°	-
582	572170	9815832	1499	-	N5W/90°	-
583	572210	9815936	1519	-	N10W/90°	-
584	572014	9816153	1523	-	N5W/90°	-

585	571765	9816142	1494	-	N5W/90°	-
586	538291	9786811	1514	Qtzophyllades+schists similar to Rukira fm, qz veins crosscut perpendicularly to S0	N155E/45°S	-
587	533107	9784714	1633	Gahengeri	N135E/Subvertical	-
588	533109	9784717	1676	Gahengeri, quartz veins at Mataba hill	-	-
589	533030	9784761	1681	Conjugate shear zone (isochronous), micro-conglomeratic sandstones	S0 N165E/70°SW	-
590	536704	9785749	1602	Musha fm	S0 N170E/80°E	-
591	536865	9785574	1654	Synsedimentary slumps, unstability linked likely to a volcanic activity, garnet and pyrite facies	-	-
592	564630	9797458	1558	Microconglomerates of Birenga fm	S0 N10W/85°S	-
593	564742	9797435	1539	Birenga fm, Nyakabungo site (Mwiri sector)	N10E/65°SE	-
594	565002	9797246	1505	Light quartzites of Kibungo fm, parallel laminations, quartzophyllades and schists	N10E/85°N	-
595	565083	9797257	1491	Light quartzites of Kibungo fm	-	-
596	565517	9797227	1501	Quartzites of Kibungo fm	-	-
597	565516	9797052	1460	Ndamira fm dominated by sandstones and quartzophyllades	-	-
598	564349	9798173	1611	Gitwe: massive quartzites with megawaves and rare clay minerals	S0 N30W/80°E	-
599	564256	9798002	1599	-	S0 N30W/80°W	-
600	562365	9796214	1622	Massive quartzites of Gitwe with regular conglomerates	-	-
601	562345	9796297	1617	Massive quartzites of Gitwe with regular conglomerates	S0 N120E/45°S	S1 N85E/30NE
602	562309	9796476	1617	-	N160E/55°SE; 40°NE	-
603	562253	9796539	1614	Zoned schists (Musha fm?)	N160E/Subvertical	-
604	562243	9796731	1608	Banded and zoned schists	NS/60°E	-
605	562046	9796813	1581	Blocks of hematites (core of anti or syn- cline) fractured zone/ weathering?	-	-
606	561991	9796788	1587	Musha ?	N10E/40°W	-
607	561943	9796798	1595	Gitwe fm	-	-
608	561930	9797038	1578	Limit between Musha and Nyabugogo fms	-	-
609	561676	9797323	1501	-	S0 N160E/55°SW	N30E/65°SE
610	561904	9797753	1481	QQP to QPP, zoned layers: Nyabugogo fm underneath Musha	-	-
611	551430	9745132	1357	Kabombo mine	-	-
612	551392	9745141	1414	Kabombo ferberite mine	-	-
613	551327	9744848	1392	Kabombo mine	-	-
614	549676	9745146	1449	massive qtzites light grey colored similar to Nyabugogo or Nduba fms but Br on map), Kibare-Mutukura wolframite Mine	S0 N170E/50°W	-

Appendix 3: Rock-samples, their locations and types of petrographic analyses

Ref.	Sample	Locality	Easting	Northing	Elev.	Mac	LM	SEM	XRF	FI study
1	JC-1	Gashenyi	577498	9740345	-	x	x	-	x	-
2	JC-2	Musaza	572560	9736590	-	x	x	-	x	-
3	JC-3	Kagera	567880	9739530	-	x	x	-	x	-
4	JC-4	Nkuri	446800	9825040	-	x	x	-	x	-
5	JC-5	Nyagatare	527400	9828000	-	x	x	-	x	-
6	JC-6	Mugonero	410875	9754757	-	x	x	-	x	-
7	JC-6-1	Ntungwa	536911	9785351	-	x	x	-	x	-
8	JC-6-3	Ntungwa	537309	9784870	-	x	-	-	-	-
9	JC-6-6	Ntungwa	539973	9783220	-	x	-	-	-	-
10	JC-6-7	Ntungwa	539969	9783228	-	x	-	-	x	-
11	JC-8	Kigoma	-	-	-	x	x	-	-	-
12	JC-9	Kibuye	-	-	-	x	x	-	-	-
13	JC-10	Kibungo	557020	9767880	-	x	x	-	x	-
14	JC-11	Rusumo	584380	9746566	-	x	x	-	x	-
15	JC-12	Kibungo	-	-	-	x	x	x	-	-
16	JC-13	East	-	-	-	x	x	-	x	-
17	JC-14	East	-	-	-	x	x	-	x	-
18	JC-15	-	-	-	-	x	-	-	-	x
19	JC-16	Ntungwa	536700	9785900	-	x	-	-	x	-
20	JC-17	Rwinkwavu	567050	9783830	-	x	-	x	-	-
21	JC-18	Mwiri	563570	9793640	-	x	-	-	x	-
22	JC-19	Musha-Ntungwa	-	-	-	x	-	-	x	x
23	JC-23	Musha-Ntungwa	538350	9787020	-	x	x	-	-	-
24	JC-24	Musha-Ntungwa	540100	9782000	-	x	x	-	x	-
25	JC-25	Musha-Ntungwa	538160	9790140	-	x	-	x	-	-
26	JC-26	Musha-Ntungwa	537780	9788030	-	x	x	x	-	-
27	JC-27	Musha-Ntungwa	537760	9787460	-	x	x	x	-	x
28	JC-28	Musha-Ntungwa	538950	9786380	-	x	x	x	-	-
29	JC-29	Musha-Ntungwa	539890	9783340	-	x	x	x	-	-
30	JC-30	Musha-Ntungwa	538170	9787160	-	x	-	-	x	-
31	JC-31	Kibungo	561260	9767440	-	x	x	x	x	-
32	JC-32	Bujumu	544900	9813300	-	x	x	-	-	x
33	JC-33	Bujumu	545000	9813500	-	x	x	x	-	-
34	JC-34	Bugarura	537570	9807770	-	x	x	x	-	-
35	JC-35	Rwankuba	537100	9798400	-	x	x	-	x	-
36	JC-36	Rwankuba	537100	9798400	-	x	x	x	x	-
37	JC-37	Nyarunazi	565700	9785200	-	x	x	x	-	-
38	JC-38	Nyarunazi	565700	9785200	-	x	x	x	-	-
39	JC-39	Kizanye	566700	9783300	-	x	x	x	x	-
40	JC-40	Rwinkwavu	561800	9780400	-	x	x	x	x	-
41	JC-392	Rwinkwavu	566250	9780950	-	x	x	x	-	-
42	JC-423	Rwinkwavu	567848	9781947	1442	x	-	-	x	-
43	JC-424	Rwinkwavu	567842	9781844	1448	x	-	x	-	-
44	JC-435	Rwinkwavu	568373	9781691	1553	x	x	-	x	-
45	JC-453	Rwinkwavu	566007	9780903	1574	x	-	-	x	-
46	JC-455	Rwinkwavu	565986	9780667	1553	x	x	x	-	-
47	JC-457	Rwinkwavu	565894	9780928	1556	x	x	-	x	x
48	JC-473	Rutonde	567474	9782600	1394	x	x	-	-	x
49	JC-515	Rwinkwavu	566159	9781360	1568	x	x	-	x	-
50	JC-520A	Ntungwa	539904	9783157	1515	x	x	-	x	-
51	JC-521	Ntungwa	539897	9783166	1605	x	x	-	x	-
52	JC-523	Ntungwa	539935	9783161	1658	x	x	-	-	-
53	JC-535	Musha	538390	9786974	1582	x	-	x	-	-
54	JC-22-6-6 639	Ntungwa	539930	9783630	-	x	-	x	-	-
55	JC-23-6-1	Rwinkwavu	568080	9780960	-	x	-	-	-	x
56	JC-23-6-3	Rwinkwavu	568230	9781750	-	x	x	-	-	x
57	JC-23-6-4	Rwinkwavu	567380	9779860	-	x	x	-	-	-

58	JC-23-6-6 638	Rwinkwavu	567885	9781929	1455	x	-	x	-	-
59	JC-23-6-6	Rwinkwavu	566840	9780350	-	x	x	-	-	-
60	JC-24-6-1	Rwinkwavu	565543	9782960	1429	x	-	-	-	x
61	JC-24-6-2	Rwinkwavu	565532	9782943	1436	x	-	-	x	-
62	JC-24-6-3	Rwinkwavu	566427	9780708	1618	x	x	-	-	-
63	JC-24-6-4 642	Rwinkwavu	565623	9782572	1499	x	-	x	-	-
64	JC-25-6-3 643	Ntungu	562188	9780331	1661	x	-	x	-	-
65	JC-25-6-3	Ntungu	540216	9783323	1535	x	x	-	-	-
66	JC-25-6-4	Ntungu	540266	9783325	1544	x	-	-	x	-
67	JC-25-6-5	Ntungu	540304	9783272	1538	x	-	-	-	-
68	JC-26-6	Bugarama	473444	9847562	1929	x	-	-	x	-
69	JC-26-6-1	Bugarama	473444	9847562	1929	x	-	-	x	-
70	JC-26-6-1 644	Bugarama	473626	9847458	1913	x	-	x	-	-
71	JC-26-6-3	Bugarama	473651	9847561	1970	x	x	-	-	-
72	JC-26-6-4	Bugarama	473651	9847561	1970	x	x	-	-	-
73	JC-28-6-1 641	Bugarura East	537261	9807353	1610	x	-	x	-	-
74	JC-28-6-2	Bugarura	537734	9807824	-	x	x	-	-	-
75	JC-28-6-2 640	Bugarura	536300	9808950	-	x	-	x	-	-
76	JC-28-6-3	Bugarura	536150	9808030	-	x	-	-	x	x
77	JC-28-6-4	Mamfu	536121	9808201	-	x	-	-	x	x
78	JC-28-6-4 645	Bugarura	536279	9809024	1639	x	-	x	-	-
79	JC-30-6-1 646	Rutongo	505080	9798900	-	x	-	x	-	-
80	JC-30-6-2	Rutongo	505180	9799260	-	x	-	-	-	x
81	JC-30-6-2 647	Rutongo	505300	9799980	-	x	-	x	-	-
82	JC-30-6-3 648	Rutongo	505430	9800800	-	x	-	x	-	-
83	JC-GHR	Gahengeri	568030	9781260	-	x	-	x	-	-
84	JC-KRM	Kirimbari	563706	9796148	1661	x	-	x	-	-
85	JC-KRM-1 676	Kirimbari	563700	9796152	-	x	-	x	-	-
86	JC-MGR	Migera	564900	9789800	-	x	-	x	-	-
87	JC-NYZ	Nyarunazi	566100	9784800	-	x	-	x	-	-
88	JC-GRAN1	Nyagatare	537642	9849022	1336	x	x	-	-	-
89	JC-GRAN2	Ngarama	526823	9830501	1466	x	x	-	-	-
90	JC-GRAN3	Nkuri	446800	9825040	-	x	x	-	-	-
91	JC-HFLS	Gatore	564353	9750367	1359	x	x	-	-	-
92	JC-24-6 LEP	Ngara	549567	9760661	1439	x	x	-	x	-

Abbreviations: x-applied technique; -: not applied; Elev.-elevation; Mac-macroscopic observations; LM-light microscopy; XRF-X Ray fluorescence; FI study-fluid inclusion study.

APPENDIX 4: Representative SEM data. The SEM-EDX data were measured with internally calibrated standards and the results were automatically normalized to 100%.

4.1 Chemical composition of micas (wt. %). The structural formula was calculated on the basis of 22 oxygens

Sample	JC-22-6-6 639		JC-26							JC-535			JC-25-6-3 639		
An.	6	8	2	10	11	12	13	19	24	2	5	6	1	2	4
WO ₃	0.0	0.3	-	-	-	-	-	-	-	-	-	-	-	-	-
P ₂ O ₅	0.0	-	-	-	0.8	-	-	-	-	-	-	-	-	-	-
Ta ₂ O ₅	0.0	0.7	-	-	-	-	-	-	-	-	-	-	-	-	-
SiO ₂	46.6	50.4	39.6	49.3	42.3	41.7	48.3	41.0	48.8	43.7	46.0	34.8	48.2	48.3	49.1
TiO ₂	0.8	0.5	1.4	-	-	2.4	-	2.2	-	0.1	0.2	0.2	-	-	-
SnO ₂	0.0	1.1	-	-	-	-	-	-	-	-	-	-	-	-	-
Al ₂ O ₃	31.9	32.0	34.9	32.5	28.0	35.2	33.3	34.2	34.6	34.4	36.0	29.9	38.7	39.1	39.4
Fe ₂ O ₃	3.8	3.7	16.9	4.5	18.8	13.7	4.3	15.2	4.4	11.4	6.2	26.8	1.2	0.0	0.0
MgO	1.1	0.6	3.1	0.8	0.9	3.6	0.7	3.8	0.6	-	0.0	0.0	-	-	-
CaO	0.0	0.1	0.5	0.1	-	-	0.3	0.5	-	0.1	0.3	0.2	0.2	-	-
MnO	0.0	-	-	-	-	-	-	-	-	-	-	-	-	-	-
BaO	0.0	-	-	1.2	-	-	-	-	-	-	-	-	0.1	-	-
Li ₂ O	0.0	-	-	-	-	-	-	-	-	-	-	-	-	-	-
Na ₂ O	1.1	0.9	3.7	1.1	0.9	3.5	1.1	3.0	0.9	1.0	1.0	0.6	1.1	1.3	-
K ₂ O	10.0	9.4	-	10.4	8.4	-	10.2	0.2	10.8	9.3	9.6	7.5	10.7	11.3	11.5
Rb ₂ O	0.0	-	-	-	-	-	-	-	-	-	-	-	-	-	-
F	4.8	0.2	-	-	-	-	2.0	-	-	-	0.6	-	-	-	-
Cl															
Tot	100	100	100	100	100	100	100	100	100	100	100	100	100	100	100
Number of cations based on 22 oxygens															
W	0.0	0.0	0.0	0.0	0.0	0.0	0.0	0.0	0.0	0.0	0.0	0.0	0.0	0.0	0.0
P	0.0	0.0	0.0	0.0	0.1	0.0	0.0	0.0	0.0	0.0	0.0	0.0	0.0	0.0	0.0
Ta	0.0	0.0	0.0	0.0	0.0	0.0	0.0	0.0	0.0	0.0	0.0	0.0	0.0	0.0	0.0
Si	6.3	6.8	5.3	6.6	5.7	5.6	6.5	5.5	6.6	5.9	6.2	4.7	6.5	6.5	6.6
Ti	0.1	0.1	0.1	0.0	0.0	0.2	0.0	0.2	0.0	0.0	0.0	0.0	0.0	0.0	0.0
Sn	0.0	0.1	0.0	0.0	0.0	0.0	0.0	0.0	0.0	0.0	0.0	0.0	0.0	0.0	0.0
Al	5.0	5.1	5.5	5.1	4.4	5.6	5.3	5.4	5.5	5.4	5.7	4.7	6.1	6.2	6.2
Fe	0.4	0.4	1.7	0.5	1.9	1.4	0.4	1.5	0.4	1.2	0.6	2.7	0.1	0.0	0.0
Mg	0.2	0.1	0.6	0.2	0.2	0.7	0.1	0.8	0.1	0.0	0.0	0.0	0.0	0.0	0.0
Ca	0.0	0.0	0.1	0.0	0.0	0.0	0.0	0.1	0.0	0.0	0.0	0.0	0.0	0.0	0.0
Mn	0.0	0.0	0.0	0.0	0.0	0.0	0.0	0.0	0.0	0.0	0.0	0.0	0.0	0.0	0.0
Ba	0.0	0.0	0.0	0.1	0.0	0.0	0.0	0.0	0.0	0.0	0.0	0.0	0.0	0.0	0.0
Li	0.0	0.0	0.0	0.0	0.0	0.0	0.0	0.0	0.0	0.0	0.0	0.0	0.0	0.0	0.0
Na	0.3	0.2	1.0	0.3	0.2	0.9	0.3	0.8	0.2	0.3	0.3	0.2	0.3	0.3	0.0
K	1.7	1.6	0.0	1.8	1.4	0.0	1.8	0.0	1.9	1.6	1.7	1.3	1.8	1.9	2.0
Rb	0.0	0.0	0.0	0.0	0.0	0.0	0.0	0.0	0.0	0.0	0.0	0.0	0.0	0.0	0.0
ΣCat	14.0	14.3	14.3	14.5	13.9	14.4	14.4	14.3	14.7	14.3	14.5	13.6	14.8	14.9	14.8

4.1 (Continued)

Sample	KRM		JC-37					JC-40						JC-392	28-6-2 640	JC-34	
Analysis	1	3	2	4	9	11	18	1	2	3	6	9	10	11	9	4	7
WO ₃	-	-	-	-	-	-	-	-	-	-	-	-	-	-	-	-	-
P ₂ O ₅	-	-	-	-	-	-	-	-	-	-	-	-	-	-	-	-	-
Ta ₂ O ₅	-	-	-	-	-	-	-	-	-	-	-	-	-	-	-	-	-
SiO ₂	47.1	42.1	47.3	49.8	47.5	44.7	47.2	45.5	48.9	47.9	47.1	48.8	41.6	48.4	44.1	48.1	47.1
TiO ₂	-	-	0.3	0.8	-	1.0	0.3	0.9	0.2	0.3	1.2	0.7	0.8	0.6	-	0.2	-
SnO ₂	-	-	-	-	-	-	-	-	-	-	-	-	-	-	-	-	-
Al ₂ O ₃	34.3	34.3	34.6	34.3	33.9	32.2	33.6	39.8	37.8	36.2	32.4	34.3	37.1	37.9	32.4	34.9	36.5
Fe ₂ O ₃	11.2	20.6	2.5	3.1	3.0	11.4	3.6	10.5	2.4	3.8	15.7	3.9	17.0	1.6	-	1.1	1.3
MgO	-	-	0.6	0.6	0.5	0.9	0.6	-	-	-	0.8	0.6	1.0	-	-	-	-
CaO	-	-	0.2	-	0.2	-	0.1	-	-	-	0.1	-	-	-	-	0.1	0.4
MnO	-	-	-	-	0.1	-	0.1	-	-	-	-	-	-	-	13.3	-	-
BaO	-	-	-	-	-	-	-	-	-	-	-	-	-	1.1	-	-	-
Li ₂ O	-	-	-	-	-	-	-	-	-	-	-	-	-	-	-	-	-
Na ₂ O	0.8	-	0.7	0.8	0.5	0.7	0.8	3.4	-	1.0	2.6	0.7	2.6	0.6	1.2	0.4	0.9
K ₂ O	5.4	2.9	9.9	10.7	10.1	9.2	9.8	-	10.6	10.6	-	10.9	-	9.3	9.0	11.0	10.8
Rb ₂ O	1.2	-	-	-	-	-	-	-	-	-	-	-	-	-	-	-	-
F	-	-	4.0	-	4.3	-	4.0	-	-	-	-	-	-	0.6	-	4.4	2.8
Cl	-	-	-	-	-	-	-	-	0.1	0.2	0.1	-	-	-	-	-	-
Tot	100	100	100	100	100	100	100	100	100	100	100	100	100	100	100	100	100
Number of cations based on 22 oxygens																	
W	0.0	0.0	0.0	0.0	0.0	0.0	0.0	0.0	0.0	0.0	0.0	0.0	0.0	0.0	0.0	0.0	0.0
P	0.0	0.0	0.0	0.0	0.0	0.0	0.0	0.0	0.0	0.0	0.0	0.0	0.0	0.0	0.0	0.0	0.0
Ta	0.0	0.0	0.0	0.0	0.0	0.0	0.0	0.0	0.0	0.0	0.0	0.0	0.0	0.0	0.0	0.0	0.0
Si	6.3	5.7	6.4	6.7	6.4	6.0	6.3	6.1	6.6	6.4	6.3	6.6	5.6	6.5	5.9	6.5	6.3
Ti	0.0	0.0	0.0	0.1	0.0	0.1	0.0	0.1	0.0	0.0	0.1	0.1	0.1	0.1	0.0	0.0	0.0
Sn	0.0	0.0	0.0	0.0	0.0	0.0	0.0	0.0	0.0	0.0	0.0	0.0	0.0	0.0	0.0	0.0	0.0
Al	5.4	5.4	5.5	5.4	5.4	5.1	5.3	6.3	6.0	5.7	5.1	5.4	5.9	6.0	5.1	5.5	5.8
Fe	1.1	2.1	0.2	0.3	0.3	1.1	0.4	1.1	0.2	0.4	1.6	0.4	1.7	0.2	0.0	0.1	0.1
Mg	0.0	0.0	0.1	0.1	0.1	0.2	0.1	0.0	0.0	0.0	0.2	0.1	0.2	0.0	0.0	0.0	0.0
Ca	0.0	0.0	0.0	0.0	0.0	0.0	0.0	0.0	0.0	0.0	0.0	0.0	0.0	0.0	0.0	0.0	0.1
Mn	0.0	0.0	0.0	0.0	0.0	0.0	0.0	0.0	0.0	0.0	0.0	0.0	0.0	0.0	1.5	0.0	0.0
Ba	0.0	0.0	0.0	0.0	0.0	0.0	0.0	0.0	0.0	0.0	0.0	0.0	0.0	0.1	0.0	0.0	0.0
Li	0.0	0.0	0.0	0.0	0.0	0.0	0.0	0.0	0.0	0.0	0.0	0.0	0.0	0.0	0.0	0.0	0.0
Na	0.2	0.0	0.2	0.2	0.1	0.2	0.2	0.9	0.0	0.3	0.7	0.2	0.7	0.1	0.3	0.1	0.2
K	0.9	0.5	1.7	1.8	1.7	1.6	1.7	0.0	1.8	1.8	0.0	1.9	0.0	1.6	1.5	1.9	1.9
Rb	0.1	0.0	0.0	0.0	0.0	0.0	0.0	0.0	0.0	0.0	0.0	0.0	0.0	0.0	0.0	0.0	0.0
∑Cat	14.1	13.6	14.1	14.6	14.0	14.3	14.1	14.4	14.6	14.7	14.0	14.6	14.1	14.5	14.4	14.1	14.4

4.2 Chemical composition of Fe-Ti-minerals (wt. %)

Sample analysis	JC-26				JC-KRM			JC-37	
	1	4	6	8	9	4	19	23	
P ₂ O ₅				2.5	1.0				
V ₂ O ₅	0.1	0.1	0.1			0.3	0.2		0.1
SiO ₂	0.7		4.3	1.3	1.4	1.1	3.8		0.6
TiO ₂	56.7	62.2	57.4	14.0	21.6	72.4	67.9		60.3
Al ₂ O ₃	0.2			2.7	1.9	0.6	2.0		
Sc ₂ O ₃		0.1							0.2
Cr ₂ O ₃	0.1	0.0				0.0	0.2		
Fe ₂ O ₃	39.6	33.9	36.2	76.1	71.5	25.2	25.6		37.3
As ₂ O ₃				3.4	2.7				
MgO	0.2	0.3	0.2			0.0	0.0		0.2
CaO	0.1	0.0	0.1			0.1	0.2		
MnO	2.2	3.4	1.6			0.4	0.2		1.5
Tot	100	100	100	100	100	100	100		100
Chemical formula based on 6 oxygens									
P	0.0	0.0	0.0	0.1	0.0	0.0	0.0		0.0
V	0.0	0.0	0.0	0.0	0.0	0.0	0.0		0.0
Si	0.0	0.0	0.2	0.1	0.1	0.0	0.2		0.0
Ti	1.9	2.1	2.0	0.5	0.7	2.5	2.3		2.1
Al	0.0	0.0	0.0	0.1	0.1	0.0	0.1		0.0
Sc	0.0	0.0	0.0	0.0	0.0	0.0	0.0		0.0
Cr	0.0	0.0	0.0	0.0	0.0	0.0	0.0		0.0
Fe	1.4	1.2	1.2	2.6	2.4	0.9	0.9		1.3
As	0.0	0.0	0.0	0.1	0.1	0.0	0.0		0.0
Mg	0.0	0.0	0.0	0.0	0.0	0.0	0.0		0.0
Ca	0.0	0.0	0.0	0.0	0.0	0.0	0.0		0.0
Mn	0.1	0.1	0.1	0.0	0.0	0.0	0.0		0.1
Σcat.	3.4	3.4	3.5	3.5	3.4	3.4	3.5		3.4

4.3 Chemical composition of zircon (wt. %) on the basis of 16 oxygens

	JC-26			JC-392				JC-457		
	16	17	21	1	2	4	5	14	15	17
P ₂ O ₅	0.0	0.8	0.0	0.0	0.0	0.0	0.0	0.0	0.0	0.0
SiO ₂	34.2	34.4	34.5	34.4	34.8	34.2	33.4	34.6	31.4	34.5
TiO ₂	0.1	0.0	0.0	0.0	0.0	0.1	0.1	0.0	0.0	0.0
ZrO ₂	62.5	62.6	65.5	65.6	65.3	63.7	63.3	65.4	63.1	64.4
HfO ₂	1.4	0.0	0.0	0.0	0.0	1.8	2.1	0.0	0.0	0.0
ThO ₂	0.0	0.4	0.0	0.0	0.0	0.0	0.0	0.0	0.0	0.0
Al ₂ O ₃	0.1	0.4	0.0	0.0	0.0	0.0	0.2	0.0	1.3	0.0
Sc ₂ O ₃	0.0	0.0	0.0	0.0	0.0	0.0	0.0	0.0	1.1	0.0
Fe ₂ O ₃	1.6	1.3	0.0	0.0	0.0	0.1	0.9	0.0	3.0	1.2
CaO	0.2	0.1	0.0	0.0	0.0	0.0	0.1	0.0	0.0	0.0
Total	100	100	100	100	100	100	100	100	100	100
Chemical formula based on 16 oxygens										
P	0.0	0.1	0.0	0.0	0.0	0.0	0.0	0.0	0.0	0.0
Si	4.1	4.2	4.2	4.2	4.2	4.1	4.0	4.2	3.8	4.2
Ti	0.0	0.0	0.0	0.0	0.0	0.0	0.0	0.0	0.0	0.0
Zr	3.7	3.7	3.9	3.9	3.8	3.8	3.7	3.9	3.7	3.8
Hf	0.0	0.0	0.0	0.0	0.0	0.1	0.1	0.0	0.0	0.0
Th	0.0	0.0	0.0	0.0	0.0	0.0	0.0	0.0	0.0	0.0
Al	0.0	0.1	0.0	0.0	0.0	0.0	0.0	0.0	0.2	0.0
Sc	0.0	0.0	0.0	0.0	0.0	0.0	0.0	0.0	0.1	0.0
Fe	0.1	0.1	0.0	0.0	0.0	0.0	0.1	0.0	0.3	0.1
Ca	0.0	0.0	0.0	0.0	0.0	0.0	0.0	0.0	0.0	0.0
ΣCat.	8.1	8.1	8.0	8.0	8.0	8.0	8.0	8.0	8.1	8.1

4.4 Representative SEM data for the cassiterite samples from Bugarura – Kuluti – Bibare. The formula was calculated on the basis of 2 oxygens.

Sample Analysis	JC-33			JC-34					JC-28-6-1 641					JC-28-6-2 640				JC-28-6-4 645	
	2	3	7	11	12	13	14	15	1	3	6	9	13	1	2	5	8	1	2
WO ₃	1.0	0.5	0.4	0.9	0.5	4.3	0.6	1.6	1.1	-	0.3	-	1.4	-	1.2	-	0.2	0.7	0.9
MoO ₃	-	0.5	-	-	-	-	-	-	-	-	-	-	-	-	-	-	-	-	-

Nb ₂ O ₅	-	-	0.1	1.2	0.8	-	0.9	9.8	0.2	-	0.1	-	0.1	0.4	0.4	0.6	-	-	-
V ₂ O ₅	-	0.1	-	-	-	-	-	-	-	-	-	-	-	-	-	-	-	-	-
Ta ₂ O ₅	-	0.6	-	2.8	1.9	5.2	1.2	8.3	0.1	0.3	0.7	-	-	0.8	-	0.1	0.3	-	-
SnO ₂	98.9	92.3	98.3	93.4	95.4	64.5	96.8	74.3	97.5	97.5	98.5	85.3	97.8	94.2	95.2	97.8	98.9	98.9	99.0
TiO ₂	-	0.4	-	0.2	0.1	0.1	0.2	0.5	0.3	0.7	0.3	0.2	0.4	-	2.3	0.1	-	0.2	0.1
GeO ₂	-	0.8	-	-	-	-	-	-	-	-	-	-	-	-	-	-	-	-	-
TcO ₂	-	0.2	-	-	-	-	-	-	-	-	-	-	-	-	-	-	-	-	-
RuO ₂	-	0.2	-	-	-	-	-	-	-	-	-	-	-	-	-	-	-	-	-
HfO ₂	-	0.3	-	-	-	-	-	-	-	-	-	-	-	-	-	-	-	-	-
SiO ₂	-	-	-	-	-	12.6	-	1.0	-	-	-	-	-	4.5	-	-	-	-	-
ZrO ₂	-	-	0.1	0.1	-	-	0.0	-	-	-	0.1	-	-	-	0.6	0.2	0.4	0.2	-
Fe ₂ O ₃	0.1	0.1	-	1.5	1.2	0.4	0.1	2.5	0.8	0.3	-	12.8	0.3	-	0.4	1.2	0.0	-	-
Cr ₂ O ₃	-	0.1	-	-	-	-	-	-	-	-	-	-	-	-	-	-	-	-	-
Ga ₂ O ₃	-	0.0	-	-	-	-	-	-	-	-	-	-	-	-	-	-	-	-	-
As ₂ O ₃	-	0.4	-	-	-	-	-	-	-	-	-	-	-	-	-	-	-	-	-
Al ₂ O ₃	-	-	-	-	-	12.8	-	-	-	1.2	-	1.6	-	-	-	-	-	-	-
MnO	-	-	0.2	-	0.2	0.2	0.2	2.0	-	-	-	-	-	-	-	-	0.2	-	-
MgO	-	-	-	-	-	-	-	-	-	-	-	-	-	0.1	-	-	-	-	-
BaO	-	-	0.9	-	-	-	-	-	-	-	-	-	-	-	-	-	-	-	-
CdO	-	0.5	-	-	-	-	-	-	-	-	-	-	-	-	-	-	-	-	-
CoO	-	0.4	-	-	-	-	-	-	-	-	-	-	-	-	-	-	-	-	-
NiO	-	0.4	-	-	-	-	-	-	-	-	-	-	-	-	-	-	-	-	-
ZnO	-	0.9	-	-	-	-	-	-	-	-	-	-	-	-	-	-	-	-	-
SrO	-	0.4	0.1	-	-	-	-	-	-	-	-	-	-	-	-	-	-	-	-
PdO	-	0.1	-	-	-	-	-	-	-	-	-	-	-	-	-	-	-	-	-
Cu ₂ O	-	0.5	-	-	-	-	-	-	-	-	-	-	-	-	-	-	-	-	-
Cl	-	0.3	-	-	-	-	-	-	-	-	-	-	-	-	-	-	-	-	-
Tot.	100.0	100.0	100.0	100.0	100.0	100.0	100.0	100.0	100.0	100.0	100.0	100.0	100.0	99.9	100.0	100.0	100.0	100.0	100.0
Number of cations based on 2 oxygens																			
W	0.01	0.00	0.00	0.01	0.00	0.03	0.00	0.01	0.01	0.00	0.00	0.00	0.01	0.00	0.01	0.00	0.00	0.00	0.01
Mo	0.00	0.00	0.00	0.00	0.00	0.00	0.00	0.00	0.00	0.00	0.00	0.00	0.00	0.00	0.00	0.00	0.00	0.00	0.00
Nb	0.00	0.00	0.00	0.01	0.01	0.00	0.01	0.11	0.00	0.00	0.00	0.00	0.00	0.00	0.00	0.01	0.00	0.00	0.00
V	0.00	0.00	0.00	0.00	0.00	0.00	0.00	0.00	0.00	0.00	0.00	0.00	0.00	0.00	0.00	0.00	0.00	0.00	0.00
Ta	0.00	0.00	0.00	0.02	0.01	0.04	0.01	0.06	0.00	0.00	0.00	0.00	0.00	0.01	0.00	0.00	0.00	0.00	0.00
Sn	0.99	0.92	0.98	0.93	0.95	0.64	0.97	0.74	0.97	0.97	0.99	0.85	0.98	0.94	0.95	0.98	0.99	0.99	0.99
Ti	0.00	0.01	0.00	0.00	0.00	0.00	0.00	0.01	0.01	0.01	0.00	0.00	0.01	0.00	0.04	0.00	0.00	0.00	0.00
Ge	0.00	0.01	0.00	0.00	0.00	0.00	0.00	0.00	0.00	0.00	0.00	0.00	0.00	0.00	0.00	0.00	0.00	0.00	0.00

Tc	0.00	0.00	0.00	0.00	0.00	0.00	0.00	0.00	0.00	0.00	0.00	0.00	0.00	0.00	0.00	0.00	0.00	0.00	0.00
Ru	0.00	0.00	0.00	0.00	0.00	0.00	0.00	0.00	0.00	0.00	0.00	0.00	0.00	0.00	0.00	0.00	0.00	0.00	0.00
Hf	0.00	0.00	0.00	0.00	0.00	0.00	0.00	0.00	0.00	0.00	0.00	0.00	0.00	0.00	0.00	0.00	0.00	0.00	0.00
Si	0.00	0.00	0.00	0.00	0.00	0.32	0.00	0.03	0.00	0.00	0.00	0.00	0.00	0.11	0.00	0.00	0.00	0.00	0.00
Zr	0.00	0.00	0.00	0.00	0.00	0.00	0.00	0.00	0.00	0.00	0.00	0.00	0.00	0.00	0.01	0.00	0.00	0.00	0.00
Fe	0.00	0.00	0.00	0.03	0.02	0.01	0.00	0.05	0.02	0.01	0.00	0.24	0.00	0.00	0.01	0.02	0.00	0.00	0.00
Cr	0.00	0.00	0.00	0.00	0.00	0.00	0.00	0.00	0.00	0.00	0.00	0.00	0.00	0.00	0.00	0.00	0.00	0.00	0.00
Ga	0.00	0.00	0.00	0.00	0.00	0.00	0.00	0.00	0.00	0.00	0.00	0.00	0.00	0.00	0.00	0.00	0.00	0.00	0.00
As	0.00	0.01	0.00	0.00	0.00	0.00	0.00	0.00	0.00	0.00	0.00	0.00	0.00	0.00	0.00	0.00	0.00	0.00	0.00
Al	0.00	0.00	0.00	0.00	0.00	0.30	0.00	0.00	0.00	0.03	0.00	0.04	0.00	0.00	0.00	0.00	0.00	0.00	0.00
Mn	0.00	0.00	0.00	0.00	0.00	0.00	0.00	0.04	0.00	0.00	0.00	0.00	0.00	0.00	0.00	0.00	0.00	0.00	0.00
Mg	0.00	0.00	0.00	0.00	0.00	0.00	0.00	0.00	0.00	0.00	0.00	0.00	0.00	0.00	0.00	0.00	0.00	0.00	0.00
Ba	0.00	0.00	0.01	0.00	0.00	0.00	0.00	0.00	0.00	0.00	0.00	0.00	0.00	0.00	0.00	0.00	0.00	0.00	0.00
Cd	0.00	0.01	0.00	0.00	0.00	0.00	0.00	0.00	0.00	0.00	0.00	0.00	0.00	0.00	0.00	0.00	0.00	0.00	0.00
Co	0.00	0.01	0.00	0.00	0.00	0.00	0.00	0.00	0.00	0.00	0.00	0.00	0.00	0.00	0.00	0.00	0.00	0.00	0.00
Ni	0.00	0.01	0.00	0.00	0.00	0.00	0.00	0.00	0.00	0.00	0.00	0.00	0.00	0.00	0.00	0.00	0.00	0.00	0.00
Zn	0.00	0.02	0.00	0.00	0.00	0.00	0.00	0.00	0.00	0.00	0.00	0.00	0.00	0.00	0.00	0.00	0.00	0.00	0.00
Sr	0.00	0.01	0.00	0.00	0.00	0.00	0.00	0.00	0.00	0.00	0.00	0.00	0.00	0.00	0.00	0.00	0.00	0.00	0.00
Pd	0.00	0.00	0.00	0.00	0.00	0.00	0.00	0.00	0.00	0.00	0.00	0.00	0.00	0.00	0.00	0.00	0.00	0.00	0.00
Cu	0.00	0.01	0.00	0.00	0.00	0.00	0.00	0.00	0.00	0.00	0.00	0.00	0.00	0.00	0.00	0.00	0.00	0.00	0.00
Σcat	1.00	1.03	1.00	1.00	1.01	1.34	1.00	1.05	1.01	1.02	1.00	1.14	1.00	1.07	1.02	1.01	1.00	1.00	1.00
Nb/Ta	-	0.00	-	0.71	0.68	0.00	1.33	1.98	4.78	0.00	0.26	-	-	0.74	-	13.06	0.00	-	-
Nb+Ta	0.00	0.00	0.00	0.03	0.02	0.04	0.02	0.17	0.00	0.00	0.01	0.00	0.00	0.01	0.00	0.01	0.00	0.00	0.00
Sn+Ti	0.99	0.93	0.98	0.94	0.96	0.65	0.97	0.75	0.98	0.99	0.99	0.86	0.99	0.94	0.99	0.98	0.99	0.99	0.99
[(Nb+Ta)/Sn]*	0.00	0.00	0.00	0.76	0.72	0.00	1.38	2.67	4.90	0.00	0.27	0.00	0.00	0.78	0.00	13.35	0.00	0.00	0.00
(Fe+Mn)/Sn**	0.00	0.00	0.00	0.03	0.03	0.02	0.01	0.12	0.02	0.01	0.00	0.28	0.00	0.00	0.01	0.02	0.01	0.00	0.00
W/Sn***	0.01	0.00	0.00	0.01	0.00	0.04	0.00	0.01	0.01	0.00	0.00	0.00	0.01	0.00	0.01	0.00	0.00	0.00	0.01
log (*)	-	-	-	-0.12	-0.14	-	0.14	0.43	0.69	-	-0.57	-	-	-0.1	-	1.13	-	-	-
log (**)	-2.82	-2.91	-2.46	-1.52	-1.58	-1.77	-2.28	-0.92	-1.79	-2.19	-	-0.55	-2.32	-	-2.13	-1.62	-2.29	-	-
log (***)	-2.17	-2.46	-2.54	-2.23	-2.51	-1.36	-2.41	-1.86	-2.14	-	-2.67	-	-2.03	-	-2.10	-	-2.84	-2.33	-2.23

Abbreviations: - Not determined.

4.5 Chemical composition of sulphides (wt. %)

Chalcopyrite ?		Arsenopyrite ?				Pyrite ?	
Sample	JC-28	JC-28				JC-28	
Analysis	2	12	14	15	27	10	
Na ₂ O	6.6	Al ₂ O ₃	4.0	28.2	nd	Na ₂ O	0.7
MgO	2.6	SiO ₂	0.5	3.7	0.4	Al ₂ O ₃	0.9
Al ₂ O ₃	10.3	SO ₃	31.0	5.0	nd	SiO ₂	14.1
SiO ₂	43.8	Cl	0.5	0.9	32.2	SO ₃	54.5
SO ₃	15.2	Fe ₂ O ₃	26.3	4.9	28.8	Cl	0.4
Cl	2.7	Cu ₂ O	2.6	1.1	nd	K ₂ O	0.4
K ₂ O	4.6	As ₂ O ₃	35.2	56.0	38.5	Fe ₂ O ₃	28.9
CaO	2.2	K ₂ O	nd	0.2	nd		
Fe ₂ O ₃	2.1	Sm ₂ O ₃	nd	0.1	nd		
Cu ₂ O	10.1	Ga ₂ O ₃	nd	nd	0.1		
Total	100	Total	100	100	100	Total	100

4.7 Representative SEM data for cassiterite samples from Rwinkwavu and Musha-Ntunga and for coltan and ferberite are compiled along chapter four.

APPENDIX 5: CHEMISTRY OF TOURMALINE. The structural formula was calculated on the basis of 24.5 oxygens.

Analysis	1	2	3	4	5	6	1	2	3	4	1	3	4	1	2	3
Sample	JC-28						JC-29				JC-37			JC-40		
Na ₂ O	3.0	3.7	3.2	3.3	2.7	3.6	3.2	3.5	2.6	2.5	2.4	2.8	2.3	2.6	3.1	2.6
MgO	1.6	4.1	3.2	2.9	2.8	2.8	2.9	2.8	3.1	1.7	4.5	1.8	4.3	0.8	1.1	1.0
Al ₂ O ₃	34.7	34.4	34.7	34.7	34.1	34.9	33.6	34.7	35.9	31.4	37.0	33.2	38.3	32.4	36.5	37.1
SiO ₂	40.9	41.8	41.3	41.6	41.5	40.5	40.8	40.6	41.9	48.4	42.5	36.4	42.2	47.1	40.7	41.6
CaO	0.3	0.5	0.8	0.6	0.7	0.6	0.7	0.6	0.6	0.2	0.8	0.9	1.0	0.1	0.0	0.0
TiO ₂	0.7	0.9	0.7	0.5	1.2	0.9	1.4	1.0	0.8	0.0	0.9	1.1	0.6	1.2	1.1	0.8
MnO	0.3	0.0	0.0	0.0	0.0	0.0	0.0	0.0	0.0	0.0	0.0	0.3	0.0	0.0	0.0	0.0
Fe ₂ O ₃	18.6	14.6	16.2	16.4	17.1	16.8	17.3	16.6	15.2	13.7	11.9	23.5	11.2	15.7	17.5	17.0
Cl	0.0	0.0	0.0	0.0	0.0	0.0	0.2	0.2	0.0	0.3	0.0	0.0	0.0	0.1	0.0	0.0
V ₂ O ₅	0.0	0.0	0.0	0.0	0.0	0.0	0.0	0.0	0.0	0.1	0.0	0.0	0.0	0.0	0.0	0.0
Y ₂ O ₃	0.0	0.0	0.0	0.0	0.0	0.0	0.0	0.0	0.0	1.8	0.0	0.0	0.0	0.0	0.0	0.0
Total	100.0	100.0	100.0	100.0	100.0	100.0	100.0	100.0	100.0	100.0	100.0	100.0	100.0	100.0	100.0	100.0
Chemical formula based on 24.5 oxygens [which assumes fixed B at 3 apfu and fixed (OH, F) at 4 apfu] (Williamson et al., 2000).																
Na	0.8	1.0	0.9	0.9	0.7	1.0	0.9	1.0	0.7	0.7	0.7	0.8	0.6	0.7	0.9	0.7
Mg	0.3	0.9	0.7	0.6	0.6	0.6	0.6	0.6	0.7	0.4	1.0	0.4	0.9	0.2	0.2	0.2
Al	5.8	5.8	5.9	5.9	5.7	5.9	5.7	5.8	6.1	5.3	6.2	5.6	6.5	5.5	6.1	6.3
Si	5.9	6.0	5.9	6.0	5.9	5.8	5.8	5.8	6.0	6.9	6.1	5.2	6.1	6.7	5.8	6.0
Ca	0.0	0.1	0.1	0.1	0.1	0.1	0.1	0.1	0.1	0.0	0.1	0.1	0.2	0.0	0.0	0.0
Ti	0.1	0.1	0.1	0.1	0.1	0.1	0.2	0.1	0.1	0.0	0.1	0.1	0.1	0.1	0.1	0.1
Mn	0.0	0.0	0.0	0.0	0.0	0.0	0.0	0.0	0.0	0.0	0.0	0.0	0.0	0.0	0.0	0.0
Fe	2.0	1.6	1.7	1.8	1.8	1.8	1.9	1.8	1.6	1.5	1.3	2.5	1.2	1.7	1.9	1.8
V	0.0	0.0	0.0	0.0	0.0	0.0	0.0	0.0	0.0	0.0	0.0	0.0	0.0	0.0	0.0	0.0
Y	0.0	0.0	0.0	0.0	0.0	0.0	0.0	0.0	0.0	0.1	0.0	0.0	0.0	0.0	0.0	0.0
∑Cat.	15.0	15.4	15.3	15.2	15.1	15.3	15.1	15.2	15.2	14.9	15.5	14.8	15.5	14.9	15.1	15.1
Fe+Mg	2.3	2.5	2.4	2.4	2.4	2.4	2.5	2.4	2.3	1.8	2.2	2.9	2.1	1.9	2.1	2.0
Fe/(Fe+Mg)	0.9	0.6	0.7	0.7	0.8	0.8	0.8	0.7	0.7	0.8	0.6	0.9	0.6	0.9	0.9	0.9

APPENDIX 6: WHOLE ROCK CHEMISTRY DATA (JC- SAMPLES).

Sample	JC-18	521	520A	25-6-4	30	24	19	16	24-6-LEP	6-7	6-1	11	6	5	4	14	13	10	3	2	JC-1
Loc.	MW	MN	MN	MN	MN	MN	MN	MN	NG	MN	MN	RU	MU	NT	NK	East	East	KB	KG	MS	GS
RT	HEM	MSED	MSED	MSED	MSED	QV	PEG	MSED	PEG	PEG	MSED	GRAN	GRAN	GRAN	GRAN	BAS	BAS	BAS	BAS	BAS	BAS
Sum	99.9	99.6	99.7	100.6	99.2	99.8	99.1	99.1	98.2	98.9	97.2	96.6	97.5	97.8	98.3	100.5	100.2	97.1	99.0	98.8	99.2
SiO ₂	0.0	89.5	87.7	82.7	79.9	95.1	66.9	72.3	47.6	62.3	65.5	68.5	71.6	70.9	74.0	52.8	53.4	47.8	53.5	57.0	53.2
Al ₂ O ₃	0.1	5.4	7.5	8.2	11.9	2.5	17.6	23.8	38.8	35.2	20.0	14.4	13.6	14.1	14.1	17.0	13.1	18.2	14.5	13.6	14.1
Fe ₂ O ₃	99.3	3.8	1.7	7.0	3.3	1.1	0.5	1.2	0.5	0.2	5.7	3.1	2.3	2.3	1.3	9.1	16.6	10.4	12.0	14.0	11.0
MnO	0.0	0.0	0.1	0.0	0.0	0.0	0.0	0.0	0.1	0.0	0.0	0.0	0.0	0.0	0.0	0.1	0.3	0.2	0.2	0.2	0.2
MgO	0.1	0.2	0.4	0.3	0.4	0.2	0.1	0.1	0.1	0.1	0.2	1.4	0.7	0.9	0.5	8.4	4.2	5.1	6.3	3.6	7.1
CaO	0.0	0.0	0.0	0.0	0.0	0.0	0.1	0.0	0.0	0.0	0.0	2.4	1.5	1.6	0.7	10.4	8.1	12.3	9.8	6.1	11.2
Na ₂ O	0.0	0.0	0.0	0.0	0.2	0.1	2.5	0.0	0.3	0.0	0.3	2.5	2.9	2.8	3.4	1.1	1.3	1.9	1.5	2.0	1.2
K ₂ O	0.0	0.3	1.9	1.7	2.5	0.7	11.4	0.0	10.6	0.9	4.2	4.2	4.9	5.6	4.9	0.6	0.4	0.3	0.1	0.2	0.7
TiO ₂	0.0	0.4	0.4	0.5	0.7	0.0	0.0	1.4	0.0	0.0	1.0	0.4	0.3	0.2	0.1	0.6	1.9	1.2	1.0	2.3	0.8
P ₂ O ₅	0.0	0.0	0.0	0.2	0.0	0.0	0.2	0.1	0.0	0.0	0.1	0.1	0.1	0.1	0.1	0.1	0.2	0.1	0.1	0.2	0.1
Sc	1	6	1	10	7	2	1	8	2	0	17	2	1	1	2	2	3	2	2	9	2
V	300	19	16	59	49	6	3	55	3	0	95	29	16	11	1	205	631	230	312	422	338
Cr	9	19	18	55	45	11	3	79	3	4	78	31	12	12	9	326	16	60	88	58	190
Cu	10	9	1	22	11	2	2	7	50	10	5	3	3	4	2	38	15	117	12	4	49
Zn	4	6	45	14	23	10	7	5	257	19	38	35	15	11	25	53	135	68	113	112	73
Cd	3	3	3	3	3	3	0	3	3	3	3	3	3	3	3	3	3	3	1	3	3
Sn	6	13	96	128	26	37	3	6	432	601	4	2	2	1	4	2	2	2	2	2	2
Mo	2	0	0	1	0	0	0	2	0	0	0	1	1	2	0	1	1	1	1	1	2
Ni	1	4	7	5	6	6	13	7	13	8	13	8	6	3	3	30	47	52	19	10	17
As	3	16	3	173	184	1	3	3	3	3	11	3	3	3	3	3	15	3	0	0	6
Br	1	0	0	1	2	2	4	3	2	2	2	4	4	3	3	2	3	4	4	4	6
Rb	0	23	1314	131	98	94	336	1	4500	404	193	197	190	217	361	30	8	16	4	4	41
Sr	1	3	8	15	17	3	74	21	14	9	37	196	123	154	166	87	96	201	114	133	70
Y	1	13	0	18	17	1	1	9	6	2	17	27	18	20	5	16	35	22	24	39	27
Zr	2	304	256	287	227	1	2	317	0	57	219	136	133	150	64	54	157	73	95	184	86
Nb	5	6	12	18	15	4	0	18	46	46	19	11	9	9	12	2	6	10	6	8	5
Sb	7	3	3	3	3	3	3	1	3	1	3	0	2	1	1	3	3	3	3	5	5
Ba	20	66	155	500	447	22	413	56	29	20	753	604	434	981	530	214	56	77	73	62	322
Tl	2	2	10	3	3	3	0	3	37	5	3	2	2	1	3	1	3	2	2	5	6
Bi	11	4	3	1	0	1	3	1	1	3	1	1	1	1	1	0	1	1	1	0	1
Ga	14	10	17	1	0	12	21	54	180	72	37	22	21	19	38	15	16	15	16	18	15
Ge	0	2	5	0	0	3	1	0	7	10	0	0	0	0	1	0	0	0	0	0	0
Se	0	0	0	0	0	0	0	0	0	0	0	0	0	0	0	0	0	0	0	0	0
Yb	4	0	1	0	1	1	1	1	1	1	1	1	1	1	1	0	2	2	0	1	1
Hf	2	14	10	0	0	2	6	21	4	28	11	7	5	5	9	2	5	3	3	4	1
Ta	1	2	6	0	0	1	1	4	147	234	3	2	1	3	3	1	1	1	1	5	1
W	134	16	20	0	0	17	6	9	8	6	9	15	14	17	16	6	4	8	5	11	7
Pb	2	8	5	19	13	4	76	38	24	26	19	21	30	32	34	3	2	3	13	20	9
Th	1	6	0	10	8	1	0	12	1	2	16	14	26	35	10	1	6	1	5	7	4
U	0	4	1	6	2	0	1	6	1	2	2	5	13	9	5	1	2	2	1	4	2

Abbreviations: HEM-hematite; MSED-meta-sediment; PEG-pegmatite; GRAN-granite; BAS-basic rock; MW-Mwiri; NG-Ngara; MN-Musha-Ntunga; RU-Rusumo; MU-Mugonero; NT-Nyagatare; NK-Nkuri.

Appendix 6 (Continued).

Sample	JC-26-6-1	JC-26-6	JC-36	JC-35	JC-28-6-4	JC-28-6-3	JC-24-6-2	JC-515	JC-457	JC-453	JC-435	JC-423	JC-40	JC-39	JC-31
Loc.	BM	BM	BR	BR	BR	BR	RW	RW	RW	RW	RW	RW	RW	RW	RW
R-Type	BS	QV	QV	QV	QV	QV	MSED	MSED	Fe-TQV	MSED	MSED	MSED	QV	QV	MSED
Sum	92.4	99.3	99.1	100.1	99.5	99.4	98.6	100.1	96.0	92.7	100.7	98.0	98.9	98.9	98.9
SiO ₂	70.8	93.7	97.2	97.9	98.5	97.9	48.6	82.5	51.5	36.1	98.5	82.4	60.0	75.6	60.4
Al ₂ O ₃	3.6	3.7	0.8	0.8	0.3	0.2	17.7	11.1	18.9	29.7	0.8	11.6	27.6	15.1	22.3
Fe ₂ O ₃	17.7	0.4	0.5	0.9	0.3	0.8	28.0	2.7	22.4	20.6	0.9	3.3	2.2	3.3	14.1
MnO	0.0	0.0	0.0	0.0	0.0	0.0	0.0	0.0	0.1	0.1	0.0	0.0	0.0	0.0	0.0
MgO	0.1	0.3	0.3	0.1	0.2	0.2	0.2	0.5	1.7	2.3	0.1	0.2	0.3	0.2	0.2
CaO	0.0	0.0	0.0	0.0	0.0	0.0	0.0	0.0	0.1	0.2	0.0	0.0	0.0	0.0	0.2
Na ₂ O	0.0	0.1	0.0	0.0	0.0	0.0	0.3	0.1	0.5	0.8	0.0	0.0	0.3	0.2	0.0
K ₂ O	0.1	0.9	0.0	0.1	0.1	0.0	2.6	2.5	0.0	0.1	0.1	0.0	7.8	4.3	0.0
TiO ₂	0.2	0.3	0.0	0.0	0.0	0.0	1.0	0.6	0.5	2.3	0.1	0.6	0.2	0.1	1.1
P ₂ O ₅	0.0	0.0	0.0	0.0	0.0	0.0	0.1	0.0	0.1	0.0	0.0	0.0	0.0	0.0	0.4
Sc	16	5	0	1	0	1	60	7	34	51	2	8	2	2	32
V	151	18	2	4	2	7	452	37	337	553	15	43	14	16	192
Cr	194	29	5	8	4	14	336	30	239	899	36	40	3	10	309
Cu	9	1	1	3	2	2	34	5	19	29	2	24	0	6	22
Zn	7	0	0	2	0	1	22	32	102	88	0	19	96	35	19
Cd	3	0	1	3	3	3	1	3	3	5	3	3	7	1	3
Sn	10	4	5	3	5	2	2	93	12	21	2	7	579	555	2
Mo	1	0	0	0	0	0	2	0	50	5	1	0	5	21	9
Ni	2	4	2	4	2	1	17	4	7	20	3	7	6	6	49
As	640	1	20	70	3	36	762	72	893	1114	2	126	134	338	6
Br	3	2	2	2	2	2	2	0	1	0	1	3	2	3	5
Rb	6	48	0	4	6	1	94	313	2	9	3	0	1470	774	1
Sr	11	15	1	2	2	1	36	35	70	131	2	7	26	17	20
Y	4	8	1	2	0	1	22	10	11	89	2	7	1	0	60
Zr	101	168	3	15	0	1	160	320	33	294	44	636	6	5	154
Nb	4	4	0	1	0	0	8	8	2	12	1	7	41	19	8
Sb	1	3	3	1	3	0	3	1	2	4	0	2	3	3	3
Ba	102	161	5	20	12	1	624	500	33	253	21	5	367	348	72
Tl	2	2	1	1	2	0	3	4	3	4	2	1	11	6	2
Bi	0	2	1	1	1	1	0	0	1	0	1	0	0	0	0
Ga	0	13	1	0	0	0	0	4	0	0	2	1	4	0	28
Ge	0	1	1	0	4	1	0	0	0	0	0	0	0	0	0
Se	0	0	0	0	0	0	0	0	0	0	0	0	0	0	0
Yb	0	1	1	1	1	1	0	0	0	1	1	1	1	1	4
Hf	0	11	3	0	2	2	2	2	2	2	7	1	0	0	2
Ta	0	0	1	0	1	1	0	0	0	0	1	0	2	0	4
W	0	200	113	5	14	4	1	13	1	1	13	0	0	0	31
Pb	15	9	1	4	2	0	25	15	51	31	2	9	20	79	47
Th	7	6	1	0	1	1	11	6	6	13	1	7	1	1	14
U	1	1	1	1	1	1	4	1	3	7	1	1	1	1	3

Abbreviations: MSED-meta-sediment; QV-quartz vein; Fe-TQV-Fe-titanium rich quartz vein; BS-black shale; BM-Bugarama; BR-Bugarura; RW-Rwinkwavu.